SAN ONOFRE NUCLEAR GENERATING STATION
UNIT 1

SEISMIC EVALUATION OF REINFORCED CONCRETE MASONRY WALLS

VOLUME 4 : FUEL STORAGE BUILDING

Prepared for:

BECHTEL POWER CORPORATION
Los Angeles, California

Prepared by:

COMPUTECH ENGINEERING SERVICES, INC.
Berkeley, California

April, 1982.

REPORT NO. R543-02

TABLE OF CONTENTS

1 GENERAL

1.1 Introduction

This report describes the procedures used and the results of the seismic evaluation of the Fuel Storage Building at the San Onofre Nuclear Generating Station, Unit 1 (SONGS-1). The structure was analyzed taking into account the material nonlinearities under severe ground motions. Linear analyses were used to obtain bounds on the non-linear analyses and a form of substructuring was used to obtain detailed results from the full three dimensional model of the structure.

1.2 Scope of Work

The evaluation of the Fuel Storage Building comprised linear and nonlinear analyses of the structure and the evaluation of the stresses and deformations in the individual components of the structure.

The structure was evaluated for two distinct conditions. Firstly, the "as-built" structure was analyzed using limit state conditions to determine whether structural integrity would be maintained under the 0.67g Housner Design Basis Earthquake. For these analyses components were evaluated in terms of ultimate capacities.

From this series of analyses the components which required modification to meet the re-evaluation criteria were identified and a separate series of analyses was carried out incorporating these modifications. The re-evaluation criteria were based on the conservatisms and factors of safety normally applied to structures under ultimate load conditions.

Separate models were used for the evaluation of horizontal and vertical earthquake effects. Vertical acceleration components from each of these models were summed to obtain total vertical input for evaluation of diaphragms.

1.3 Report Format

Section 1 of this report provides an introduction, the scope of work and a general description of the building. In Section 2 the criteria and methodology used in the evaluation are discussed and the procedure used to select appropriate time histories is detailed. The formulation for the non-linear elements is briefly described in Section 3. Section 4 provides details of the model used to analyze the structure for horizontal earthquake loadings and Section 5 the model for vertical loadings. In Section 6 the analyses performed on each of the models are described and the results of these analyses are summarized in Section 7. Detailed evaluation of the structure is reported in Sections 8 and 9 on the "as-built" and "as-modified" structure respectively. Conclusions drawn from the evaluation are presented in Section 10.

Appendices A and B provide details of the non-linear formulation for the in-plane and out-of-plane masonry walls respectively. In Appendices C through H detailed results from each of the final non-linear analyses are listed.

1.4 Description of Building

The Fuel Storage Building provides storage for both spent fuel and new fuel. The upper level also contains a decontamination area and equipment for the transfer of fuel between this building and the adjacent containment structure. The lower level of the building contains 480V switchgear in a section adjacent to the spent fuel pool.

The spent fuel storage area is a reinforced concrete pool with massive concrete walls founded on a mat foundation. This pool extends from elevation -3.9' to elevation 42'-0" and the side of the pool forms one wall of the adjacent 480V switchgear room. This room extends from reinforced concrete strip footings at elevation 14'-0" to elevation 42'-0" with a mezzanine floor at elevation 31'-0". The walls of this room are reinforced concrete masonry. At elevation 42'-0" a reinforced concrete slab covers the switchgear room at the top of pool level. From this elevation to the roof level at approximately 65'-0" the structure consists of light steel framing carrying the vertical roof loads and reinforced concrete masonry walls carrying the shear loads.

The roof is a seismically designed steel decking welded to steel roof members. This roof has a hatch at the east end for the fuel transfer

operations.

A general view and typical sections of the structure are as shown in Figures 1.1, 1.2 and 1.3. The location of each masonry wall is identified in Figure 1.4.

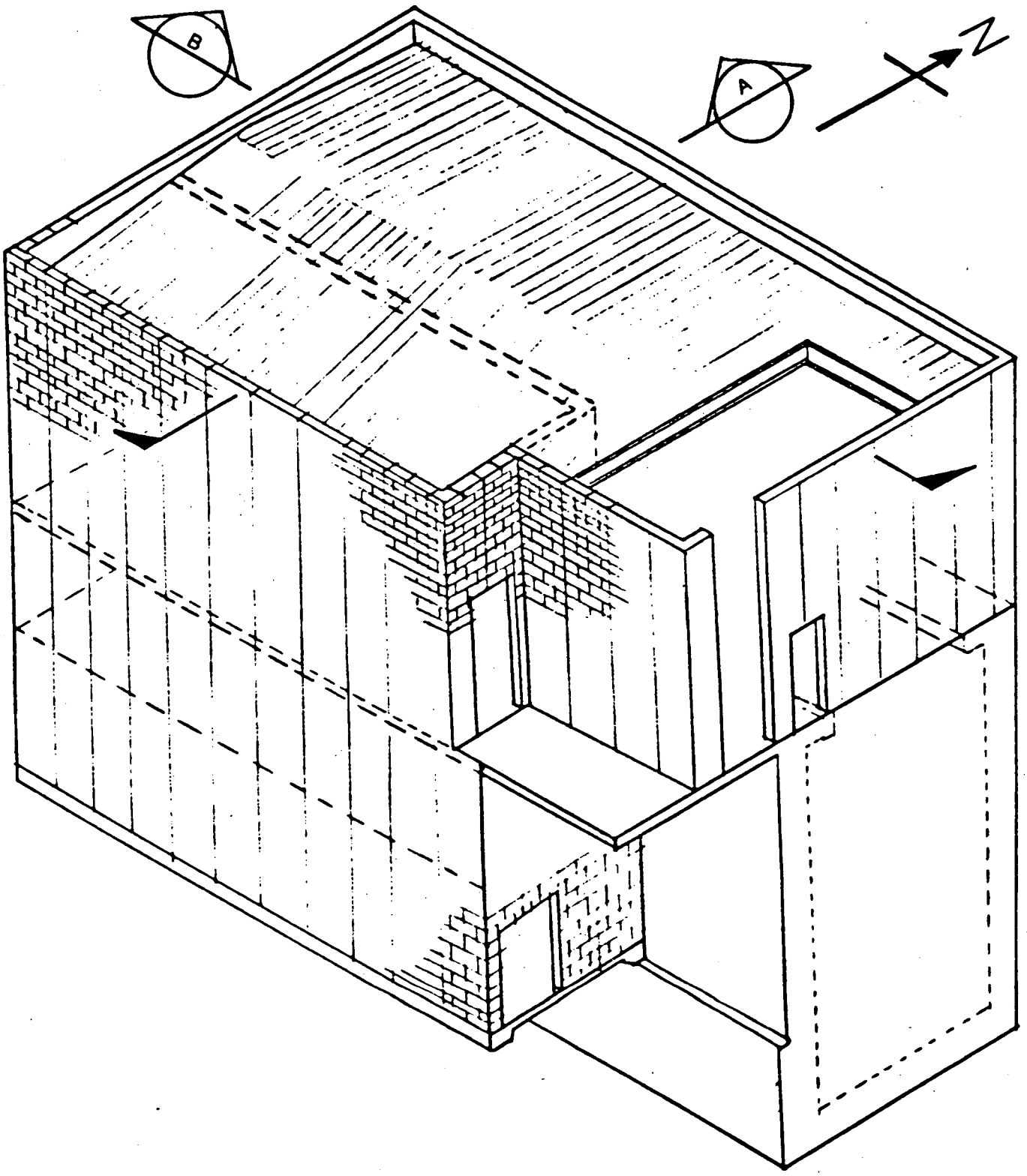

FIGURE 1.1 : GENERAL VIEW OF STRUCTURE

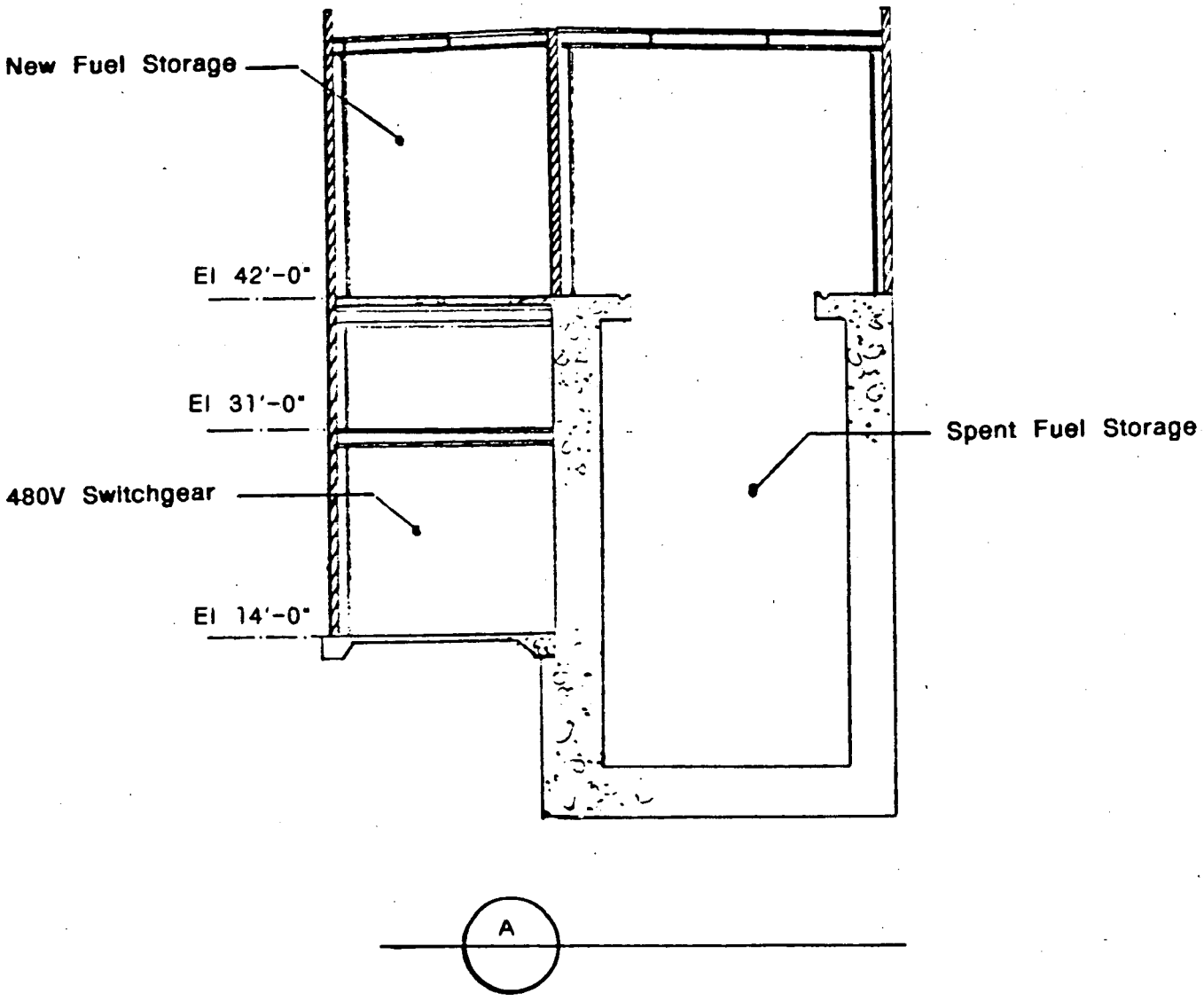

FIGURE 1.2 : TYPICAL TRANSVERSE SECTION

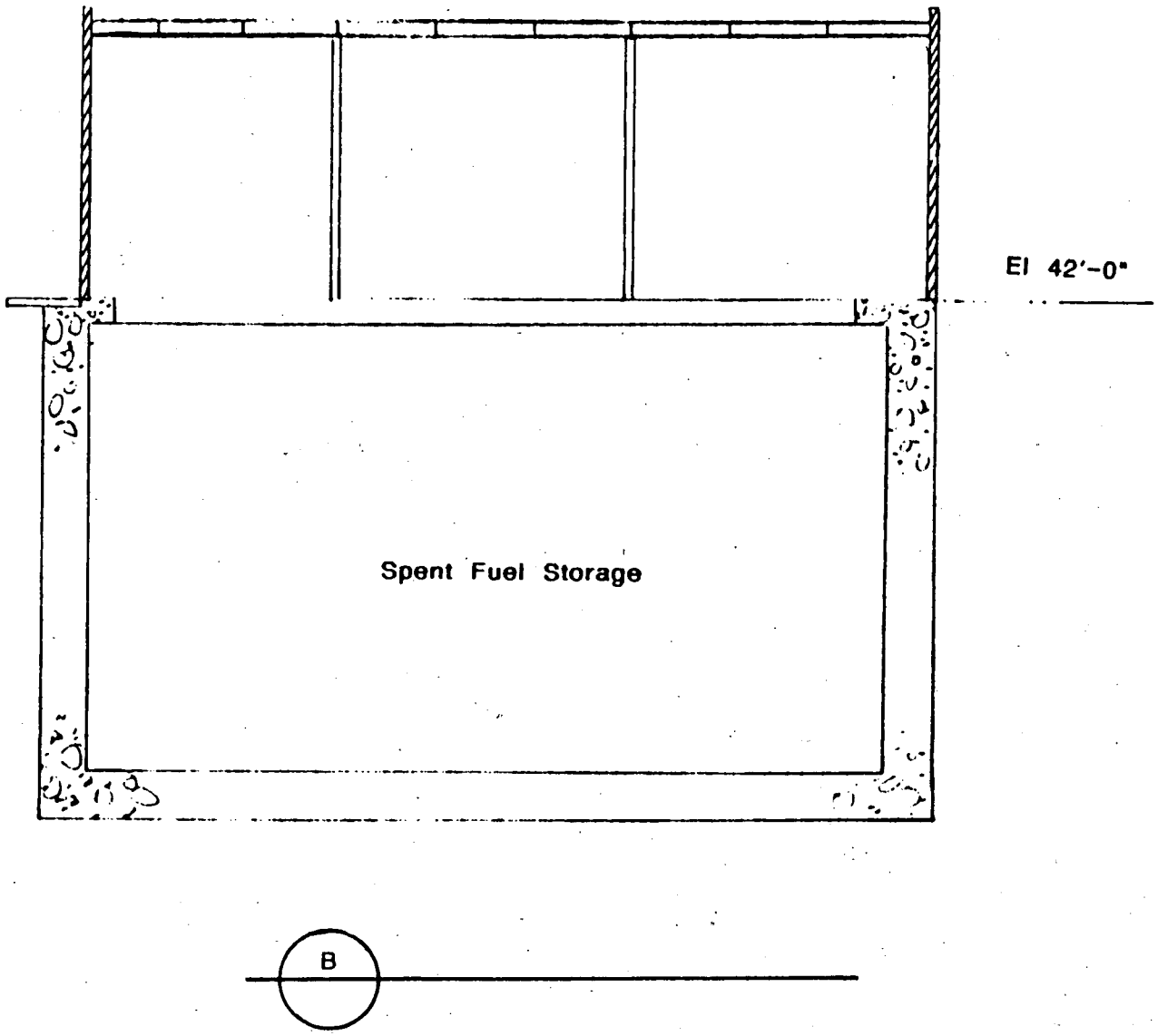

FIGURE 1.3 : TYPICAL LONGITUDINAL SECTION

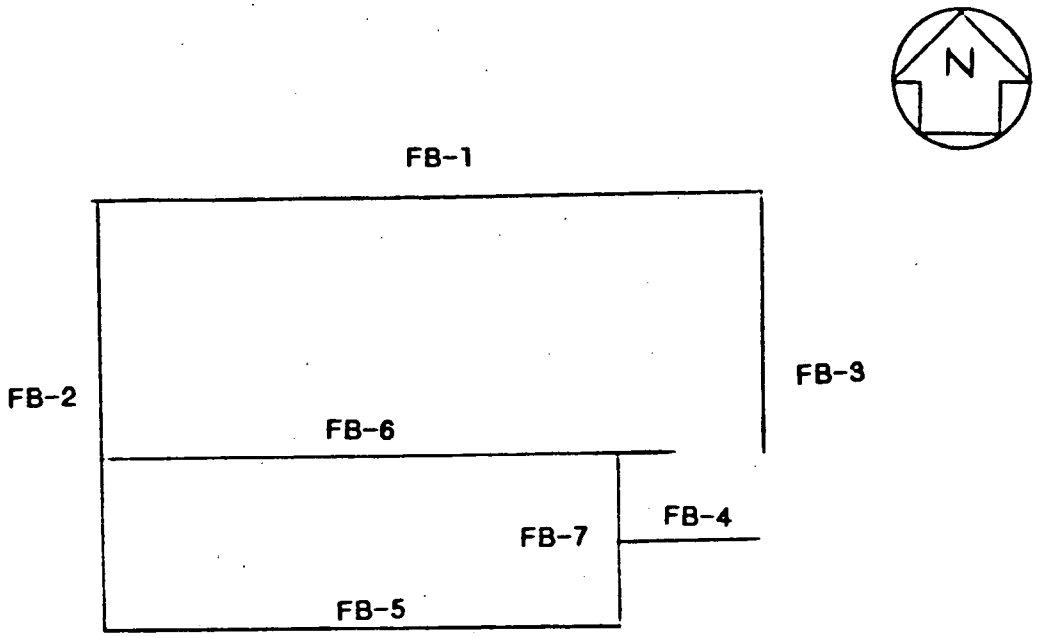

ELEVATION 42'-0"

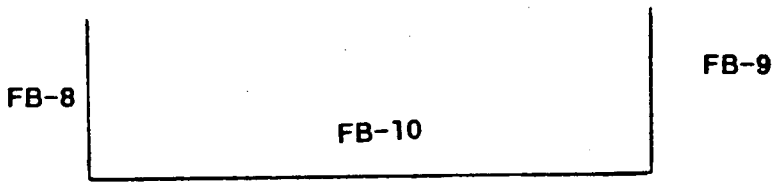

ELEVATION 14'-0"

FIGURE 1.4 : KEY PLAN FOR MASONRY WALLS

2 CRITERIA AND METHODOLOGY

2.1 Analytical Methodology

The building was analyzed using both linear and non-linear techniques. The analyses were carried out using the time history method with actual recorded time histories scaled to an intensity appropriate for the load level at the San Onofre, Unit 1 plant. All analyses were carried out using computer programs available in the public domain. In particular SAP-IV for the linear analyses and ANSR-II for the non-linear analyses were utilized.

The methodology for linear portions of the structure followed generally accepted analytical procedures. For the non-linear components, that is the masonry walls responding both in-plane and out-of-plane, methodologies were developed based on engineering mechanics principles and on available test data.

For out-of-plane reinforced masonry wall analysis the detailed methodology is reported in Volume 2 of this report. For the in-plane response the method used is detailed in Section 3.1 and in Appendix A of this Volume.

2.2 Earthquake Record Selection

A similar criteria for selection of the time histories for the non-linear analyses was used as for the Masonry Wall Evaluation reported in Volume 3 of this report. Three earthquake records were selected which when scaled according to spectral intensity together enveloped the Housner Response Spectrum normalized to 0.67g.

Each of the earthquake records had recorded horizontal motions in two orthogonal directions. For the building analysis each of these two components was applied simultaneously to the major axes of the model. The record was then rotated 90 degrees relative to the model axes and the analysis repeated for the same two earthquake components. This gave a total of six complete time history analyses.

The earthquake records as used for the previous evaluations provided a large degree of conservatism with respect to the design spectrum over

a wide range of frequencies. Therefore, for the assessment of structural integrity under "as-built" conditions the earthquake records were modified to reduce this conservatism. This was done by varying the frequency content of the recorded record in the primary direction such that the differences between the earthquake spectrum and the design spectrum were minimized. The records used are discussed further in later sections of this volume.

2.3 Fuel Building Specified Damping Ratios

The BOPSSR criteria for the SONGS-1 plant (Reference 1) provides a table of DBE damping values to be used for seismic reevaluation. This table is reproduced as Table 2.1. The Fuel Storage building is constructed of masonry block, bolted steel framing and reinforced concrete. At the level of load specified for the DBE the masonry may be assumed to be cracked. Therefore all materials in the structure have a damping percentage of 7% of critical.

For the fuel pool foundations Woodward Clyde Consultants supplied data (Reference 2) which included damping ratios associated with soil structure interaction, as listed in Table 2.2.

2.4 Re-evaluation Acceptance Criteria

The re-evaluation acceptance criteria are based on the BOPSSR criteria [1], which references the relevant material codes [3,4,5]. The seismic loading on the structure is the 0.67g Housner Design Basis Earthquake (DBE).

The re-evaluation criteria for the masonry walls which respond in the inelastic range for in-plane and/or out-of-plane loading are not included in the BOPSSR report. For these walls, criteria are reported in Volume 1 of this report and are expanded in Appendix A to include permissible strains under in-plane loadings.

The out-of-plane criteria specify stability considerations, maximum steel strain ratio limits of 45 and maximum masonry stress limits of 0.85 f'm. The criteria for in-plane strains limit the maximum strain to 0.00264 for walls which are required to carry full lateral loads. This is based on the strain level at which strength degradation is observed to commence

experimentally. For braced walls, (i.e. walls which have alternate lateral load resistance through other structural mechanisms such as steel framing) this limit is increased to 0.00528, based on the strain at which spalling of the face shells might be initiated. These criteria are sufficient to ensure that no face shell spalling will occur in any wall and that no strength loss will occur in the primary load carrying walls.

2.5 Structural Integrity Acceptance Criteria

For the "as-built" evaluation to ensure structural integrity, acceptance criteria have been developed that are based on the actual material strengths. These criteria permit higher allowable forces in the diaphragm and connections and also use a more refined envelope curve for the in-plane stiffness formulation.

The roof diaphragm stresses are limited to a maximum of 3 times the allowable shear stress provided by the manufacturer. This is based on the lower bound ultimate strength obtained in tests and is 20% higher than the factor of 2.5 used for the re-evaluation criteria. The connection forces are assessed based on a shear strength of 3 times the UBC values and a tensile strength of 2 times the UBC values. This compares with the factor of 1.5 that was used for the shear and tensile forces in the re-evaluation criteria. The in-plane stiffness formulation for structural integrity is discussed in Appendix A.

ITEM	DBE Damping (percent of critical)
Concrete Grade A Masonry Block	
Cracked	7
Uncracked	5
Welded Steel Structures	4
Bolted and/or Riveted Structures	7
Reinforced Concrete Structures	7
Prestressed Concrete Structures	5

TABLE 2.1 DBE DAMPING VALUES FOR SEISMIC REEVALUATION

Spring Type	Spatial Damping	Hysteretic Damping	Total DBE Damping
Vertical	27.0%	13.0%	40.0%
Translational N-S	16.0%	13.0%	29.0%
Translational E-W	16.0%	13.0%	29.0%
Rotational N-S	7.7%	13.0%	20.7%
Rotational E-W	1.5%	13.0%	14.5%
Torsional	4.0%	13.0%	17.0%

TABLE 2.2 FUEL POOL MAT DAMPING VALUES

3 NON-LINEAR MASONRY ELEMENTS

3.1 In-Plane Properties

The in-plane response of the masonry walls falls into two distinct categories, according to whether the loads are applied as imposed inertial loads or as applied displacements. Therefore the model used for the walls must accurately represent the response of reinforced masonry walls under both conditions.

Benchmark response curves were selected from a series of tests carried out at the Earthquake Engineering Research Center at the University of California, Berkeley. Parameters for a degrading stiffness model were then selected so as to match these curves. Details of the element parameters used and the correlation obtained are included in Appendix A of this volume.

3.2 Out-of-Plane Properties

A methodology for the evaluation of masonry walls responding to out-of-plane loads has been presented in Volume 2 of this report. In Volume 3 the results of the application of this methodology to the walls in three of the buildings at the San Onofre, Unit 1 plant have been reported.

The Fuel Storage Building out-of-plane wall models were based on this methodology. Rather than using the multi-mass formulation as in the above analyses the hysteresis as developed in Volume 2 was incorporated into the yield function of a two-dimensional beam. This beam provided a similar global response as the more complex plane-stress/gap element model but required far fewer degrees of freedom. The model does not provide the detailed results of material response which are to be evaluated in terms of the criteria in volume 1 of this report. However the well defined yield function and deflected shape of the wall in its predominant mode allows geometric derivation of formulas to extract material stresses and deformations from the output displacement and plastic rotations. This method is detailed in Appendix B which also gives details of the element formulation and provides verification of the predicted response compared with that of the more detailed model.

4 MODEL FOR HORIZONTAL RESPONSE

The main effort in the Fuel Storage Building evaluation was directed toward the response to horizontal earthquake motions. A detailed ANSR-II model as described in this section was therefore coded to obtain the response to these loads.

The lateral load resisting elements, i.e. the fuel pool walls and the superstructure masonry walls, have very high axial stiffness values and therefore no amplification of the vertical motions would be expected from these elements. The only structural elements which would be subject to vertical acceleration amplification are the roof beams and the beams at elevation 31'-0". These members are not included in the global model for horizontal response as they are considered at the sub-structure levels. Therefore vertical accelerations were not applied to the ANSR-II model. A simpler model for vertical load analysis was set up as described in Section 5 and the vertical acceleration time histories obtained from this model were combined with the ANSR-II results to obtain input for the diaphragm substructures.

4.1 General Concepts

A real structure has an almost infinite number of degrees of freedom and so any analytical model requires selection of particular degrees of freedom sufficient to describe all aspects of the response which are important for the purposes of the analysis. In general the solution techniques also impose constraints on the number of degrees of freedom to be selected. Non-linear techniques in general use in structural engineering essentially solve a series of linear structures, and thus the level of effort required for a linearly elastic analysis is multiplied many times over. For this reason it is desirable for a non-linear model to include fewer degrees of freedom than an elastic model of the same system.

The method of substructuring is a means of attaining detailed results from a global model which is simpler than would otherwise be necessary. The basic concept is to split the structure up into a number of substructures each typically containing a group of similar components. A model of each substructure is assembled and the global properties computed. These properties relate the overall forces and deformations in the substructure to a limited number of degrees of freedom. These degrees of freedom for each substructure are then assembled into a global model. The global model results are transformed back into detailed stresses and displacements by

applying them to the detailed models.

A number of computer programs are currently available which incorporate substructuring within the analysis package. However such programs have not as yet had as extensive use or as complete verification as other nonlinear programs which have been longer in the public domain. Therefore the decision was made to carry out the substructuring outside the main analysis program. This allowed complete flexibility in the detailed substructure formulations and back substitution and also maintained complete user control over the selected global degrees of freedom.

4.2 Overall Structural Behavior

The bulk of the mass and stiffness of the structure is concentrated in the water filled spent fuel storage pool and its associated soil interaction. This pool provides the main driving force for the structure under seismic loads and its response is the dominant factor in the forces and displacements induced into the other structural elements. In particular, the masonry walls of the switchgear room will have imposed displacements from the rotation of the pool on its soil springs. The walls above elevation 42'-0" will be excited by the motions at the top of the spent fuel pool.

4.3 Fuel Pool Modelling

The spent fuel pool is a reinforced concrete water retaining box. The walls and base are from 4 feet to 5 feet thick. This provides very high stiffness and the structure essentially acts as a rigid box translating and rotating on the base soil. The model was developed to reproduce this rigid box action, with the side walls formed of plane stress elements of thickness equal to the concrete walls. Around the top and bottom of the pool beam elements with properties based on the pool dimensions were included to prevent distortion of the structure. Similar vertical beams were also used over the height of the pool to provide support for the spring elements modelling the water action and also to provide support where the side walls from the switchgear room connected to the side of the fuel pool.

The substructure used to model the pool does not provide a detailed stress pattern in the structure. Therefore a separate detailed linear model was developed to carry out parametric runs and also to obtain stresses for

the structural evaluation of the pool itself. This model had a very detailed representation of the pool itself and a smaller number of elements to enable the overall influence of the superstructure mass and stiffness to be included.

Plots of the fuel pool mesh for both the global modal and the detailed substructure model are reproduced in Figures 4.1 and 4.2.

4.4 Soil-Structure Interaction

Woodward Clyde Consultants provided soil structure interaction parameters for each of the structures. These values included translational and rotational spring values and the associated damping percentages for the base of the fuel pool and for the foundation beneath the switchgear room. The non-linear model used these values to define the extent of soil-structure interaction as did the detailed sub-structure models where appropriate. In the following section the incorporation of the parameters into the model is discussed.

4.4.1 Fuel Pool Mat

The properties supplied for the soil springs and the damping for the base of the fuel pool were developed for an earlier model with a single node at the base of the pool. For the analyses reported here the spatial characteristics of the pool were included in the model, allowing the springs to be distributed over the area of the pool base. A series of springs were incorporated at the corners of the model and along the mid-side in the long direction. These springs provided equal spring constants in the three translational and three rotational directions as the values for the single node model.

Because the springs interacted to some extent, for example with the distributed vertical springs providing some of the rotational stiffness, the associated damping values used were different than those originally used. The derivation of the element damping is discussed in more detail in Section 4.8, where it is shown that the damping values used always provided modal damping less than or equal to the specified values.

The soil springs layout is given in Figure 4.3.

4.4.2 Wall Footings

Spring values for the wall footings around the perimeter of the switchgear room were supplied for an earlier model. These values were computed based on a footing tributary area and therefore equivalent values were computed for the actual nodal distribution in the final model. As the masonry walls were assumed pinned at elevation 14'-0" translational springs only were required.

4.5 Masonry Walls

The masonry walls provide essentially all the in-plane stiffness from elevation 42'-0" to roof level. Below elevation 42'-0" the walls are loaded by applied displacements from the fuel pool.

The structure was designed and constructed such that the masonry walls carry no vertical loads other than their self-weight and from equipment mounted on the walls. The roof and floor loads are carried by structural steel columns.

The nonlinear wall response is significant both for in-plane and out-of-plane behavior. The methods of including these effects in the model were discussed briefly in section 2 and in more detail in Appendices A and B.

4.5.1 In-Plane Walls

Stiffness and strength properties of these walls were derived as discussed in Appendix A. To incorporate these walls into the ANSR-II models correction factors to allow for the relatively coarse grid and for the presence of openings were developed. To obtain these factors detailed substructure models were coded using plane stress elements in the SAP-IV program. These models were then analyzed for static lateral loads and deflections obtained. A simpler model using the ANSR-II element was similarly analyzed using SAP-IV and the equivalent deflection obtained. For these results a correction factor to be applied to the element thickness was obtained.

Examples of both the complex and simple models for one of the walls with openings, FB-8, are reproduced in Figures 4.4 and 4.5.

4.5.2 Out-of-plane Walls

The yield function of these walls was as discussed in Appendix B. Each masonry wall was typically represented in the ANSR-II model by two or three element sets with properties lumped for the length of wall represented by each element. The mass was lumped such that 50% was at the mid-height node and 25% at both the top and bottom of the wall. Equivalent stiffness based on 1.5 times the cracked moment of inertia and yield moments derived for a one foot strip of wall were factored by the effective length of wall to obtain input properties. For walls with significant openings the properties were derived taking into account the reduced width.

Two walls, FB-7 and FB-4, had horizontal spans between support of less than one half the vertical spans between supports. For these walls out-of-plane wall models were not included in the global model. They were later evaluated based on two way spanning as discussed in Section 9 on component evaluation.

4.5.3 Control Joints

The masonry walls at both elevation 14'-0" and 42'-0" have vertical control joints at approximately 24'-0" on centers. These control joints are specified as "DUR-O-WALL" rapid control joints (wide flange). The detail of this joint is shown on Drawing 567682-4.

This type of control joint is a solid rubber section with a neoprene compound edge that can be compressed tightly in the joint. The joint provides a vertical stress relieving joint in the in-plane direction but has sufficient shear strength in the out-of-plane direction to provide wall lateral stability. This is achieved by keying a section of the rubber joints into the masonry block on either side of the joint. The shear strength attained has been tested at 470 psi, higher than the shear strength of a mortar joint.

The structural significance of this type of joint is that out-of-plane compatibility of displacements is enforced on either side of the joint and so the wall section may be considered continuous in this direction. In the plane of the wall the joint allows relative vertical slippage between the wall sections on either side of the joint. For horizontal displacements

separation of the wall sections may or may not occur depending on the relative stiffness of the wall portions on either side of the joint and on the direction of loading. In general the joint passes through the masonry wall only and not through the top and bottom support members. Therefore the wall will have equal horizontal displacements enforced at least at these positions by the chord members.

Based on the above the presence of the joints was accounted for in the analytical model by allowing relative vertical movement between the plane stress elements modelling the wall on each side of the joint but constraining these nodes to have equal horizontal displacements along the plane of the wall. For the out-of-plane wall model the nature of the connection was such that no account need be taken of the control joint.

4.6 Roof Diaphragm

The roof diaphragm is comprised of light gage metal decking welded onto steel supporting members. The roof was designed for a seismic shear force using the table of allowable in-plane shears provided by the manufacturer.

The diaphragm was modelled using plane stress elements. To obtain the properties of these elements the stiffness was correlated with implied stiffness values inherent in the manufacturers deflection coefficients. This required a two part parametric study, first to obtain an equivalent element thickness assuming sufficient elements to give an accurate solution and secondly to correlate these values to the coarser grid used in the global model. Each of these two substructure studies are discussed in the following section.

4.6.1 Theoretical Diaphragm Properties

The stiffness of a metal deck is a function not only of the modulus of elasticity of the material but also of the corrugated shape of the section and the weld pattern used to fasten the deck. For this reason the stiffness is not determinate from theoretical considerations, and so deflection coefficients are provided by the manufacturer based on tests. The first parametric study was concerned with converting these coefficients into element properties which could be used in the mathematical representation of the deck.

To obtain plane stress element thickness values giving equivalent deflections to those provided by the coefficients the grid shown in Figure 4.6 was analyzed. This grid is a simple rectangular diaphragm with edge supports and chord members. The deflection was computed from the coefficients under a uniform load of 1000 lb/foot as 0.0120" due to flexure of the chords and 0.0125" shear deformation in the decking, giving a total deflection of 0.0245".

The grid was then analyzed using various values of the deck thickness. Note that as the deflection is a function of the chord plus deck deformations the thickness cannot be arrived at directly from the results of a single analysis even though the response is assumed linearly elastic. It was found that an element thickness of 0.0207" gave a deflection of 0.0245", equal to the target value. This thickness is actually equal to about one third the thickness of a 16ga plate, of which the deck is formed. The study was repeated for three different roof gages and it was found that this conversion factor of one third the actual thickness was typical.

4.6.2 Roof Model Properties

Based on the conversion factor for thickness derived as discussed in the previous section a model of the actual Fuel Building roof was set up using an element thickness of 0.0207". This model, as shown in Figure 4.7, produced a deflection under uniform load of 0.045". This compared well with a deflection of 0.043" computed using the tabulated diaphragm stiffness properties and the actual span layout.

The analysis was then repeated using a coarser grid corresponding to the layout in the global model, as shown in Figure 4.8. It was found that the equivalent deflection pattern could be obtained by adjustment to the thickness of elements along the nothern edge. With this modification the maximum deflection of this simplified model was 0.044", again close to the target value of 0.045".

4.7 Floor Diaphragms

The structure has diaphragms at elevations 42'-0", 31'-0" and at the base

of the fuel pool. The fuel pool mat is four feet thick reinforced concrete and thus is essentially rigid for earthquake type loadings. This mat has therefore been modelled as rigid in the analysis.

At elevation 42'-0" the floor above the switchgear room and adjacent to the top of the pool is typically a 9" thick reinforced concrete slab. Over part of the floor in the cask laydown area the slab is locally thickened to 17.5". This floor is modelled as plane stress elements with thickness equal to the actual thickness. Part of this floor acts in flexure at the south-east corner of the structure where the floor is supported on structural steel columns. In this region beam elements have been added along the periphery of the diaphragm to transfer the shear induced by slab bending. The properties of these beams were computed based on an effective width of four times the slab thickness. Results are relatively insensitive to the properties of these beams and so a more accurate assessment is not necessary.

Elevation 31'-0" has steel framing horizontally over the area of the switchgear room. The eastern end of this framing is covered by a steel grid, which would enforce partial diaphragm action. The stiffness of this grillage of beams in-plane is not such that shear force transfer into the masonry walls would occur. However the framing does provide pin supports to the masonry walls for out-of-plane response at approximately 12'-0" on centers.

This support for the masonry wall has been incorporated into the model by the inclusion of truss members spanning from the fuel pool side wall to the out-of-plane masonry walls at elevation 31'-0". This support causes the walls to respond out-of-plane as two span continuous members but does not effect the response of the in-plane masonry wall elements.

4.8 Damping

The energy loss mechanism in elastic systems is assumed to occur through viscous damping, i.e. damping forces proportional to the velocity. For non-linear analysis there is energy loss through hysteretic damping which is accounted for in the yield functions for the materials. The means of incorporating these damping effects vary for the linear and non-linear models. In this section the procedures to obtain mathematical formulations to provide the specified damping are discussed.

4.8.1 Theoretical Considerations

The Standard Review Plan provides for the use of either stiffness or mass weighting functions for determining an equivalent modal damping matrix. For models that take soil-structure interaction into account by the lumped soil spring approach the former method, i.e. stiffness weighted damping, should be used. In this procedure the equivalent modal damping is computed as:

$$\bar{B}_j = \frac{(\phi)^T [\bar{K}] (\phi)}{(\phi)^T [K] (\phi)}$$

where $\bar{B}_j$ = equivalent modal damping ratio of the jth mode
$[K]$ = assembled stiffness matrix
(ϕ) = jth normalized modal vector
$[\bar{K}]$ = modified stiffness matrix formed as the product of the damping ratio for the element and its stiffness matrix.

This procedure is based on the uncoupling of the normal modes of vibration and therefore is restricted to elastic systems.

To obtain the modal damping ratios from the above formulation requires a knowledge of the material damping of various elements, the stiffness matrix of the elements and the shape of the various modes.

4.8.1.1 Linear Analysis

The procedures for the linear dynamic analysis in this project used the uncoupled modes. Therefore the composite modal damping ratios computed as described above was incorporated directly into the equations of motion for each of the individual modes.

Using the composite modal damping Bj the generalized damping for mode j was determined as:

$$C_j = 2 B_j w_j M_j$$

where

C_j is the generalized damping
M_j is the generalized mass

4.8.1.2 Non-linear Analysis

Non-linear analysis techniques solve the equations of motion for the total system without uncoupling the response into its normal modes. The formulation for deriving composite modal damping is not directly compatible with these solution techniques. However consideration of the uncoupled modes allows values to be assigned to the parameters defining the form of the damping matrix.

For the uncoupled system damping, the relationship between the generalized damping, mass and stiffness for mode j is:

$$C_j = a\ M_j + b\ K_j$$

where

$$C_j = 2\ B_j\ w_j\ M_j$$

and

$$K_j = w_j\ M_j$$

therefore any specified values of a and b imply damping in the jth mode of

$$B_j = \frac{a}{2w_j} + \frac{bw_j}{2}$$

Stiffness dependent damping, b, implies higher damping with higher frequencies and mass dependent damping the reverse.

If both a and b are specified two simultaneous equations may be set up to define the damping in two modes and the damping values for all frequencies are then specified. If only one of the two constants is used the modal damping is set for a single mode and defines all other damping values.

For practical implementation the mass damping value is set at the structure level and thus applies equally to all elements of the structure. The stiffness damping factor, b, is applied at the element level and may be varied for elements or groups of elements.

4.8.2 Implementation in Models

4.8.2.1 Element Damping

For the superstructure the element damping is available from the tabulated values for each of the material types. However the fuel pool soil damping values are based on a pool model with only six degrees of freedom at the basemat. In this form of model the element damping and the composite modal damping are effectively the same for the three translational and three rotational springs and for the six modes associated with these springs.

When the fuel pool is modelled as a three dimensional model with the soil springs spatially distributed the spring damping values are the composite modal damping values but because of the coupling between different springs for some modes the element damping values are unknown.

To obtain the element damping for the springs the stiffness weighted formulation given previously is solved for the six basic pool modes, with the composite modal damping and eigenvectors known and the element damping ratios associated with each of the springs as the unknowns.

Although there are six unknowns, i.e. the element damping values, and six equations, the solution of the system has the additional constraint that all damping ratios be greater than or equal to zero. For this reason the element damping values may not necessarily be able to exactly match the supplied composite modal damping values.

Solving these equations gives damping ratios for each spring value as shown in Table 4.1. Also in Table 4.1 is a comparison of the target and obtained composite modal damping. It can be seen that the correct damping will be applied in all modes except the vertical, where the applied damping of 26% is only 65% of the target value of 40%. However this value is conservative for any vertical amplification and is thus acceptable.

Note that these values were computed assuming complete uncoupling of modes, i.e. "pure" mode shapes in each of the six directions. Later studies using the detailed fuel pool model showed that composite model damping values computed using these element

damping values and the actual mode shapes were very close to those calculated as discussed above. Therefore the assumed mode shapes were very close to the actual shapes.

4.8.2.2 Damping Constants for Non-linear Analysis

The damping in the non-linear analysis is specified as a combination of the mass and stiffness matrices. The damping implied by the factors applied to these matrices is frequency dependent, and so as the frequency of particular modes changes due to non-linear material behavior the effective damping will also change.

The procedure adopted for specification of the two parameters describing the damping was to select a value of "a" to factor the mass matrix such that the applied damping with this factor alone would in no case exceed the minimum specified damping for any element group in the frequency ranges expected in the analysis. The minimum damping in any element is 7% and preliminary studies showed that the minimum frequency of the most non-linear elements was about 0.33hz, i.e. a period of 3 seconds.

A value of "a" equal to 0.2932 will give 7% of critical damping at a period of 3 seconds. For lower periods the damping will be less than 7% and for higher periods the damping will be greater than 7%.

For each element group the required damping was then obtained by specifying a "b" factor so as to give the correct damping at the elastic frequency of the component.

To specify "b" it was assumed that the contribution of an element to the overall structural response would be slight at frequencies higher than that elements own elastic natural frequency. Therefore the effect of specifying a "b" value so as to give damping in a particular element higher than that specified at frequencies higher than the elements natural frequency is acceptable.

Figures 4.9 and 4.10 are examples of "b" factors selected by this procedure for the out-of-plane masonry walls, with an elastic period of 0.47 secs, and the fuel pool vertical springs which are required

to have a damping ratio of 26% of critical at a period of 0.10 secs.

Figure 4.9 shows that for the out of plane wall a "b" factor of 0.00883 gives effective element damping less than the specified value of 7% for the period range of 0.47 to 2.54 seconds. In Figure 4.10 the value of "b" produces the correct element damping ratio of 26% at the elastic period of 0.10 secs. Above this period the damping drops sharply but as the element frequency does not change this is acceptable.

DIRECTION	ELEMENT DAMPING	COMPOSITE MODAL DAMPING	
		TARGET	ACHIEVED
Rotation E-W	6.8%	14.5%	14.5%
Rotation N-S	0.0%	20.7%	20.7%
Vertical	26.0%	40.0%	26.0%
Torsional	-	17.0%	17.0%
Translational E-W	29.0%	29.0%	29.0%
Translational N-S			
Corner	8.8%		
Middle	35.7%	29.0%	29.0%

TABLE 4.1 ELEMENT AND MODAL DAMPING VALUES

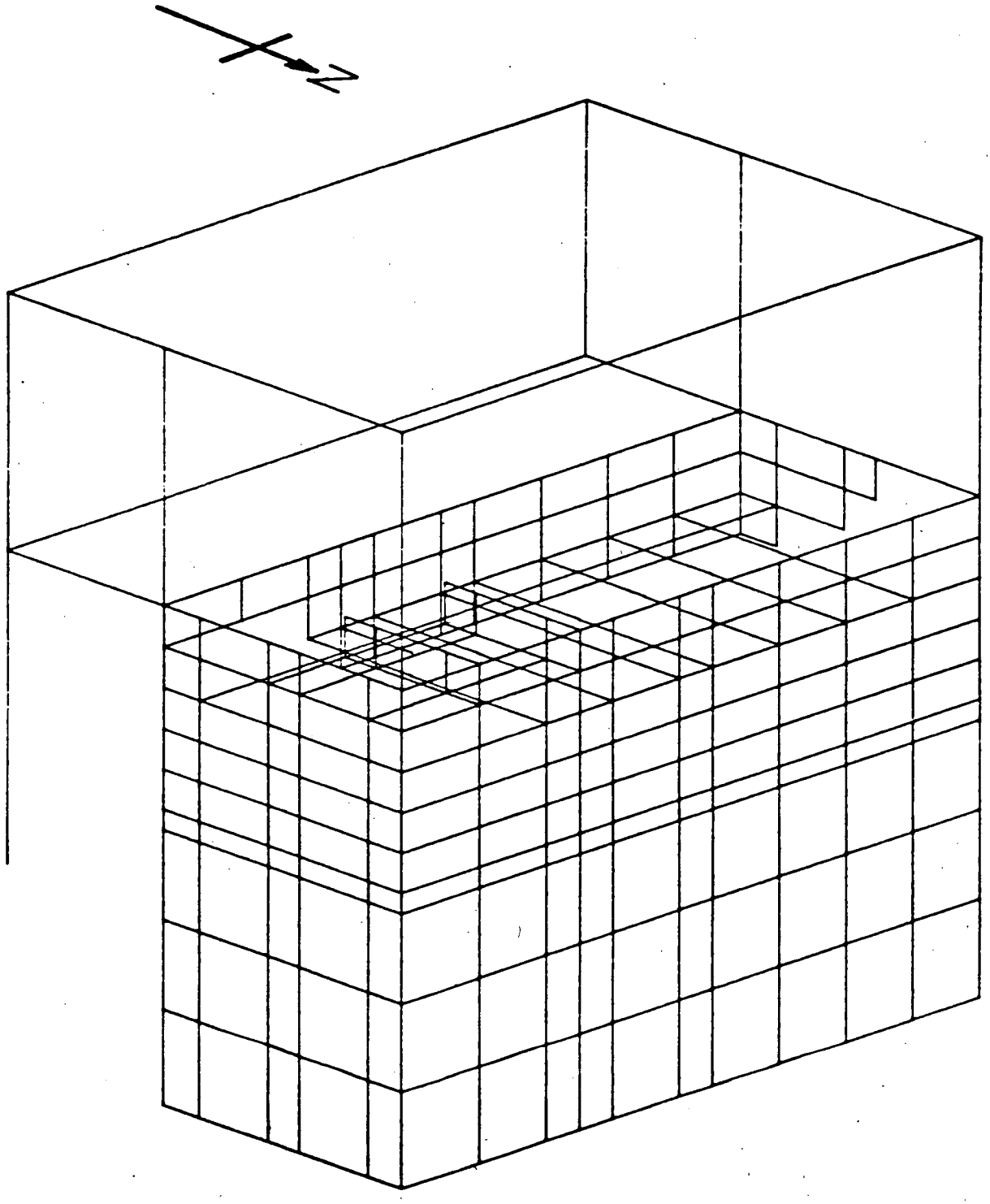

FIGURE 4.1 : DETAILED FUEL POOL MODEL

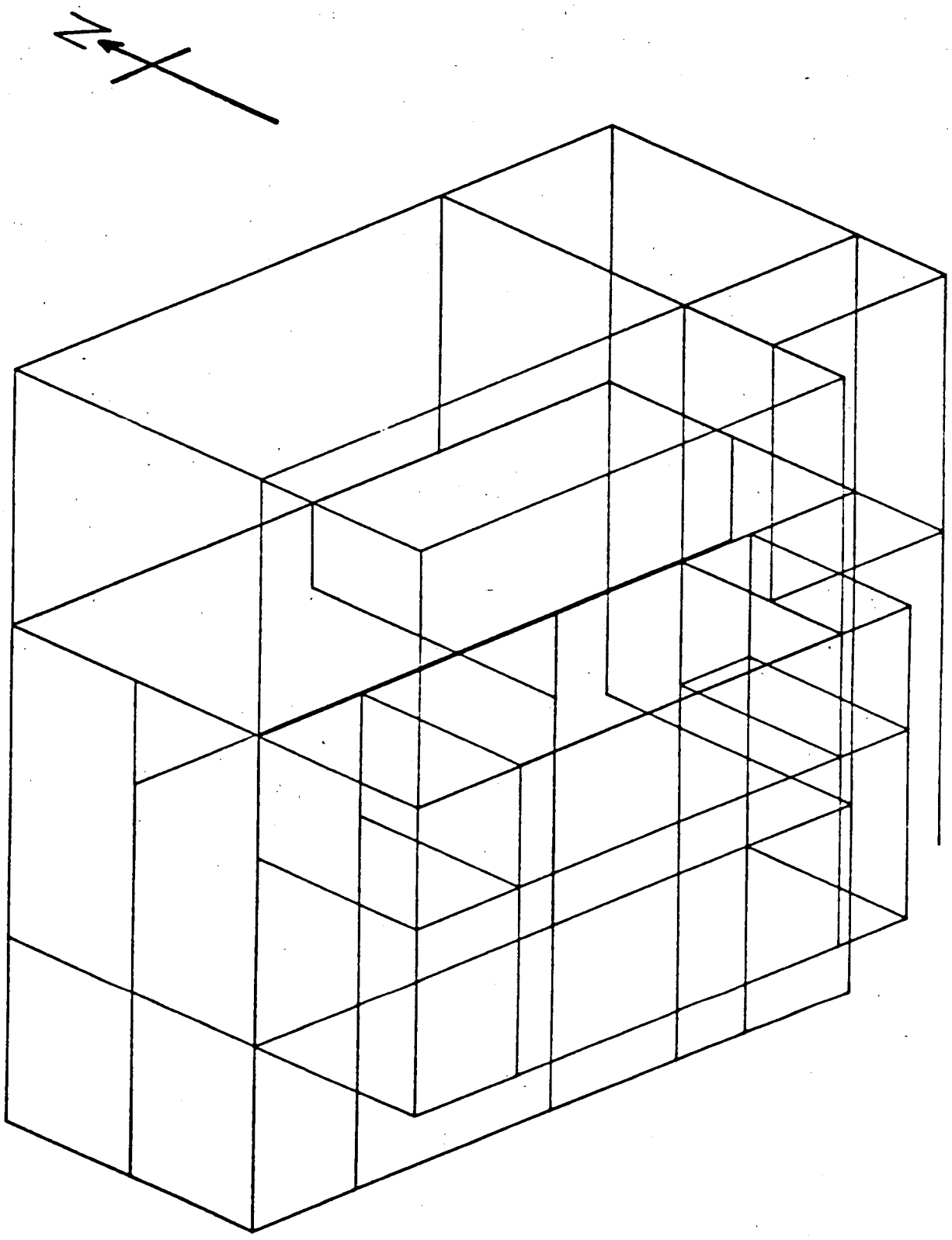

FIGURE 4.2 : GLOBAL FUEL POOL MODEL

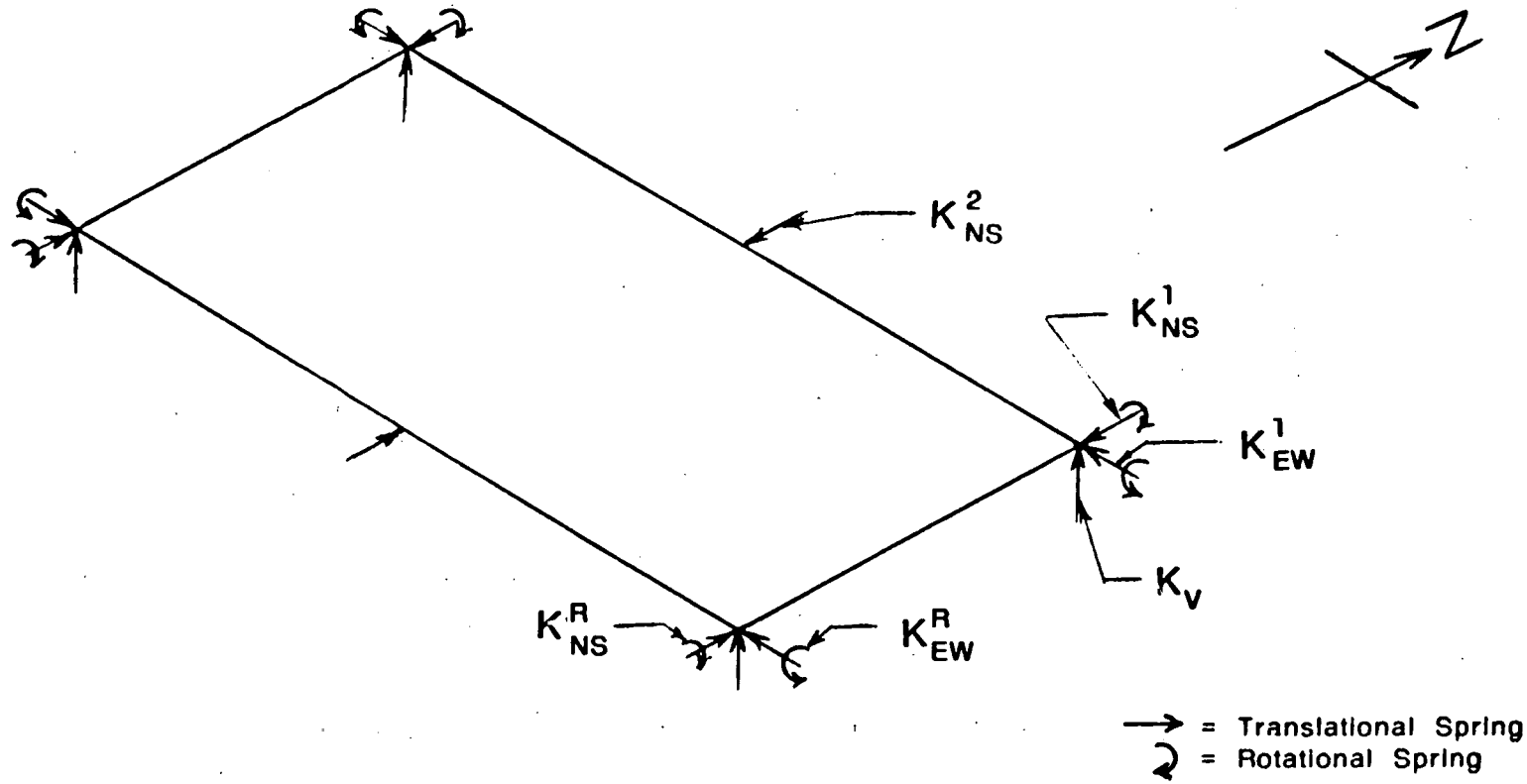

SPRING	STIFFNESS	UNITS	ELEMENT DAMPING
K_V	60525	kip/ft	26.0%
K^1_{EW}	181950	kip/ft	29.0%
K^1_{NS}	45414	kip/ft	8.8%
K^2_{NS}	273073	kip/ft	35.7%
K^R_{NS}	18609725	k-ft/rad	0.0%
K^R_{EW}	18509930	k-ft/rad	6.8%

FIGURE 4.3 : SOIL SPRINGS AT FUEL POOL BASE

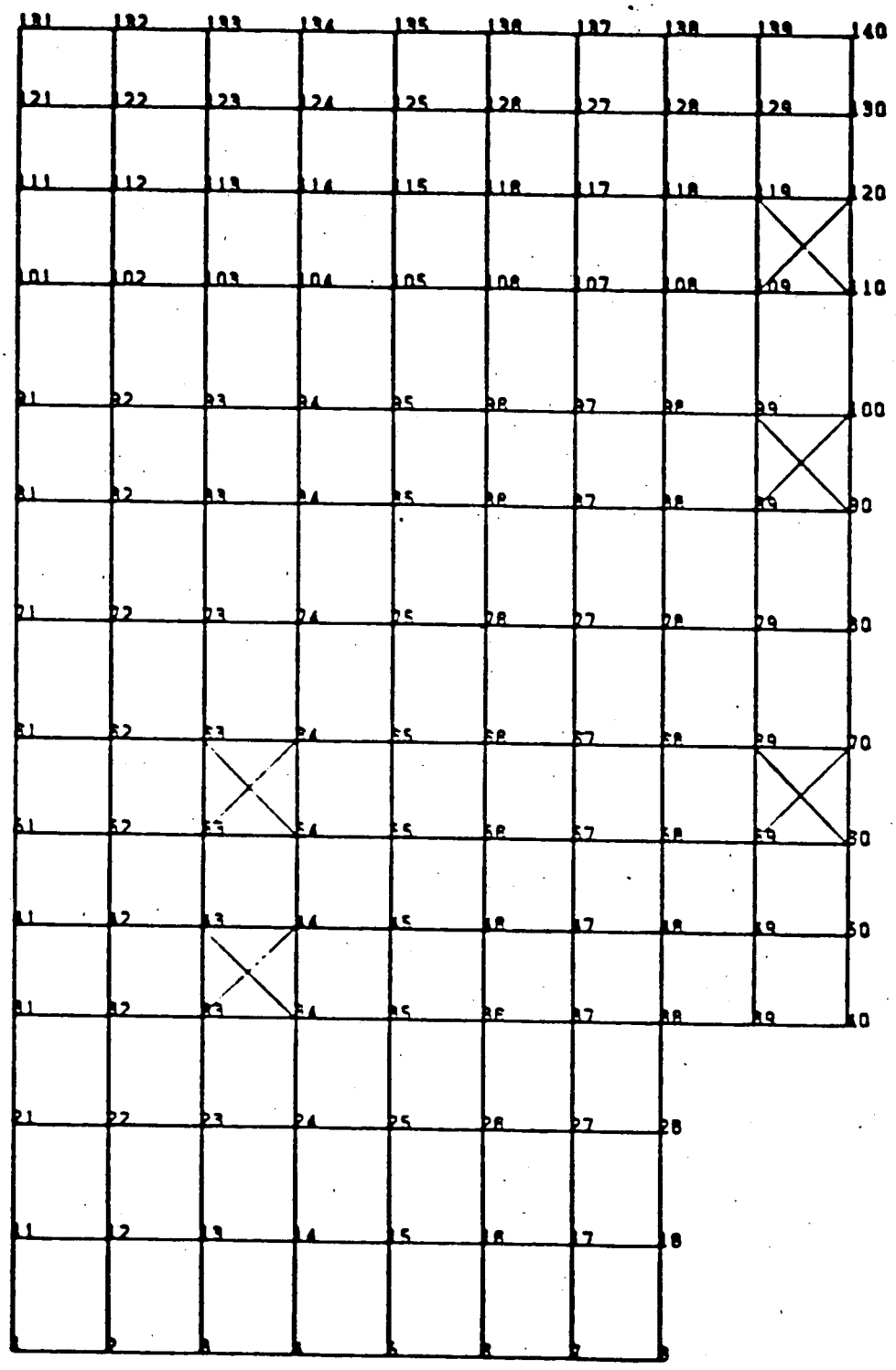

FIGURE 4.4 : DETAILED MODEL OF WALL FB-8

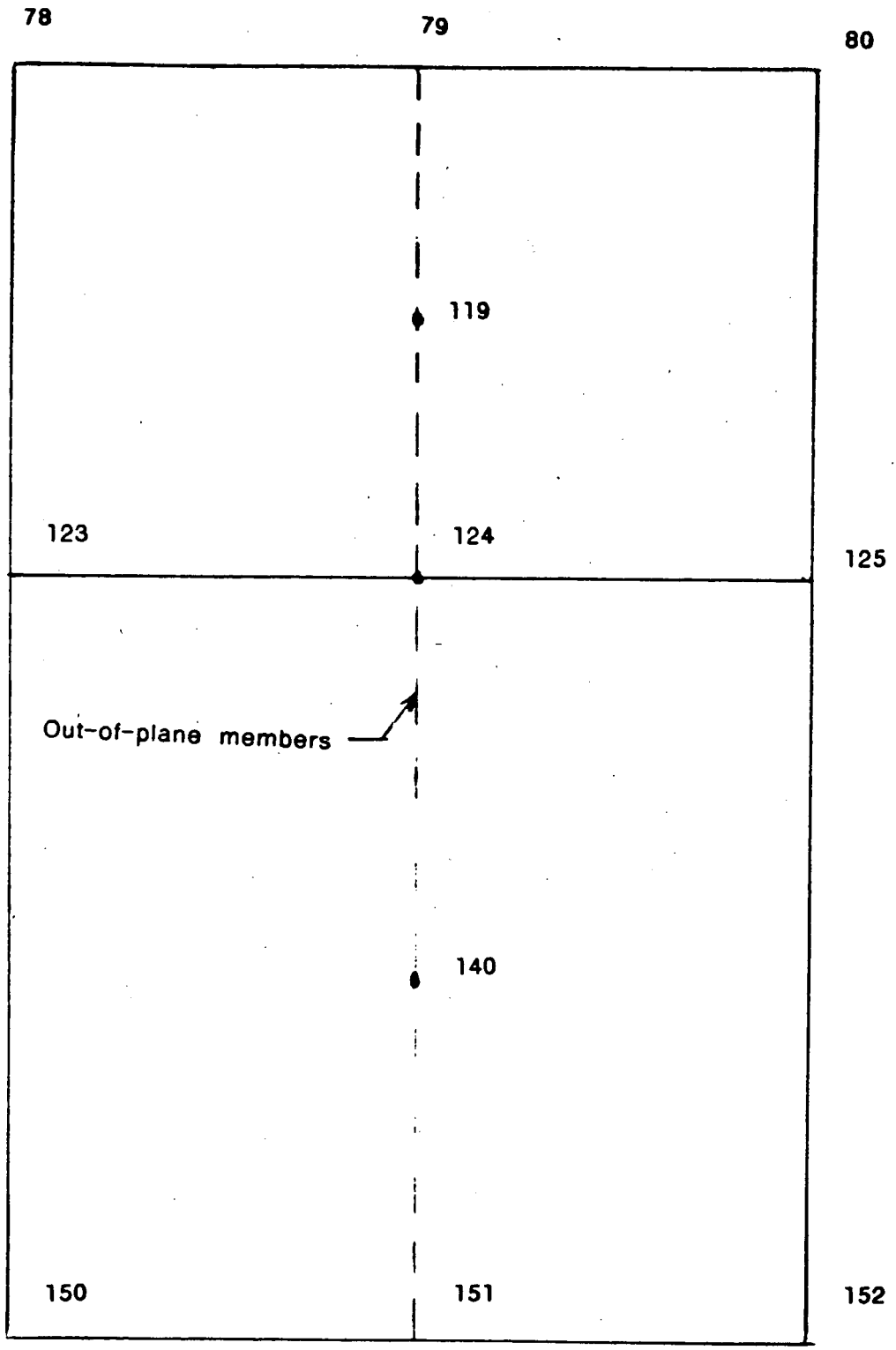

FIGURE 4.5 : GLOBAL MODEL OF WALL FB-8

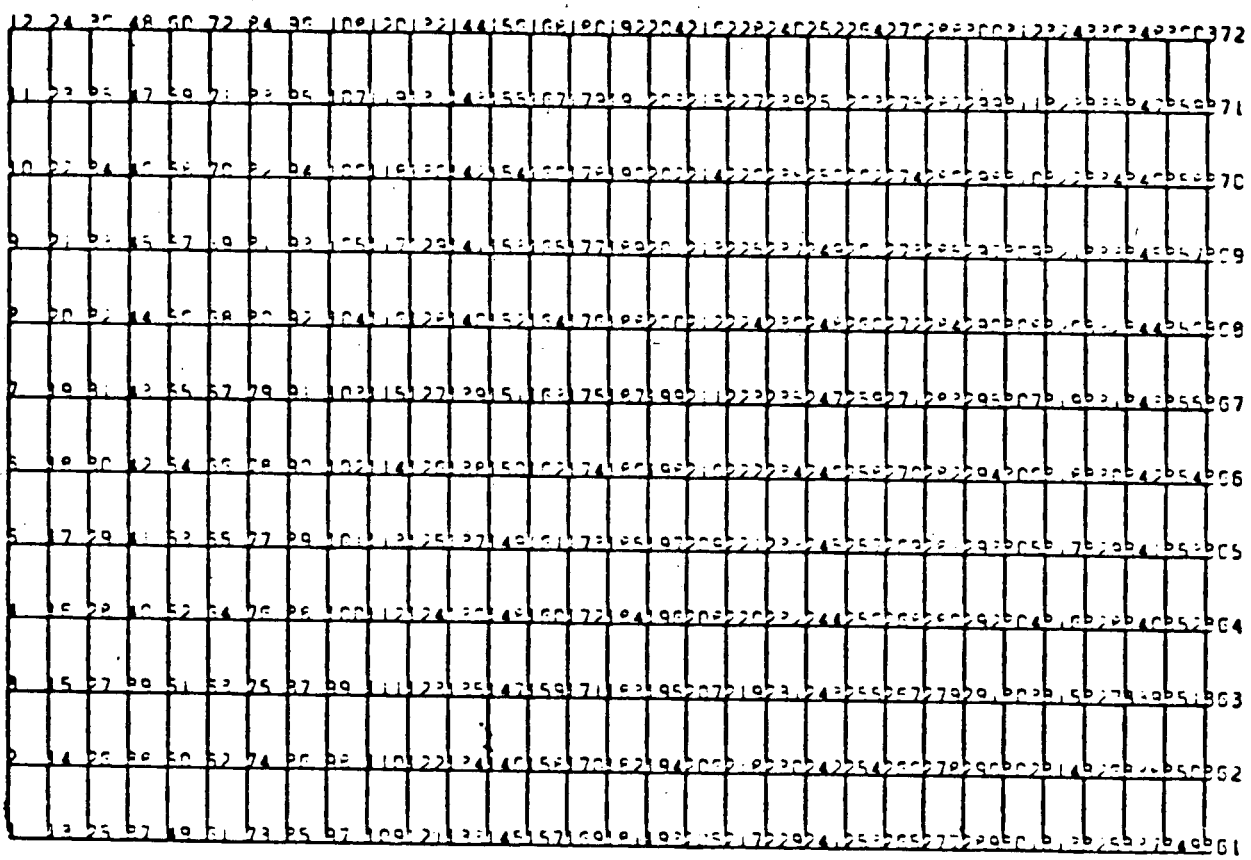

FIGURE 4.6 : MODEL FOR DETERMINATION OF ROOF THICKNESS

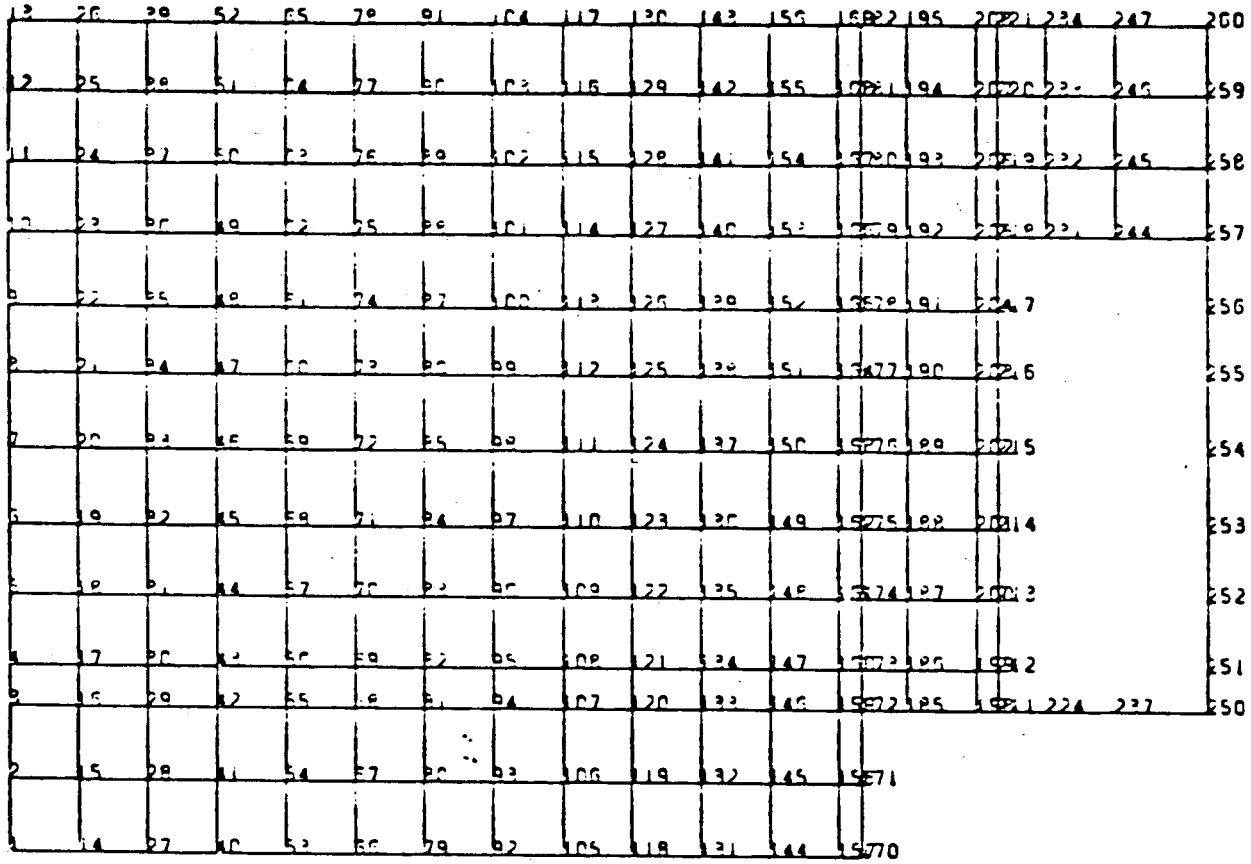

FIGURE 4.7 : DETAILED ROOF DIAPHRAGM MODEL

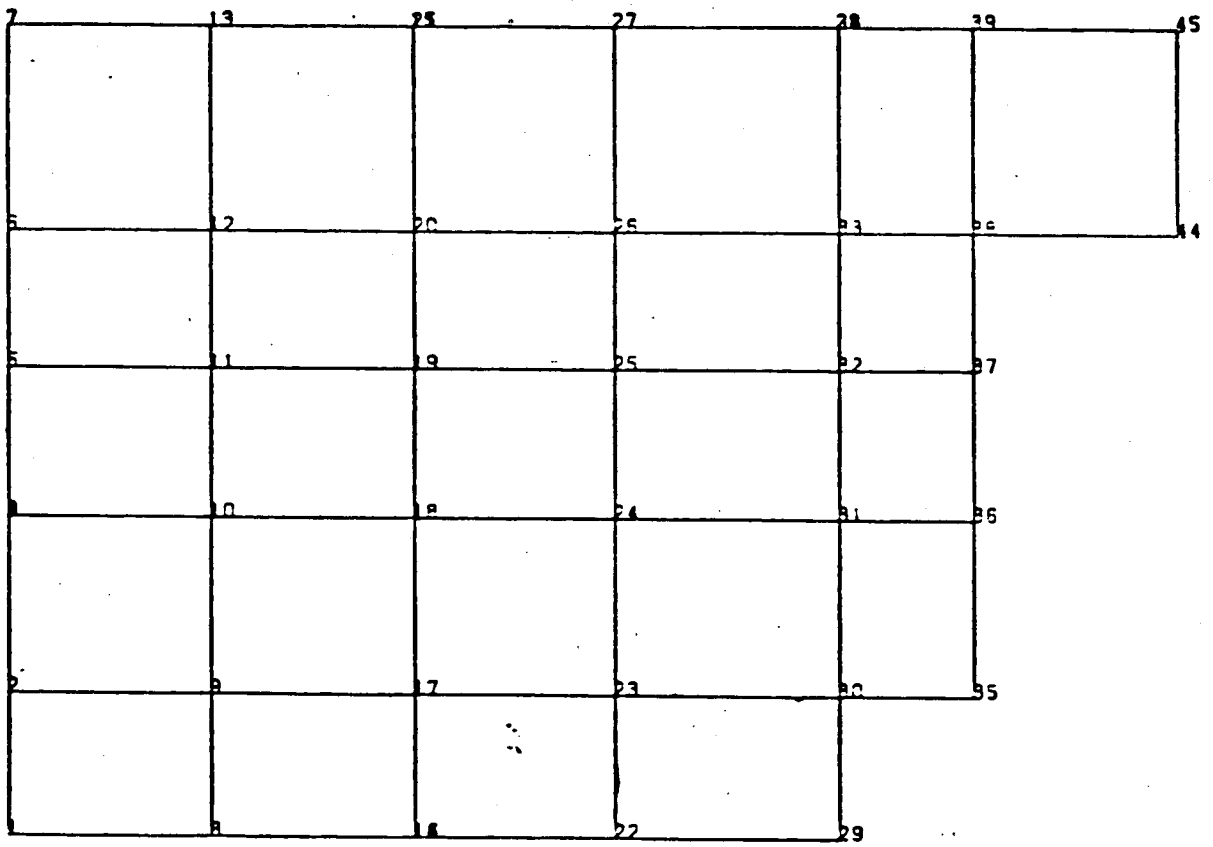

FIGURE 4.8 : GLOBAL ROOF DIAPHRAGM MODEL

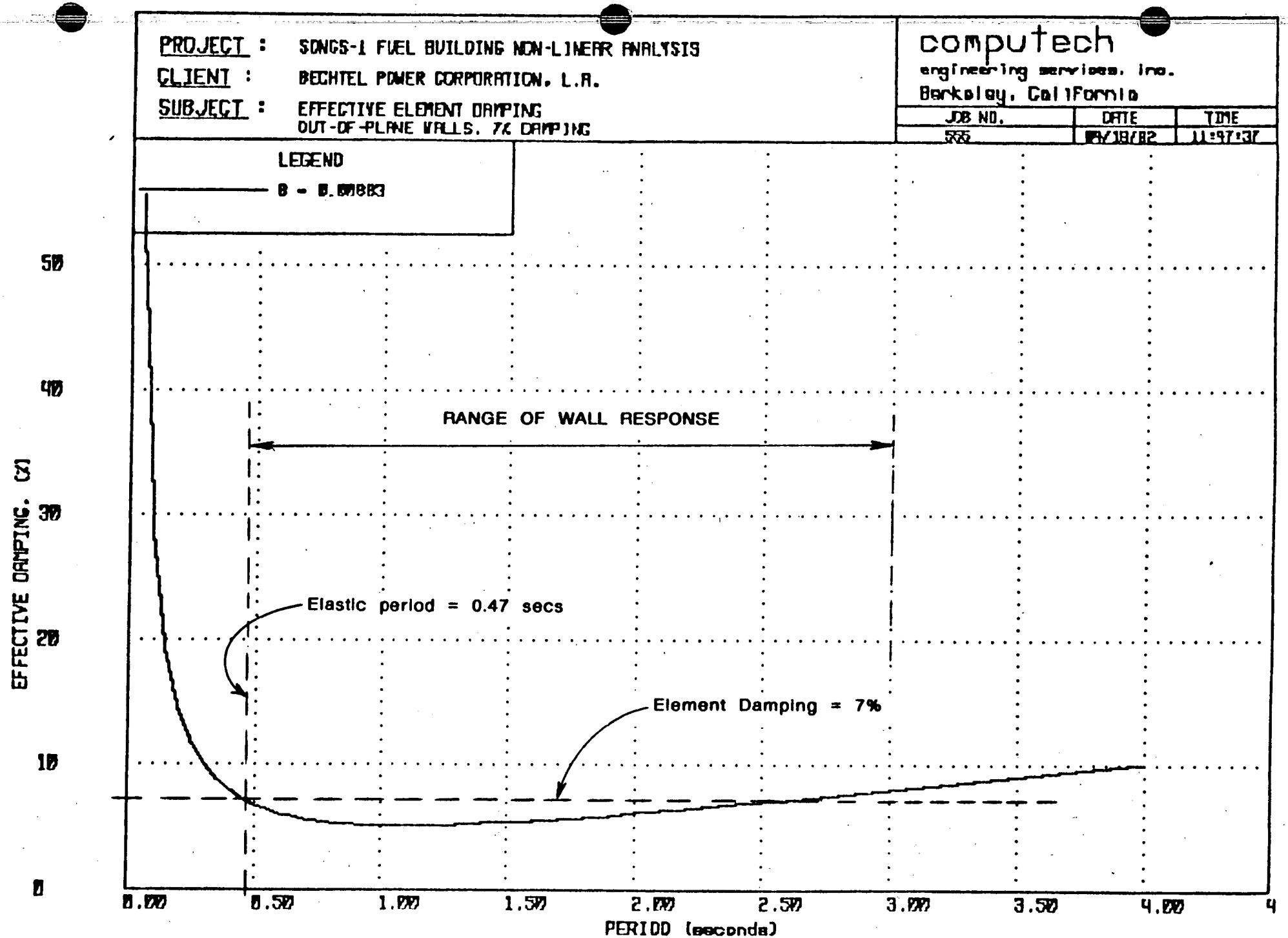

FIGURE 4.9 : DAMPING IN OUT-OF-PLANE WALLS

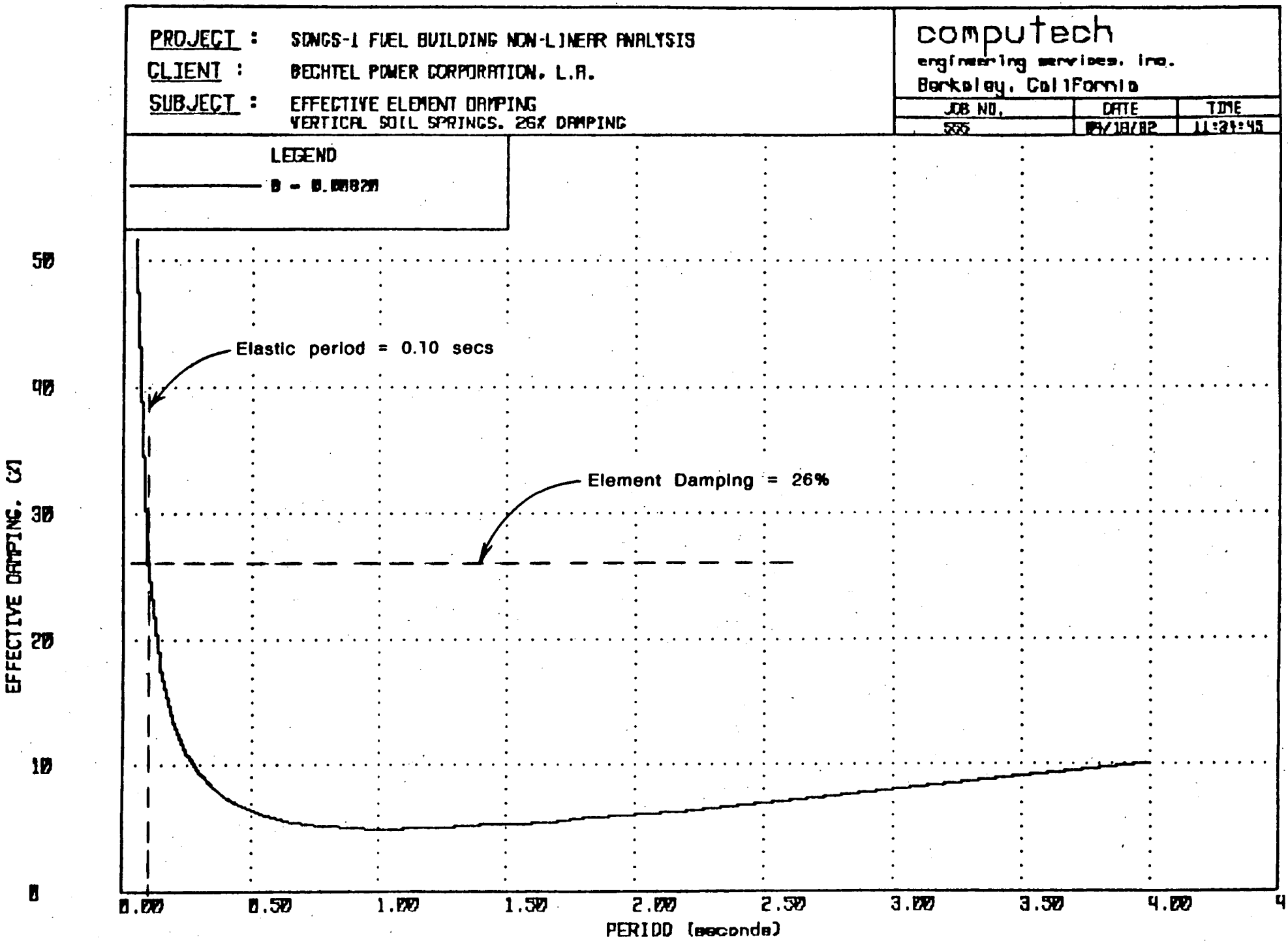

FIGURE 4.10 : DAMPING IN VERTICAL SPRINGS

5 MODEL FOR VERTICAL RESPONSE

The detailed non-linear model was assembled from the individual substructures as described in the preceding sections and a number of abbreviated static and dynamic analyses carried out to determine the overall characteristics of the structural response. One of the parameters investigated was the effect of a vertical acceleration record. A 5 second analysis using the scaled vertical acceleration record from the El Centro 1940 N-S record showed that the response under these loads was almost pure vertical translation on the base springs with negligible rocking and no non-linearity.

This result is not unexpected in that all the elements providing resistance to horizontal loads, i.e. the masonry and concrete walls, have a very high axial stiffness. Elements which may be subject to vertical amplification are the roof and Elevation 31'-0" diaphragm members, which were included in the substructure models but not in the global model for horizontal response. The global model was analyzed for horizontal earthquake motions only and a simpler model was used to obtain the vertical response time histories at each diaphragm elevation. These time histories were then added to the vertical components obtained from the horizontal analyses to give an input time history for later analysis of the detailed substructures.

Preliminary studies revealed that the vertical response of the global structure was essentially that of a single spring mass system. However to allow for possible rocking effects about the E-W axis, where the switchgear room springs introduce non-symmetry into the structure, a plane frame model of a section perpendicular to this axis was constructed. This model contained lumped representation of the mass and stiffness properties of the global structure and use of the planar model allowed the spatial distribution of the mass and springs to be included.

A representation of the model used for the vertical analyses is shown in Figure 5.1.

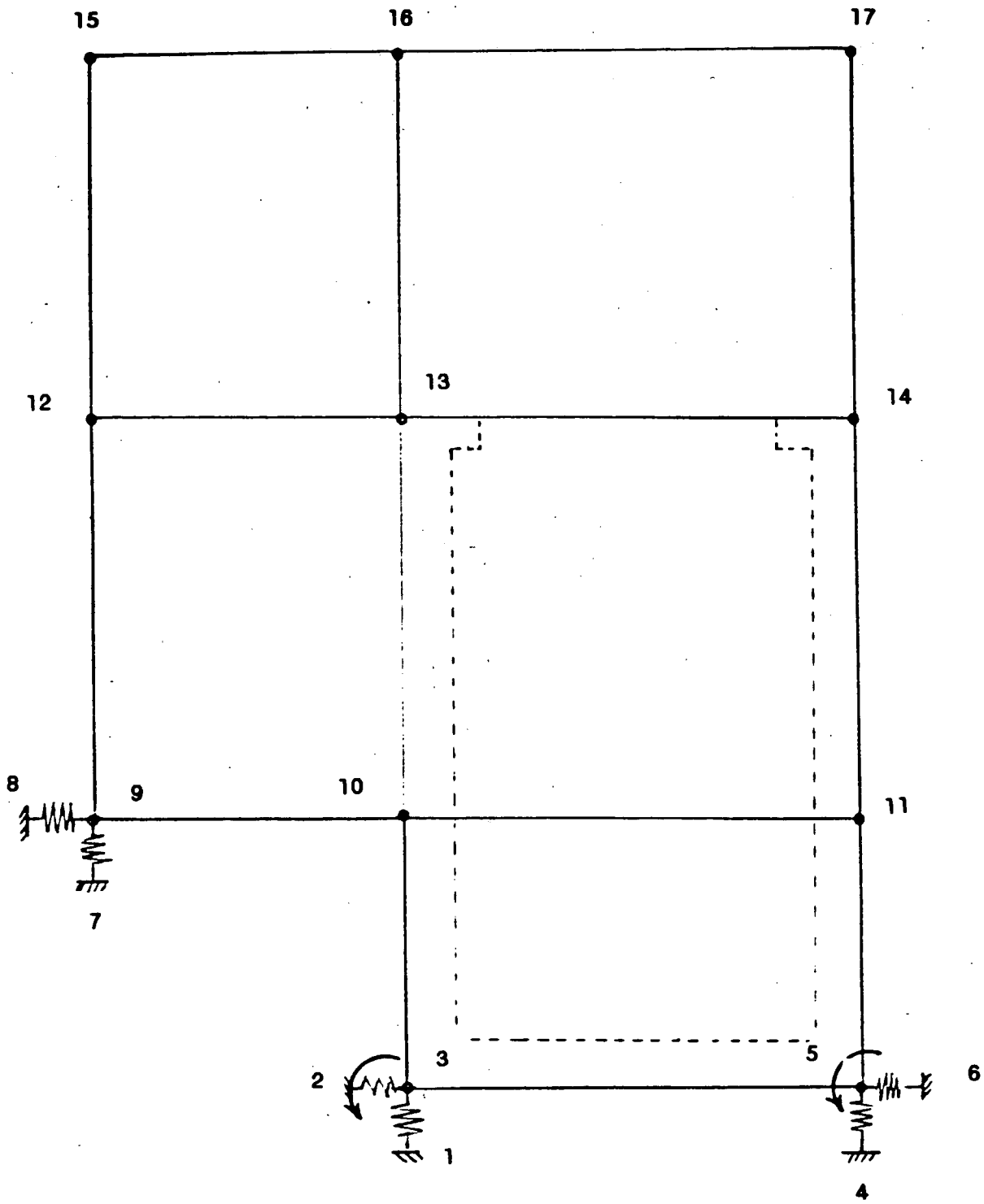

FIGURE 5.1 : VERTICAL MODEL

6 DESCRIPTION OF ANALYSES

Most of the analytical effort was devoted to the non-linear model in the as-modified condition. The linear model was used to aid in an understanding of the global model behavior and as an overall check on the order of magnitude results. The "as-built" model was used primarily to carry out initial runs and to identify areas where modifications were required to meet the re-evaluation criteria of Section 2.4. This model was then modified to reflect the ultimate state conditions to assess structural integrity. The vertical load model was used to provide vertical components of response to be added to those obtained from the global non-linear model.

In the following sections the analyses carried out on each of these models are briefly described.

6.1 Linear Model

The linear model was an exact duplicate of the non-linear model except for the non-linear elements, i.e. the in-plane and out-of-plane masonry walls. The main advantage of constructing this equivalent model was that it enabled the normal modes of the system to be extracted. While these frequencies and mode shapes were not used in the evaluation in themselves they contributed greatly to an understanding of the overall dynamic behavior of the structure. These frequencies were also used to obtain damping constants for the elements in the non-linear model.

Analyses carried out on this linear model were as follows:

a. Eigenanalysis of the entire structure with masonry elements in their original elastic state.

b. Eigenanalysis of the entire structure with masonry elements having an elastic stiffness equal to the stiffness in each wall at the end of the ANSR-II analyses, i.e. using the minimum equivalent stiffness.

c. A series of eigenanalyses for the superstructure alone with the masonry in-plane elements in various degraded conditions.

In the initial stages of the project consideration was given to the use of

this model for response spectrum analyses to obtain forces to check against the global model if this proved necessary. However the non-linear response of the global model did not produce any inconsistent results and the additional effort required to carry out a response spectrum analysis was not warranted, especially in view of the wide variation in composite modal damping caused by the soil spring damping values. This would have required the generation of a very large set of spectra for the range of damping values for each earthquake to obtain reasonable response.

6.2 Non-Linear Model - "As-Built"

The first analyses were carried out on the model of the structure in the "as-built" condition using the scaled El Centro 1940 earthquake. The model was then modified to reflect ultimate state conditions and a further analysis carried out. The modification to the model was mainly to the properties of the in-plane walls. The stiffness envelope for these walls was developed assuming that strain levels would be low. The first two runs revealed high strains in some in-plane walls and so the envelope was modified to correctly model the response up to these higher strain levels. Results were therefore obtained for each of the following load cases:

a. El Centro 1940, N-S applied in the N-S direction, with "original" in-plane element properties.

b. El Centro 1940, E-W appled in the N-S direction, with "original" in-plane element properties.

c. El Centro 1940 N-S modified to reduce conservatism with respect to the Housner spectrum. Element properties modified to reflect ultimate state conditions.

Note that in each of the runs above two orthogonal components of horizontal acceleration were applied simultaneously along each of the axes of the structure. The component listed is for the "principal" direction. The same scale factor as applied to the "principal" component to envelope the design spectrum was applied to the "lesser" component. The "principal" component is defined here as the earthquake component which was used to obtain the spectral intensity and thus the scaling factor relative to the 0.67g Housner spectrum, as listed below:

EARTHQUAKE		COMPONENT	EERL DESIGNATION	SCALING FACTOR
EL CENTRO	May 18, 1940	S00E	A001/S00E	1.57
TAFT	July 21, 1952	S69E	A004/S69E	2.90
OLYMPIA	April 13, 1949	N04W	B029/N04W	2.51

The first two analyses showed that the critical loading case was clearly when the major component was applied along the building N-S axis where
the lateral load resistance was a minimum. Therefore only this case was analyzed for the third case to assess structural integrity. For this third run the major change to the model was in the principal direction acceleration
time history and in the stiffness of the in-plane elements at high strain levels. The results were evaluated in terms of ultimate conditions, rather than for design limits as for the other analyses.

6.3 Non-Linear Model - As Modified

The initial two runs using the "as-built" model indicated that the in-plane shear strains in wall FB-7 were very high. The strains using the modified time history were below the level at which complete loss of load carrying capability would occur but failed to meet the re-evaluation criteria. At high strain levels this wall degraded and the consequent redistribution of lateral loads caused high diaphragm stresses in the roof. Therefore a conceptual modification was identified to enable this wall (and consequently the roof) to meet the criteria. This conceptual modification, which is shown in Figure 6.1, was incorporated in the analytical model.

This modified model was then analyzed under the complete suite of six earthquake loadings, each of 30 seconds duration, as listed below:

a. El Centro 1940 N-S applied along N-S axis.

b. El Centro 1940 E-W applied along N-S axis

c. Olympia 1949 N04W applied along N-S axis

d. Olympia 1949 N86E applied along N-S axis.

e. Taft 1952 S69E applied along N-S axis

f. Taft 1952 S21W applied along N-S axis.

As for the previous analyses two components, each scaled by the same fact were used for each analysis and applied simultaneously along each of the principal axes of the structure.

6.4 Vertical Load Model

The plane frame model for vertical acceleration response was analyzed for the vertical components for each of the three ground motions used in this evaluation, i.e.

a. El Centro, 1940

b. Olympia, 1949

c. Taft, 1952

Each of these records was scaled by the same factor as was derived such that the principal horizontal direction had equal spectral intensity to the Housner spectrum. This ensured consistency between the two models such that when the results were combined the response was obtained for the model responding to the three recorded components of the same earthquake each scaled by the same factor.

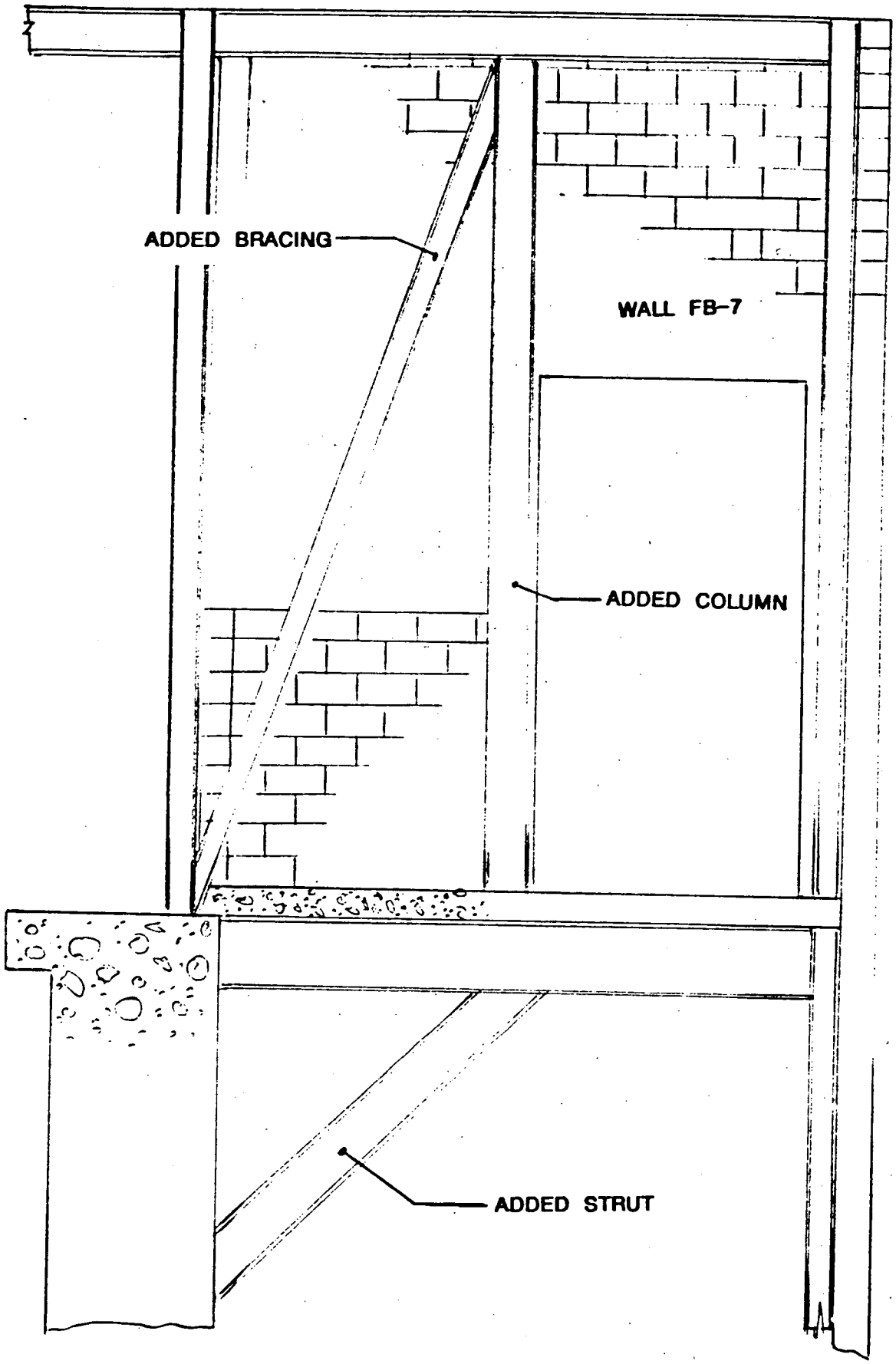

FIGURE 6.1 : CONCEPTUAL MODIFICATION TO WALL FB-7

7 RESULTS OF ANALYSES

In this section the results of the linear analyses, the "as-built" and as modified non-linear analyses and the vertical load analysis are presented. The most comprehensive series of analyses was the non-linear evaluation of the building in the as-modified condition.

The results presented in this section are used in Section 8 for the evaluation of the structure in the "as-built" condition and in Section 9 for the evaluation of the modified structure.

7.1 Linear Analyses

The linear analyses were used to obtain the normal modes of the structure both for the original stiffness and for the degraded condition. These modes provided data for the computation of the frequency dependent damping constants and also provided checks on the overall dynamic response of the structure.

The natural frequencies and participation factors obtained from these SAP-IV analyses are listed in Tables 7.1 and 7.2 for both the original stiffness and the degraded stiffness analyses.

7.2 Non-Linear Analyses - "As-Built"

The structure in the "as-built" condition was analyzed three times, using the scaled El Centro 1940 earthquake components with two different orientations and then using the El Centro record modified to reduce the conservatism relative to the Housner spectrum.

The first two analyses were of a testing nature in that they were used to verify assumptions about the degree of non-linearity and the frequency content of the response on which such parameters as damping constants and in-plane wall stiffness depended. The results of these analyses revealed high strain levels in one of the masonry walls, FB-7, and consequent overloading of portions of the roof diaphragm. This required modifications to the model and so consequent analyses considered the structure in two conditions:

1. As-Modified Structure: Steel strengthening members were added to the model at the location of wall FB-7. Results of the analyses for the structure in this condition are described in the following sub-section. The re-evaluation criteria which was used for this condition is stated in Section 2.4.

2. As-Built Structure with Ultimate State Conditions: Properties of the in-plane walls and damping constants were adjusted to reflect the level of response determined from the two preliminary analyses. The earthquake record was modified and evaluation was carried out in terms of assessing the structural integrity using the acceptance criteria in Section 2.5.

The earthquake record used for the structural integrity run is plotted in Figure 7.1 and the response spectrum of this record is compared with the Housner spectrum in Figure 7.2. This spectrum was computed in accordance with Section 7.1 of the Standard Review Plan (SRP). The results of critical elements are summarized in Section 8. The stress strain hysteresis for the most critical wall, FB-7, is reproduced in Figure 7.3.

7.3 Non-Linear Analyses - As Modified

Results for each of the six non-linear analyses are summarized in Appendices C to H. For each analysis tables of maximum displacements and the response of critical elements are provided. Time history plots are also reproduced in the Appendices for critical displacements and elements along with response spectra at the top of pool level to illustrate the filtering effect of the soil springs.

From these six sets of results absolute maximum quantities have been extracted, and these values are summarized in Tables 7.3 to 7.7. It should be noted that these values are envelope values from the set of records selected to envelope the 0.67g Housner response spectrum. The tables provide maximum values of the following:

a. Table 7.3 : Maximum Displacements. This table lists the maximum displacements at the building corners at the roof level, the top of pool (Elevation 42'-0") and the base of the pool.

Displacements are given for both horizontal directions.

b. Table 7.4 : Maximum In-Plane Wall Response. The maximum shear stresses and shear strains for each of the masonry walls are tabulated. The ratio of the maximum strain to the allowable strain as specified in the criteria is also listed.

c. Table 7.5 : Maximum Out-Of-Plane Wall Response. Maximum steel strain ratios, masonry stress and center displacement are listed for each of the vertically spanning masonry walls. These values are derived from the output plastic rotations as described in Appendix B.

d. Table 7.6 : Maximum Connection Forces : These values are the maximum shear and tensile forces at the interface between the masonry walls and the steel roof framing members and the concrete diaphragm at elevation 42'-0". For elevation 31'-0" diaphragm tension forces only are given as the diaphragm does not transfer shear stresses.

e. Table 7.7 : Maximum Diaphragm Forces : These forces are the maximum shear stresses in the roof diaphragm at the critical points adjacent to the masonry walls. Note that these values do not necessarily correspond to the connection forces in the previous table as not all the wall shears are transferred through the diaphragm.

Figure 7.4 is a plot of the envelope spectrum from the six time histories compared with the San Onofre, Unit 1 specified DBE earthquake load level of 0.67g ZPA on the Housner spectrum. These spectra are plotted for a damping ratio of 7%. Figures 7.5 to 7.10 show representative time histories for the most critical elements, as follows:

a. Figure 7.5 : Maximum roof displacement.

b. Figure 7.6 : Maximum displacement at the center of the out-of-plane wall with the greatest deflection.

c. Figure 7.7 : Hysteresis plot of the shear stress versus shear strain for wall FB-7.

d. Figure 7.8 : Shear modulus of wall FB-7 showing progressive degradation.

e. Figure 7.9 : Displacement plot of the top of the masonry wall adjacent to the roof opening on the East wall.

f. Figure 7.10 : Displacement plot of the top of the masonry wall adjacent to the roof opening on the South wall.

These results were used in the detailed component evaluation reported in Section 9. Where applicable, e.g. for the steel framing, the results from the analyses of the vertical load model were added to those from the horizontal analyses to obtain total force levels for the evaluations.

MODE	FREQUENCY (hertz)	PARTICIPATION FACTORS		
		X (E-W)	Y (N-S)	Z (VERT)
1	0.194	60.32	-0.00	-0.00
2	0.350	-0.00	35.70	-0.01
3	2.233	0.81	106.20	-3.32
4	2.535	-20.23	0.10	0.37
5	2.545	1.04	-0.19	-0.02
6	2.547	0.38	0.27	-0.04
7	2.547	-0.48	-0.42	0.00
8	2.726	0.87	66.42	-3.01
9	3.406	-43.61	1.53	3.11
10	3.668	-98.18	3.40	12.26
11	3.714	2.83	2.95	0.41
12	3.809	10.36	-0.50	-2.35
13	4.048	-1.29	0.20	1.75
14	4.265	-8.48	-4.52	-172.40
15	4.405	3.48	-0.05	5.03
16	5.418	-0.12	1.13	0.65
17	6.331	1.45	6.36	-2.86
18	6.576	0.04	0.17	9.78
19	6.812	-7.55	-24.67	10.12
20	8.436	-10.08	1.88	4.77
21	9.635	6.67	0.08	7.62
22	9.642	102.40	1.29	4.32
23	9.908	-63.17	-2.29	7.40
24	10.840	-0.64	107.00	-0.50
25	10.950	-5.82	35.18	0.19
26	11.620	-0.62	-3.62	-0.11
27	11.710	-4.76	-7.79	-1.84
28	11.810	-3.09	0.68	-0.19
29	12.220	-2.58	0.29	-0.19
30	12.940	2.46	-4.06	-2.56
31	13.040	0.81	5.76	2.01
32	13.970	-0.39	0.20	1.39
33	14.460	0.36	-0.31	0.00
34	14.790	-0.81	-5.18	-0.13
35	15.740	-1.27	-0.92	-1.11
36	16.520	0.26	1.38	0.19
37	16.690	-0.76	0.78	-0.33
38	17.660	-0.22	0.24	0.35
39	17.850	0.19	-0.14	-0.32
40	19.090	-0.14	0.29	-0.15

TABLE 7.1 : FREQUENCIES "AS-MODIFIED" - ORIGINAL STIFFNESS

MODE	FREQUENCY (hertz)	PARTICIPATION FACTORS		
		X (E-W)	Y (N-S)	Z (VERT)
1	0.194	60.32	-0.00	-0.00
2	0.350	-0.00	35.72	-0.01
3	2.205	0.75	108.00	-2.32
4	2.534	20.35	-0.06	-0.36
5	2.545	-1.04	0.24	0.04
6	2.547	-0.41	-0.33	0.05
7	2.547	0.47	0.49	-0.01
8	2.715	-0.81	-63.05	2.01
9	3.404	-44.98	1.36	3.33
10	3.659	97.60	-3.35	-11.97
11	3.714	2.39	3.14	0.24
12	3.809	9.45	-0.47	-2.21
13	4.048	-1.16	0.19	1.74
14	4.254	-8.37	-3.24	-172.40
15	4.405	-3.40	0.31	-3.58
16	5.418	-0.15	0.96	0.67
17	6.258	-7.45	-22.09	9.23
18	6.330	-3.88	-8.72	2.75
19	6.576	-0.00	-0.04	-9.82
20	7.537	6.84	-3.95	-7.20
21	8.902	0.30	0.84	3.41
22	9.206	36.81	-1.56	9.52
23	9.635	0.49	0.01	7.32
24	9.755	-114.80	-3.37	2.98
25	10.560	0.23	-41.16	1.12
26	10.580	9.01	-11.28	1.18
27	10.870	0.07	98.60	0.57
28	11.000	-4.76	36.74	-0.36
29	11.620	0.20	2.99	-0.05
30	11.810	3.21	-1.17	0.08
31	12.210	2.37	-1.11	-0.01
32	12.310	-2.33	-3.14	-0.42
33	13.210	-0.14	-1.91	-0.09
34	13.600	0.17	-1.16	0.68
35	14.240	-1.36	-4.39	-2.56
36	14.460	0.36	-0.23	0.03
37	14.960	0.18	3.91	-0.87
38	15.610	-0.22	-0.38	-0.17
39	16.950	0.10	-0.98	-0.34
40	17.010	-0.14	0.50	0.10

TABLE 7.2 : FREQUENCIES "AS-MODIFIED" - FINAL STIFFNESS

LOCATION	DISPLACEMENT (Inches)	
	X (E-W)	Y (N-S)
ROOF		
N-W Corner	0.502	1.433
S-W Corner	0.602	1.408
N-E Corner	0.533	1.537
S-E Corner	0.537	1.525
TOP OF FUEL POOL		
N-W Corner	0.311	0.846
S-W Corner	0.328	0.850
N-E Corner	0.311	0.905
S-E Corner	0.326	0.905
BASE OF FUEL POOL		
N-W Corner	0.098	0.075
S-W Corner	0.102	0.075
N-E Corner	0.098	0.118
S-E Corner	0.102	0.117

NOTES:

1. Values are absolute maxima from all earthquake records.

2. These results are from the "as-modified" non-linear analysis.

TABLE 7.3: MAXIMUM DISPLACEMENTS

WALL NUMBER	SHEAR STRESS (p.s.i)	SHEAR STRAIN	RATIO OF MAXIMUM STRAIN TO ALLOWABLE
FB-1	42.4	0.00030	0.114
FB-2	116.6	0.00116	0.439
FB-3	69.6	0.00049	0.186
FB-4	71.3	0.00051	0.193
FB-5	50.9	0.00036	0.136
FB-6	55.4	0.00039	0.148
FB-7	178.4	0.00478	0.905
FB-8	132.4	0.00159	0.602
FB-9	157.1	0.00237	0.898
FB-10	104.9	0.00092	0.349

NOTES:

1. Values are absolute maxima from all earthquake records.

2. These results are from the "as-modified" non-linear analysis.

3. Maximum allowable strain for unbraced walls (all except FB-7) is 0.00264.

4. Maximum allowable strain for braced walls (FB-7) is 0.00528

5. Masonry wall identification is as given in Figure 1.4.

TABLE 7.4: MAXIMUM IN-PLANE WALL RESPONSE

WALL	STEEL STRAIN RATIO		MASONRY STRESS	CENTER DISPLACEMENT
	CENTER	END	fm (p.s.i.)	(inches)
FB-1	21.0	24.6	656	10.56
FB-2	12.7	15.9	656	6.62
FB-3	15.5	15.9	656	8.11
FB-4			Horizontal	Spanning
FB-5	16.8	16.8	656	7.46
FB-6	23.0	26.4	656	11.19
FB-7			Horizontal	Spanning
FB-8	1.2	0.6	656	0.98
FB-9	1.3	0.6	656	0.97
FB-10	1.5	0.9	656	1.34

NOTES:

1. Values are absolute maxima from all earthquake records.
2. These results are from the "as-modified" non-linear analysis.
3. Maximum allowable steel strain ratio is 45.
4. Maximum allowable masonry compressive stress is 1147 psi.
5. Masonry wall identification is as given in Figure 1.4.

TABLE 7.5: MAXIMUM OUT-OF-PLANE WALL RESPONSE

WALL NUMBER	LOCATION	SHEAR STRESS (lb/ft)	TENSION (lb/ft)	RATIO OF MAXIMUM/ALLOWABLE
FB-1	Roof	707.1	257.9	0.47
FB-2	Roof	1045.2	233.8	0.82
FB-3	Roof	355.0	113.6	0.14
FB-4	Roof	378.4	-	0.31
FB-5	Roof	714.2	227.2	0.46
FB-6	Roof	1447.9	214.7	1.35
FB-7	Roof	1831.0	-	1.48
FB-8	El 42'-0"	2929.2	656.7	0.48
FB-9	El 42'-0"	1046.1	159.2	0.08
FB-10	El 42'-0"	2127.0	697.6	0.30
FB-8	El 31'-0"	-	711.2	0.57
FB-9	El 31'-0"	-	619.2	0.50
FB-10	El 31'-0"	-	1059.6	0.86

NOTES:

1. Values are absolute maxima from all earthquake records.
2. These results are from the "as-modified" non-linear analysis.
3. See Section 9.5 for derivation of maximum allowable values.
4. Masonry wall identification is as given in Figure 1.4.

TABLE 7.6: MAXIMUM CONNECTION FORCES

WALL NUMBER	LOCATION	SHEAR STRESS (lb/ft)	RATIO OF MAXIMUM/ALLOWABLE
FB-1	Roof	1113.3	0.37
FB-2	Roof	1581.1	0.53
FB-3	Roof	848.0	0.29
FB-4	Roof	955.8	0.32
FB-5	Roof	1017.9	0.34
FB-6	Roof	2687.7	0.91
FB-7	Roof	2687.7	0.91
FB-8	El 42'-0"	4272.5	0.42
FB-9	El 42'-0"	4900.0	0.48
FB-10	El 42'-0"	2826.4	0.28

NOTES:

1. Values are absolute maxima from all earthquake records.
2. These results are from the "as-modified" non-linear analysis.
3. Maximum allowable shear in metal decking at roof level is 2962.5 lb/ft.
4. Maximum allowable shear in concrete slab at Elevation 42'-0" is 10251 lb/ft.
5. Values are peak stresses in diaphragms, not average values.
6. Masonry wall identification is as given in Figure 1.4.

TABLE 7.7: MAXIMUM DIAPHRAGM FORCES

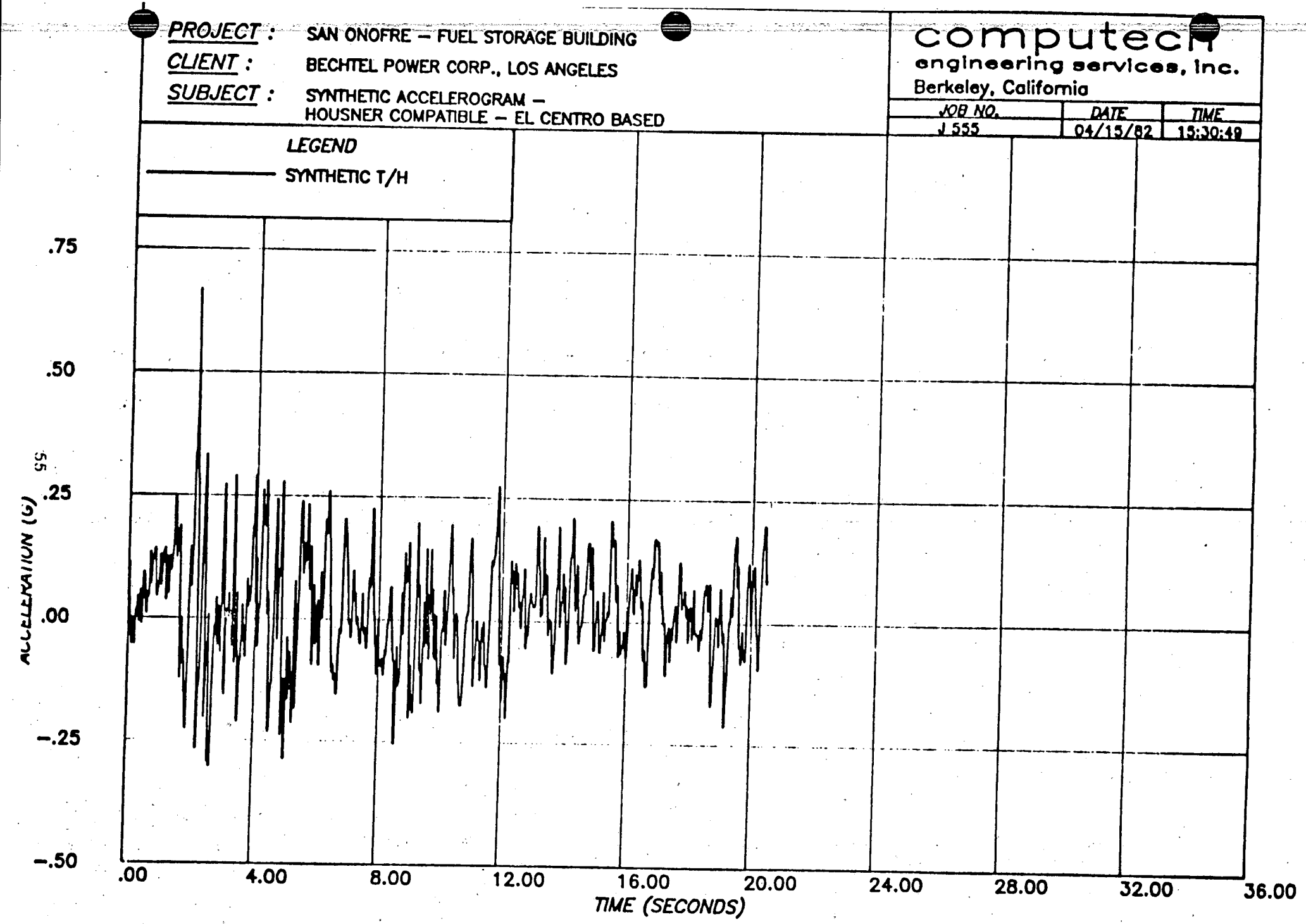

FIGURE 7.1 : TIME HISTORY FOR "AS-BUILT" ANALYSIS

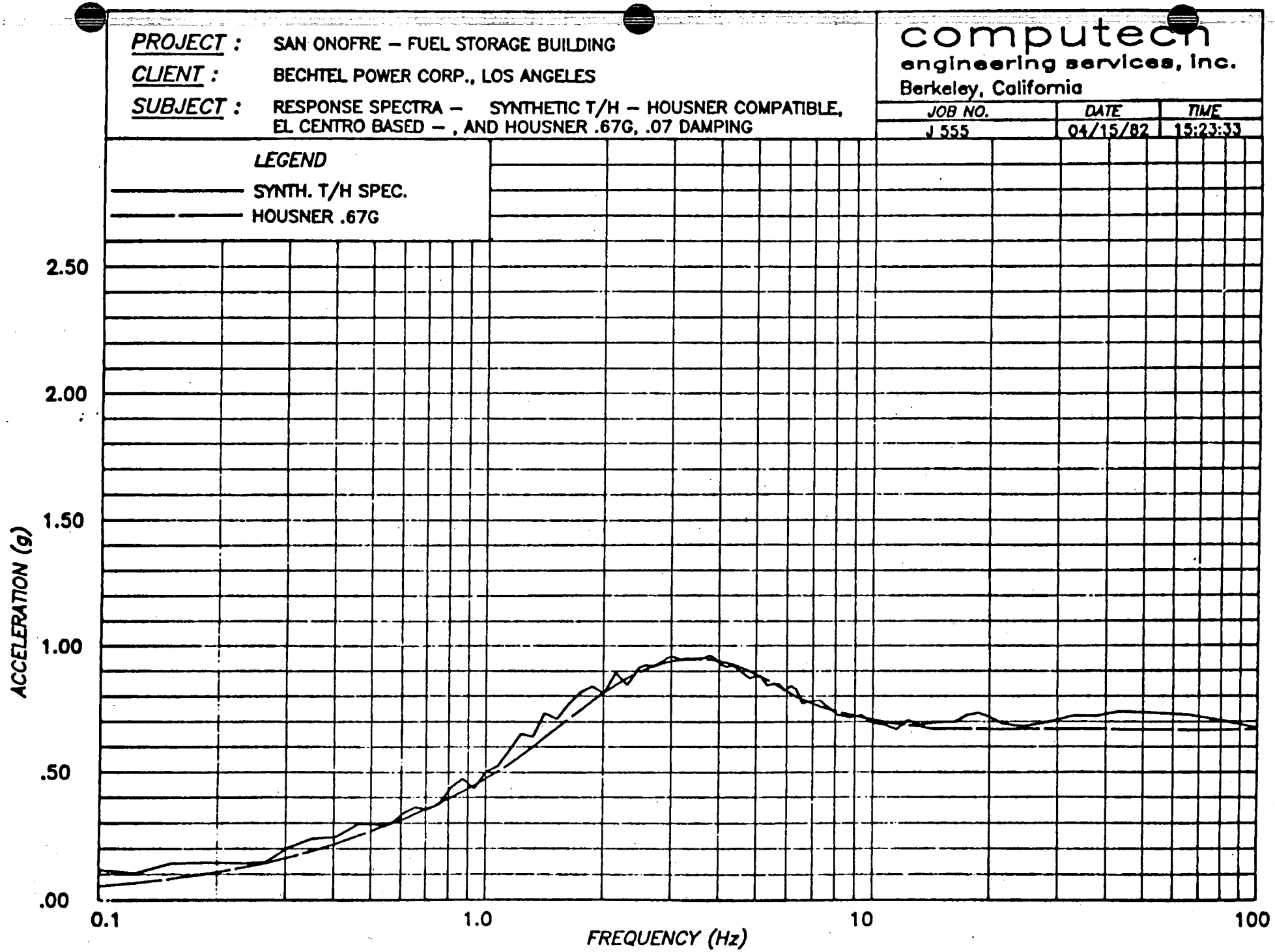

FIGURE 7.2 : RESPONSE SPECTRUM FOR "AS-BUILT" ANALYSIS

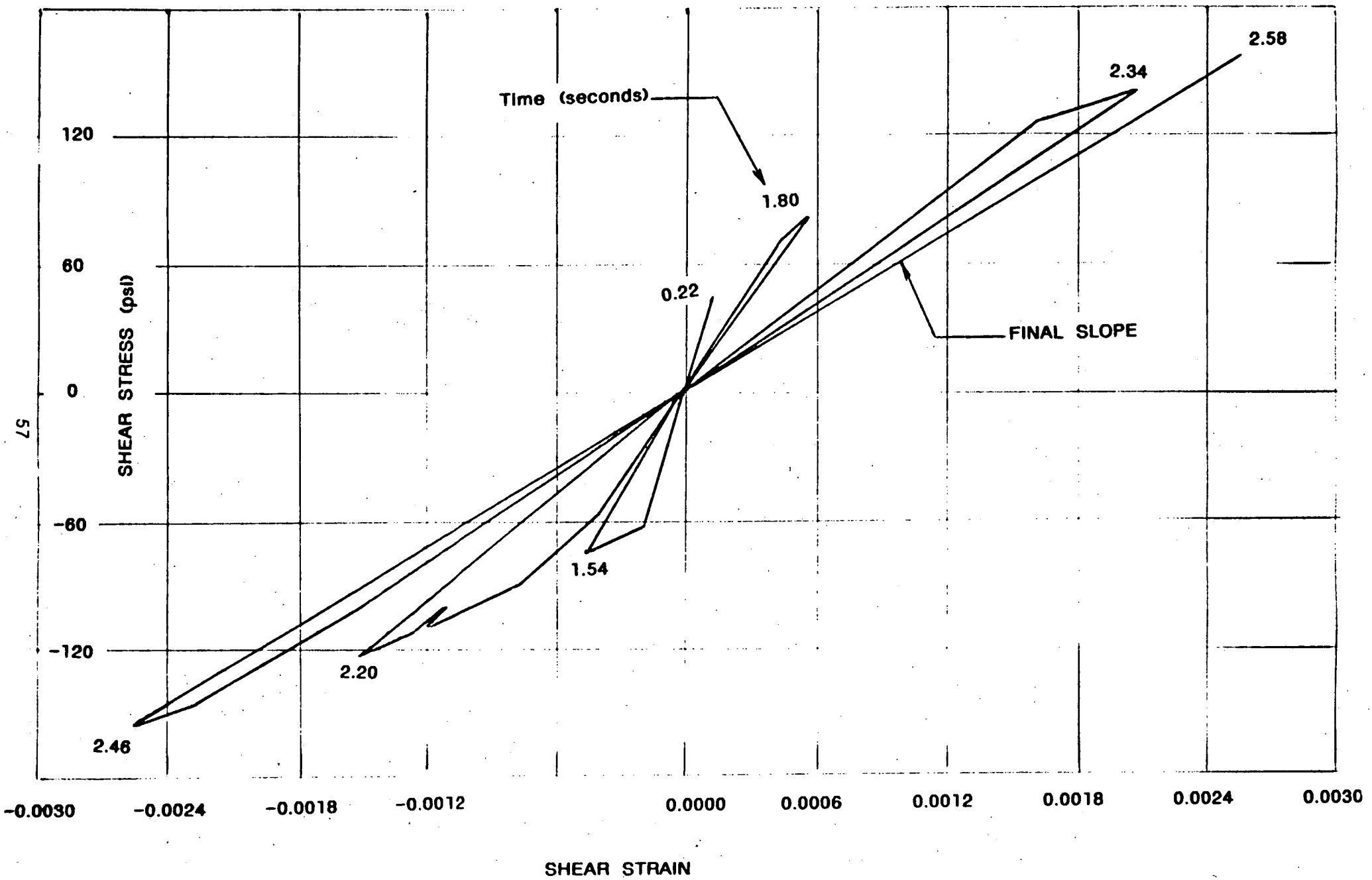

FIGURE 7.3 : STRESS-STRAIN HISTORY OF WALL FB-7 ("AS-BUILT" ANALYSIS)

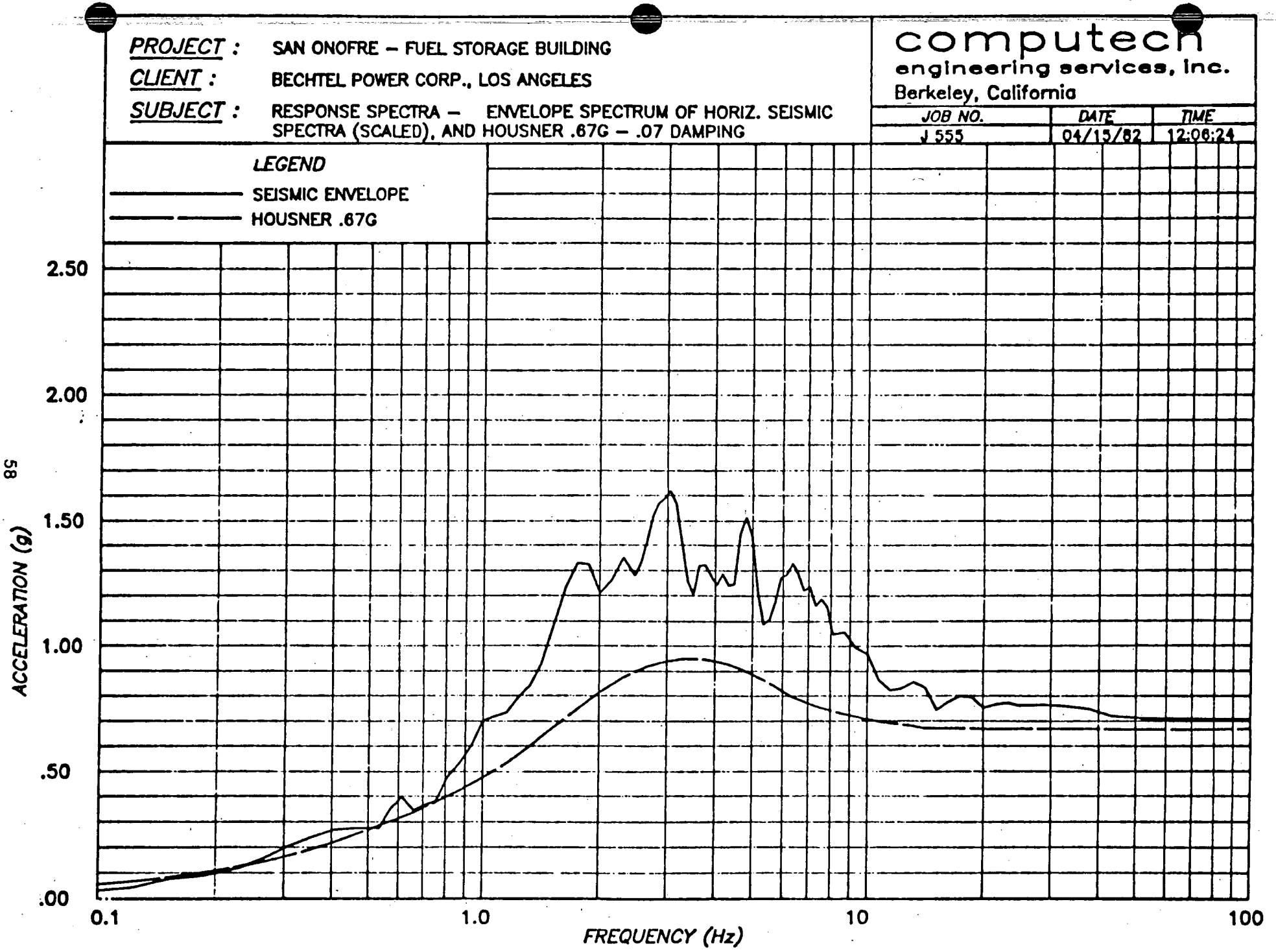

FIGURE 7.4 : ENVELOPE SPECTRUM – "AS-MODIFIED" ANALYSIS

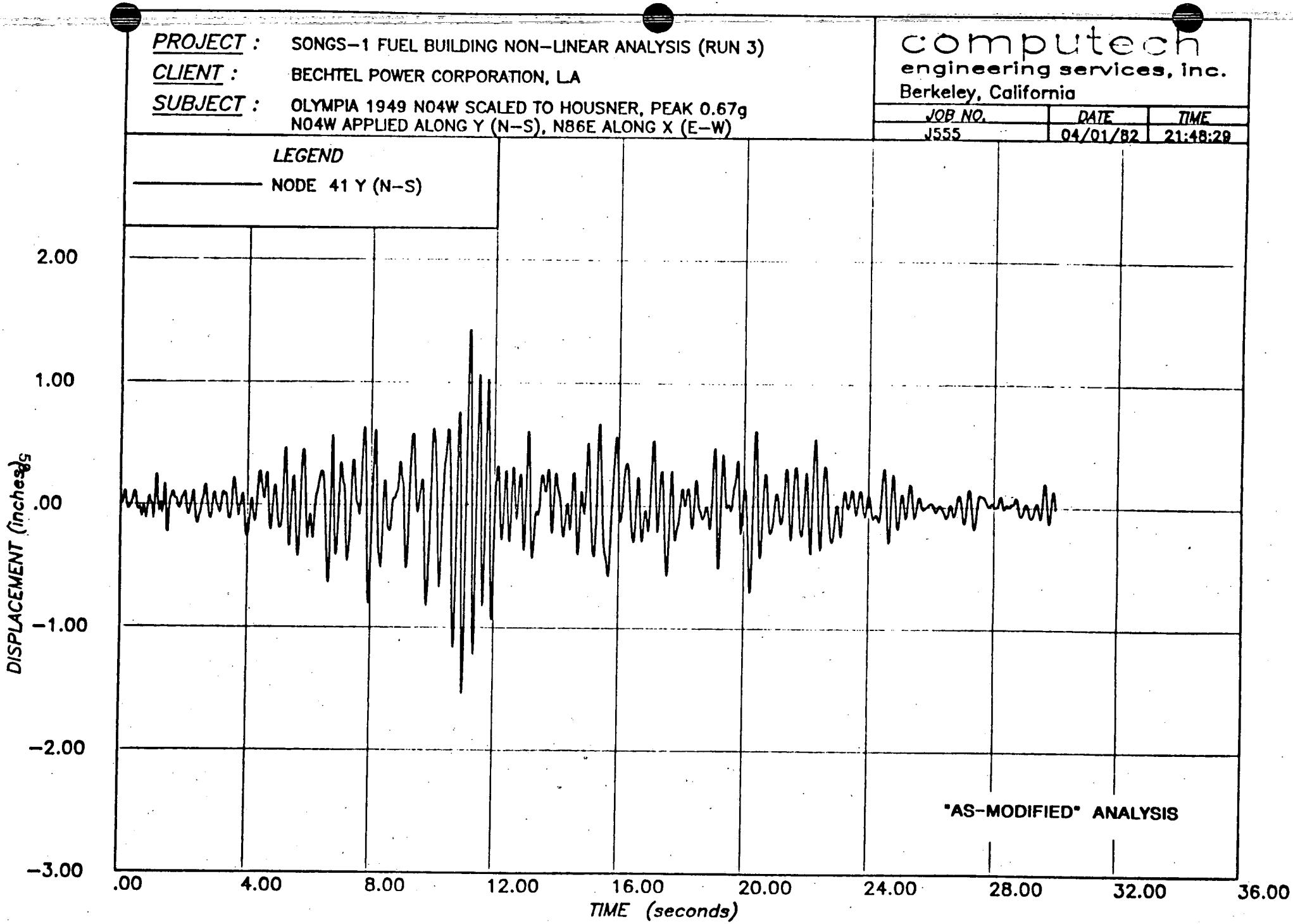

FIGURE 7.5 : MAXIMUM ROOF DISPLACEMENT TIME HISTORY

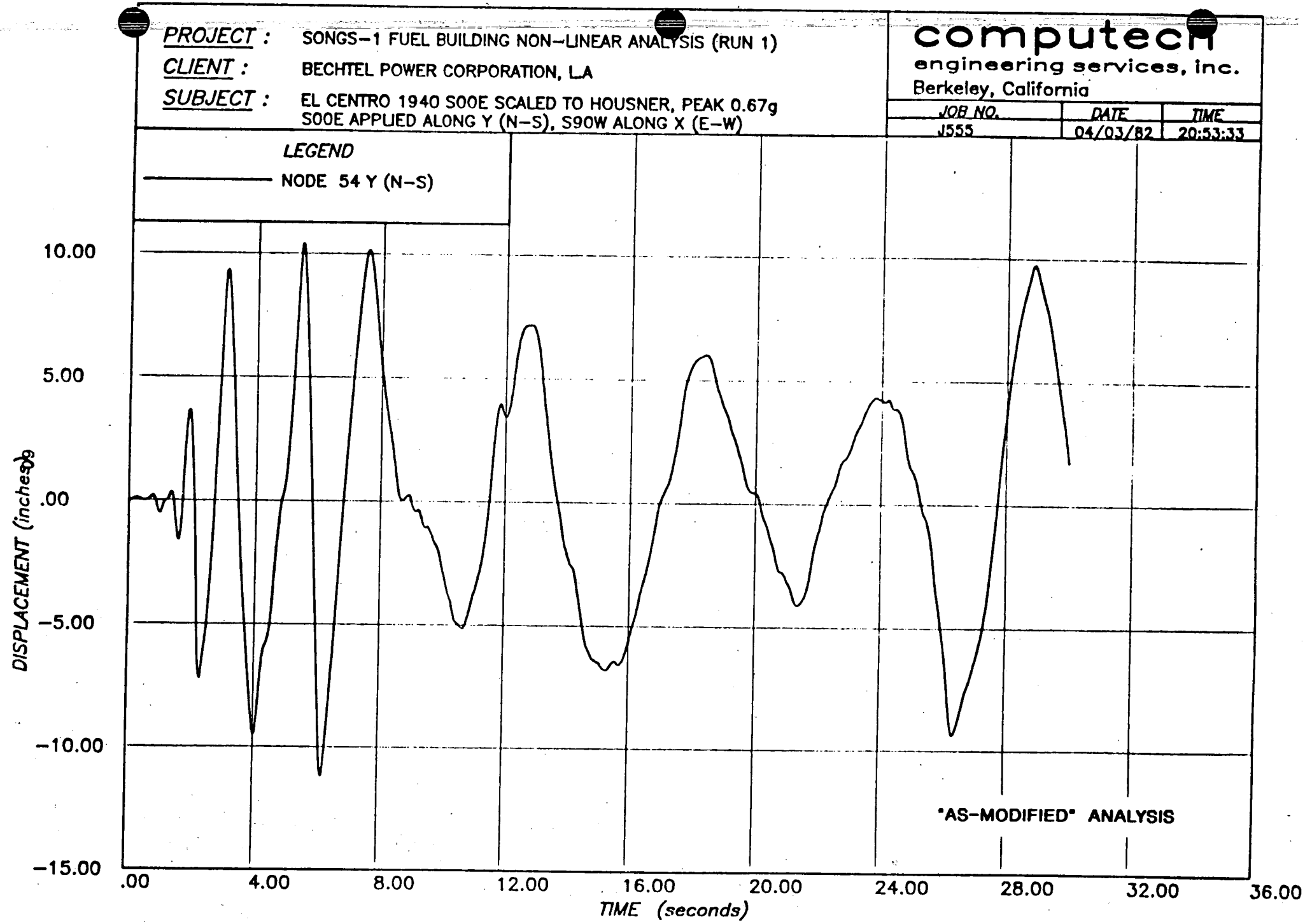

FIGURE 7.6 : MAXIMUM OUT-OF-PLANE MASONRY WALL DISPLACEMENT

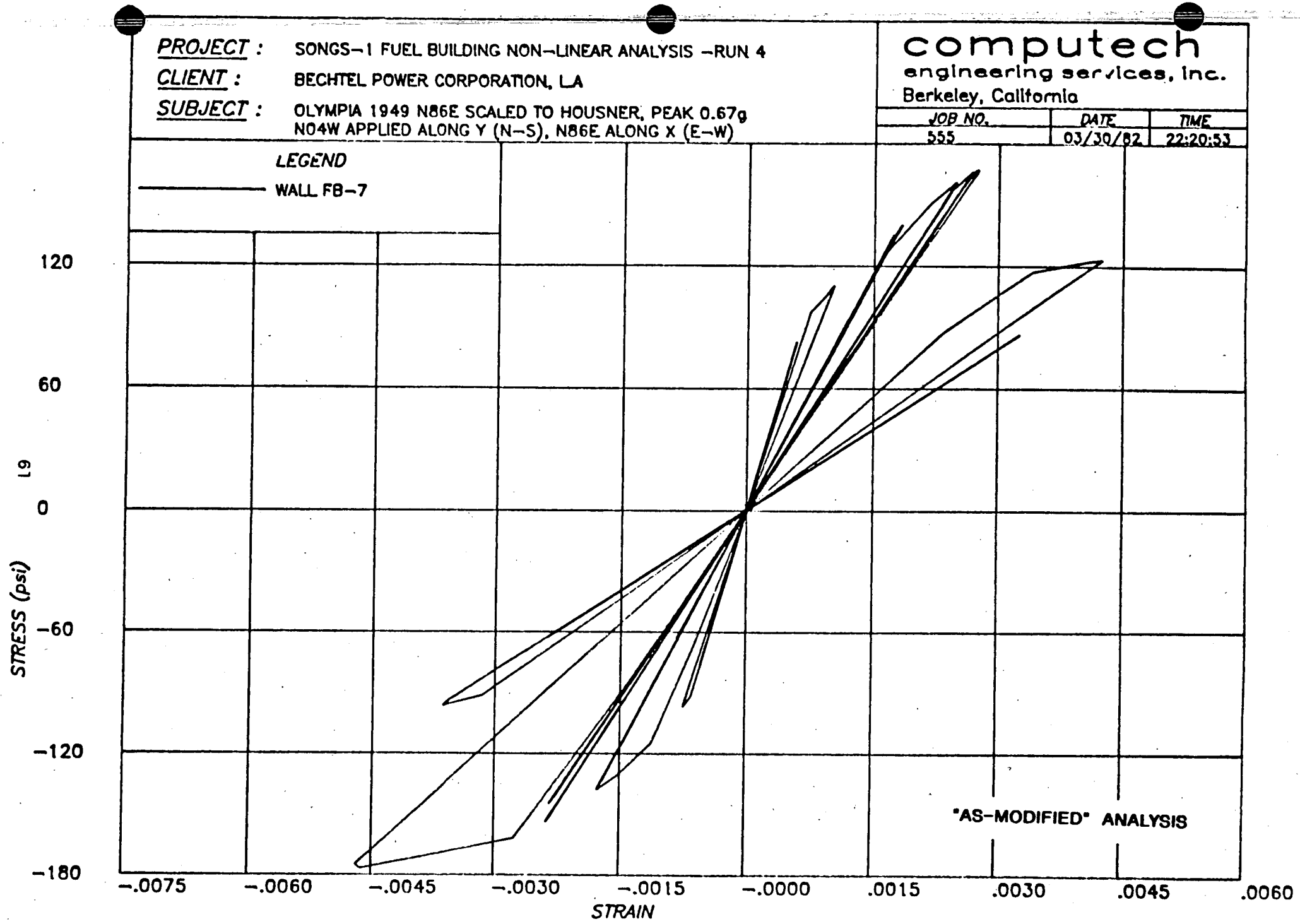

FIGURE 7.7 : MAXIMUM IN-PLANE MASONRY WALL STRESS-STRAIN

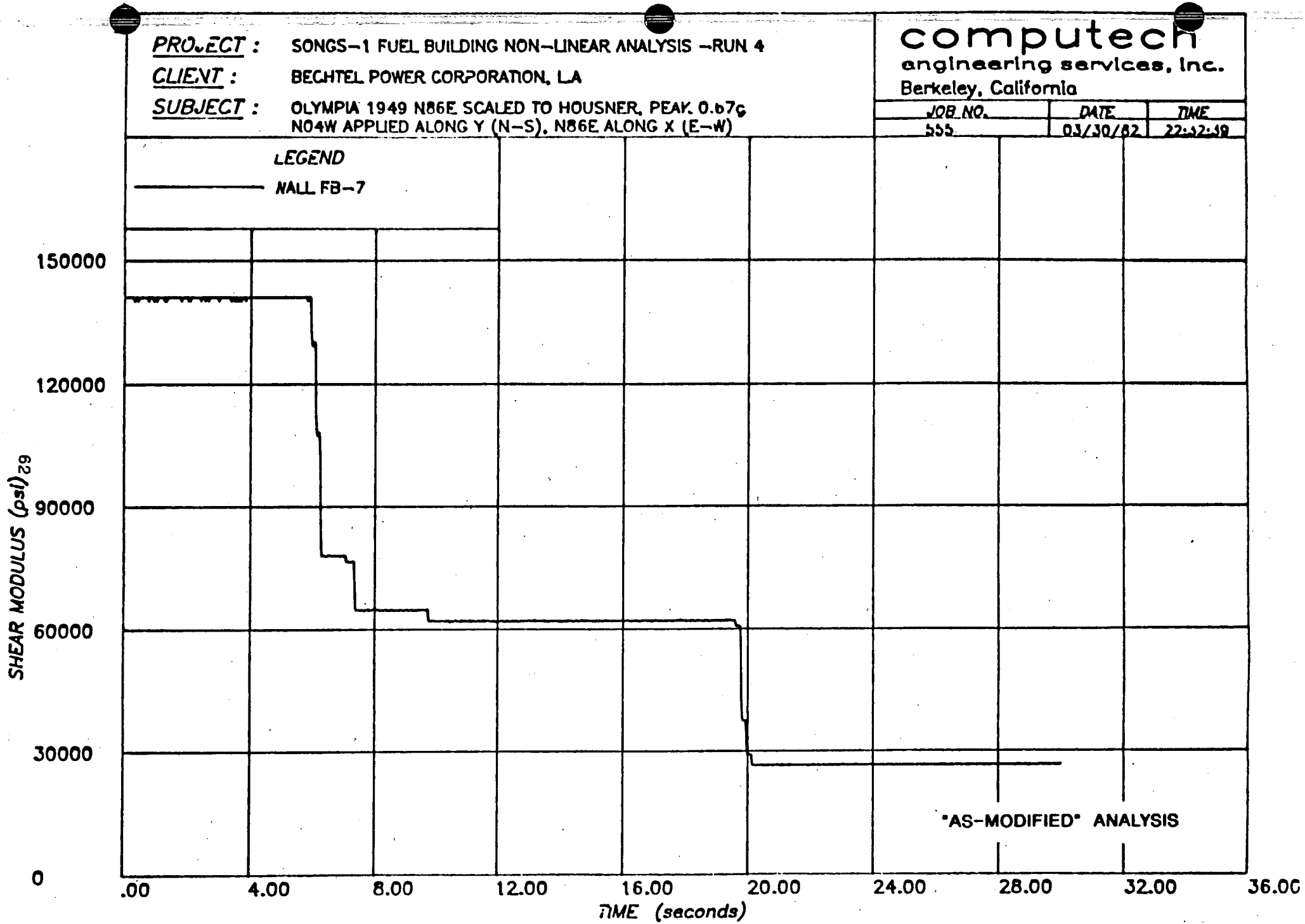

FIGURE 7.8 : MAXIMUM IN-PLANE WALL STIFFNESS DEGRADATION

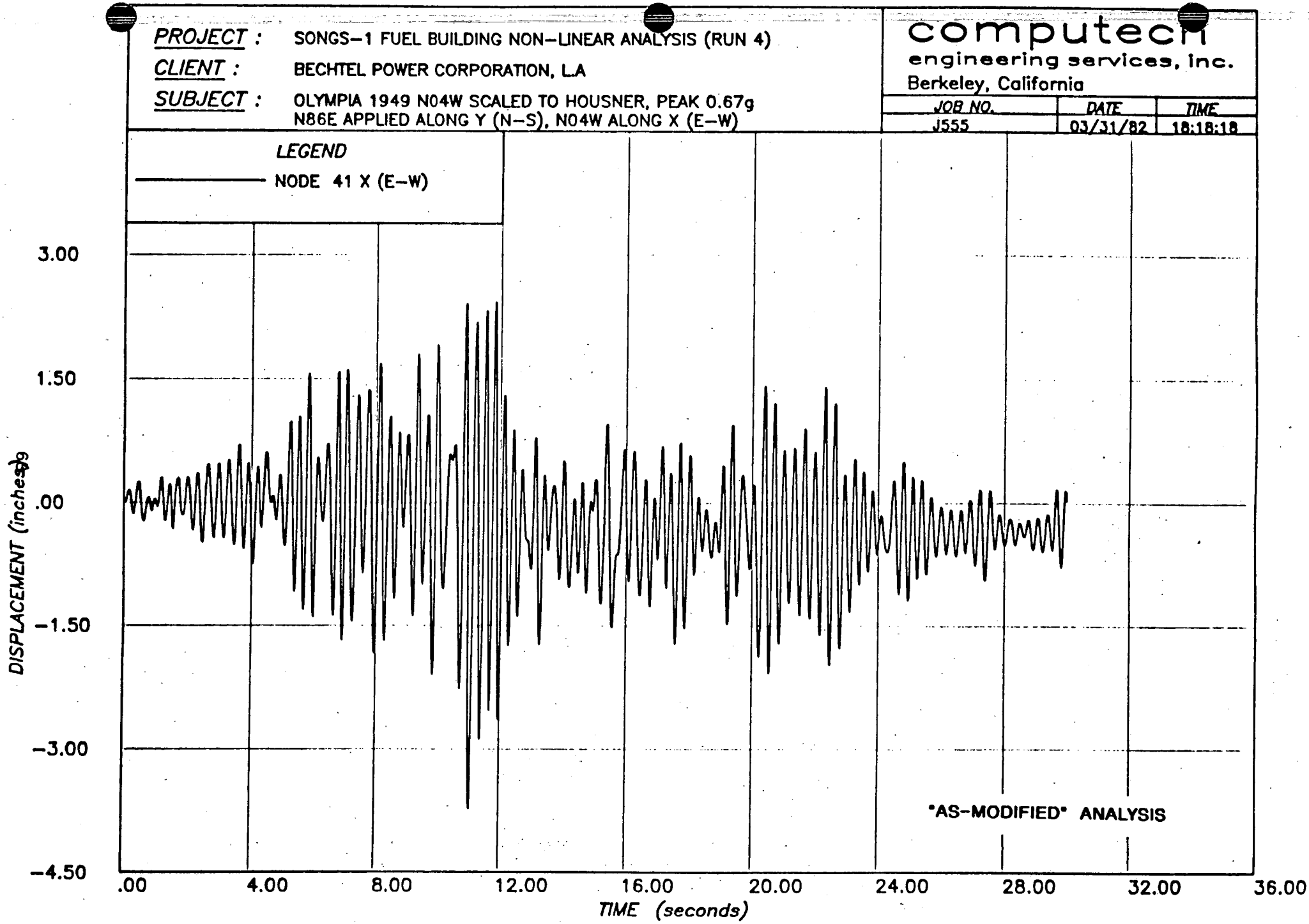

FIGURE 7.9 : MAXIMUM WALL DISPLACEMENT AT ROOF OPENING (E-W)

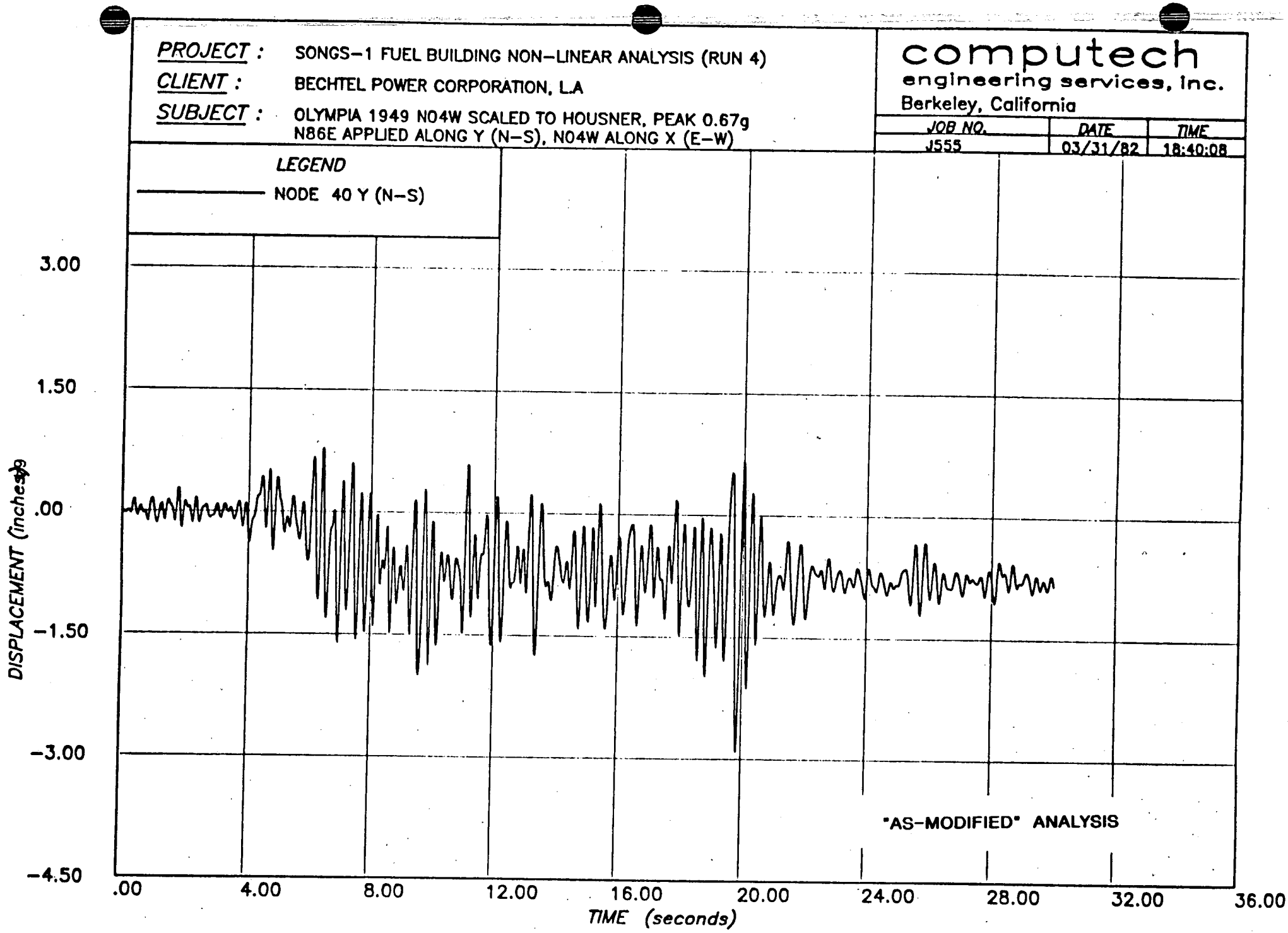

FIGURE 7.10 : MAXIMUM WALL DISPLACEMENT AT ROOF OPENING (N-S)

8 EVALUATION OF "AS-BUILT" STRUCTURE

The evaluation of the "as-built" structure was limited in scope as its purpose was solely to assess the structural integrity of the structure during the limited interval of time until the modifications are incorporated into the structure to restore design margins. The criteria used for this evaluation are stated in Section 2.5.

This assessment was carried out using limit state conditions. The diaphragm was assessed based on an ultimate strength factor of 3.0, the minimum safety margin determined from test results. For the in-plane walls damping constants were based on the degraded modulus of the strain envelope and the slopes were adjusted to reflect test curves up to the ultimate strain limit for unbraced walls of 0.00264. For connections recent test results have indicated that the UBC tables of allowable stresses on bolts are very conservative especially for shear forces and so higher stress limits were used.

The main difference between the "as-built" and "as-modified" structure is the presence of steel strengthening members in the latter case. These elements have an impact only on the superstructure and do not effect the overall pool response. Therefore the evaluation of the "as-built" structure was restricted to this location. The out-of-plane wall response is similarly unaffected by the presence of the strengthening and so these elements were not evaluated at this stage. Based on these considerations the evaluation considered only the maximum in-plane strains in the masonry walls at the superstructure level, the maximum shear stresses in the diaphragms and the connection forces. Each of these components is considered in the following sub-sections.

8.1 Superstructure Walls

The maximum shear stresses and shear strains in the superstructure walls FB-1 to FB-7 are listed in Table 8.1. The maximum shear strain for all these load carrying walls from the criteria is 0.00264 and the ratio of maximum strain to this value is also listed in Table 8.1.

Strain levels were moderate in all walls except FB-7 which had a value of greater than 97% of the criteria limit. This wall is relatively short and carries a disproportionate amount of the total lateral load due to the discontinuity of the diaphragm caused by the roof opening. The remaining

walls resisting the North-South lateral loads, FB-2 and FB-3 had strains less than 20% of the allowable value.

The walls resisting East-West lateral loads are much longer than those in the North-South direction and this is reflected in the maximum stresses and strains in walls FB-1, FB-4, FB-5 and FB-6 all of which have in-plane strains less than 10% of the allowable value.

8.2 Connection Forces

The maximum forces on the connections between the masonry walls and the roof diaphragm are listed in Table 8.2. The shear component arises from in-plane wall response and the tension from the out-of-plane wall bending. The ratio of maximum to allowable in Table 8.2 has been computed using the interaction formula given in Section 9.5 of this Volume. Because the ultimate strength is being assessed the capacity of the embedded bolts was computed using 3 times the UBC values in shear and 2 times the UBC values in tension, based on the results of research currently being undertaken at Clemson University which has shown the UBC values to be very conservative, especially in shear.

These ultimate factors produce allowable shear of 2475 lb/ft and allowable tension of 1650 lb/ft. Using the interaction formula of section 9.5 the ratio of maximum to allowable is in all cases less than 0.60, and all but two walls have loads less than 50% of the ultimate value.

8.3 Diaphragm Stresses

The maximum shear stresses in the roof diaphragm are listed in Table 8.3 together with the ratio of this maximum stress to the ultimate stress. The ultimate stress is taken as three times the working stress value as the manufacturer's test results have all produced a minimum factor of safety of three on these allowable stresses.

The maximum stresses are very close to this ultimate limit, with walls FB-1 and FB-3 each having peak stresses at 95% of this value. Note that the listed values are the maximum values occurrring in any element along the wall. If an average value along the wall were taken the stress would be

considerably lower. Deformations at the ultimate limit would be sufficient to redistribute load along the entire length of the wall and at this stage of loading an average value would be less than the results shown in Table 8.3.

WALL NUMBER	SHEAR STRESS (p.s.i)	SHEAR STRAIN	RATIO OF MAXIMUM STRAIN TO ALLOWABLE
FB-1	25.2	0.00007	0.026
FB-2	76.4	0.00046	0.174
FB-3	74.5	0.00042	0.159
FB-4	67.2	0.00026	0.099
FB-5	34.0	0.00010	0.038
FB-6	31.8	0.00009	0.034
FB-7	156.3	0.00257	0.974

NOTES:

1. Values are absolute maxima from modified El Centro record.

2. Maximum allowable strain for all walls is 0.00264.

3. These results are for the "as-built" structure.

4. Masonry wall identification is as given in Figure 1.4.

TABLE 8.1: MAXIMUM IN-PLANE WALL RESPONSE

WALL NUMBER	LOCATION	SHEAR STRESS (lb/ft)	TENSION (lb/ft)	RATIO OF MAXIMUM/ALLOWABLE
FB-1	Roof	1601	258	0.53
FB-2	Roof	1636	224	0.54
FB-3	Roof	1412	113	0.40
FB-4	Roof	121	-	0.05
FB-5	Roof	693	226	0.16
FB-6	Roof	895	215	0.22
FB-7	Roof	824	-	0.33

NOTES:

1. Values are absolute maxima from modified El Centro record.
2. See Section 8.2 for derivation of maximum allowable values.
3. These results are for the "as-built" structure.
4. Masonry wall identification is as given in Figure 1.4.
5. The ratio of maximum to allowable is computed according to the interaction formula given in Section 9.5.

TABLE 8.2: MAXIMUM CONNECTION FORCES

WALL NUMBER	LOCATION	SHEAR STRESS (lb/ft)	RATIO OF MAXIMUM/ALLOWABLE
FB-1	Roof	3373	0.95
FB-2	Roof	2019	0.57
FB-3	Roof	3373	0.95
FB-4	Roof	613	0.17
FB-5	Roof	1197	0.34
FB-6	Roof	2019	0.57
FB-7	Roof	1782	0.50

NOTES:

1. Values are absolute maxima from modified El Centro record.

2. Maximum untimate shear in metal decking at roof level is 3555 lb/ft.

3. Values are peak stresses in diaphragms, not average values.

4. These results are for the "as-built" structure.

5. Masonry wall identification is as given in Figure 1.4.

TABLE 8.3: MAXIMUM DIAPHRAGM FORCES

9 EVALUATION OF "AS-MODIFIED" STRUCTURE

The as-modified structure was evaluated in terms of the original design margins, with allowable stresses based on ultimate strength design procedures and masonry strains based on servicability limits.

The individual components of the structure were evaluated in terms of the criteria adopted for the project. For the concrete and steel structures the acceptance criteria were based on the appropriate sections of the BOPSSR criteria [1]. For the non-linear masonry walls the re-evaluation acceptance criteria are as stated in Section 2.4.

In the following sections each of the major element groups of the structure are listed together with mention of the criteria used and the results of the evaluation. These evaluations are based on the results presented in Section 7.3 plus vertical load effects where applicable.

9.1 Fuel Pool

The fuel pool comprises reinforced concrete walls and base slab. The pool elements remain elastic throughout all the analyses and were evaluated using ultimate strength design procedures for reinforced concrete as detailed in the ACI-318 code [5].

The design load combinations for the pool were horizontal and vertical earthquake loads plus the dead load of the water. The earthquake loads in the horizontal direction were obtained from the results of the time history analyses on the as-modified structure. This model included the effects of the hydrodynamic loadings caused by the water. To these forces were added the loads caused by the dead load of the water amplified by the vertical accelerations.

The loads were applied to substructure models of the fuel pool walls modelled as assemblages of plate bending elements. Output shear forces and bending moments were then checked against ultimate strength values computed from the section geometry and reinforcing layout. These results are tabulated in Tables 9.1 and 9.2.

For each wall the maximum moment from the analysis was first checked

against the cracking moment of the concrete section. If the moment exceeded this value it was checked against the ultimate moment capacity. For all walls except that on the North side. Table 8.1 shows that the maximum moment was less than the cracking moment. In the North wall the moment exceeded the cracking level but was less than the ultimate moment capacity.

The maximum shear stresses in each wall are as tabulated in Table 9.2. To check the shear the capacity of the concrete alone was first evaluated. In all walls this capacity was greater than the applied shears by considerable margins. Therefore any contribution from the steel reinforcing to the shear strength was neglected. The steel pool liner is non-structural and sufficiently flexible to conform to the deformed shape of the massive concrete walls. Therefore as the concrete is within the allowable stress limits the pool integrity is maintained.

9.2 Diaphragms

The Fuel Building diaphragms occur at the roof level and at elevation 42'-0" with a partial diaphragm at Elevation 31'-0". The steel framing elements occuring in each of these levels are considered separately in Section 9.4. In this section the steel decking and concrete slab are evaluated.

9.2.1 Roof Level

Table 7.7 lists the maximum steel deck stresses and the ratio of shear force to allowable shear force. The allowable force is based on the working stress shear factored by 2.5 for ultimate strength conditions as recommended by the manufacturer. This allows a factor of safety as the allowable stresses are based on one third the minimum test ultimate capacity.

This factor produced an allowable shear load of 2962.5 lb/ft. Using this value the maximum ratio computed in the diaphragm was 91% of the allowable. These ratios were computed based on the peak stresses in the elements modelling the diaphragm rather than the average values along the length of the wall.

9.2.2 Elevation 42'-0"

The concrete diaphragm shear forces from horizontal loadings are tabulated in Table 7.7 together with the ratio of maximum stress to ultimate strength. The latter values were computed using the ACI-318 ultimate strength procedures based on an allowable concrete shear stress of 134 psi. The maximum shear stress was 48% of the allowable value.

The concrete slab is subjected to out-of-plane loads both from gravity and from vertical earthquake effects. The rigidity of the floor system at Elevation 42'-0" is such that it may be considered in the rigid range for vertical accelerations. Therefore to obtain vertical earthquake effects the gravity loads may be increased by a factor corresponding to the ZPA of the response spectrum at that elevation.

At Elevation 42'-0" the average ZPA of the vertical response spectra is 0.775g. Therefore the slab was analyzed using a total load of 1.775 times the gravity loads. One way action between the floor beams was assumed and the maximum positive and negative moments were 3.00 and 3.30 k.ft/ft respectively. These values are less than 25% of the ultimate strength capacity of the slab, 13.57 k.ft/ft.

9.3 Masonry Walls

Masonry walls are subjected to the combined effects of out-of-plane and in-plane loadings. The criteria developed for the San Onofre, Unit 1 evaluation provide limits on steel strain ratios and masonry stress for the former and on maximum strain levels for the latter. In the following section the various walls are evaluated.

9.3.1 Superstructure Walls

The superstructure walls, FB-1 to FB-7, span between the top of pool at Elevation 42'-0" and the roof level at approximately 65'-0". With the exception of walls FB-7 and FB-4 all walls span vertically and thus are evaluated in terms of the criteria developed in Volume 1 of this report for their out-of-plane response. For in-plane response the

criteria for ultimate strain limits the maximum strain levels to 0.00264 for load carrying walls.

Conceptual modifications have been identified for wall FB-7 (Figure 6.1) using steel strengthening members which carry the applied shears and therefore greater strain levels are permissible in this wall.

The maximum out-of-plane response of these walls are listed in Table 7.5. Wall FB-6 has the maximum deflection at the center, 11.19 inches. At this level of displacement the maximum steel strain ratios are 23.0 and 26.4 at the central and base hinges respectively, slightly greater than 50% of the criteria limit of 45. The masonry compressive stress expressed as a uniform stress over the face shell is limited by the yield force in the steel and therefore is effectively constant over all yielding walls at 656 psi, about 57% of the allowable value of 1147 psi which is based on 0.85f'm.

Table 7.4 lists the maximum in-plane stresses and strains for each of the masonry walls. Except for wall FB-7 the strains were relatively low, with the peak value of 44% of the limit occurring in wall FB-2. The other walls were less than 20% of the allowable. Wall FB-7 with steel strengthening members is braced and thus is not required to perform load carrying functions. A higher strain limit of 0.00528 is thus accepted for this wall, based on the level at which face shell spalling has been observed in tests. Wall FB-7 reached 91% of this value.

Two of the superstructure walls, FB-7 and part of FB-4, have horizontal spans considerably less than their vertical spans. The out-of-plane stiffness for these walls was not included in the global model for horizontal response. To evaluate these walls the envelope response spectrum obtained from the non-linear analyses was used as loading input to a SAP5A plate finite element model.

The walls were modelled as assemblages of plate bending elements with moment fixity at their edges and pinned supports at roof level. The stiffness was based on 1.5 times the cracked moment of inertia. The response spectrum used had a ZPA of 1.05g and a maximum amplified acceleration of 4.15g. Modal responses were combined by the square root of the sum of the squares method.

In both walls the maximum moments in each direction were considerably less than the ultimate moment capacity. The maximum horizontal moments were 43% and 21% of ultimate in walls FB-4 and FB-7 respectively. The vertical moment was 25% of ultimate in FB-4 and only 4% of ultimate in wall FB-7. Therefore both walls were concluded to be satisfactory.

9.3.2 480V Switchgear Walls

Walls FB-8, FB-9 and FB-10 enclose the switchgear room from elevation 14'-0" to elevation 42'-0" with an intermediate support by the mezzanine floor at elevation 31'-0".

Maximum out-of-plane response of these walls as given in Table 7.5 is relatively small due to the reduced spans. The maximum displacements were only slightly above the yield level and thus steel strain ratios reflected minimal yielding. The masonry stress was of similar magnitude to that of the superstructure walls.

Two of the walls, FB-8 and FB-9, are subjected to imposed displacements from the rocking of the adjacent fuel pool. Table 7.4 shows that these walls have high in-plane strain levels, but less than 90% of the limiting strain. The third wall, FB-10, has only about one half as much strain.

9.4 Steel Framing

The structure has steel framing at the superstructure level and in the switchgear room. This steel framing functions solely to carry vertical loads as its stiffness is negligible compared with the horizontal load carrying masonry shear walls. The steel columns carry the full dead load of the diaphragms but because of the nature of the connections between the steel perimeter beams and the masonry walls any additional superimposed loads would be shared between the steel columns and the walls.

The steel columns have been evaluated for the effects of gravity loads and it has been assumed that vertical earthquake effects would be transferred into the masonry walls. The steel beam members in the roof and the mezzanine floor at elevation 31'-0" have been evaluated for vertical earthquake

effects by response spectrum analysis using the envelope spectra obtained from the vertical model of the structure. For Elevation 42'-0" which has a stiffness such that the response will be in the ZPA range of the vertical response spectrum the average ZPA of 0.775g has been added to the gravity load effects.

Results for the most critical of each of the steel member types are summarized in Table 9.3. The capacity for the horizontal members carrying combined loads from gravity plus earthquake has been based on ultimate strength conditions using the section modulus times the steel strength of 36 ksi. For the columns carrying gravity loads only allowable stresses from AISC have been used.

The maximum ratio of applied moment to allowable moment is 71% and in the columns the axial loads reach a maximum of 72% of allowable values. The 24 WF 94 at Elevation 42'-0" has an axial force due to the horizontal component of the reaction from the strut beneath. This force is 279 kips and produces a stress of 30% of the allowable axial stress. Therefore the total interaction ratio for flexural and axial stress is (0.69+0.30)=0.99, very close to the allowable value. Note however that this assumes no transfer of axial load into the slab and is the resultant of a horizontal earthquake motion that is very conservative with respect to the 0.67g Housner DBE. Therefore the steel framing was concluded to be satisfactory.

9.5 Connections

Connection forces between the vertical and horizontal elements of the structure are tabulated in Table 7.6. In general the connections have both a shear and a tensile component except for Elevation 31'-0", which transfers no shear force, and the top of the two walls which span horizontally under out-of-plane loads, FB-4 and FB-7. These walls do not produce any significant tension loads on the connection.

Evaluation of the adequacy of the connections has been carried out using the interaction formula given in References 6 and 7:

$$\left(\frac{V}{V_a}\right)^{\frac{5}{3}} + \left(\frac{T}{T_a}\right)^{\frac{5}{3}} \leq 1.0$$

where

Va = Allowable shear
V = Maximum shear from analysis
Ta = Allowable tension
T = Maximum tension from analysis.

For the masonry to steel connections the allowable shear and tension are computed from the tabulated UBC values [3] and factored by the ultimate strength factor of 1.5 giving allowable values of 1237.5 lb/ft for both shear and tension.

The connection at elevation 42'-0" between the masonry wall and the concrete slab is by way of steel rebars anchored into the concrete slab and into the grouted bond beam in the wall. The allowable shear force has been computed using the ACI shear friction formulation as 4718 lb/ft. For tension the limiting value has been computed using the allowable bond stress over the anchored rebar, giving an allowable value of 5550 lb/ft.

In two walls, FB-6 and FB-7, the ratio of maximum to allowable from the above interaction formula was greater than unity, indicating that the connections are understrength in terms of the re-evaluation criteria of Section 2.4. Recent test results not yet fully evaluated suggest that these criteria may be overly conservative. Of the remaining walls only three had ratios greater than 50%.

WALL	MOMENTS (lb-in/in)					
	TYPE	Mmax	Mcr	Mult	Mmax/Mcr	Mmax/Mult
EAST	Mx	125860	193150	-	0.652	-
	My	103400	193150	-	0.535	-
WEST	Mx	125850	193150	-	0.652	-
	My	103390	193150	-	0.535	-
NORTH	Mx	266940	193150	325150	1.382	0.821
	My	373660	193150	1273700	1.935	0.293
SOUTH	Mx	158090	193150	-	0.818	-
	My	135350	193150	-	0.701	-

NOTES:

1. These results are from the "as-modified" non-linear analysis.

2. Mx is the moment caused by bending in a horizontal strip and My the moment on a vertical strip.

3. Mmax is the moment obtained from the specified load combination. Mcr is the moment at which cracking occurs and Mult is the ultimate moment capacity.

4. For all walls Mult is greater than Mcr.

TABLE 9.1 : MOMENTS IN FUEL POOL WALLS

WALL	SHEAR STRESS (psi)				
	Vmax	Vc	Vs	Vmax/Vc	Vmax/(Vc+Vs)
EAST	74.1	268.3	-	0.276	-
WEST	74.1	268.3	-	0.276	-
NORTH	216.6	268.3	-	0.807	-
SOUTH	149.7	268.3	-	0.558	-

NOTES:

1. These results are from the "as-modified" non-linear analysis.

2. Vmax is the maximum shear stress obtained from the specified load combination. Vc and Vs are the allowable shear stresses for the concrete and steel respectively computed from the ACI-318 allowable values.

3. Where the concrete alone was sufficient to take the total applied shear stress the contribution of the steel was neglected.

TABLE 9.2 : SHEAR STRESSES IN FUEL POOL WALLS

LOCATION	MEMBER	FORCE	MAXIMUM	ALLOWABLE	RATIO
ROOF	12 B 19	Moment (k-in)	509	766.8	0.66
	12 WF 45.3	"	1381	2092	0.66
EL 42'-0"	24 WF 94	"	5534	7992	0.69
	14 WF 53	"	1722	2801	0.61
	21 WF 62	"	2131	4572	0.71
EL 31'-0"	14 WF 38	"	545	1966	0.28
	16 WF 40	"	606	2329	0.26
	8 C 11.5	"	201	293	0.69
EL 14'-0" to	6 WF 15.5	Axial Load (k)	15.1	21.0	0.72
EL 65'-0"	8 WF 40	"	72.3	153.0	0.47

1. These results are from the "as-modified" non-linear analysis.

TABLE 9.3 : STEEL FRAMING EVALUATION

10 CONCLUSIONS

The Fuel Storage Building at San Onofre, Unit 1 was evaluated in terms of the re-evaluation criteria and the structural integrity acceptance criteria. Linear and non-linear analysis techniques with substructuring of portions of the structure were used for these evaluations.

To meet the re-evaluation criteria of Section 2.4 required the conceptual design of modifications to one wall, FB-7, and the addition of connections between the wall and the roof at the top of walls FB-6 and FB-7. Recent test results (which have not yet been fully evaluated) suggest that the re-evaluation criteria for these connection forces may be overly conservative. A series of analyses carried out incorporating these conceptual modifications demonstrated that the structural response was satisfactory under the postulated earthquake motions.

The "as-built" structure was subjected to earthquake motions of the specified DBE level of 0.67g Housner for San Onofre, Unit 1 and complied with the structural integrity acceptance criteria under this load.

11 REFERENCES

[1] Bechtel Power Corporation, "Balance of Plant Seismic Re-Evaluation Criteria" San Onofre Nuclear Generating Station, Unit 1, February, 1981.

[2] Woodward Clyde Consultants, "Balance of Plant (BOP) SONGS Unit 1 Soil Structure Methodology Report", Revision 1.

[3] Uniform Building Code (UBC), 1979 Edition.

[4] "Specification for the Design, Fabrication and Erection of Structural Steel for Buildings", American Institute of Steel Construction (AISC), November, 1978.

[5] "Building Code Requirements for Reinforced Concrete", ACI Standard 318-77, American Concrete Institute (ACI).

[6] "Headed Steel Anchors under Combined Loading", McMackin, Slutter and Fisher, Engineering Journal, Second Quarter, 1973, Volume 10, Number 2, AISC.

[7] "Embedment Properties of Headed Studs", Design Data 10 (1977) by TRW Nelson Division.

APPENDIX A

IN-PLANE FINITE ELEMENT

A1. INTRODUCTION

The in-plane inelastic behavior of the masonry walls of the fuel storage building are modeled using a standard 4-node inelastic finite element. The inelastic characteristics of the model provide for both strength and stiffness degradation. The properties used to define the inelastic characteristics of the finite element model are based on a series of thirty-five tests on concrete block masonry piers [1-3]. Another series of four tests [4] are used to validate the critical shear strain of the model.

A summary of the experimental test results used to define the inelastic characteristics of the model is given in Section A2. A description of the in-plane finite element model and its inelastic properties is given in Section A3. Derivation of the parameters from the experimental results are given in Section A4. The parameters used in the finite element model of the fuel storage building are given in Section A5. A comparison of the experimental results and those obtained using the analytical finite element model are given in Section A6.

A2. EXPERIMENTAL TEST RESULTS

The experimental in-plane inelastic behavior of masonry walls has been the subject of an extensive research program at the Earthquake Engineering Research Center, University of California, Berkeley, over the past eight years. The program's objectives have been to investigate the inelastic behavior of masonry walls subjected to in-plane cyclic loads. Three different types of materials were included in the program - hollow concrete block, hollow clay brick and grouted core clay brick. Three different height-to-width ratios of the piers were included - 2 to 1, 1 to 1, and 1 to 2. Other parameters included the amount and distribution of horizontal and vertical reinforcement, and the effects of full and partial grouting.

There were a total of thirty-five hollow concrete block piers included in the test program. There were 12 piers with height-to-width (H/W) ratio of 1 to 1, 6 piers with H/W ratio of 1 to 2, and 17 piers with a H/W ratio of 2 to 1. During each test a series of three cycles of amplitude-controlled load were applied to the test specimen. As each test progressed, the amplitude of each set of three cycles of load was gradually increased. After each set of three cycles of load, the pier was inspected and the extent of cracking was documented by photographs. The major result from each test was the hysteretic behavior shown in Fig. A1. This provides a continuous plot of the applied horizontal in-plane deflection at the top of the wall versus the resulting horizontal in-plane load. The full set of results for each test is given in references [1-3].

The typical hysteretic behavior shown in Fig. A1 characterizes the cyclic behavior of the masonry piers. In order to compare the behavior of different test specimen a hysteresis envelop is constructed from the hysteresis loops. The hysteresis envelop is the average of the maximum positive and negative forces for each set of three cycles of load at a given amplitude. Typical hysteresis envelopes are shown in Figs. A2.

The important characteristics to note from the experimental hysteresis envelopes and loops are:

1. The pier is essentially non-linear elastic up to a deflection of 0.05 inches for the piers with a H/W ratio of 1:1.

2. There is significant stiffness degradation throughout the entire load sequence of the piers.

3. Diagonal cracks occur in the pier at the peak of the hysteresis envelopes. Cracking prior to the formation of these diagonal cracks is minor.

4. Strength degradation occurs after the peak load is attained.

A3. IN-PLANE FINITE ELEMENT MODEL

The in-plane finite element model is based on the two-dimensional plane/axisymmetric element that was developed for the ANSR-II computer program. The inelastic characteristics of the model include all the non-linearities observed in the experimental tests and are discussed in Subsection A3.1.

A3.1 Non-Linear Characteristics

The non-linear characteristics of the finite element model include all the non-linearities observed in the masonry wall test results. The non-linear characteristics are based on a shear stress-shear strain envelop curve as shown in Figure A3 that permits both strength and stiffness degradation. The characteristics of the model are as follows:

1. The basic input of the model consists of a shear stress-shear strain envelope curve as shown in Figure A3, discretized into a series of straight line segments, each defined by a tangent shear modulus and a transition strain (Gi, δi). The envelope curve may have up to 9 straight line segments. Beyond the critical strain, a transition line is defined. This line influences the behavior of the element once the critical shear strain is exceeded, and permits strength degradation to be incorporated in the cyclic behavior of the model (see 6 below). The properties of each section of the envelop curve are deduced from the

experimental results as discussed in Section A5. The stress-strain envelope relates average shear stress to average shear strain, and is symmetric about the origin of the hysteresis plane.

2. The element state determination at the end of each load step is based on the shear strain in the element. That is, the shear strain is used to determine current stiffness of the element.

3. The cyclic behavior of the model is is shown in Figure A4. For simplicity, the envelope curve in Figure A4 incorporates only three transition strains. As the element is loaded, the initial elastic shear modulus (G1) determines the initial element stiffness. This initial stiffness is maintained until the first transition strain ($\delta 1$) is reached in either the positive or negative sense.

4. When the first ($\delta 1$) and subsequent transition strains (δi) are reached, the element stiffness is reformed using the tangent shear modulus as defined by the envelope curve at that point until the direction of loading is reversed.

5. The loading continues along the envelope curve until such time as the load reverses in sense (point A in Figure A.4). The element stiffness is then based on the "secant" shear modulus needed to unload the element through the origin of the hysteresis plane. The element retains this stiffness until it hits the envelope curve (point A1), at which time it follows the envelop curve once again. While the element is on the "secant" stiffness part of the hysteresis loop, load reversals occur without causing a change in element stiffness. This form of cyclic behavior is maintained until the critical shear strain is attained.

6. Once the element shear strain exceeds the critical shear strain (in either the positive or negative sense), the subsequent element behavior is modified from that described above. On the first excursion beyond the critical strain, the element continues along the final slope of the envelope curve (G4) until the load changes sign (point C). Once this occurs, the element unloads with a "secant" stiffness through the origin as it did previously. However, this stiffness is only maintained until the element state intersects the final transition line (point C1). At this point the element stiffness is based on the shear modulus corresponding to the final slope of the envelope curve (G4). This stiffness is maintained until load reversal (point D) and a new "secant" stiffness is calculated This is repeated as shown through the load sequence of points D, D1, E, E1, F, F1, etc., until the secant stiffness degrades to a value equal to the stiffness based on the final slope

of the envelope curve. From this point on, the element's behavior is essentially elastic, with this very low stiffness.

A4. DETERMINATION OF MATERIAL PARAMETERS

The generalized inelastic characteristics of the finite element model are capable of defining the cyclic behavior of any structural element whose experimental performance is similar to that shown in Figures A3 and A4. For the analytical model to be applicable to a particular material and/or structural element the following parameters are required:

1. Critical Shear Strain - δc.
2. Initial Shear Modulus - G1.
3. Transition Strains and Associated Tangent Shear Moduli (Gi).
4. Slope of the Transition Line ($\alpha \delta c$).

These parameters for masonry walls are derived from the experimental test results given in References [1-3] and described in the following subsections. The thirty-five pier tests described in Section A2 contained variations in the height-to-width ratio of the piers, amount and distribution of reinforcement and full and partial grouting. The masonry walls in the fuel storage building are partially grouted walls with a height-to-width ratio of approximately 1 to 1. Thus, the test results of partially grouted walls with a height-to-width ratio of 1 to 1 are used to define the parameters of the analytical model.

A4.1 Critical Shear Strain

Critical shear strains are derived for walls subjected to in-plane shear loads in Section A4.1.1 and for braced walls with an alternate load carrying member in Section A4.1.2.

A4.1.1 Shear Walls

The critical shear strain shown in Figure A3 defines the peak of the hysteretic envelop curve. For the masonry walls, it also corresponds to the onset of diagonal cracking for walls exhibiting a shear mode of response. Since this is one of the most important parameters of the analytical model, its value is deduced from both fully and partially grouted walls with a height-to-width ratio of 1. The value obtained from these tests is then used to predict the onset of diagonal cracking in piers with height-to-width ratio of 1 to 2 and 2 to 1 [1 and 3], and the tests performed by Williams [4].

to evaluate the adequacy of the value obtained from the 1 to 1 walls.

A. Walls with H/W=1 [2]

The walls are subjected to a series of displacement controlled, in-plane shear loads and are either fully or partially grouted.

Table A.1 gives the lateral displacement which corresponds to the onset of diagonal cracking determined from the hysteresis envelopes and the corresponding photographs. The lateral displacement is measured at the top of the walls.

The percentage of shear and bending components of the displacement is estimated by using the following beam formula:

$$\frac{PL^3}{12EI} + \frac{1.2PL}{AG}$$

where P = Applied Shear Force
L = Height of Wall
I = Bending Moment of Inertia of Wall
A = Cross Sectional Area of Wall
E = Young's Modulus
G = Shear Modulus
(= E/2.3, use p = 0.15)

Fully Grouted Walls

The percentage of shear and bending components of the displacement are estimated by using the following values [1]:

L = 56 inch
I = 70.272 inch**4
A = 366 inch**2

The percentages are calculated as follows:

$$\frac{P}{E}\left(\frac{56^3}{12x70272} + \frac{1.2x56x2.3}{366}\right)$$

$$= \frac{P}{E}\ (0.21 + 0.42)$$

Hence, the shear and bending components are 67% and 33% of the average displacement, respectively.

Table A.1 gives the average displacement corresponding to the onset of diagonal cracking of 0.23 inch at the top of the walls.

The displacement due to shear alone is then obtained as follows:

$$\delta cr(s) = 0.23 \times 0.67 = 0.154 \text{ inch}$$

Partially Grouted Walls

The percentage of shear and bending components of the displacement are estimated by using the following values [2]:

L = 56 inch
I = 56,960 inch**4
A = 210 inch**2

The percentages are calculated as follows:

$$\frac{P}{E}\left(\frac{56^3}{12 \times 56960} + \frac{1.2 \times 56 \times 2.3}{210}\right)$$

$$= \frac{P}{E}\,(0.257 + 0.736)$$

Hence, the shear and bending components are 74% and 26% of the average displacement, respectively.

Table A.1 gives the average displacement corresponding to the onset of diagonal cracking of 0.20 inch.

The displacement due to shear alone is obtained as follows:

$$\delta cr(s) = 0.20 \times 0.74 = 0.148 \text{ inch}$$

Critical Shear Strain

The test results on both fully and partially grouted walls indicate that diagonal

cracks develop when the displacement due to the shear component of deformation reaches 0.148 inch. The critical shear strain δcr. is therefore obtained as follows:

$$\gamma_{cr} = \frac{\delta cr(s)}{Height} = \frac{0.148}{56} = 0.00264$$

This critical strain value is used in Subsections B and C to predict the onset of diagonal cracking in other test walls with different height-to-width ratios.

B. Walls With H/W = 0.5 and 2

Cyclic loading tests were also performed on fully grouted walls with H/W = 0.5 and 2 [3, 1]. The critical shear strain derived from tests on walls with a H/W = 1 is applied to these walls to predict the lateral displacement at which diagonal cracking occurs. The predicted displacement is compared with the values obtained from the test results to evaluate the adequacy of the critical shear strain obtained from the 1 to 1 walls.

Walls With H/W = 0.5 [3]

The percentages of shear and bending components of displacement are estimated for these walls by using the following values:

L = 40 inch
I = 325.333 inch**4
A = 610 inch**2

$$\frac{P}{E}\left(\frac{40^3}{12x325333} + \frac{1.2x40x2.3}{610}\right)$$

$$= \frac{P}{E}(0.0164 + 0.181)$$

Therefore the shear and bending components of the displacement are 92% and 8%, respectively. Thus diagonal cracking is predicted to occur when the lateral displacement at the top of the walls reaches:

$$\delta cr = \frac{\gamma_{cr} \times Height}{0.92} = \frac{0.00264x40}{0.92}$$

$$= 0.115 \text{ inch}$$

The average displacement at which diagonal cracks occur in tests is 0.102 inch as given in Table A.2. Therefore, the predicted displacement exceeds the test results by about 11%.

Walls With H/W = 2 [1]

The percentage of shear and bending components of displacement are estimated for these walls by using the following values:

L = 64 inch
I = 15,360 inch**4
A = 180 inch**2

$$\frac{P}{E}\left(\frac{64^3}{12x15360} + \frac{1.2x64x2.3}{180}\right)$$

$$= \frac{P}{E}\,(1.42 + 0.98)$$

Therefore the shear and bending components are 41% and 59%, respectively. Thus diagonal cracking is predicted to occur when the lateral displacement at the top of the walls reaches:

$$\delta cr = \frac{\gamma cr \times Height}{0.41} = \frac{0.00264x64}{0.41}$$

$$= 0.41 \text{ inch}$$

The average displacement at which diagonal cracks occur in the tests is 0.33 inch as given in Table A.3. Therefore the predicted displacement exceeds the test results by 20%.

C. Cantilever Walls [4]

All the walls referenced in the preceding sections were tested with fixed-fixed moment boundary conditions. In Williams' [4] tests the top of the wall was free to rotate, thereby simulating a cantilever wall. The walls of this test program had a height-to-width ratio of approximately 1 to 1.

The critical shear strain obtained from Subsection A is again used to predict the lateral displacement at which diagonal cracking develops in these walls.

The percentage of shear and bending components of displacement are

estimated by using the following values and formula for cantilever beams:

L = 48 inch
I = 33.408 inch**4
A = 174 inch**2

$$\frac{P}{E}\left(\frac{48^3}{3x33408} + \frac{1.2x48x2.3}{174}\right)$$

$$= \frac{P}{E}\,(1.10 + 0.76)$$

Therefore the shear and bending components of the displacement are 41% and 59%, respectively. Thus diagonal cracking is predicted to occur when the lateral displacement at the top of the walls reaches:

$$\delta cr = \frac{\gamma cr \times Height}{0.41} = \frac{0.00264x48}{0.41} = 0.31 \text{ inch}$$

No photographs were provided in the referenced report, however personal communication with the author revealed that diagonal cracking occurred on the first load cycle at the point where there was a drop in the load. Table A.4 gives the lateral displacement at which diagonal cracking is estimated to have occurred in the test walls. The average displacement obtained is 0.385 inch. Therefore, the predicted displacement underestimates the test results by about 24%. The prediction of the onset of diagonal cracking using the critical shear strain derived from the 1-to-1 walls was well within acceptable limits for the 2-to-1 and 1-to-2 walls. For the cantilever walls, the prediction was conservative by approximately 26%. Since the critical shear strain is one of the most important parameters of the analytical model, the value of 0.00264 is well validated by the available test data.

The shear strains that result from the analysis of the walls are limited to this same value of critical shear strain. This value corresponds to minimal levels of cracking within the walls and it also prevents any strength degradation of the walls.

A4.1.2 Braced Walls

In the fuel storage building a conceptual modification consisting of a steel braced frame was developed for Wall FB-7. The modification acts as an

alternate load carrying path for the wall. The basic inelastic formulation of the analytical model for this braced wall is identical to the others, including the critical shear strain and transition line shown on Figure A3. The maximum strain this wall can withstand is higher than for unbraced walls since strength degradation will cause a redistribution of load to the bracing. Thus, for Wall FB-7, the limiting strain or displacement is governed by the displacement at which the integrity of the wall is maintained. This was established to be 0.40 inches and corresponds to a critical shear strain of 0.00528.

A4.2 Shear Moduli and Transition Strains

The transition strains (δi) and shear moduli (Gi) of the hysteresis envelop shown in Figure A3 define the stiffness degradation that occurs in the analytical model. The curve is discretized into a series (up to 9) straight segments and each one is defined by a shear modulus (i.e., slope of the segment) and a transition strain.

The values of these parameters for the masonry walls are obtained from the test results on the partially grouted walls with a H/W ratio of 1. To utilize the test results, it is necessary to evaluate the parameters in a generalized form so they can be used for walls with different dimensions. This is done by expressing the shear modulus of each segment as a percentage of the initial shear modulus. The transition strains for each region are defined as a fraction of the critical shear strain. The hysteresis envelops for the test results are given in Figure A2. The hysteresis envelopes for each of the tests are divided into three regions up to the critical displacement (δ)cr of 0.20 inch. The regions are 0 to 0.05 inches (1/4 δ cr), 0.05 to 0.10 inches (1/2 δ cr) and 0.10 to 0.20 inches (δcr) . Table A5 gives the corresponding shear force increments for each of these regions for each test.

The shear modulus, Gi for each region, is calculated using the following formula:

$$G = \frac{1.2\Delta PL}{A\Delta\delta s}$$

where
- L = Height of Wall (= 56 inch)
- A = Cross Sectional Area (= 210 inch)
- ΔP = Increment of Shear Force
- $\Delta\delta s$ = Increment of Displacement Due to Shear Deformation (75% of Total Displacement)

The average of the resulting shear moduli are given below:

Region	Shear Modulus psi
1	207,000
2	72,000
3	45,000

In order to express these moduli as a percentage of the initial shear modulus, it is necessary to calculate the initial shear modulus of the test results. This is obtained from the experimentally determined elastic modulus (E = 1,140,000 psi), and Poisson's ratio of 0.15 from the standard relationship as follows:

$$G_o = \frac{E}{2(1+\nu)} = \frac{1,140,000}{2(1+0.15)}$$

$$= 495,650 \text{ psi}$$

The resulting percentage of the shear modulus for each of the three regions to the initial shear modulus is determined from the above values and summarized below:

Region	Percentage Reduction G/Go (%)
1	41.8
2	14.5
3	9.1

These percentages are utilized in Section A5 to define the parameters of the hysteresis envelopes for the walls of the fuel storage building.

A4.3 Slope of the Transition Line

The transition line shown in Figure A3 provides the mechanism for strength degradation in the analytical model after the maximum load or critical shear strain is attained. The slope of the transition line affects the severity of the strength degradation. From the hysteresis envelopes of the partially grouted walls shown in Figure A2, the maximum displacement the walls can withstand is over twice the displacement at which the maximum load is attained. Therefore, if the slope of the transition line is defined as a line from the point of maximum load to a point on the abscissa of 1.5 times the critical strain, then the strength degradation will be conservatively defined. This is illustrated in Section A6 where the analytical model is compared to the test results.

A5. PARAMETERS USED FOR THE FUEL STORAGE BUILDING

The generalized characteristics of the analytical finite element model were presented in Section A3. Parameters of this model that are applicable to masonry walls were derived from experimental test results in Section A4. The parameters that were used in the analysis of the in-plane walls of the fuel storage building are shown schematically in Figure A3 and their quantitative values are as follows:

A. Critical Shear Strain

The critical shear strain δc is 0.00264. This value was obtained from the test walls with a H/W ratio of 1 which is similar to the H/W ratio of the masonry walls of the fuel storage building.

B. Shear Moduli and Transition Strains

Three tangent shear moduli and two transition strains were used to define the three regions of stiffness degradation up to the point where the critical shear strain is attained. In Section A4.2 the values of shear moduli obtained from the experimental results were expressed as a percentage of the initial shear modulus and the transition shear strains as a fraction of the critical shear strain. The initial shear modulus for the masonry walls of the fuel storage building was obtained from Young's Modulus and Poisson's Ratio. The elastic modulus is assumed to be equal to 600 f'm where f'm is taken as the minimum specified value of 1350 psi. Poisson's ratio is assumed to be equal to 0.15. Therefore the initial shear modulus is:

$$G_o = \frac{E}{2(1+\nu)} = \frac{600\ f'm}{2(1+\nu)}$$

$$= \frac{600 + 1350}{2(1 + 0.15)} = 352{,}000\ \text{psi}$$

The three regions are therefore defined as follows:

Region	Range of Shear Strain	Shear Modulus as % of Go
1	0 - 1/4 δ cr	40
2	1/4 δcr - 1/2 δ cr	13
3	1/2 δcr - δ cr	9

Region	Range of Shear Strain	Shear Modulus psi
1	0 - 0.00067	141,000
2	0.00067 - 0.00134	45,800
3	0.00134 - 0.00268	31,700

For the structural integrity evaluation, the initial shear modulus used for Region 1 was 352,000 psi up to a transition strain of 0.00018. The other values remained the same. This value was used over a smaller strain range in the initial region to reflect the probable strength of the walls.

C. Slope of Transition Line

The slope of the transition line shown on Figure A3 is defined by an δ value of 1.5.

A6. VERIFICATION OF ANALYTICAL MODEL

The analytical model and the parameters derived in Section A4 were used to determine how accurately they would predict three of the partially grouted test wall results. The walls selected for the analysis were Test Nos. 5, 8 and 10 of Reference 2. The first two were analyzed individually while the third was averaged with the first two and the average of the three test results was used.

The modeling procedures used for the test walls were similar to those used for the walls of the fuel storage building. The procedures are as follows:

1. The parameters for the hysteresis envelopes of Figure A3 for the 3 tests are given in Table A6. The tangent shear moduli for each test is taken directly from the test curves by the method given in Section A4.2.

2. The analytical model of the wall uses only two finite elements. The equivalent thickness for the wall is obtained by performing a detailed elastic finite element analysis of the wall with a fine mesh and comparing the deflections obtained from the two element elastic analysis. The two element model is too stiff and consequently its equivalent thickness must be adjusted. The equivalent solid thickness of the partially grouted walls is 4.375 inches and this was adjusted to 3.62 inches so the two element model had the correct overall stiffness.

3. The analytical model uses an element of uniform thickness to model the partially grouted test walls. As a result, the proportion of shear deformation in the analytical model was less than that of the test walls. This difference was accounted for in the analytical model by adjusting the critical and transition shear strains by the ratio of 0.67/0.75. This ratio was the proportion of shear deformation in the fully and partially grouted test walls as shown in the following table:

	Fully or Solid Grouted Walls	**Partially Grouted Walls**
Shear	67%	75%
Bending	33%	25%

The critical and transition shear strains used in the analytical model of the test walls are given in Table A6.

4. The boundary conditions and sequence of loading of the analytical model were similar to those used in the tests. The boundary conditions were such that the walls were fixed against rotation and free to move laterally at the top. The loading was cyclic and displacement controlled with a gradually increasing displacement. In the tests, three cycles of load at each specified displacement were used. However, in the analytical model, only one cycle of load was used at each specified displacement.

Figure A5 provides a comparison of the cyclic behavior of the analytical model of Test 5 with the observed test behavior. Figures A6, A7 and A8 compare the hysteresis envelopes of the analytical models of Tests 5, 8 and the average of Tests 5, 8 and 10 with the experimental hysteresis envelopes. In each case, the agreement is very good, and indicates that the analytical model used for the in-plane masonry walls of the fuel storage building is able to accurately predict the experimental behavior of walls of similar construction.

REFERENCES

1. R.L. Mayes, et al., "Cyclic Shear Tests of Masonry Piers, Vol. 1 - Test Results," EERC Report No. 76-8, University of California, Berkeley, 1976.

2. S.J. Chen, et al., "Cyclic Loading Tests of Masonry Single Piers, Vol. 2 - Height to Width Ratio of 1," EERC Report No. 78/28, University of California, Berkeley, 1978.

3. P.A. Hidalgo, et al., "Cyclic Loading Tests of Masonry Single Piers, Vol. 3 - Height to Width Ratio of 0.5," EERC Report No. 79/12, University of California, Berkeley, 1979.

4. D. Williams, "Seismic Behaviour of Reinforced Masonry Shear Walls," Ph.D. Thesis, University of Canterbury, New Zealand, 1971.

5. Mondkar, D.P. and Powell, G.H., "2D Plane/Axisymmetric/EERC-80/14," EERC, University of California, Berkeley, May 1980.

TABLE A.1

Critical Lateral Displacement
Corresponding to Onset of
Diagonal Cracking (H/W = 1)

Test No.	Critical Lateral Displacement δ_{cr} (inch)	
	Fully Grouted	Partially Grouted
4	0.21	
5		0.185
6	0.29	
7	0.175	
8		0.20
9	0.20	
10		0.21
11	0.28	
Average	0.23	0.20

TABLE A.2

Critical Lateral Displacement
Corresponding to Onset of
Diagonal Cracking (H/W = 0.5)

Test No.	Critical Lateral Displacement δ_{cr} (inch)
1	0.123
2	0.10
3	0.10
4	0.10
5	0.10
6	0.090
Average	0.102

TABLE A.3

Critical Lateral Displacement
Corresponding to Onset of
Diagonal Cracking (H/W = 2)

Test No.	Critical Lateral Displacement δ_{cr} (inch)
1	0.24
2	0.24
3	0.40
4	0.35
5	0.31
6	0.37
7	0.31
8	0.39
Average	0.33

TABLE A.4

Critical Lateral Displacement
Cantilever Walls

Test No.	Critical Lateral Displacement δ_{cr} (inch)
CB1	0.39
CB2	0.39
CB3	0.38
CB4	0.38
Average	0.385

TABLE A.5

Discretized Shear Force – Lateral Displacement
Hysteresis Envelope Curves
(H/W = 1)

Test No.	Region 1 ($0 \leq \delta \leq 0.05$)		Region 2 ($0.05 \leq \delta \leq 0.10$)		Region 3 ($0.10 \leq \delta \leq 0.20$)	
	ΔP (kip)	$\Delta \delta$ (in.)	ΔP (kip)	$\Delta \delta$ (in.)	ΔP (kip)	$\Delta \delta$ (in.)
8	22.0	0.05	4.7	0.05	9.5	0.10
5	24.1	0.05	11.5	0.05	9.5	0.10
10	26.7	0.05	8.9	0.05	12.7	0.10
Average	24.3	0.05	8.4	0.05	10.6	0.10

TABLE A.6

Shear Modulus - Transition Shear Strain
For Verification Examples

Example No.	Test No.	Boundary Condition	γ_{cr}	Shear Strain - Shear Modulus							
				Region 1		Region 2		Region 3		Region 4	
				γ_1	G_1 (ksi)	γ_2	G_2 (ksi)	γ_3	G_3 (ksi)	γ_4	G_4 (ksi)
1	5	Fixed	0.00241	0	238	0.00060	96	0.00121	52	0.00241	13
2	8	Fixed	0.00241	0	209	0.00060	44	0.00121	44	0.00241	11
3	Avg. of 5,8, 10	Fixed	0.00241	0	236	0.00060	75	0.00121	51	0.00241	13

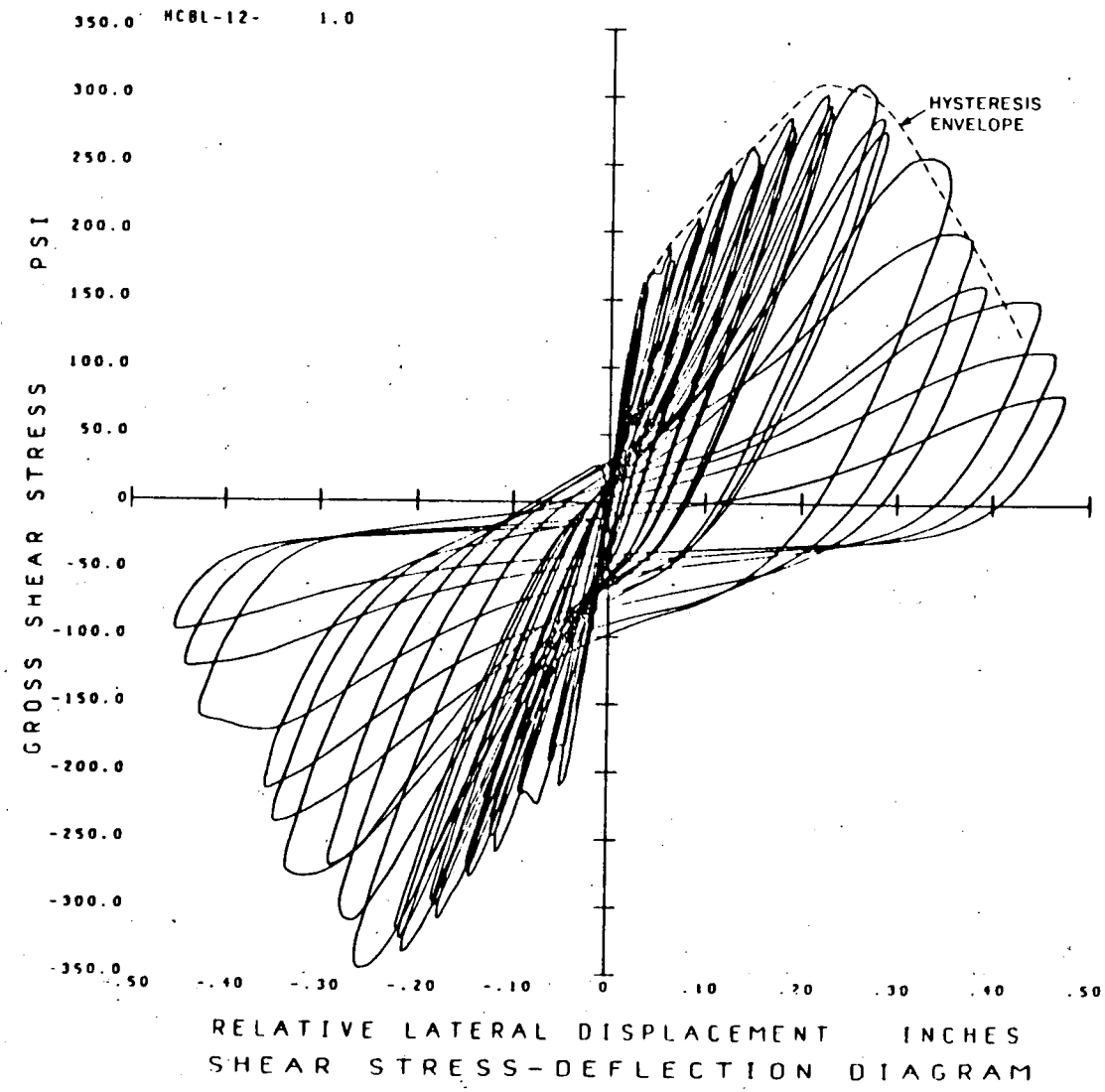

FIG A1 TYPICAL HYSTERESIS LOOPS AND ENVELOPES

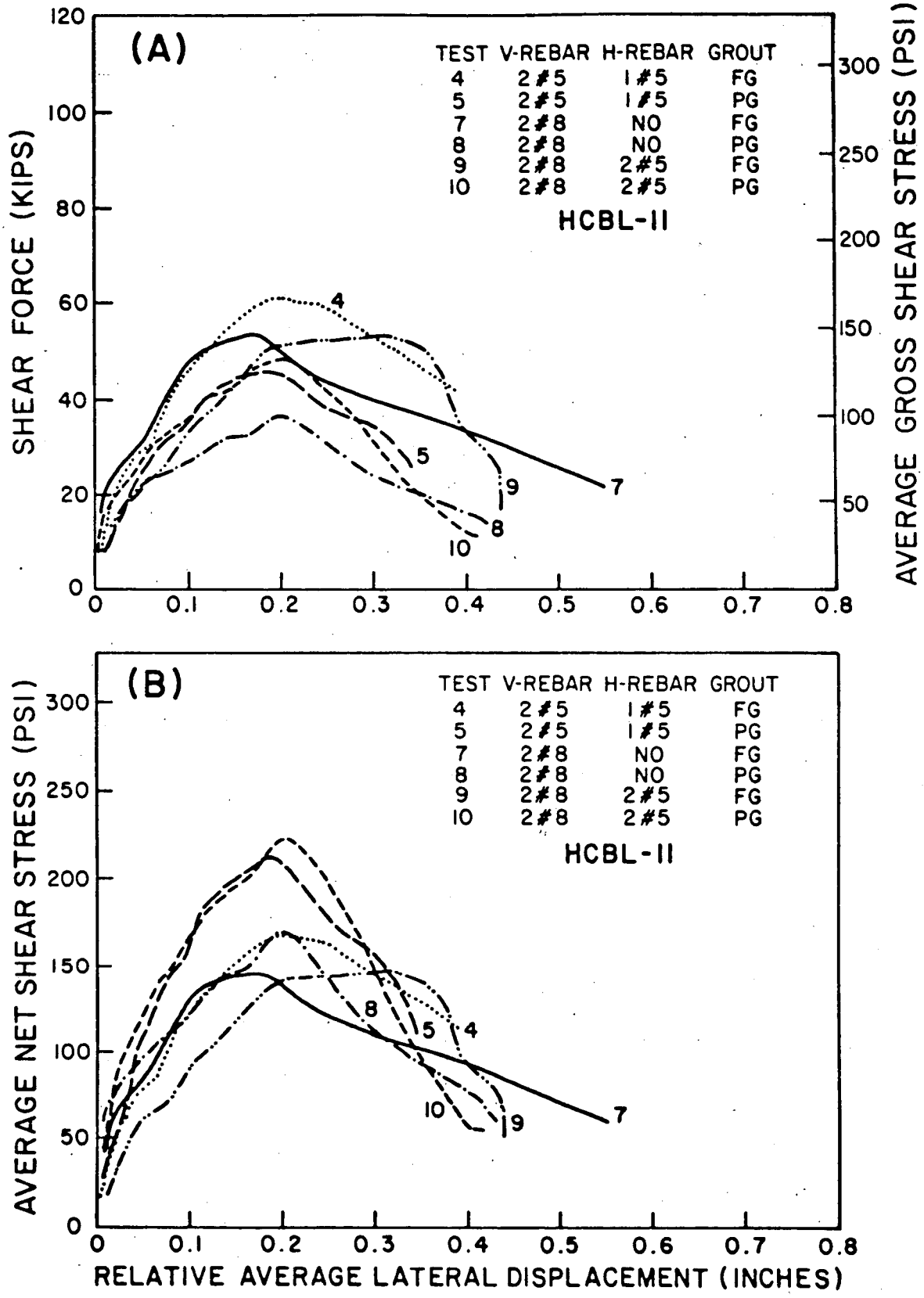

FIG A2 EFFECT OF PARTIAL GROUTING ON HYSTERESIS ENVELOPES

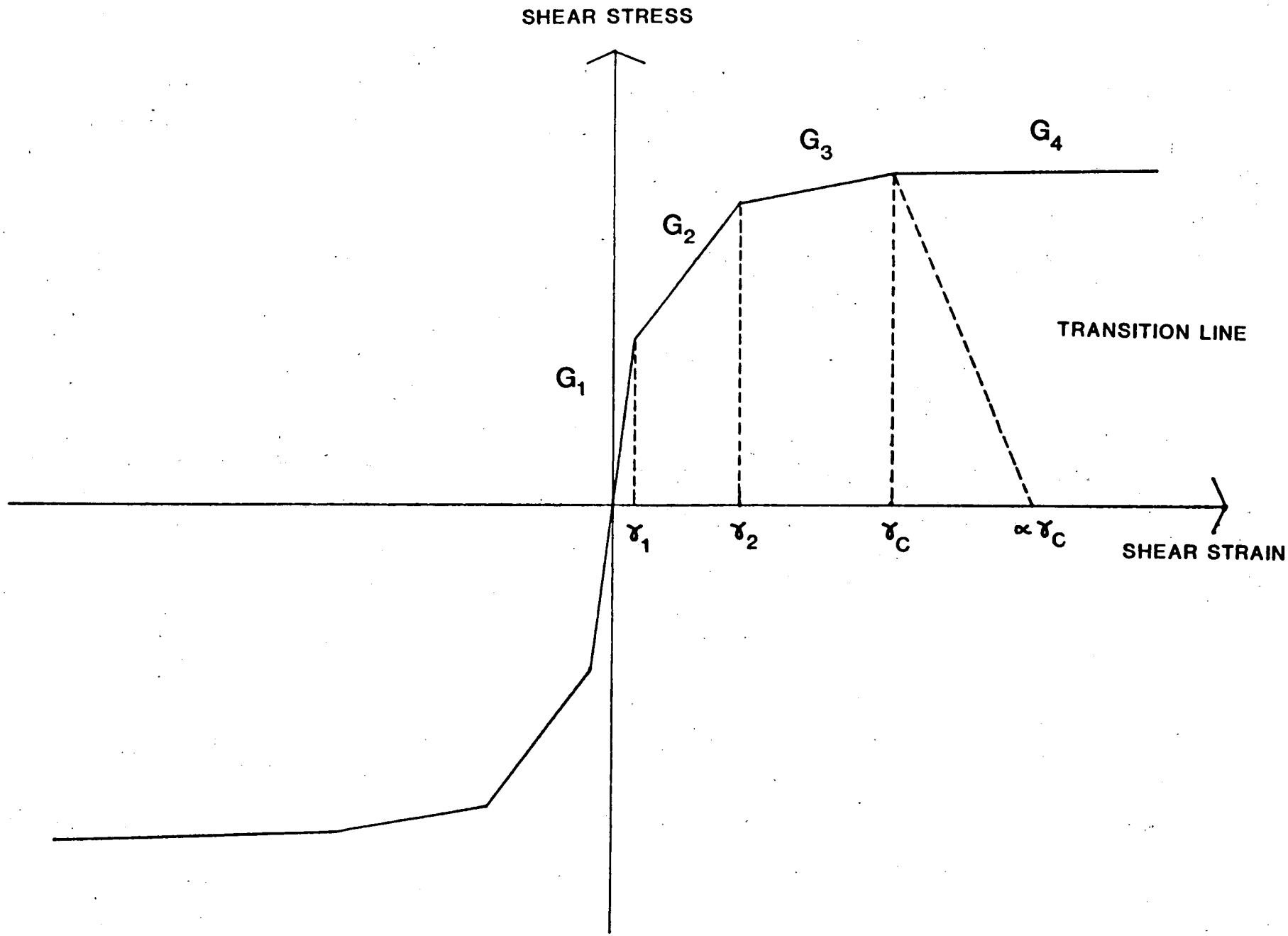

FIG A3 SHEAR STRESS-STRAIN ENVELOPE CURVE

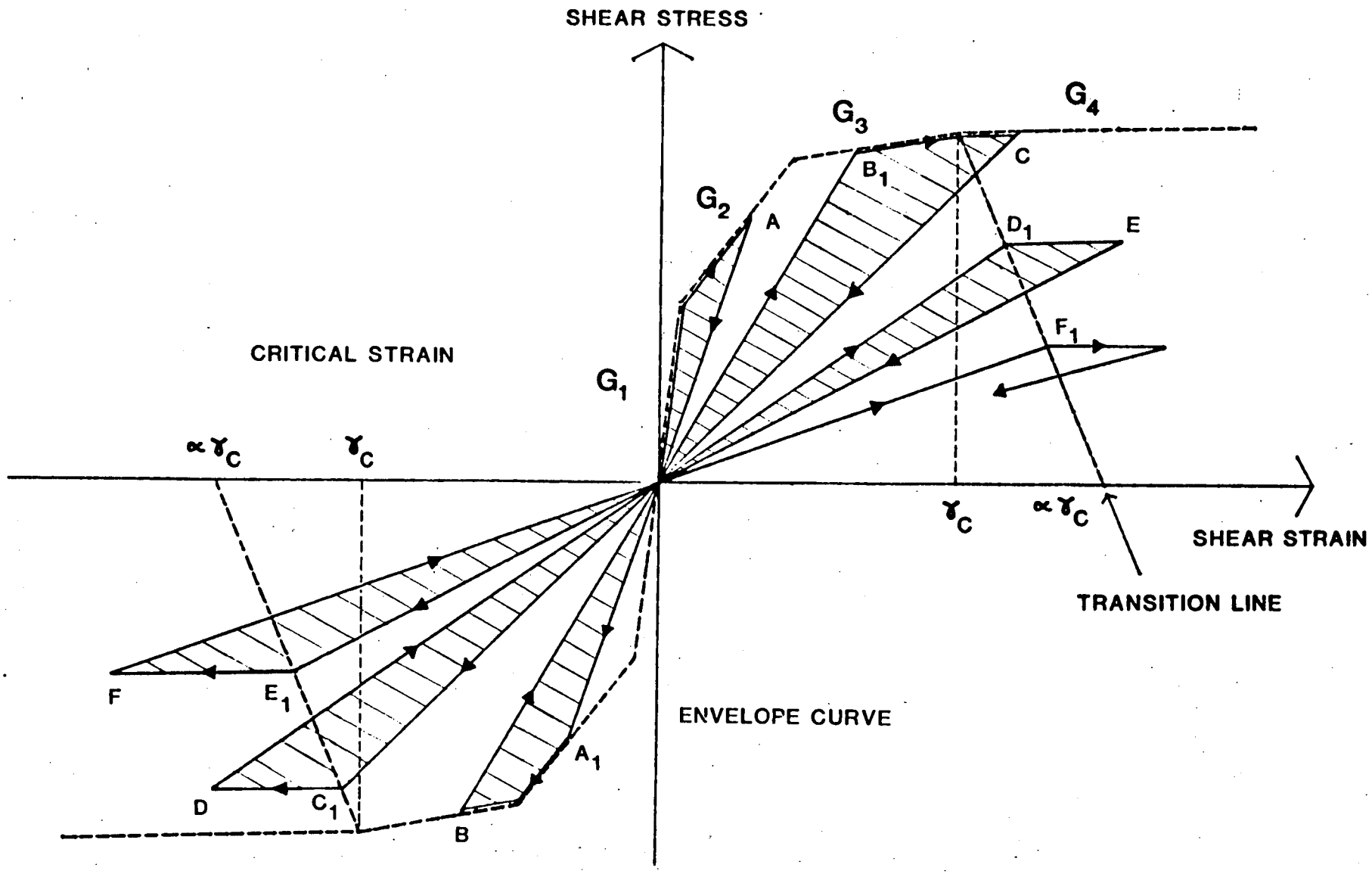

FIG A4 HYSTERETIC BEHAVIOR OF ANALYTICAL MODEL

TEST 5

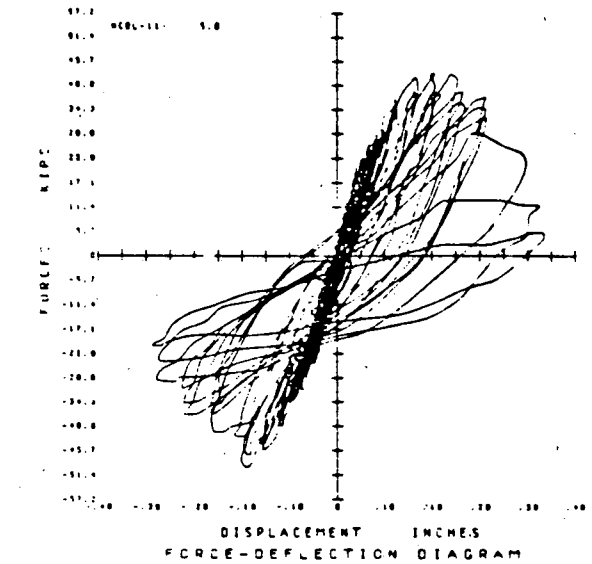

ANALYTICAL MODEL

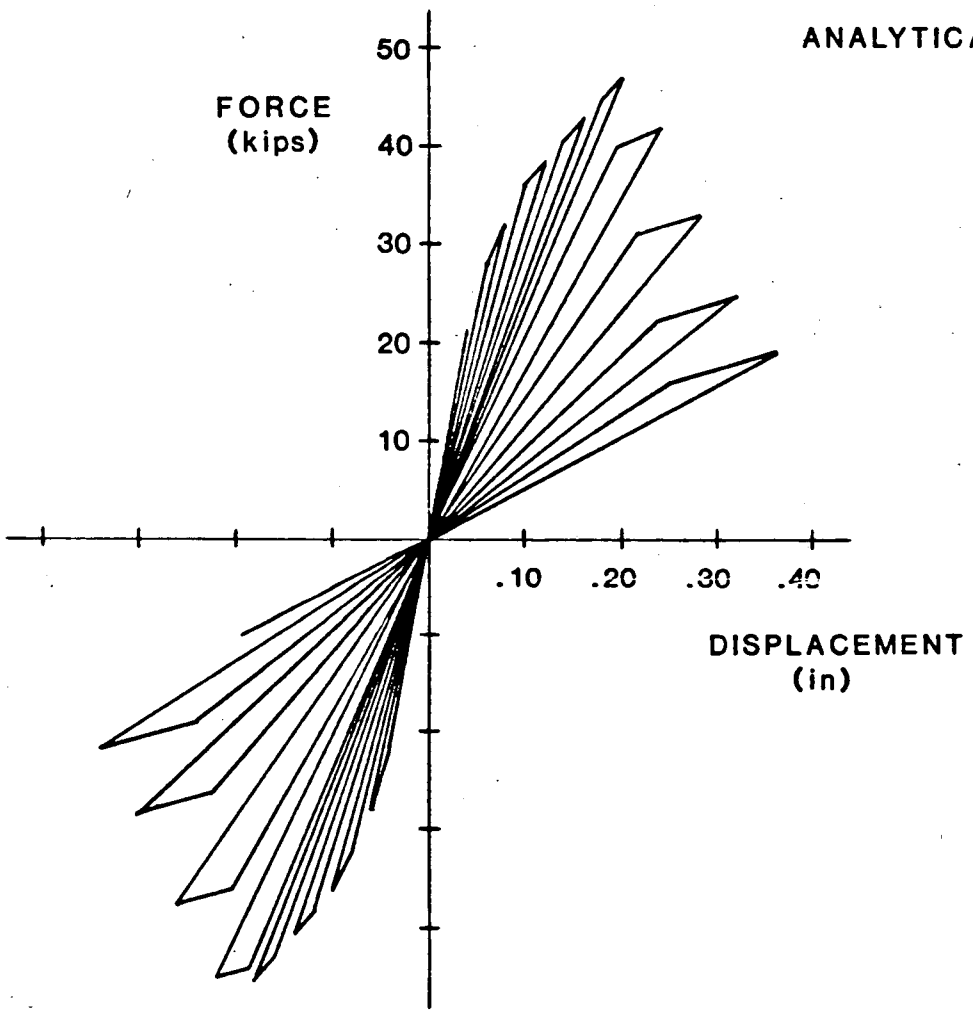

FIGURE A5. Comparison of hysteresis curves for TEST 5

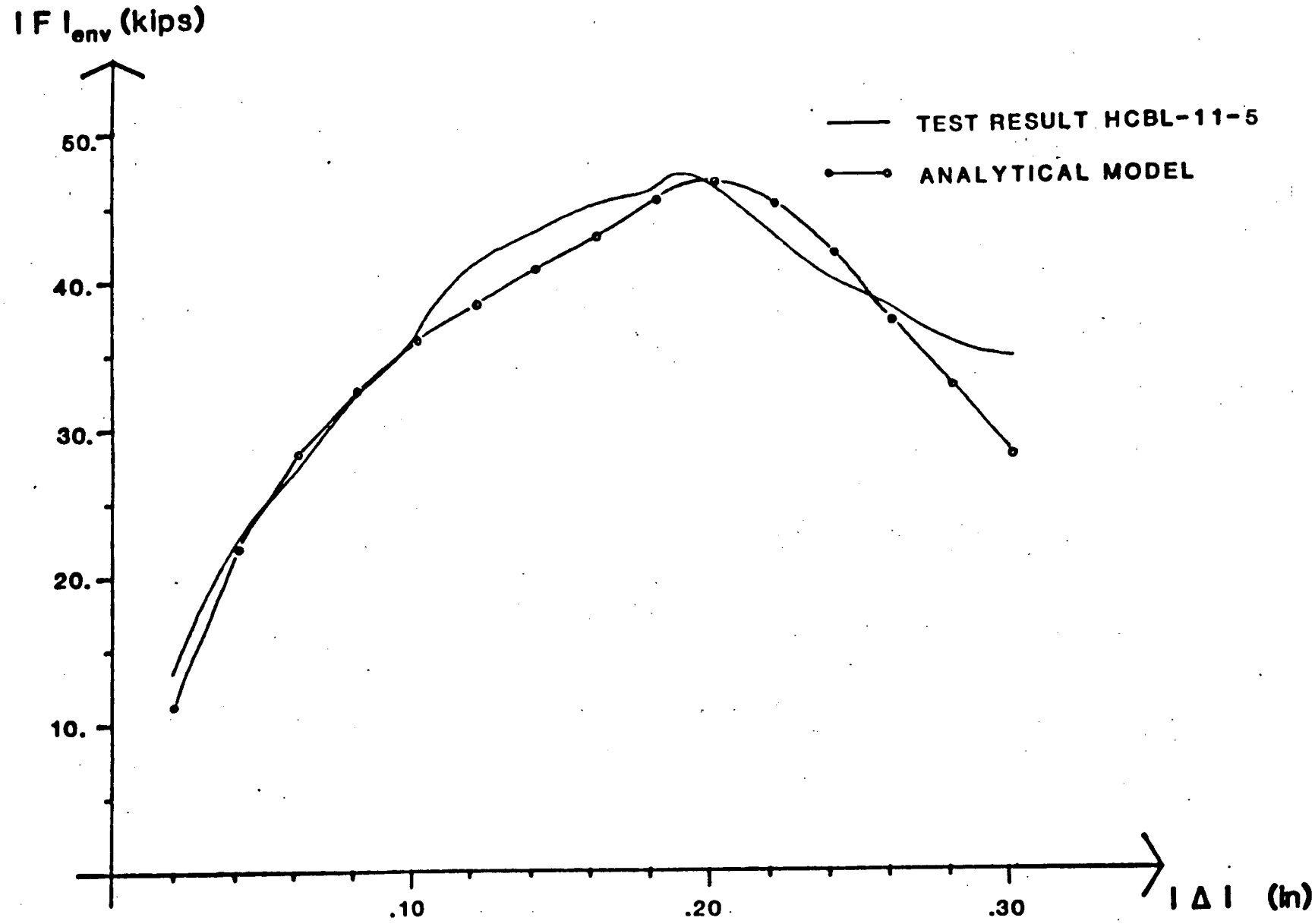

FIG A6 COMPARISON OF HYSTERESIS ENVELOPES FOR TEST 5

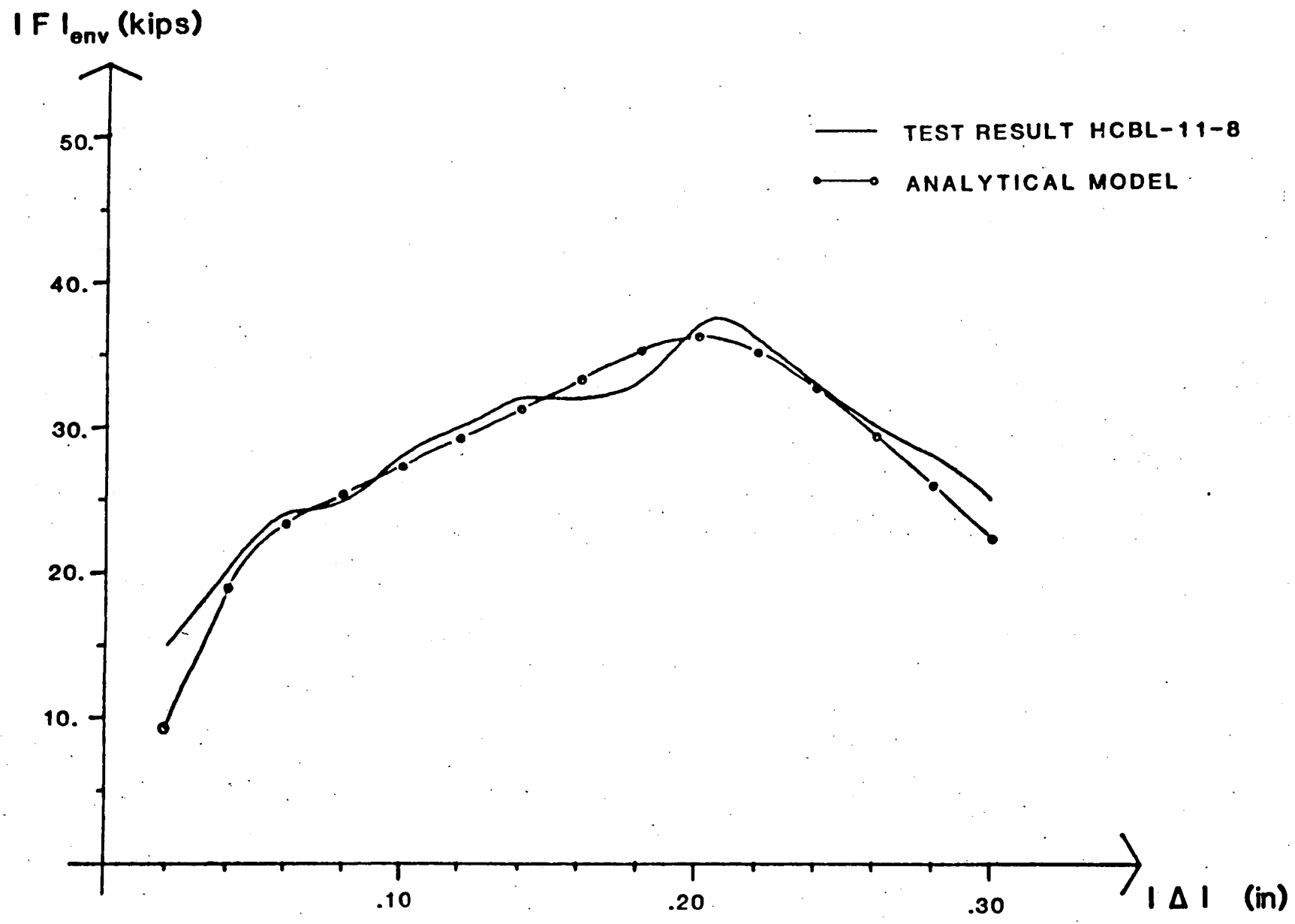

FIG A7 COMPARISON OF HYSTERESIS ENVELOPES FOR TEST 8

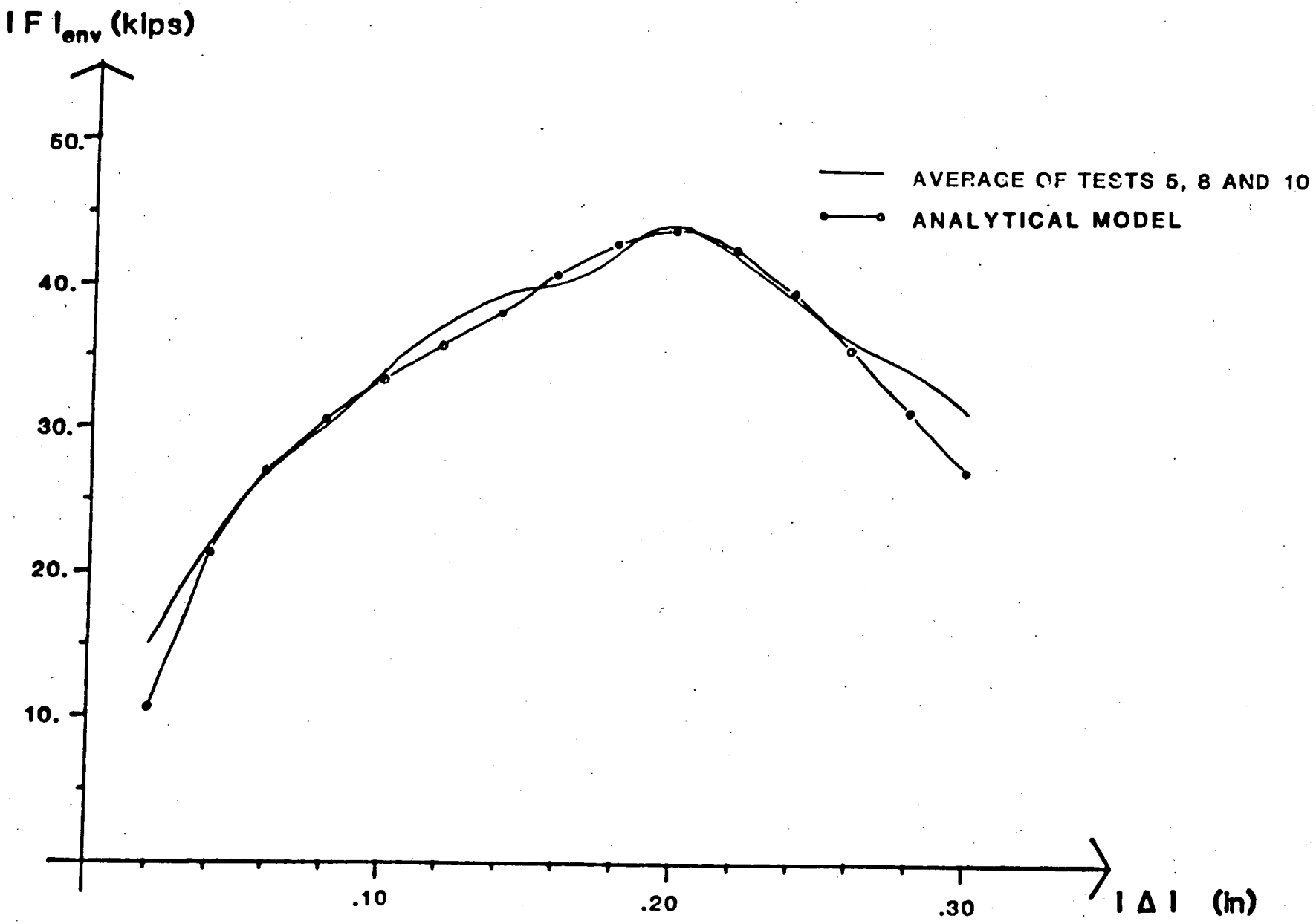

FIG A8 COMPARISON OF AVERAGE HYSTERESIS ENVELOPES FOR TESTS 5, 8 AND 10

APPENDIX B

NON-LINEAR MASONRY ELEMENT FORMULATION : OUT-OF-PLANE

TABLE OF CONTENTS

B1 : INTRODUCTION

In Volume 2 of this report a methodology for the non-linear evaluation of masonry walls subjected to out-of-plane loadings was developed. This model was used for analysis with either the DRAIN-2D or ANSR-II computer programs to evaluate the masonry walls in the Turbine Building, the Ventilation Building and the Reactor Auxiliary Building. Results of these evaluations are presented in Volume 3 of this report.

The most important parameter in the methodology development was shown to be the hysteresis curve peculiar to centrally reinforced elements where the reinforcing is always in tension. It was noted in Volume 2 that the tracking of this moment curvature curve was essential to non-linear modelling of the walls, and the model formulation developed was capable of achieving this.

For the above buildings the models used were formed of assemblages of truss, gap and plane stress elements, typically with over 100 nodes. It was apparent that for the global Fuel Storage Building model it would not be practicable to model all out-of-plane walls with this degree of complexity. Therefore a simpler formulation was developed as discussed in the following section.

B2 : ELEMENT FORMULATION

The form of the moment curvature hysteresis for a centrally reinforced masonry wall is as shown in Figure B1. Although this curve may be approximated as two linear slopes it differs from the hysteresis for doubly reinforced sections in that the loops are not stable over successive cycles but rather grow with each yield excursion as the rebar is subjected to increasing plastic tensile strains.

This form of hysteresis was coded into the standard ANSR-II two dimensional beam model. This was simply achieved by varying the rules which the element follows on inelastic loading and unloading.

Testing of the element was then carried out by comparing the static and dynamic response of a model composed of these simple elements and the more complex model derived according to the methodology of Volume 2. The shape of the hysteresis curve ensured that the correct static cyclic behavior was obtained. To obtain the correct response under dynamic earthquake loads a number of parameter studies were carried out to enable the element properties to be

refined. A comparison of the final single-mass model response and the response for the detailed multi-mass model is given in Figure B2.

Figure B2 shows that the simple model provided a very close match for the amplitude of response to the factored El Centro 1940 earthquake. The frequency content is also similar for the first few cycles but the two responses tend to diverge for an increasing number of cycles. This is because of the very low stiffness over part of the reversing cycle. At this stage of the response the model is very sensitive to small differences in the stiffness formulation.

As the amplitude agreed very well with the complex model and the frequency response only differed after the initial cycles it was concluded that the simple model provided an adequate representation of the out-of-plane walls for the global Fuel Storage Building model. The elements were implemented into the model as discussed in the following section.

B3 : IMPLEMENTATION IN MODEL

The dynamic parameter studies described in the preceding section defined the element properties to be used for the Fuel Storage Building analysis. The following procedures were then adopted for all walls:

a. Each wall was modelled as two beam elements, one elastic and one with the centrally reinforced hysteresis curve at the wall center. Stiffness proportional damping was applied to the elastic element only.

b. Wall yield moments were calculated based on the reinforcing yield strength and wall geometry.

c. Wall stiffness was based on the masonry elastic modulus and 1.5 times the cracked moment of inertia.

d. Wall mass was lumped 50% at the wall center and 25% at the top and bottom supports.

e. Plastic hinge strain hardening was based on 2.15% of the original stiffness.

f. Wall end conditions were as follows:

i. All walls pinned at roof level.

ii. Walls on strip footings were assumed pinned because of possible footing rotation (Elevation 14'-0").

iii. Walls continuous past a diaphragm were assumed to have full moment capacity at the diaphragm position.

iv. Superstructure walls dowelled into the fuel pool were assumed to have a yield moment capacity at the base computed from the area of dowel reinforcement.

g. Wall properties as computed for a 1'-0" strip were factored by the length of wall represented by each element.

h. Where several pairs of beam elements were used to represent portions of the same wall center displacements were constrained to be equal.

These constraints were followed for the 8 vertically spanning out of plane walls in the Fuel Storage Building. From the analysis the output quantities obtained were the beam center displacement, maximum moment and the maximum plastic rotation. These quantities were used to extract detailed material response as discussed in the following section.

B4 : REDUCTION OF RESULTS

The criteria for the evaluation of masonry walls given in Volume 1 of this report provide limits on the maximum steel strain ratio, the maximum masonry compressive stress and the wall stability. The wall stability is obtained from the output displacement plots. To obtain the other two parameters requires the reduction of the output data for the beam element obtained from the ANSR-II analysis.

The steel strain ratio may be obtained from the output plastic rotation given the steel yield stress, the length of the plastic hinge, the wall thickness and the elastic modulus of the reinforcing bar. The relationship so derived is given in Figure B3.

To obtain the masonry compressive stress the assumption is made as given in the criteria that the ultimate condition is a uniform stress over the width of the face shell. The ultimate moment is then:

$$Mu = fm\ t\ b\ (D/2-t/2)$$

where

t = face shell thickness
b = wall section width
D = wall thickness

The ultimate moment, Mu, is obtained from the ANSR-II output and the equation above solved for the masonry stress, fm, as the unknown.

B5 : SUMMARY

It has been shown that use of the hysteresis loop typical to centrally reinfoced sections in the ANSR-II beam element will produce essentially the same response as the complex model developed for the out-of-plane wall evaluation. The amplitude of the response is very similar although the frequency of the response tends to diverge after a number of cycles.

From the parameter studies carried out a number of rules for the implementation of the out-of-plane wall models in the global ANSR-II model were detailed. By consideration of geometry and a knowledge of the material properties detailed material stresses and deformations could be obtained from the output quantities for comparison with criteria limits.

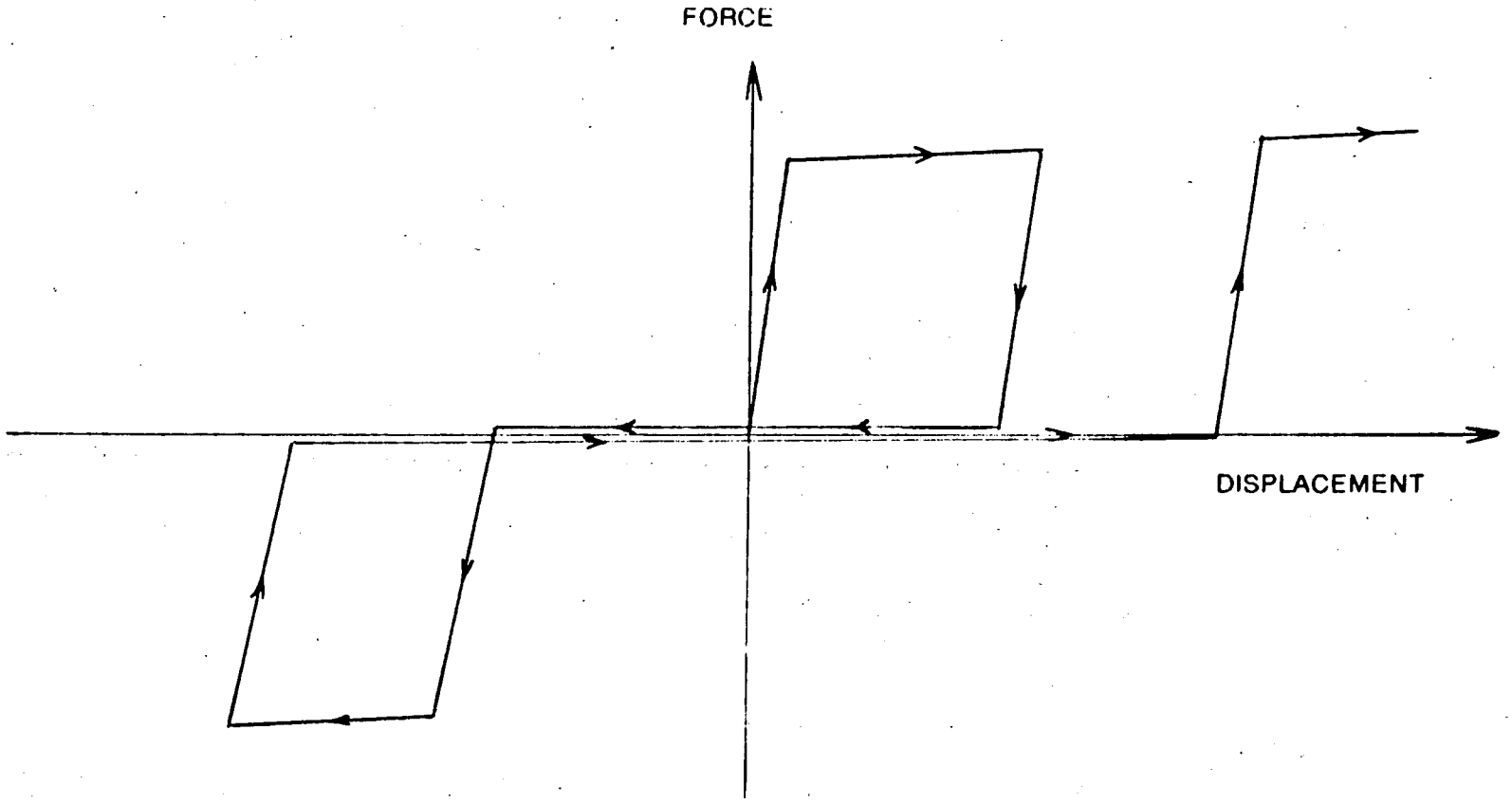

FIGURE B1 : HYSTERESIS FOR CONTRALLY REINFORCED WALLS

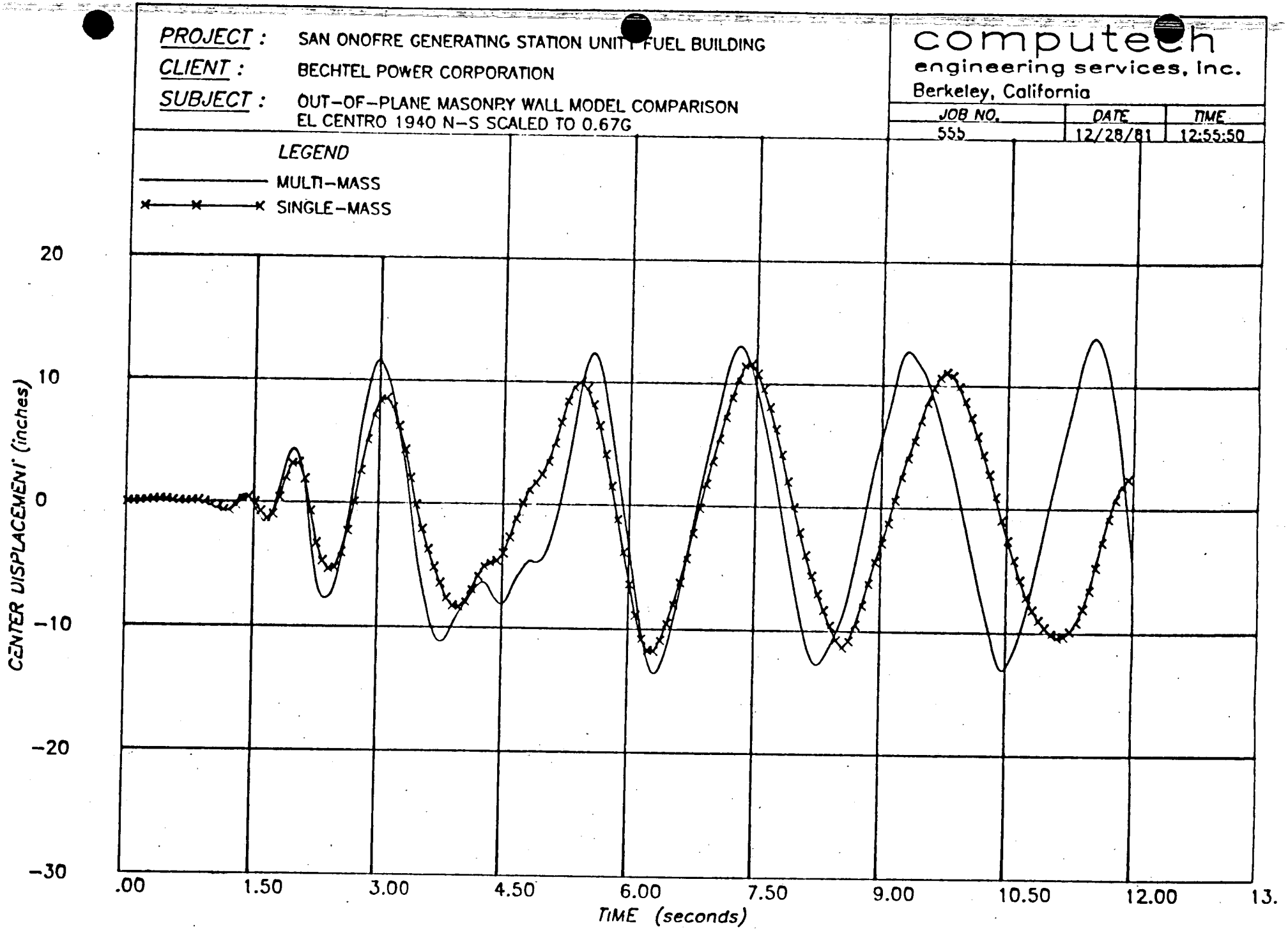

FIGURE B2 : COMPARISON OF SIMPLE AND COMPLEX MASONRY WALL MODELS

Define :

ε_u = bar ultimate strain

ε_y = bar yield strain

Δ_u = bar ultimate extension

Δ_y = bar yield extension

θ_y = yield rotation

θ_u = plastic rotation

= $(\theta_u - \theta_y)$

Δ_{pl} = plastic bar extension

= $(\Delta_u - \Delta_y)$

From Geometry:

$\Delta_y = \theta_y D/2$

$\Delta_{pl} = \theta_{pl} D/2$

$\varepsilon_u = \Delta_u / Lp$

$\varepsilon_y = \Delta_y / Lp$

$$\therefore \frac{\varepsilon_u}{\varepsilon_y} = \frac{\Delta_u}{\Delta_y}$$

$$= \frac{\Delta_{pl} + \Delta_y}{\Delta_y}$$

$$= \frac{\theta_{pl} D/2 + \theta_y D/2}{\theta_y D/2}$$

$$= 1 + \theta_{pl}/\theta_y$$

$\theta_y = 2\Delta_y/D = (F_y Lp/E)\ 2/D$

$$\frac{\varepsilon_u}{\varepsilon_y} = 1 + \theta_{pl}(ED/2F_yLp)$$

$E/F_y = 750$

$D = 7.625"$

therefore,

$$\frac{\varepsilon_u}{\varepsilon_y} = 1 + 2859(\theta_{pl}/Lp)$$

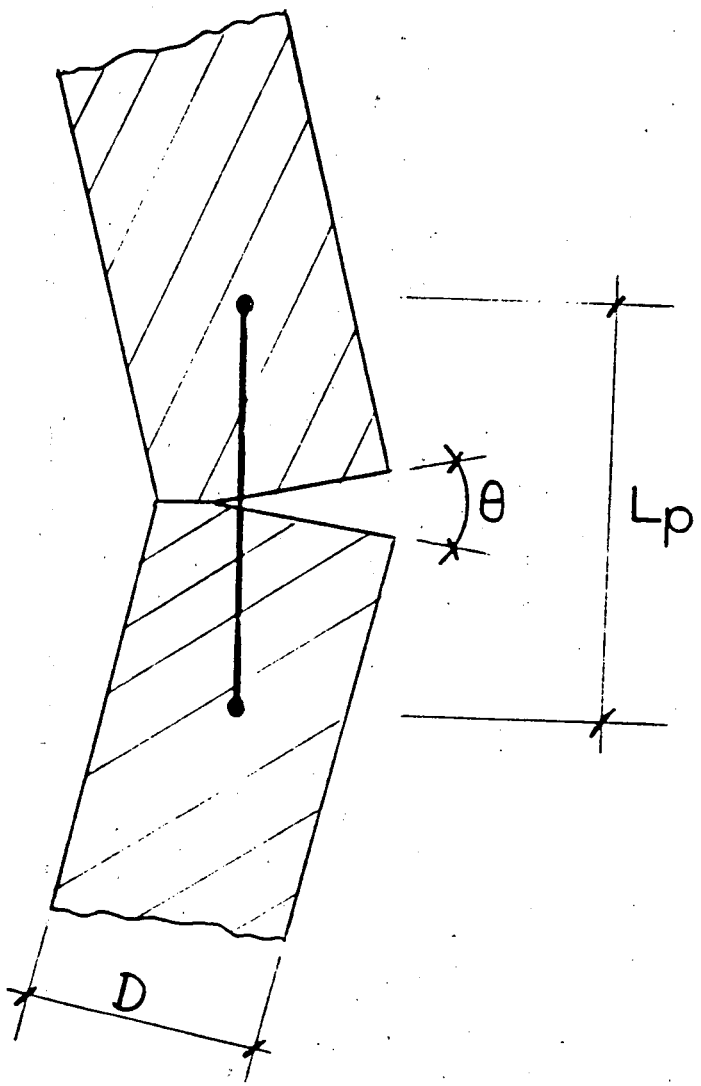

FIGURE B3 : DERIVATION OF STEEL STRAIN RATIO

APPENDIX C: DETAILED RESULTS

Y(N-S) EARTHQUAKE: El Centro 1940 N-S. Scaled 1.57, 0.67g Peak

X(E-W) EARTHQUAKE: El Centro 1940 E-W. Scaled 1.57

LOCATION	DISPLACEMENT (inches)	
	MAXIMUM	MINIMUM
ROOF		
N-W Corner	1.222	-1.011
S-W Corner	1.203	-0.984
N-E Corner	1.269	-1.113
S-E Corner	1.288	-1.073
TOP OF FUEL POOL		
N-W Corner	-0.692	-0.640
S-W Corner	-0.695	-0.643
N-E Corner	0.739	-0.678
S-E Corner	-0.740	-0.679
BASE OF FUEL POOL		
N-W Corner	0.054	-0.075
S-W Corner	0.054	-0.075
N-E Corner	0.084	-0.107
S-E Corner	0.084	-0.107

ANALYSIS NUMBER: 1

EARTHQUAKE: El Centro

PRINCIPAL COMPONENT DIRECTION: Y

TABLE C1: MAXIMUM DISPLACEMENTS

("AS-MODIFIED" STRUCTURE)

WALL NUMBER	SHEAR STRESS (p.s.i)	SHEAR STRAIN	RATIO OF MAXIMUM STRAIN TO ALLOWABLE
FB-1	24.08	0.00017	0.0644
FB-2	91.25	0.00065	0.2462
FB-3	91.25	0.00043	0.1629
FB-4	-44.88	-0.00032	0.1212
FB-5	-33.22	-0.00024	0.0909
FB-6	-32.92	-0.00023	0.0871
FB-7	166.7	0.00277	0.5246
FB-8	-113.6	-0.00110	0.4167
FB-9	132.4	0.00159	0.6023
FB-10	68.09	0.00048	0.1818

ANALYSIS NUMBER: 1

EARTHQUAKE: El Centro

PRINCIPAL COMPONENT DIRECTION: Y

TABLE C2 : MAXIMUM IN-PLANE WALL RESPONSE
("AS-MODIFIED" STRUCTURE)

WALL	STEEL STRAIN RATIO		MASONRY STRESS	CENTER DISPLACEMENT
	CENTER *	END *	fm (p.s.i.)	(inches)
FB-1	20.99	24.57	655.9	10.56
FB-2	5.35	8.86	656.0	3.63
FB-3	5.49	9.51	655.9	3.92
FB-4			Horizontal	Spanning
FB-5	11.55	12.30	655.9	6.18
FB-6	22.95	26.44	655.3	11.19
FB-7			Horizontal	Spanning
* FB-8	.60	.36	392.1	.55
* FB-9	.59	.31	384.0	.49
* FB-10	.94	.71	619.1	1.07

* (a) "End" is at El 31'-0"

(b) "Center" is maximum of 2 spans

ANALYSIS NUMBER: 1

EARTHQUAKE: El Centro

PRINCIPAL COMPONENT DIRECTION: Y

TABLE C3: MAXIMUM OUT-OF-PLANE MASONRY WALL RESPONSE

("AS-MODIFIED" STRUCTURE)

WALL NUMBER	LOCATION	SHEAR STRESS (lb/ft)	TENSION (lb/ft)
FB-1	Roof	646.6	257.9
FB-2	Roof	959.8	232.8
FB-3	Roof	355.0	113.3
FB-4	Roof	273.6	-
FB-5	Roof	675.8	227.2
FB-6	Roof	954.8	214.7
FB-7	Roof	1625.2	-
FB-8	El 42'-0"	1983.3	329.4
FB-9	El 42'-0"	921.4	112.3
FB-10	El 42'-0"	1517.1	370.7
FB-8	El 42'-0"	-	394.8
FB-9	El 42'-0"	-	330.5
FB-10	El 42'-0"	-	910.7

ANALYSIS NUMBER: 1

EARTHQUAKE: El Centro

PRINCIPAL COMPONENT DIRECTION: Y

TABLE C4: MAXIMUM CONNECTION FORCES

("AS-MODIFIED" STRUCTURE)

WALL NUMBER	LOCATION	SHEAR STRESS (lb/ft)	RATIO OF MAXIMUM STRESS TO ALLOWABLE
FB-1	Roof	919.2	0.3103
FB-2	Roof	1340.6	0.4525
FB-3	Roof	848.0	0.2862
FB-4	Roof	691.3	0.2334
FB-5	Roof	903.7	0.3050
FB-6	Roof	2444.3	0.8251
FB-7	Roof	2444.3	0.8251
FB-8	El 42'-0"	2373.8	0.2316
FB-9	El 42'-0"	2610.3	0.2546
FB-10	El 42'-0"	2610.3	0.2546

ANALYSIS NUMBER: 1

EARTHQUAKE: El Centro

PRINCIPAL COMPONENT DIRECTION: Y

TABLE C5 : MAXIMUM DIAPHRAGM FORCES
("AS-MODIFIED" STRUCTURE)

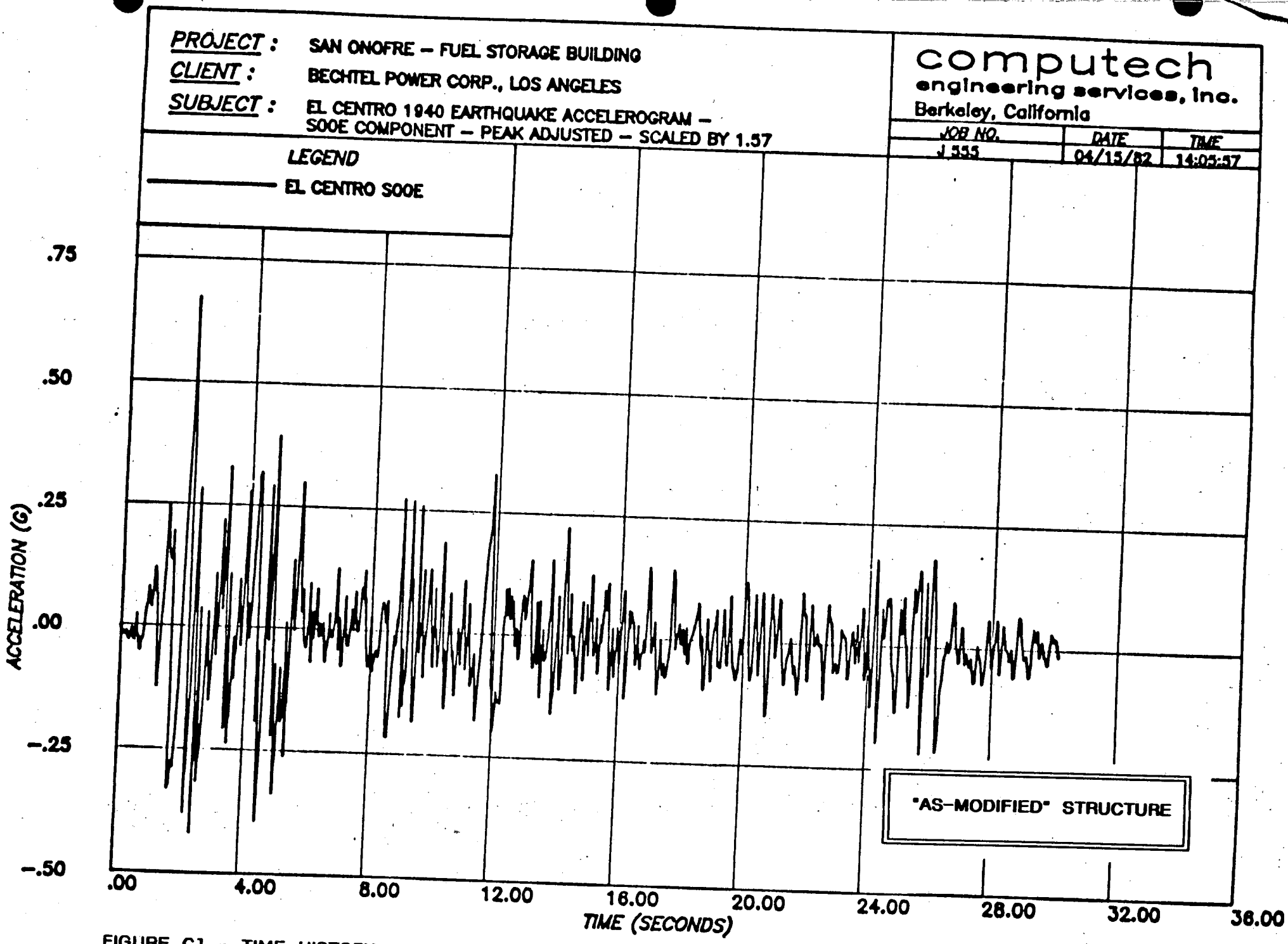

FIGURE C1 – TIME HISTORY AS SCALED [Y(N-S)]

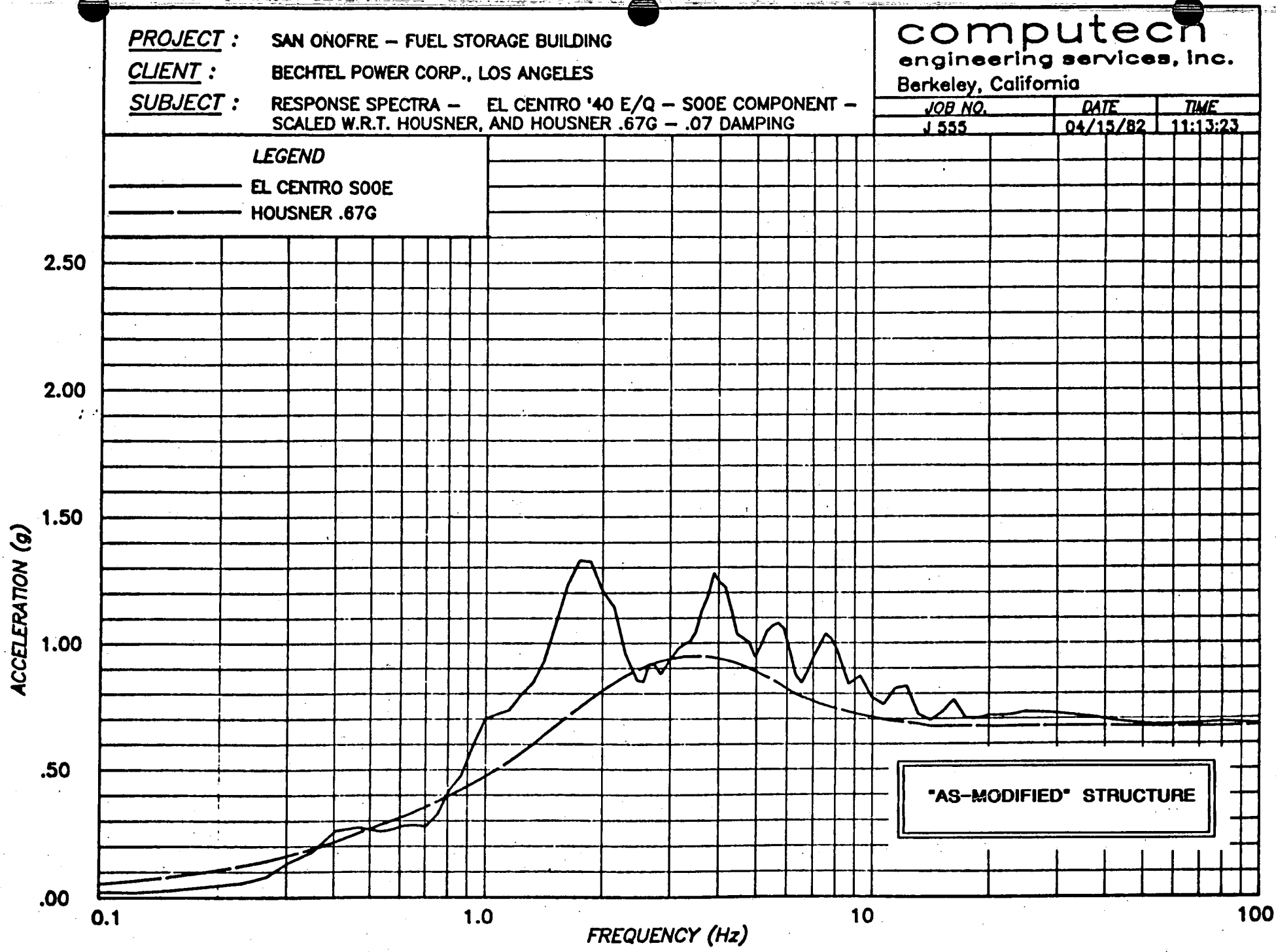

FIGURE C2 – RESPONSE SPECTRUM [Y(N-S)]

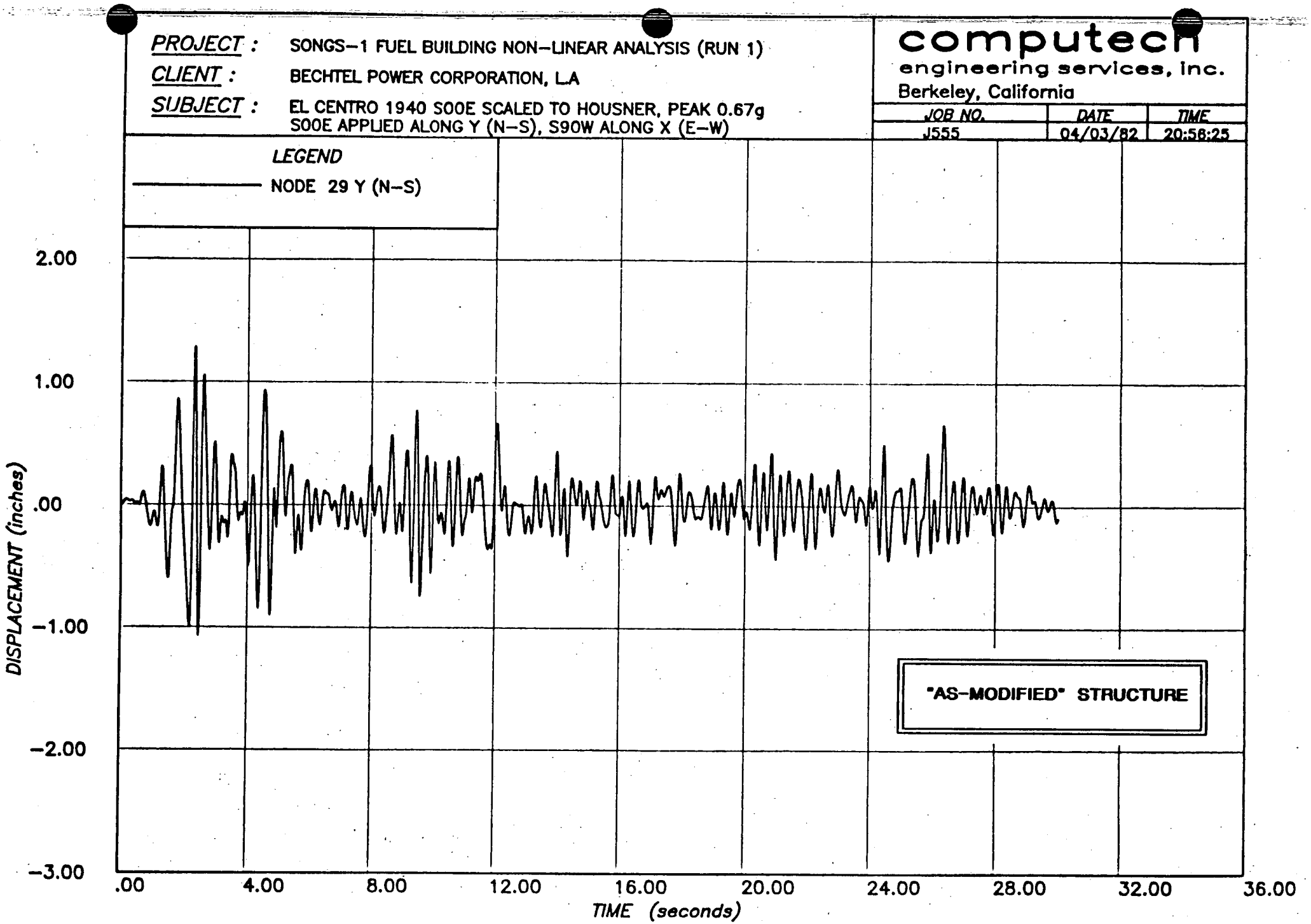

FIGURE C3 – ROOF DISPLACEMENT

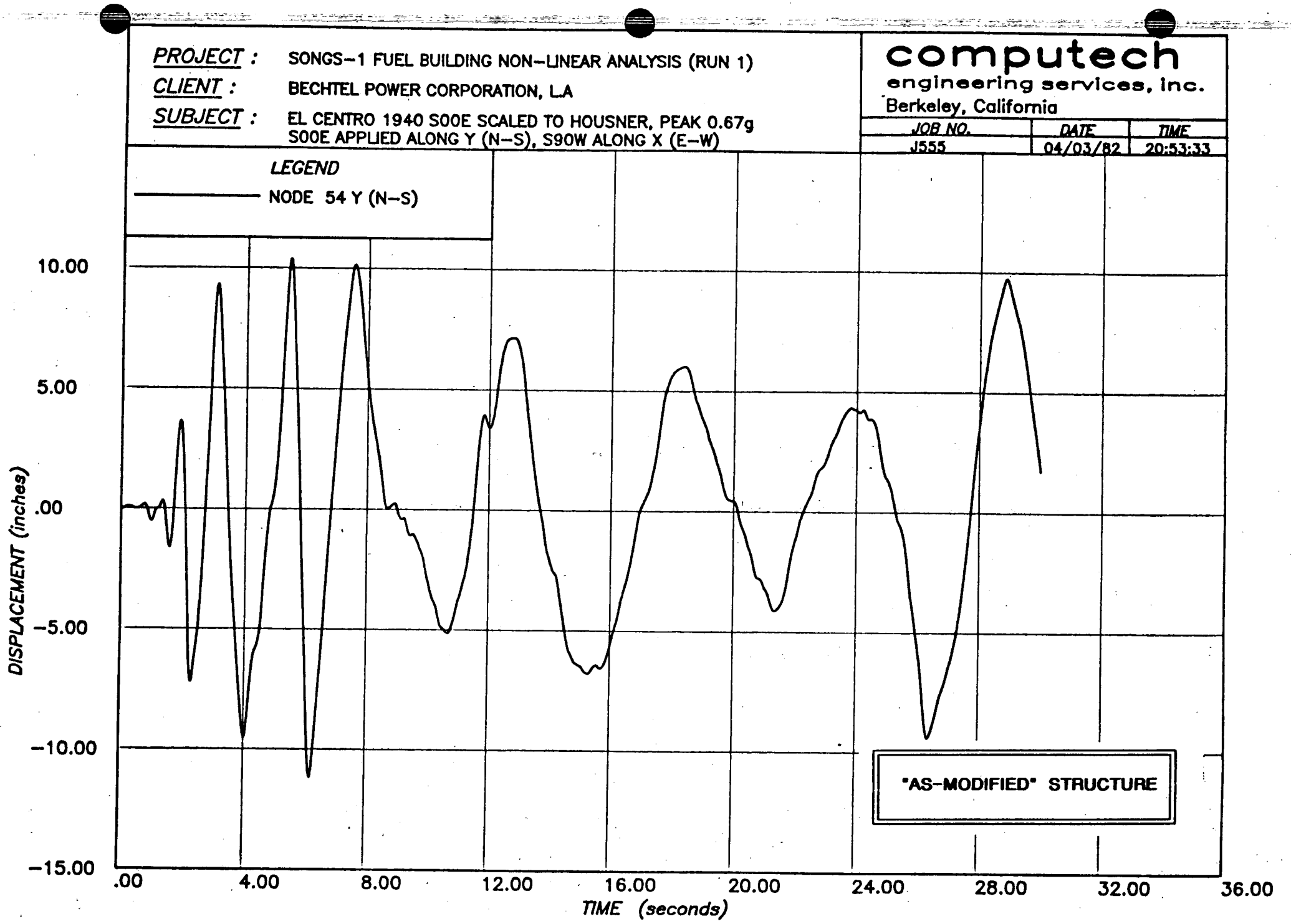

FIGURE C4 - OUT-OF-PLANE WALL DISPLACEMENTS - CENTER

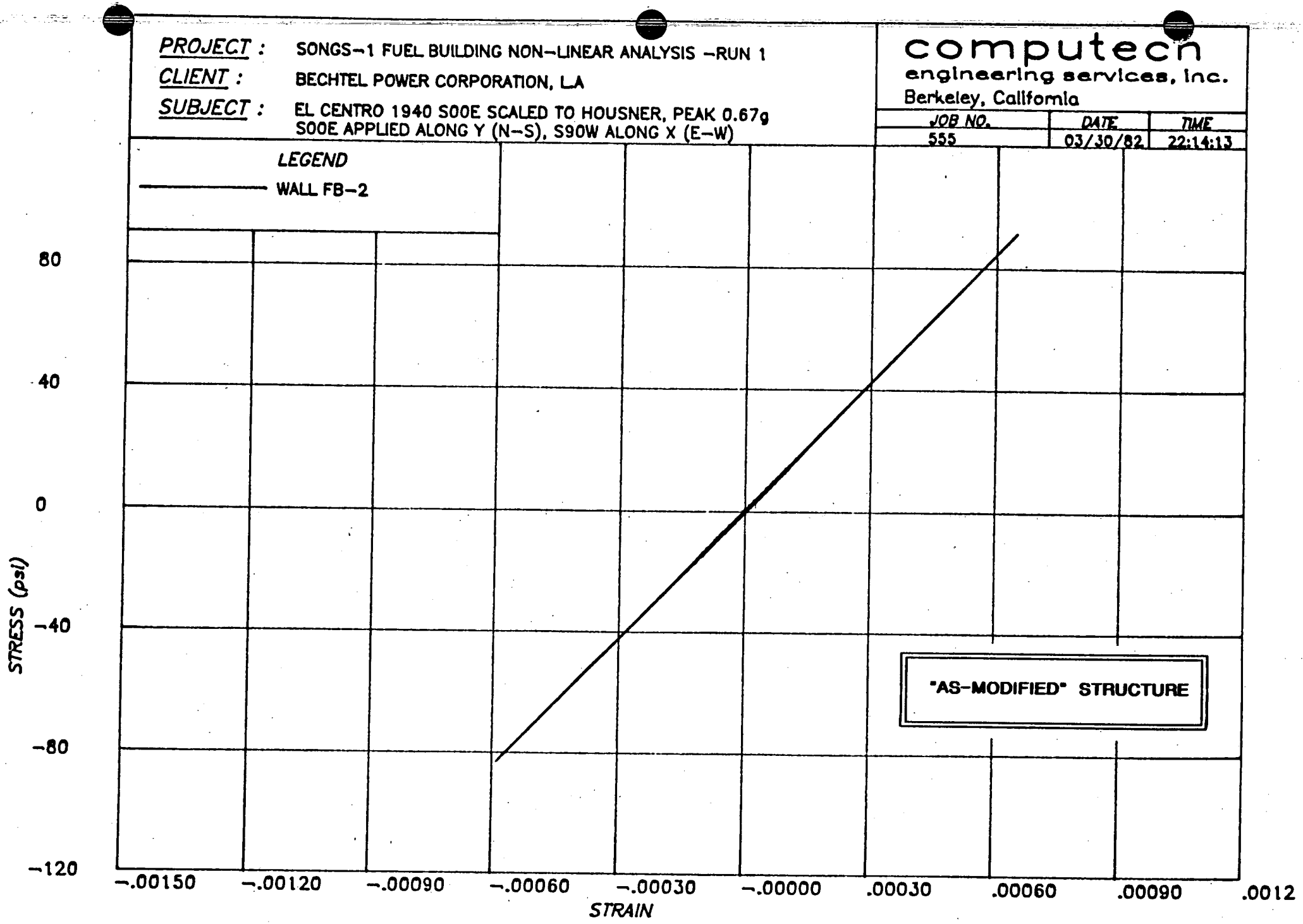

FIGURE C5 - IN-PLANE WALL STRESS-STRAIN - EL 42'

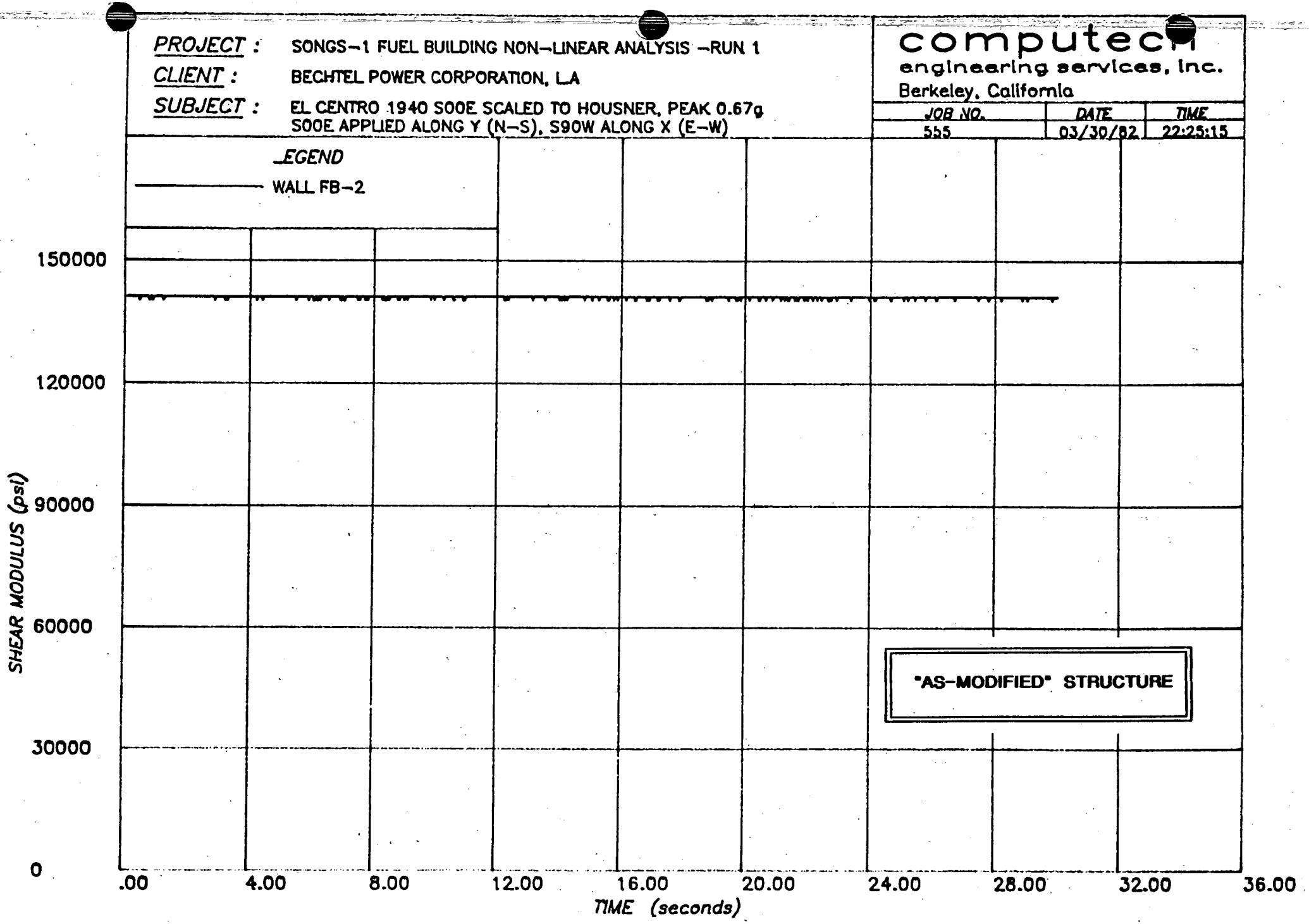

FIGURE C6 - IN-PLANE WALL STIFFNESS - EL 42'

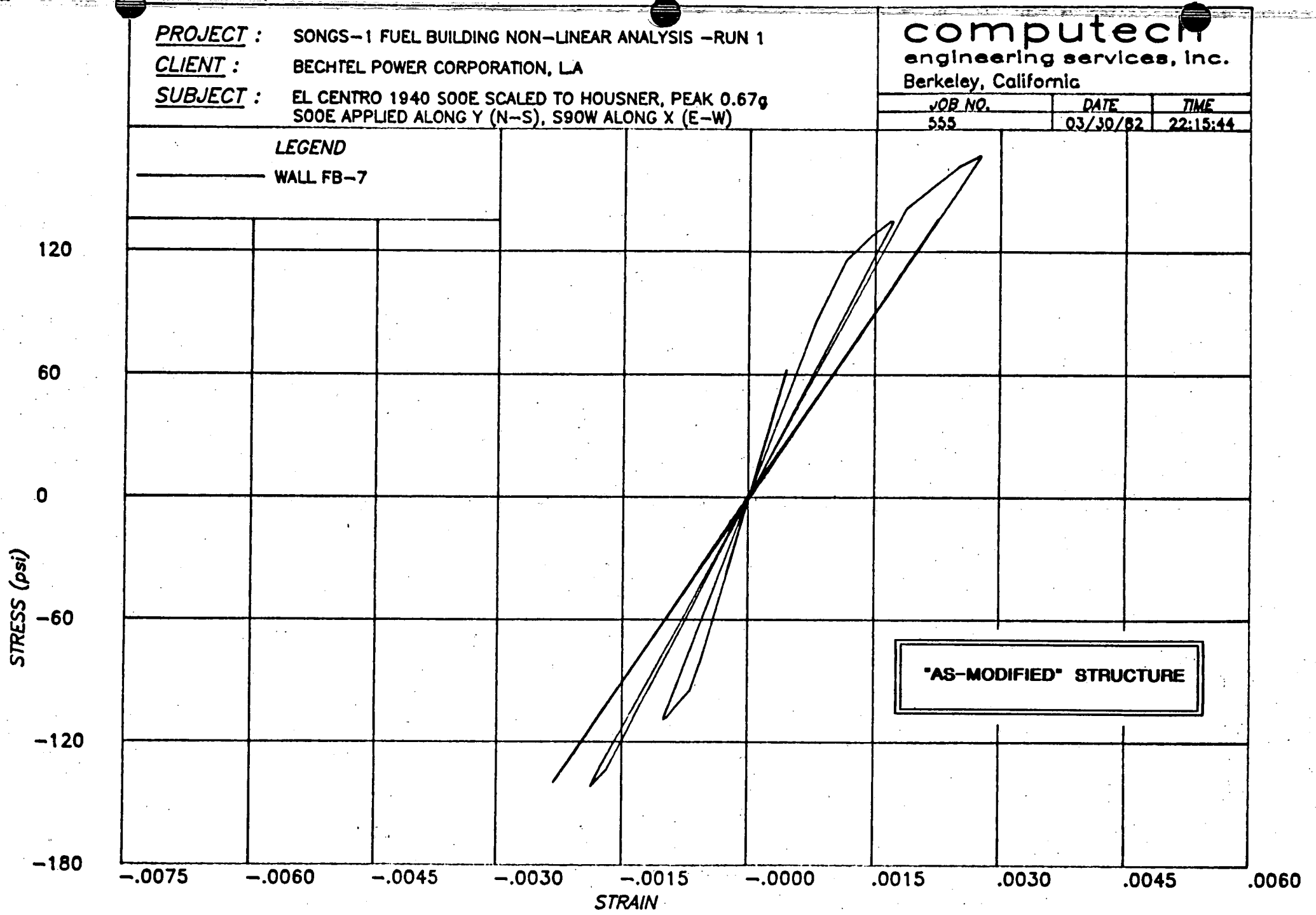

FIGURE C7 - IN-PLANE WALL STRESS-STRAIN - EL 42'

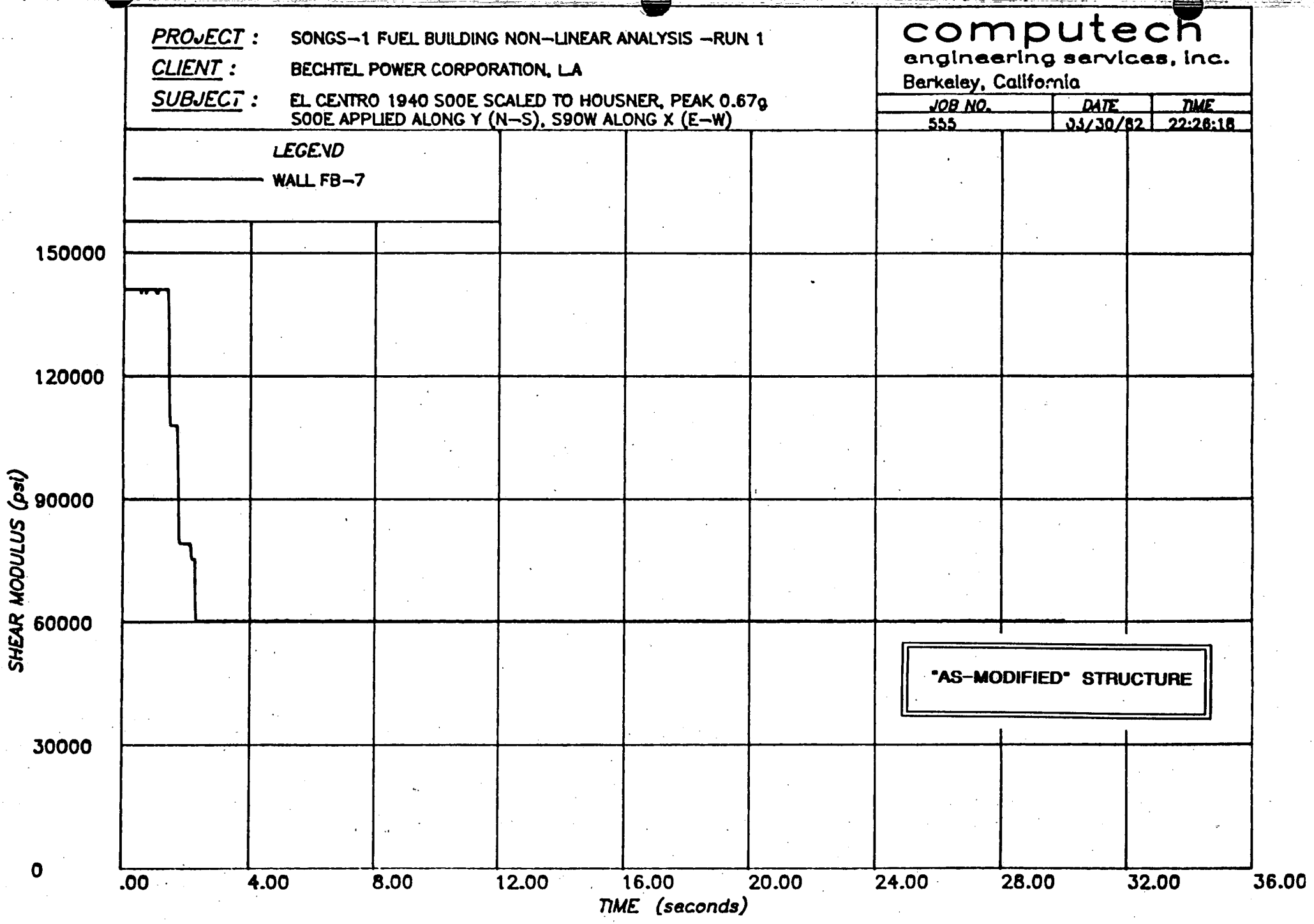

FIGURE C8 - IN-PLANE WALL STIFFNESS - EL 42'

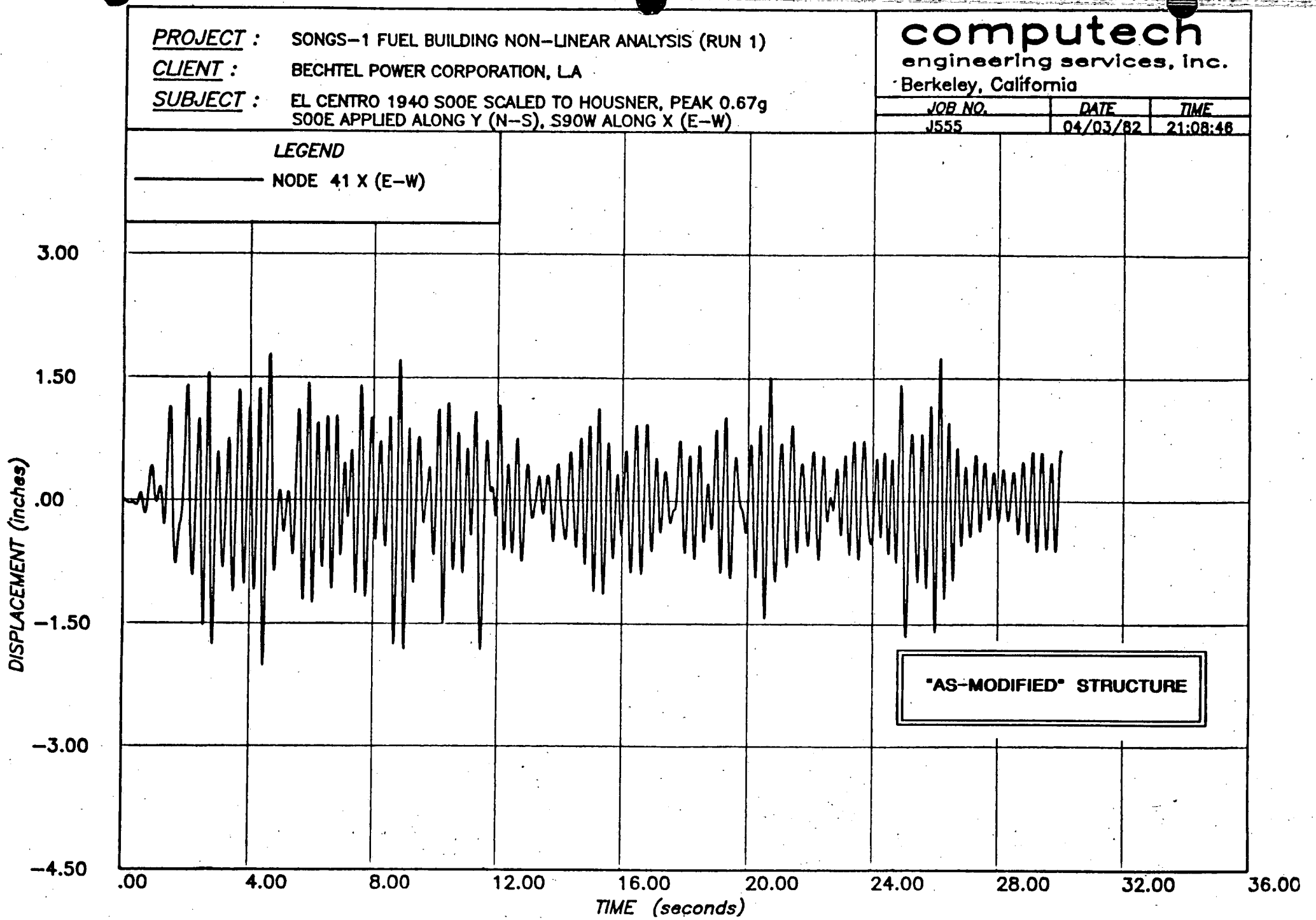

FIGURE C9 - DISPLACEMENT AT ROOF OPENING - EAST

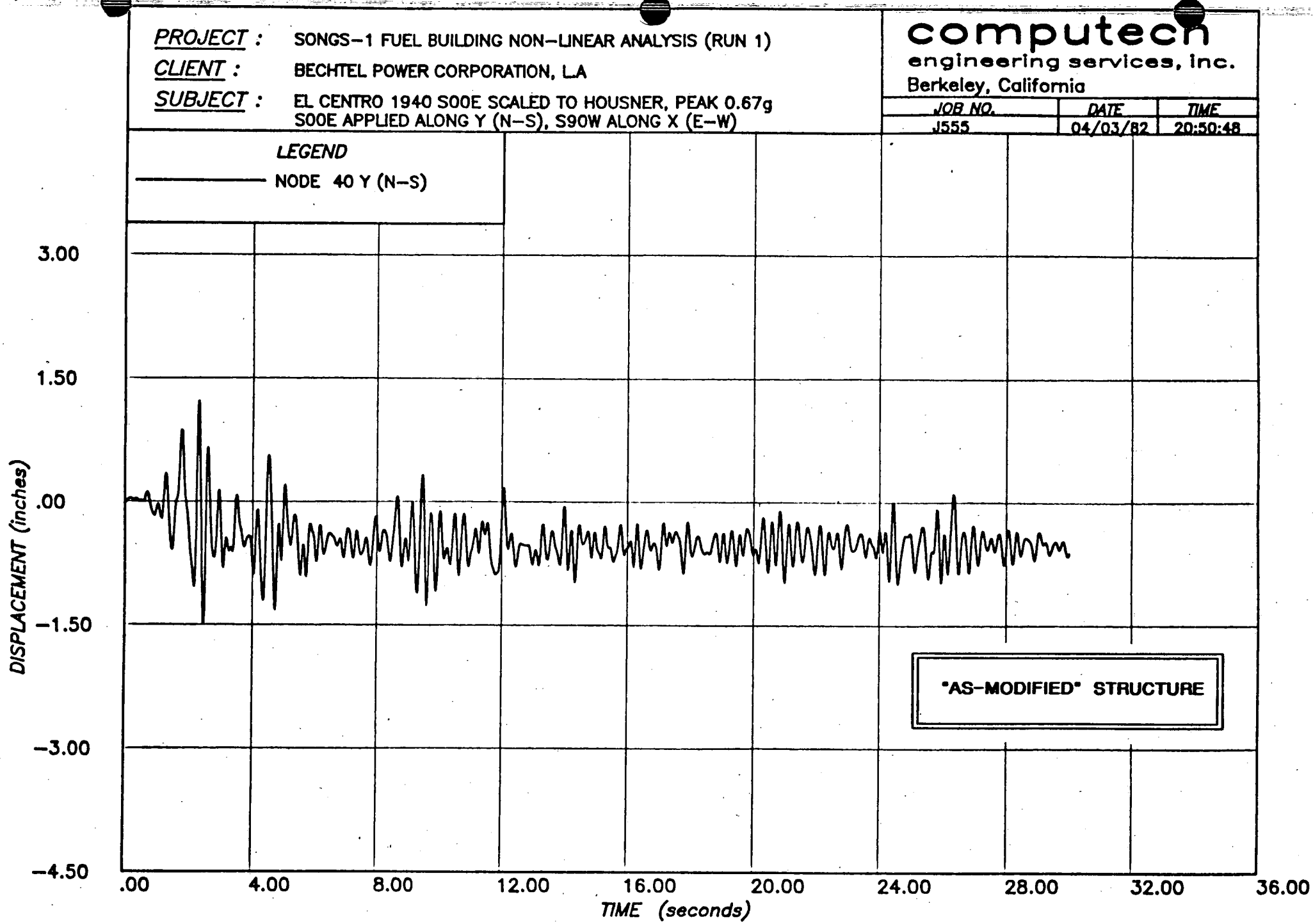

FIGURE C10 - DISPLACEMENT AT ROOF OPENING - SOUTH

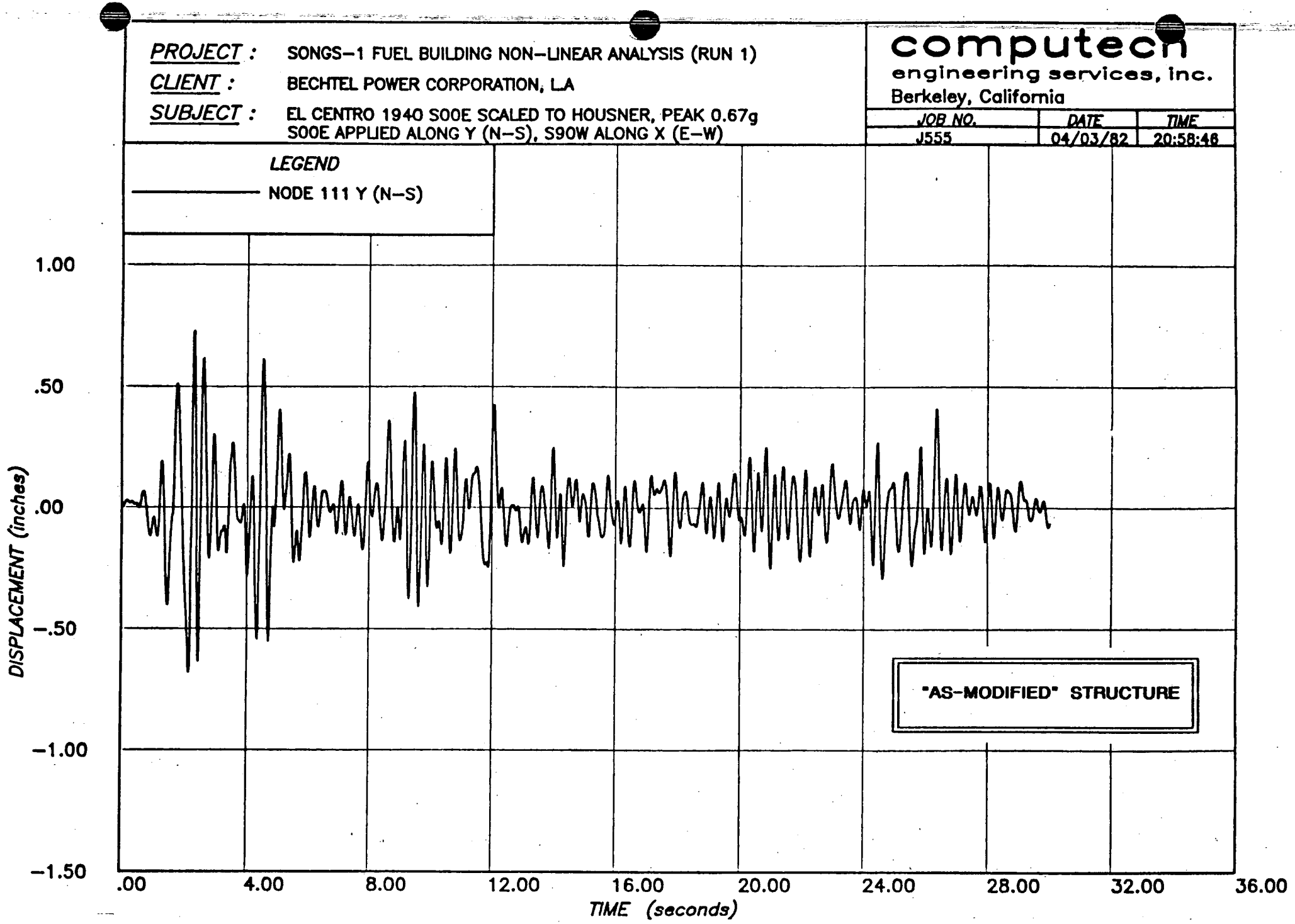

FIGURE C11 - TOP OF POOL: DISPLACEMENT

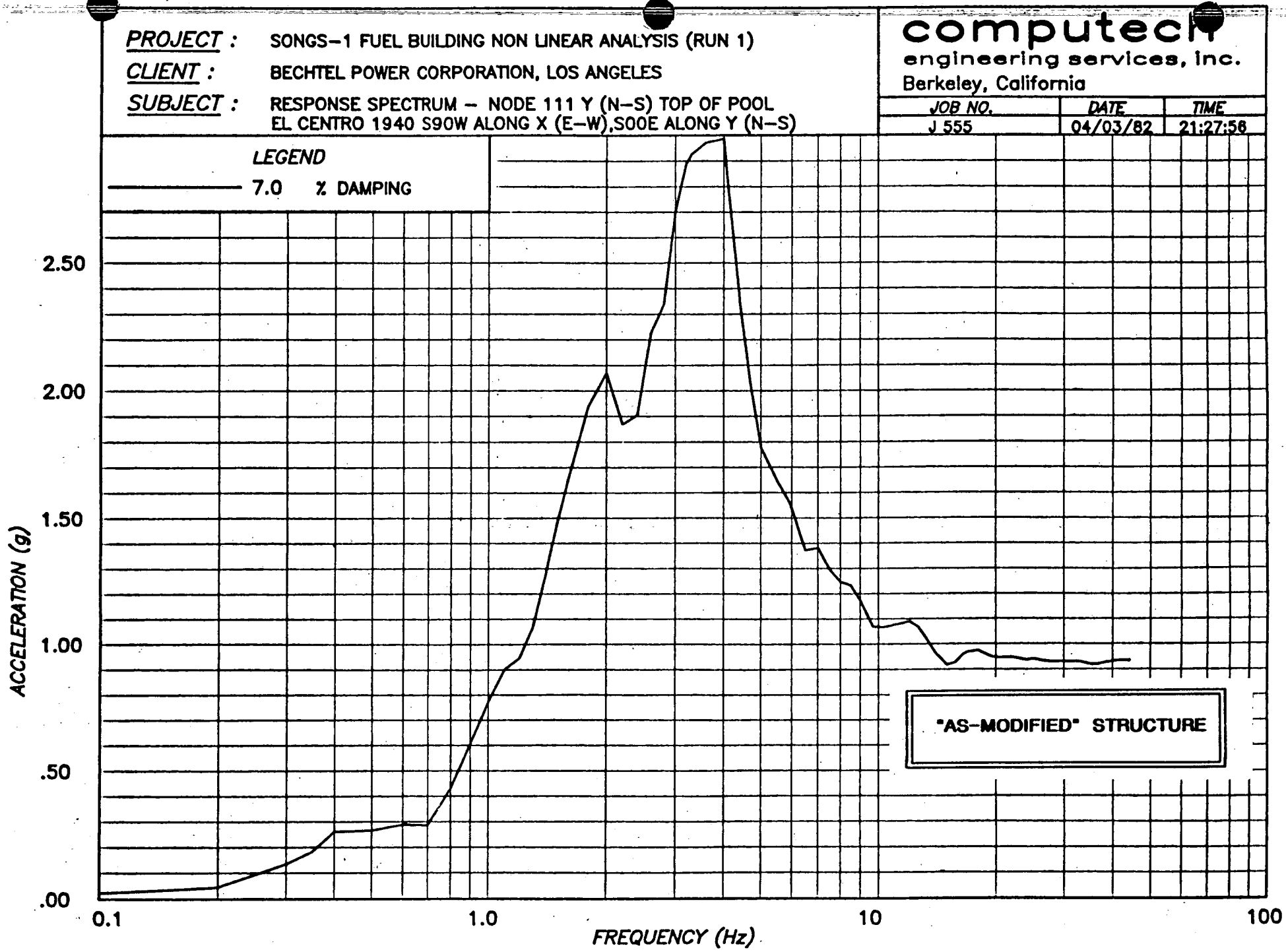

FIGURE C12 - TOP OF POOL: RESPONSE SPECTRUM - HORIZONTAL

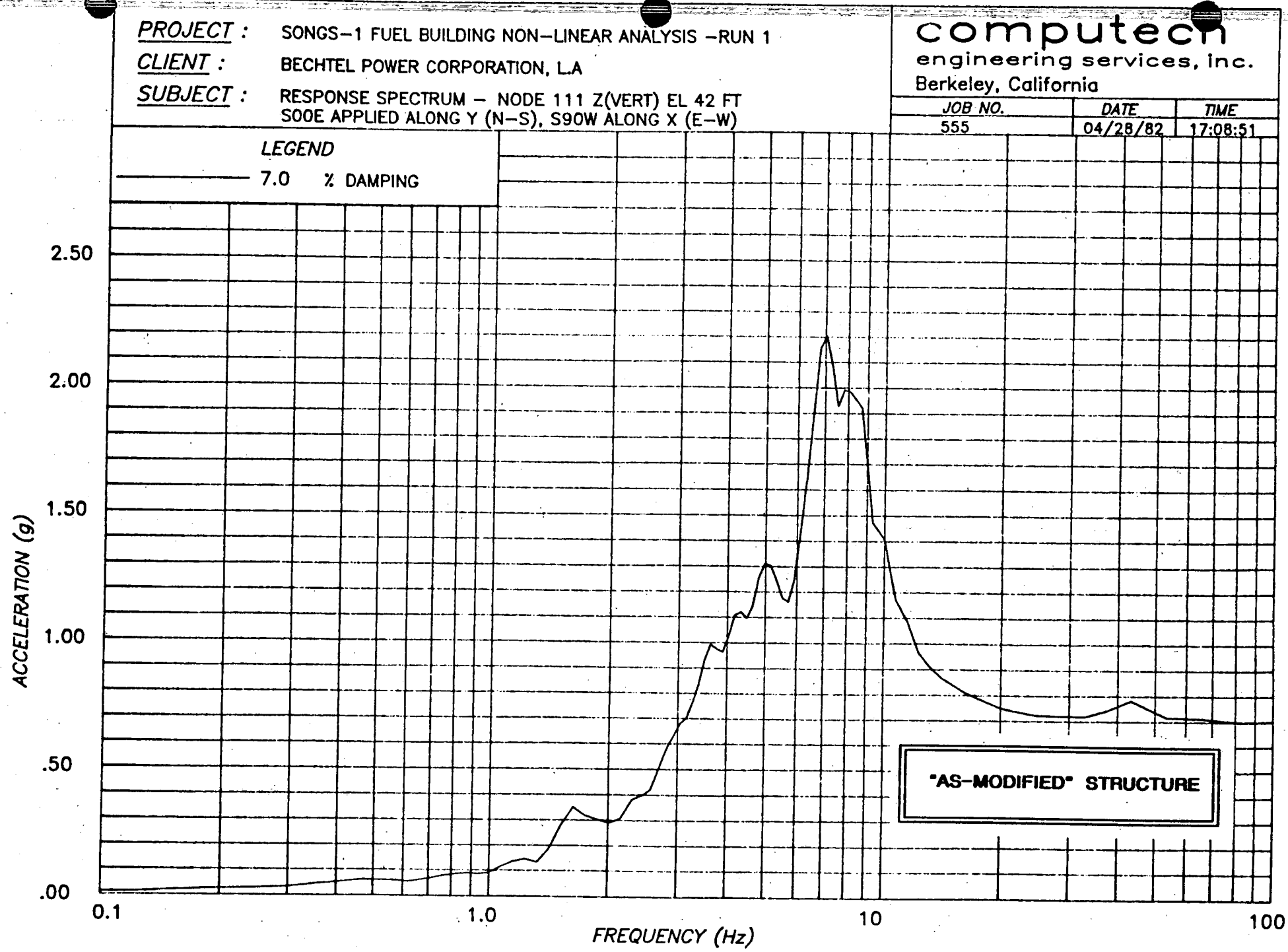

FIGURE C13 - TOP OF POOL: RESPONSE SPECTRUM - VERTICAL

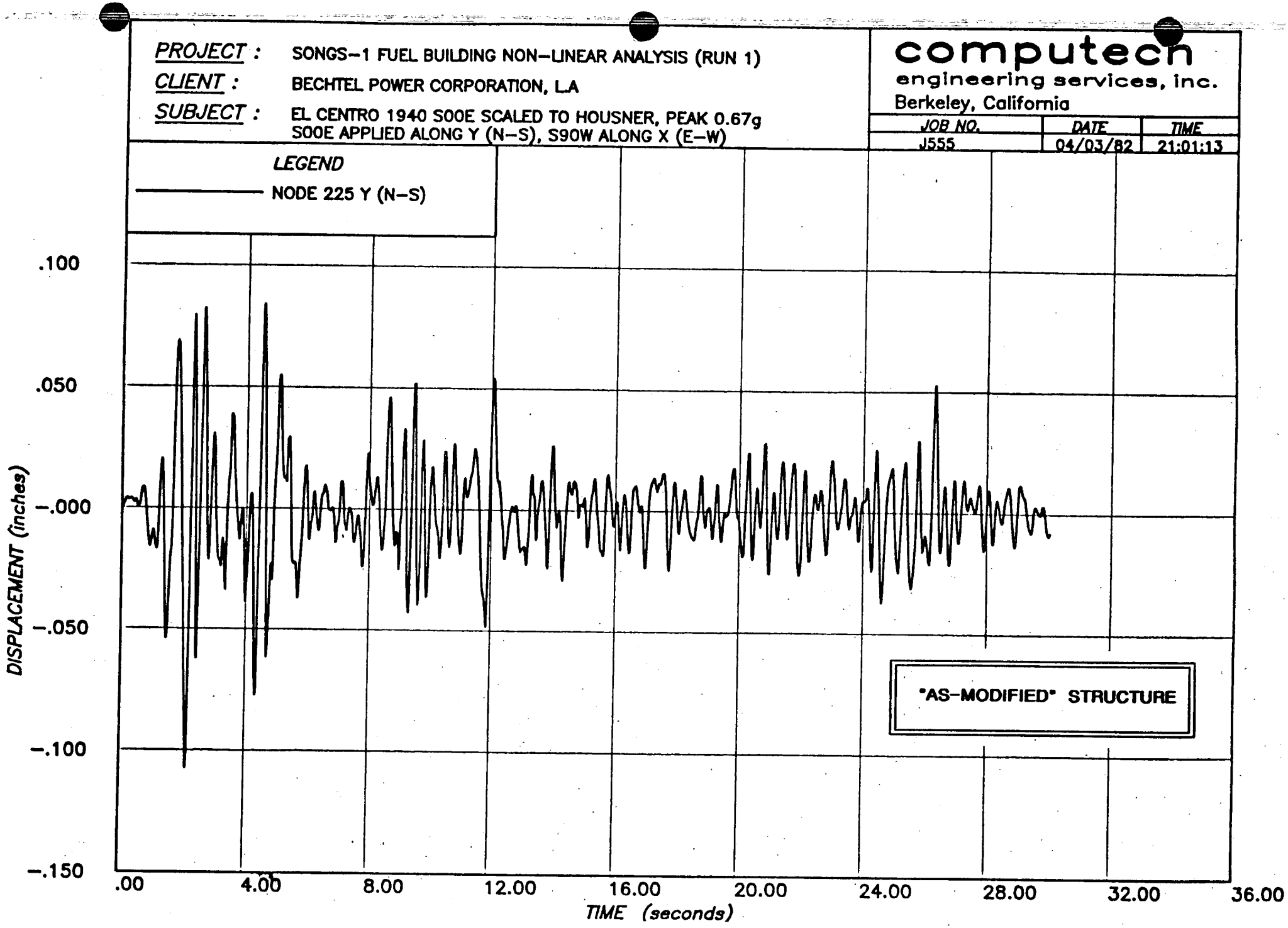

FIGURE C14 – BASE OF POOL: DISPLACEMENT

APPENDIX D: DETAILED RESULTS

Y(N-S) EARTHQUAKE: El Centro 1940 E-W, Scaled 1.57

X(E-W) EARTHQUAKE: El Centro 1940 N-S, Scaled 1.57, Peak 0.67g

LOCATION	DISPLACEMENT (inches)	
	MAXIMUM	MINIMUM
ROOF		
N-W Corner	0.502	-0.502
S-W Corner	0.463	-0.509
N-E Corner	0.481	-0.502
S-E Corner	0.492	-0.499
TOP OF FUEL POOL		
N-W Corner	0.277	-0.311
S-W Corner	0.289	-0.326
N-E Corner	0.277	-0.311
S-E Corner	0.288	-0.325
BASE OF FUEL POOL		
N-W Corner	0.064	-0.098
S-W Corner	0.066	-0.102
N-E Corner	0.064	-0.098
S-E Corner	0.067	-0.102

ANALYSIS NUMBER 2

EARTHQUAKE: El Centro

PRINCIPAL COMPONENT DIRECTION: X

TABLE D1: MAXIMUM DISPLACEMENTS

("AS-MODIFIED" STRUCTURE)

WALL NUMBER	SHEAR STRESS (p.s.D	SHEAR STRAIN	RATIO OF MAXIMUM STRAIN TO ALLOWABLE
FB-1	38.05	0.00027	0.1023
FB-2	66.22	0.00047	0.1780
FB-3	33.61	0.00024	0.0909
FB-4	61.13	0.00043	0.1629
FB-5	35.46	0.00025	0.0947
FB-6	48.78	0.00035	0.1326
FB-7	135.4	0.00169	0.3201
FB-8	95.58	0.00072	0.2727
FB-9	111.8	0.00106	0.4015
FB-10	-93.33	-0.00067	0.2538

ANALYSIS NUMBER: 2

EARTHQUAKE: El Centro

PRINCIPAL COMPONENT DIRECTION: X

TABLE D2 : MAXIMUM IN-PLANE WALL RESPONSE
("AS-MODIFIED" STRUCTURE)

WALL	STEEL STRAIN RATIO		MASONRY STRESS	CENTER DISPLACEMENT
	CENTER	END	fm (p.s.i.)	(inches)
FB-1	9.70	13.57	655.9	5.65
FB-2	4.79	8.07	656.0	3.11
FB-3	15.49	19.20	655.9	8.11
FB-4				
FB-5	4.74	5.55	655.9	2.95
FB-6	9.70	13.56	655.3	5.66
FB-7				
FB-8	1.24	.64	655.9	.98
FB-9	1.11	.54	655.9	.87
FB-10	.49	.38	323.5	.64

ANALYSIS NUMBER: 2

EARTHQUAKE: El Centro

PRINCIPAL COMPONENT DIRECTION: X

TABLE D3: MAXIMUM OUT-OF-PLANE MASONRY WALL RESPONSE

("AS-MODIFIED" STRUCTURE)

WALL NUMBER	LOCATION	SHEAR STRESS (lb/ft)	TENSION (lb/ft)
FB-1	Roof	501.2	257.8
FB-2	Roof	739.2	233.8
FB-3	Roof	180.3	113.6
FB-4	Roof	208.9	-
FB-5	Roof	495.5	225.4
FB-6	Roof	1133.0	214.6
FB-7	Roof	1425.9	-
FB-8	El 42'-0"	2593.9	656.7
FB-9	El 42'-0"	770.1	155.8
FB-10	El 42'-0"	1761.1	534.5
FB-8	El 42'-0"	-	669.7
FB-9	El 42'-0"	-	558.1
FB-10	El 42'-0"	-	519.8

ANALYSIS NUMBER: 2

EARTHQUAKE: El Centro

PRINCIPAL COMPONENT DIRECTION: X

TABLE D4: MAXIMUM CONNECTION FORCES

("AS-MODIFIED" STRUCTURE)

WALL NUMBER	LOCATION	SHEAR STRESS (lb/ft)	RATIO OF MAXIMUM STRESS TO ALLOWABLE
FB-1	Roof	730.2	0.2465
FB-2	Roof	880.8	0.2973
FB-3	Roof	430.7	0.1454
FB-4	Roof	527.9	0.1782
FB-5	Roof	693.3	0.2340
FB-6	Roof	1672.7	0.5646
FB-7	Roof	1672.7	0.5646
FB-8	El 42'-0"	3780.0	0.3687
FB-9	El 42'-0"	3670.3	0.3580
FB-10	El 42'-0"	2080.1	0.2029

ANALYSIS NUMBER: 2

EARTHQUAKE: El Centro

PRINCIPAL COMPONENT DIRECTION: X

TABLE D5 : MAXIMUM DIAPHRAGM FORCES

("AS-MODIFIED" STRUCTURE)

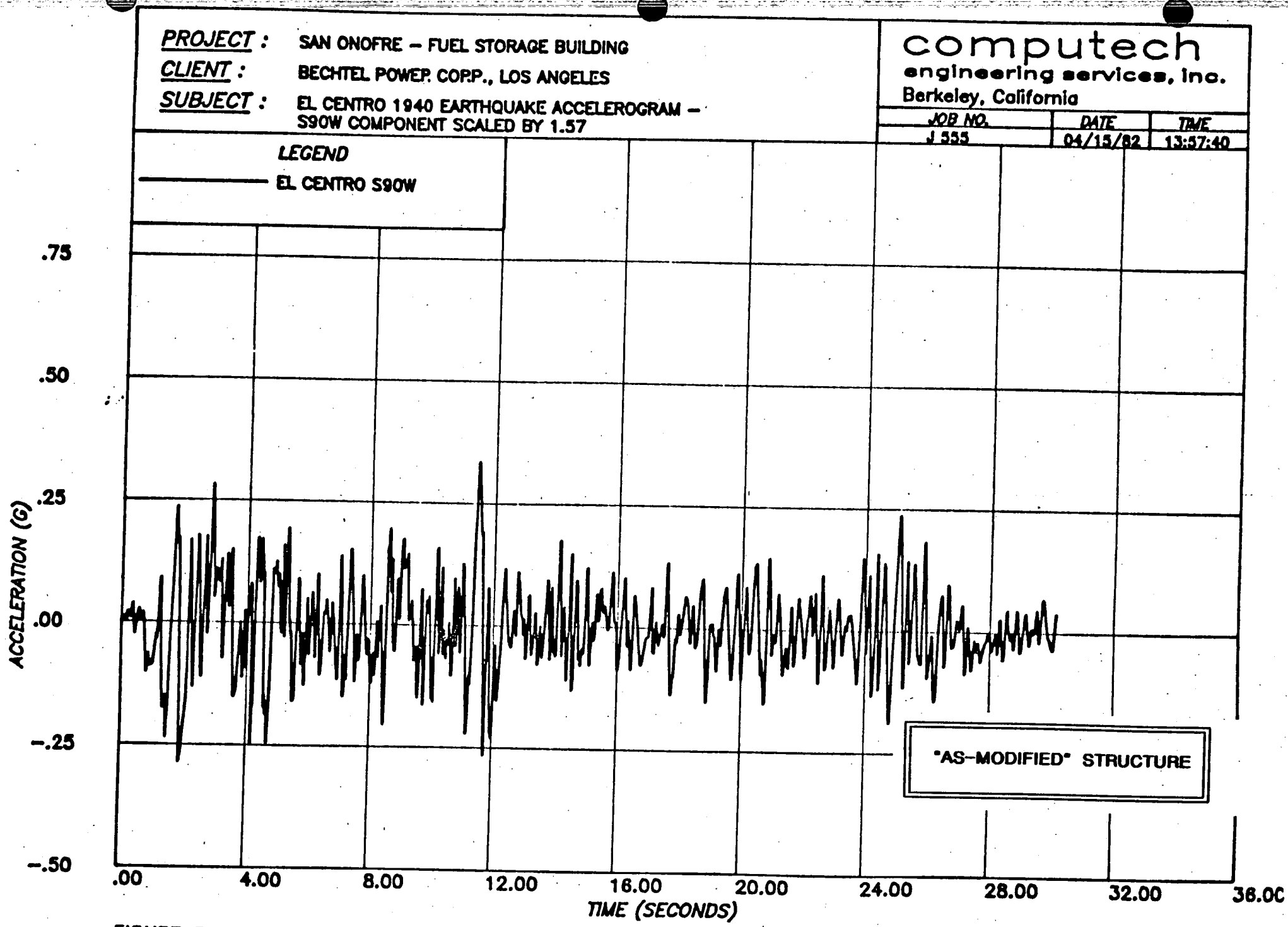

FIGURE D1 – TIME HISTORY AS SCALED [Y(N-S)]

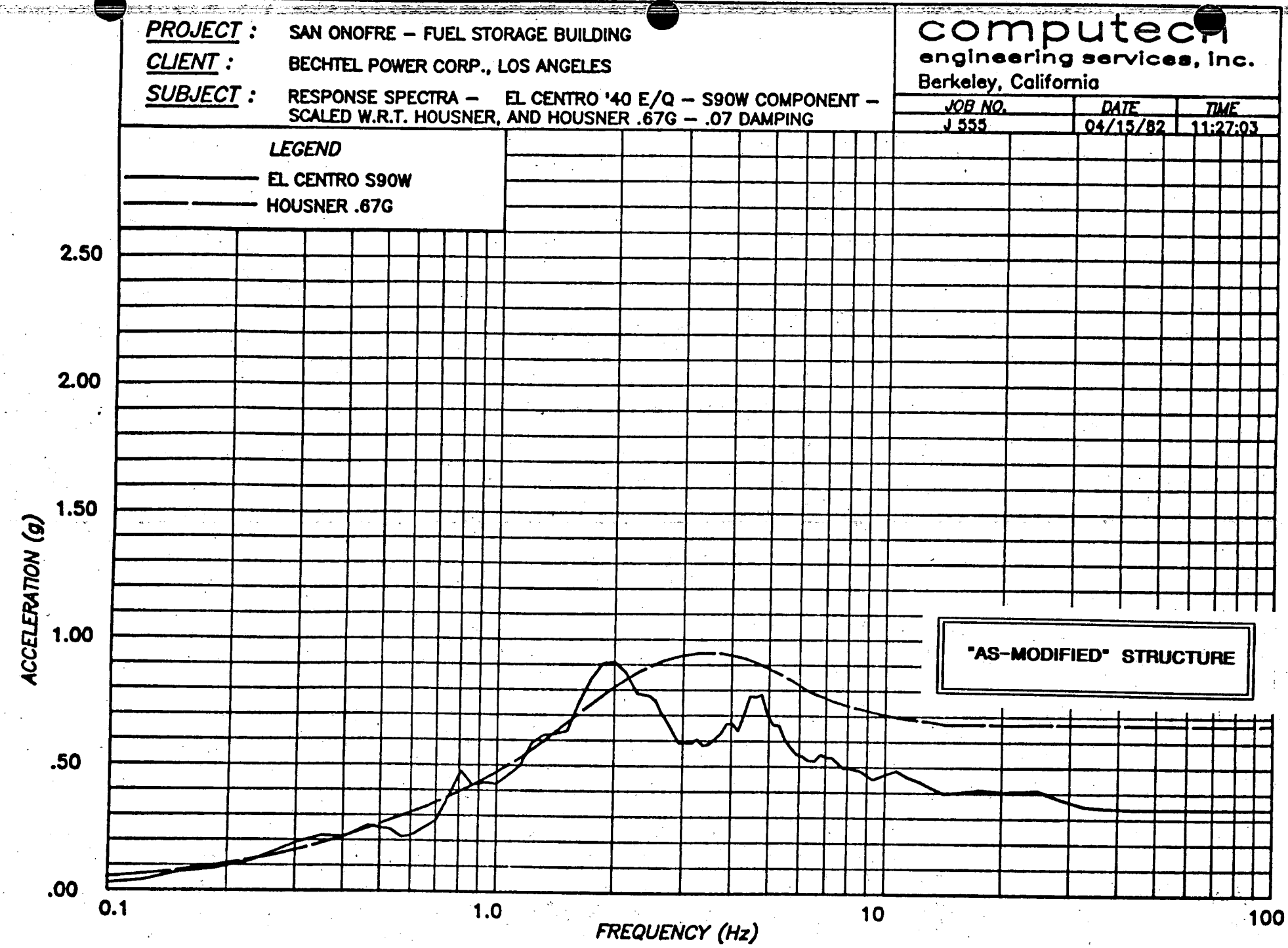

FIGURE D2 – RESPONSE SPECTRUM [Y(N-S)]

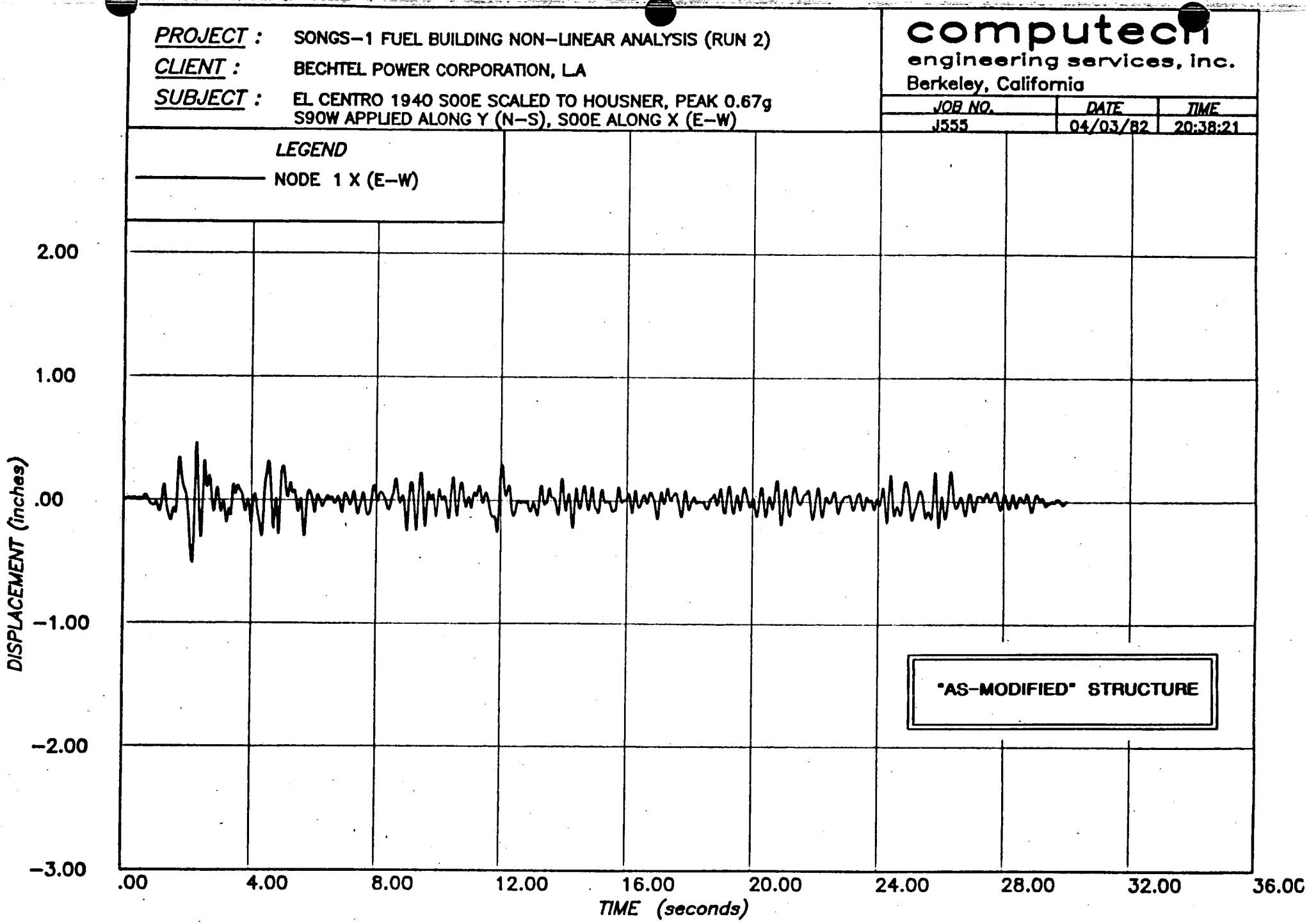

FIGURE D3 – ROOF DISPLACEMENT

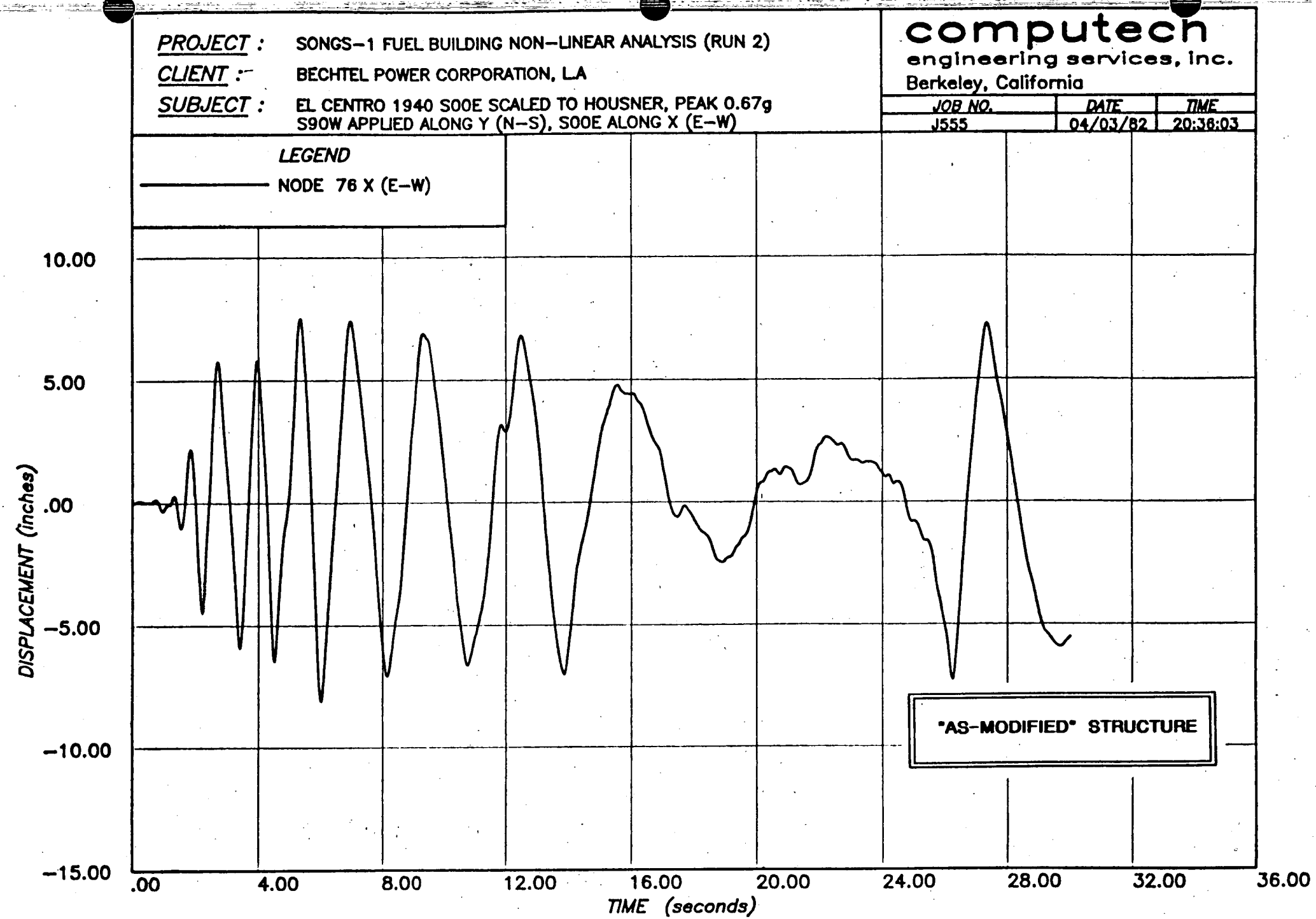

FIGURE D4 - OUT-OF-PLANE WALL DISPLACEMENTS - CENTER

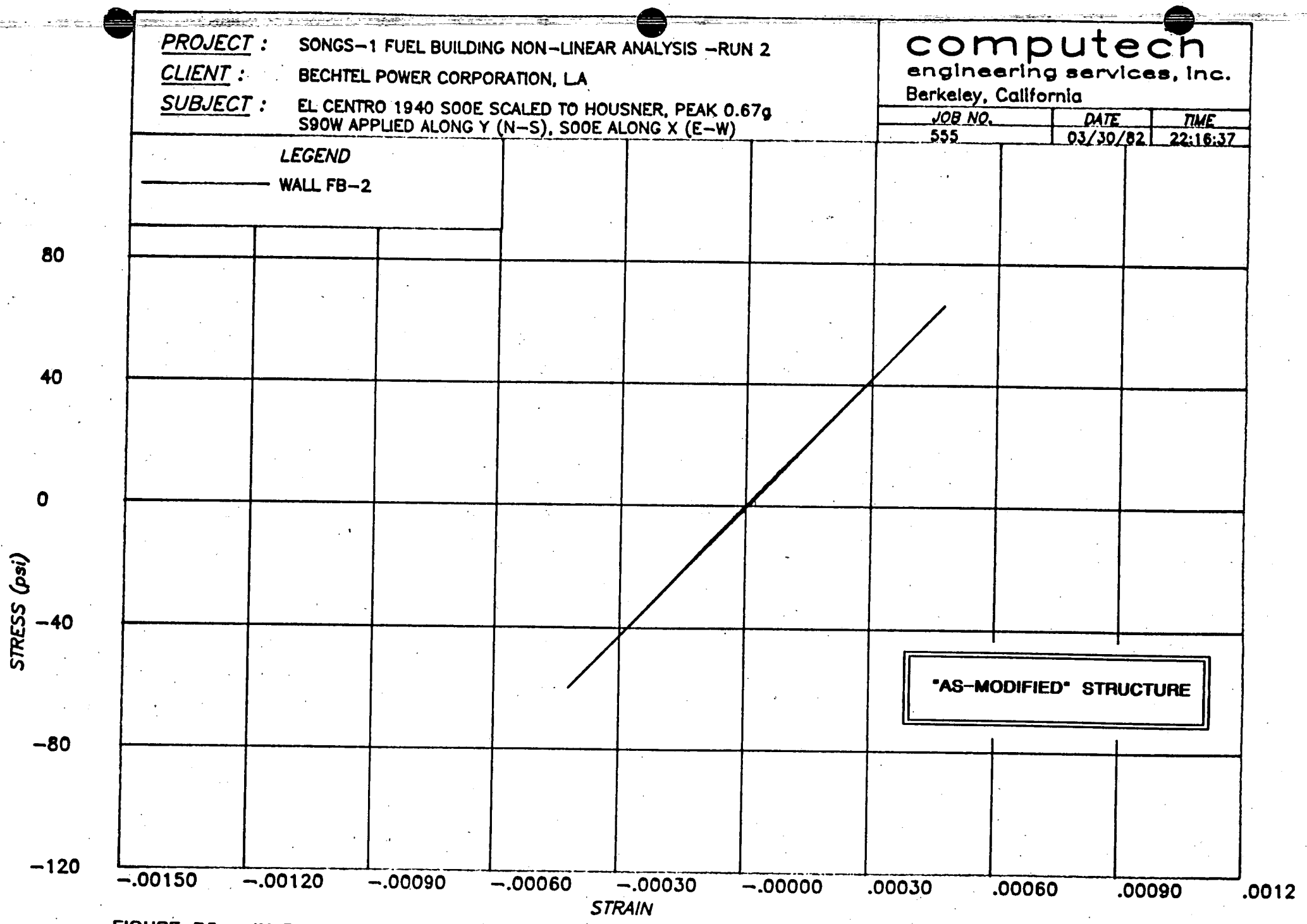

FIGURE D5 - IN-PLANE WALL STRESS-STRAIN - EL 42'

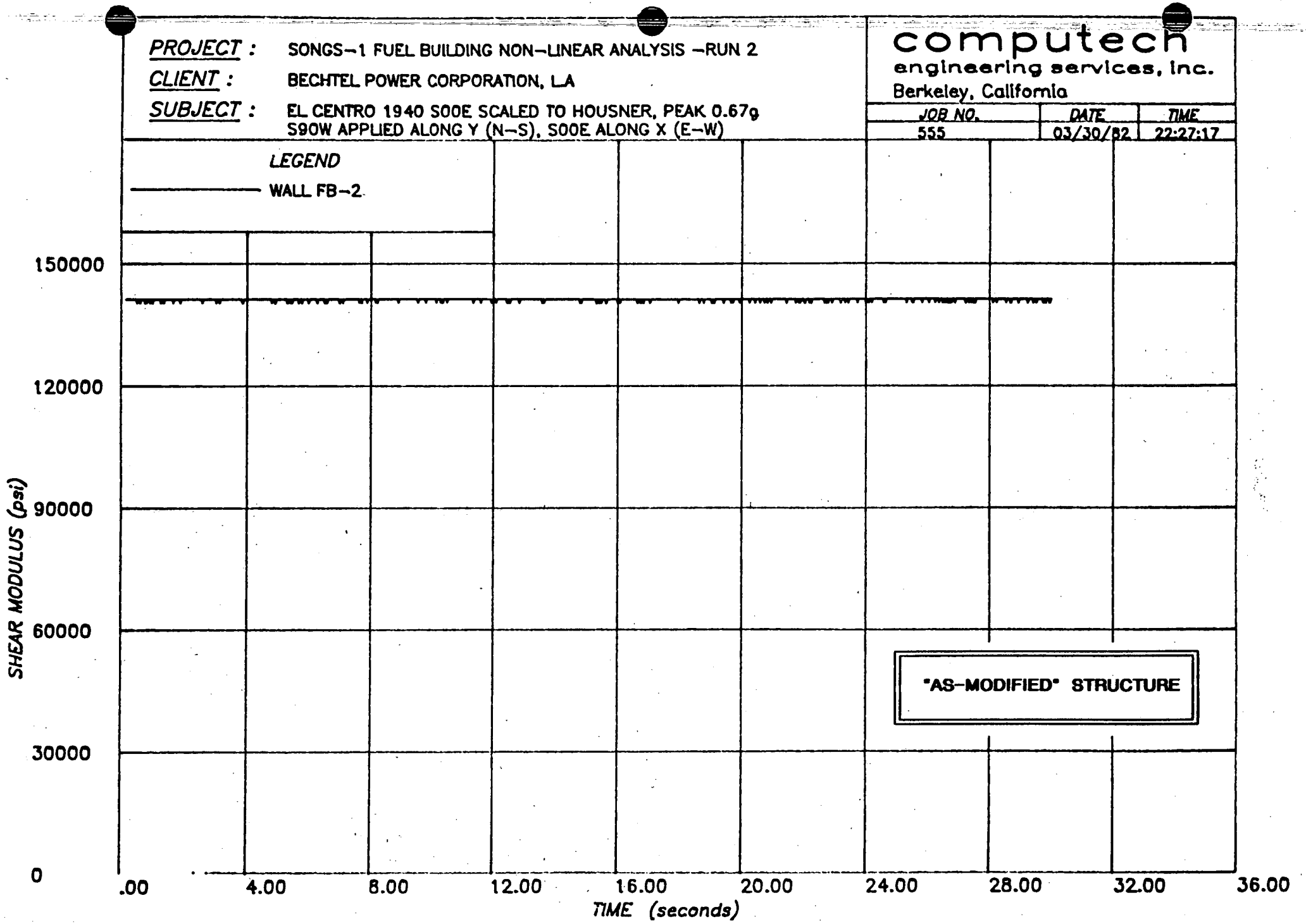

FIGURE D6 - IN-PLANE WALL STIFFNESS - EL 42'

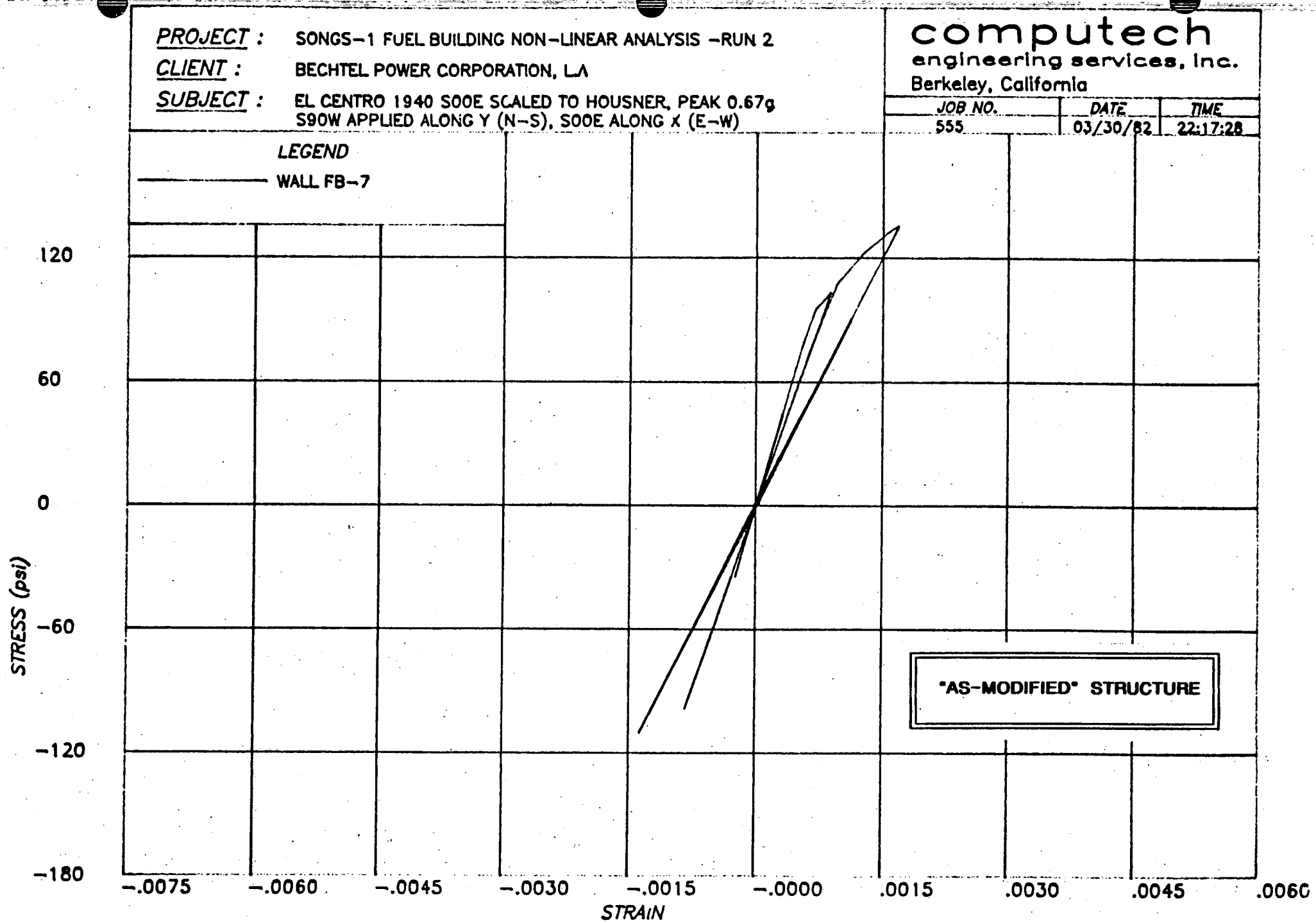

FIGURE D7 - IN-PLANE WALL STRESS-STRAIN - EL 42'

PROJECT : SONGS-1 FUEL BUILDING NON-LINEAR ANALYSIS -RUN 2

CLIENT : BECHTEL POWER CORPORATION, LA

SUBJECT : EL CENTRO 1940 S00E SCALED TO HOUSNER, PEAK 0.67g
S90W APPLIED ALONG Y (N-S), S00E ALONG X (E-W)

computech
engineering services, inc.
Berkeley, California

JOB NO.	DATE	TIME
555	03/30/82	22:28:18

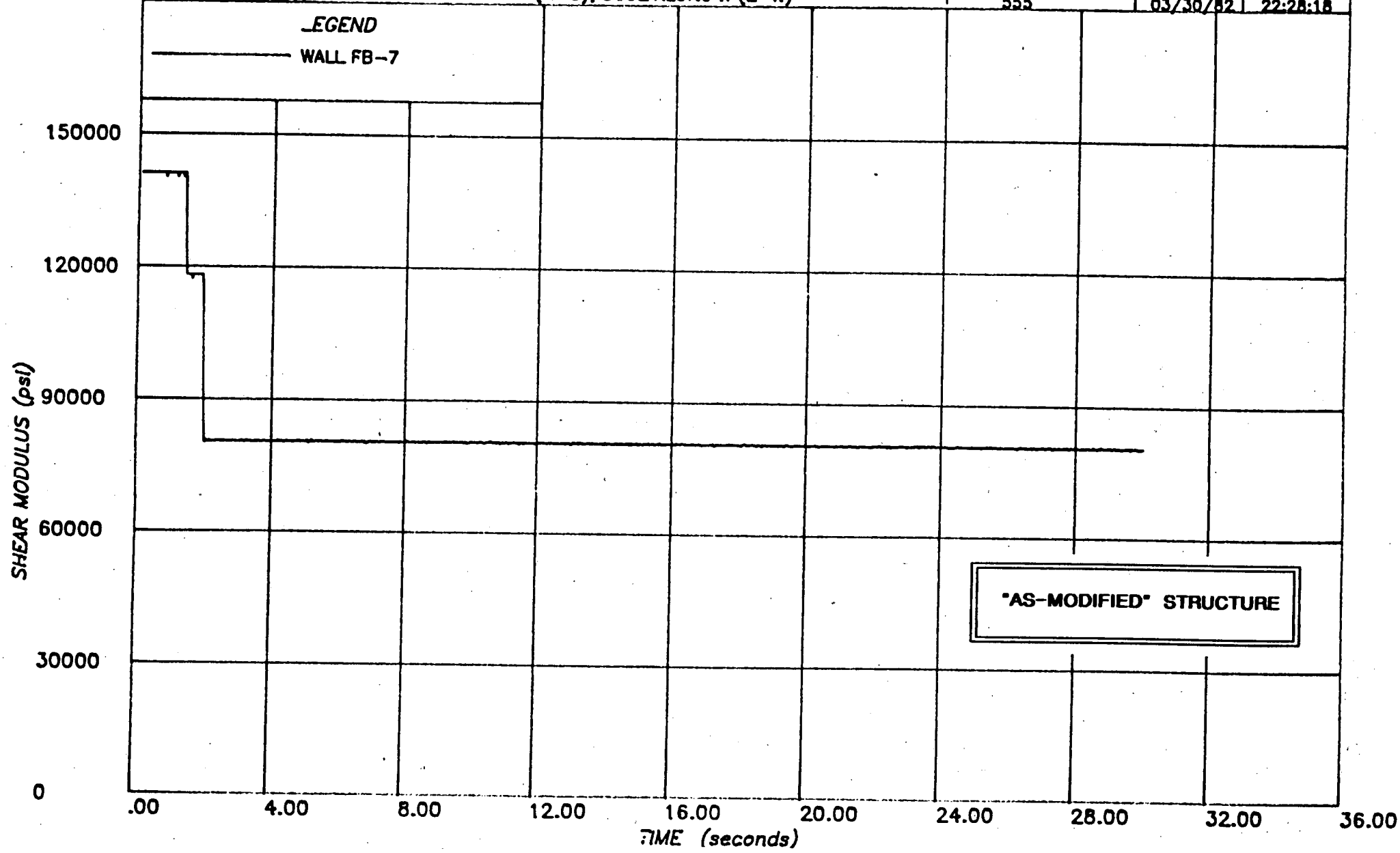

FIGURE D8 - IN-PLANE WALL STIFFNESS - EL 42'

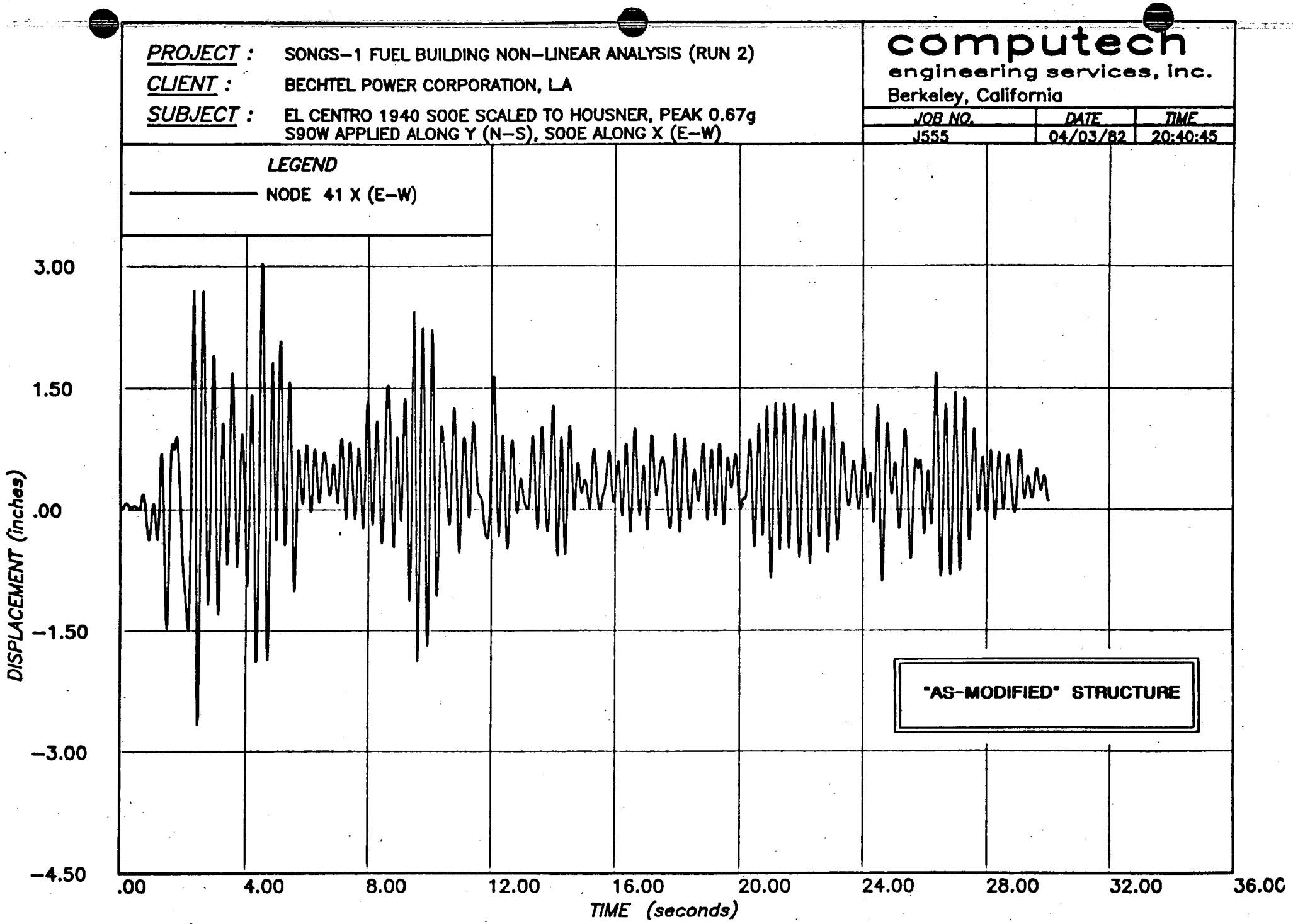

FIGURE D9 – DISPLACEMENT AT ROOF OPENING – EAST

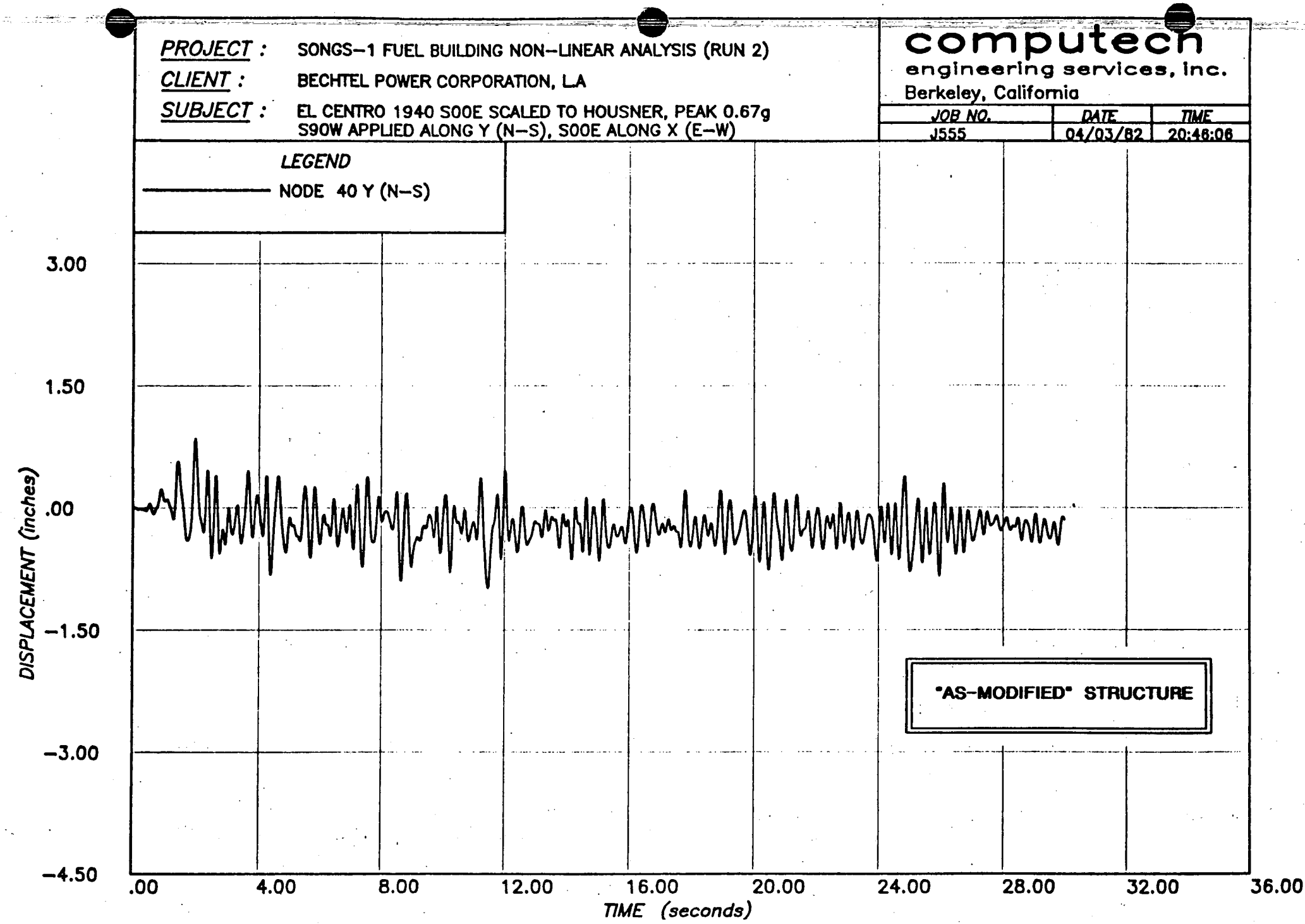

FIGURE D10 – DISPLACEMENT AT ROOF OPENING – SOUTH

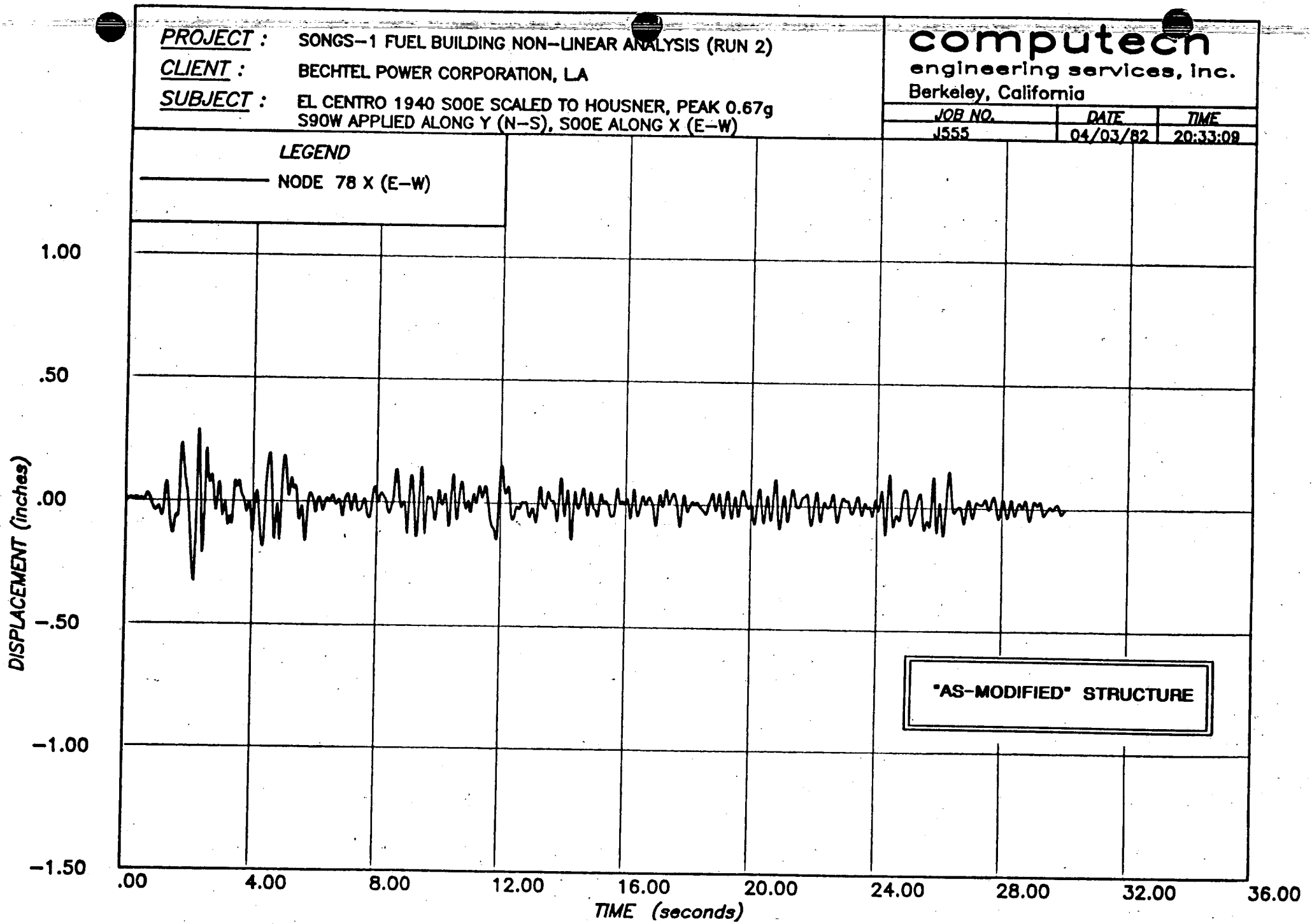

FIGURE D11 – TOP OF POOL: DISPLACEMENT

PROJECT : SONGS-1 FUEL BUILDING NON LINEAR ANALYSIS (RUN 2)

CLIENT : BECHTEL POWER CORPORATION, LOS ANGELES

SUBJECT : RESPONSE SPECTRUM - NODE 78 X (E-W) TOP OF POOL
EL CENTRO 1940 S00E ALONG X (E-W),S90W ALONG Y (N-S)

computech
engineering services, inc.
Berkeley, California

JOB NO.	DATE	TIME
J 555	04/03/82	21:22:10

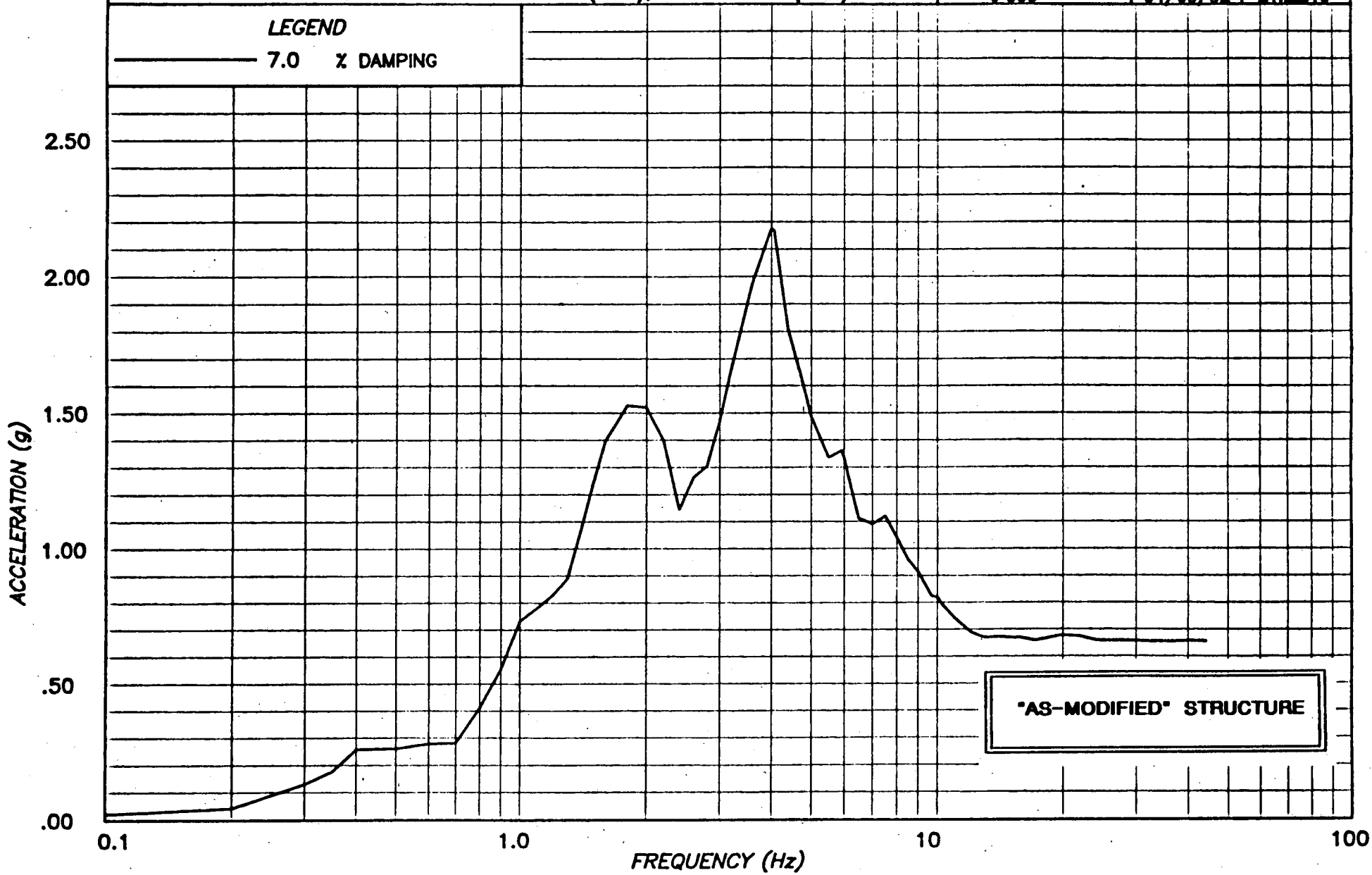

FIGURE D12 - TOP OF POOL: RESPONSE SPECTRUM - HORIZONTAL

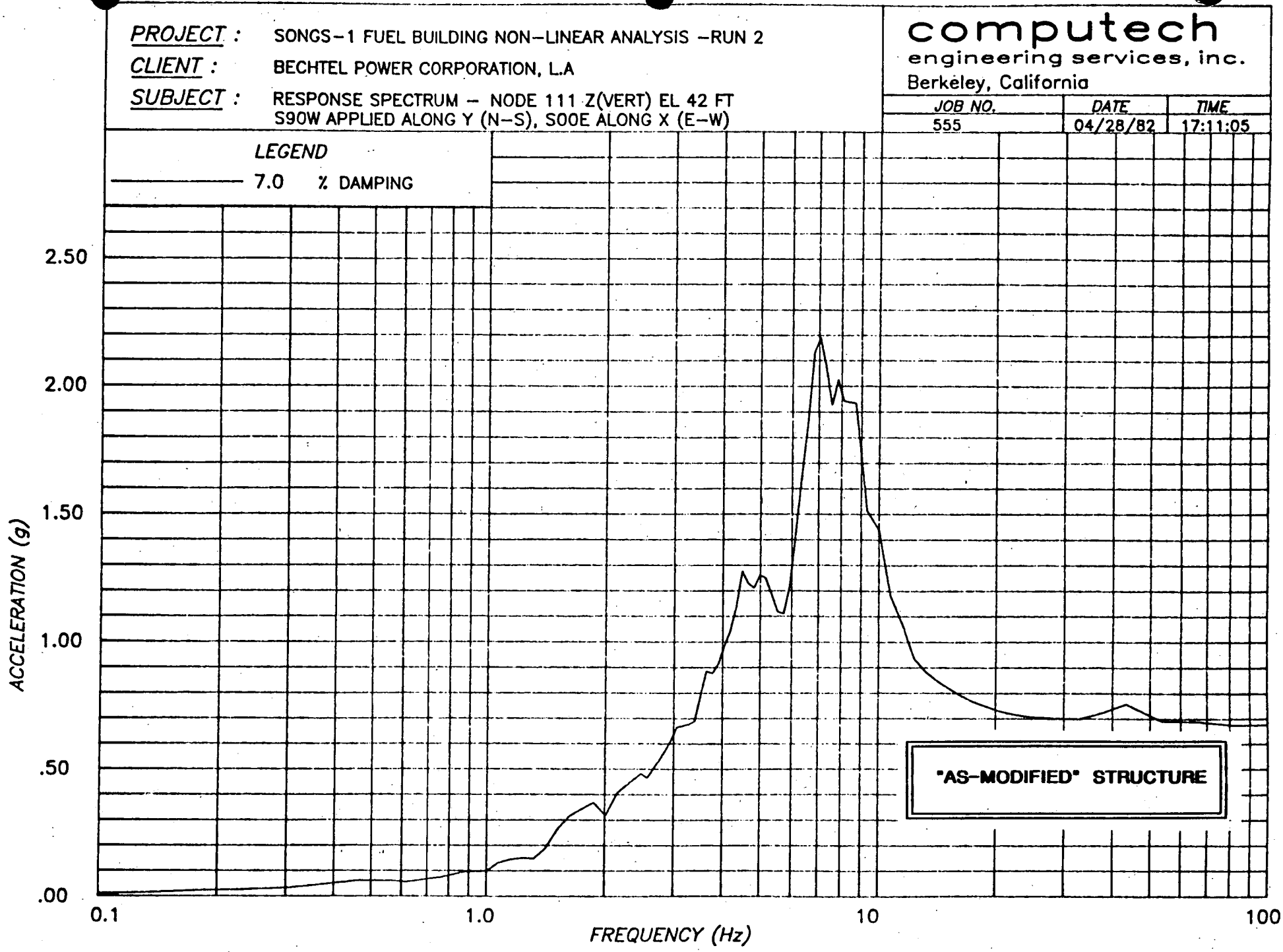

FIGURE D13 - TOP OF POOL: RESPONSE SPECTRUM - VERTICAL

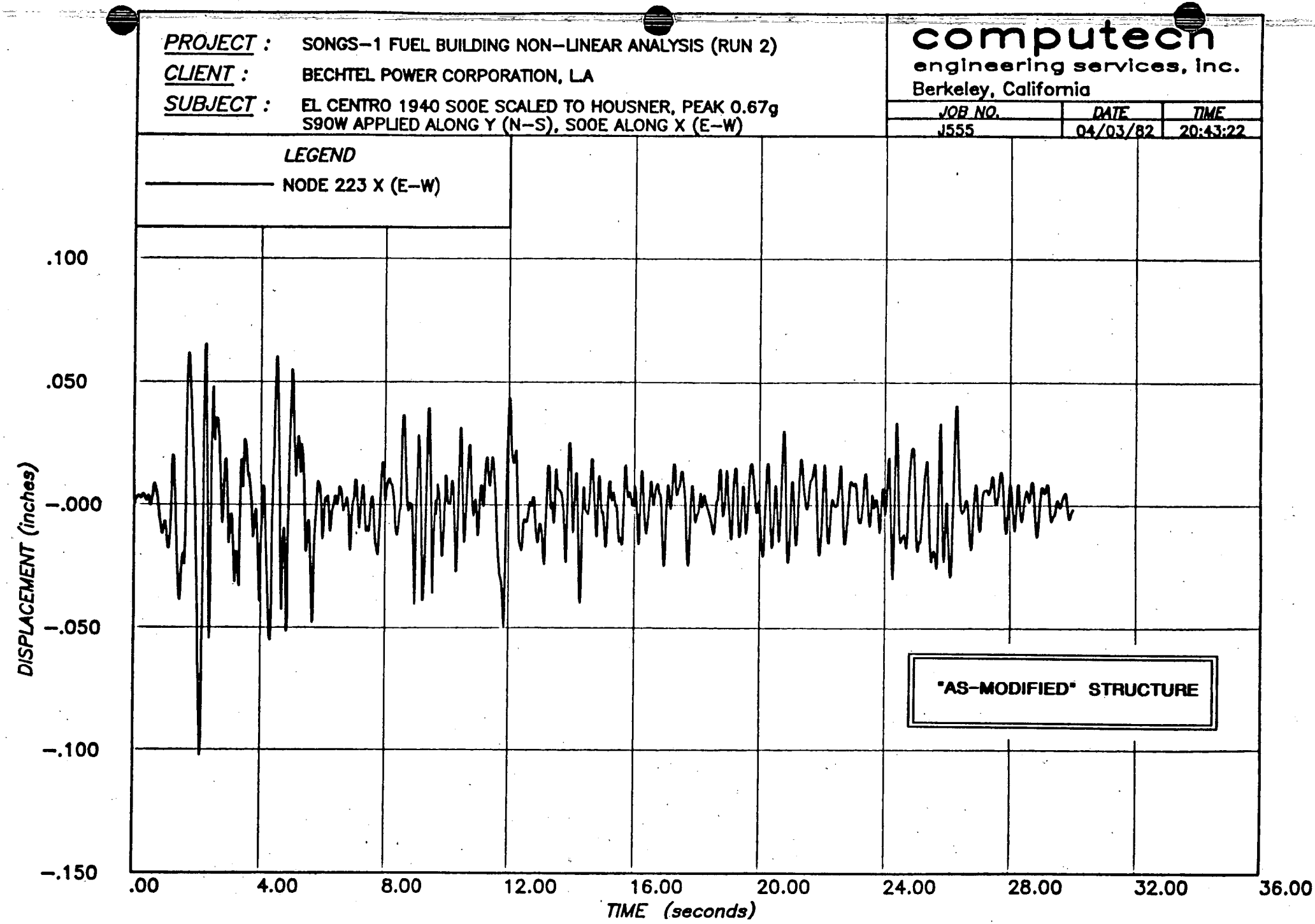

FIGURE D14 – BASE OF POOL: DISPLACEMENT

APPENDIX E: DETAILED RESULTS

Y(N-S) EARTHQUAKE: Olympia 1949 N04W, Scaled 2.51, 0.67g Peak

X(E-W) EARTHQUAKE: Olympia 1949 S86E, Scaled 2.51,

LOCATION	DISPLACEMENT (Inches)	
	MAXIMUM	MINIMUM
ROOF		
N-W Corner	1.3344	-1.4331
S-W Corner	1.2812	-1.4082
N-E Corner	1.4272	-1.5371
S-E Corner	1.3950	1.5247
TOP OF FUEL POOL		
N-W Corner	0.83167	-0.84631
S-W Corner	0.83566	-0.85036
N-E Corner	0.87726	-0.90485
S-E Corner	0.87783	-0.90552
BASE OF FUEL POOL		
N-W Corner	0.068223	-0.061634
S-W Corner	0.068176	-0.061597
N-E Corner	0.10948	-0.10707
S-E Corner	0.10943	-0.10701

ANALYSIS NUMBER 3

EARTHQUAKE: Olympia

PRINCIPAL COMPONENT DIRECTION: Y

TABLE E1: MAXIMUM DISPLACEMENTS

("AS-MODIFIED" STRUCTURE)

WALL NUMBER	SHEAR STRESS (p.s.D	SHEAR STRAIN	RATIO OF MAXIMUM STRAIN TO ALLOWABLE
FB-1	-47.98	-0.00034	0.1288
FB-2	100.6	0.00082	0.3106
FB-3	-69.58	-0.00049	0.1856
FB-4	-71.28	-0.00051	0.1932
FB-5	-43.47	-0.00031	0.1174
FB-6	-55.35	-0.00039	0.1477
FB-7	-172.70	-0.00353	0.6686
FB-8	-125.7	-0.00138	0.5227
FB-9	-150.9	-0.00217	0.8220
FB-10	-104.9	-0.00092	0.3485

ANALYSIS NUMBER: 3

EARTHQUAKE: Olympia

PRINCIPAL COMPONENT DIRECTION: Y

TABLE E2 : MAXIMUM IN-PLANE WALL RESPONSE
("AS-MODIFIED" STRUCTURE)

WALL	STEEL STRAIN RATIO		MASONRY STRESS	CENTER DISPLACEMENT
	CENTER	END	fm (p.s.i.)	(inches)
FB-1	12.52	16.20	655.9	6.30
FB-2	12.73	15.89	656.0	6.62
FB-3	9.41	13.26	655.9	5.52
FB-4				
FB-5	12.12	12.62	655.9	6.14
FB-6	11.02	14.78	655.3	5.87
FB-7				
FB-8	1.18	.64	655.9	1.00
FB-9	1.33	.58	655.9	.97
FB-10	1.53	.86	656.0	1.34

ANALYSIS NUMBER: 3

EARTHQUAKE: Olympia

PRINCIPAL COMPONENT DIRECTION: Y

TABLE E3: MAXIMUM OUT-OF-PLANE MASONRY WALL RESPONSE

("AS-MODIFIED" STRUCTURE)

WALL NUMBER	LOCATION	SHEAR STRESS (lb/ft)	TENSION (lb/ft)
FB-1	Roof	1507.5	256.9
FB-2	Roof	1045.2	233.3
FB-3	Roof	347.1	113.3
FB-4	Roof	310.5	-
FB-5	Roof	599.2	226.6
FB-6	Roof	1447.9	213.6
FB-7	Roof	1704.1	-
FB-8	El 42'-0"	2929.2	652.8
FB-9	El 42'-0"	621.6	159.2
FB-10	El 42'-0"	2127.0	697.6
FB-8	El 42'-0"	-	711.2
FB-9	El 42'-0"	-	619.2
FB-10	El 42'-0"	-	1059.6

ANALYSIS NUMBER: 3

EARTHQUAKE: Olympia

PRINCIPAL COMPONENT DIRECTION: Y

TABLE E4: MAXIMUM CONNECTION FORCES

("AS-MODIFIED" STRUCTURE)

WALL NUMBER	LOCATION	SHEAR STRESS (lb/ft)	RATIO OF MAXIMUM STRESS TO ALLOWABLE
FB-1	Roof	1113.3	0.3758
FB-2	Roof	1455.6	0.4913
FB-3	Roof	829.2	0.2799
FB-4	Roof	784.4	0.2648
FB-5	Roof	1017.9	0.3436
FB-6	Roof	2640.5	0.8913
FB-7	Roof	2640.5	0.8913
FB-8	El 42'-0"	4272.5	0.4168
FB-9	El 42'-0"	4900.0	0.4780
FB-10	El 42'-0"	2826.4	0.2757

ANALYSIS NUMBER: 3

EARTHQUAKE: Olympia

PRINCIPAL COMPONENT DIRECTION: Y

TABLE E5 : MAXIMUM DIAPHRAGM FORCES

("AS-MODIFIED" STRUCTURE)

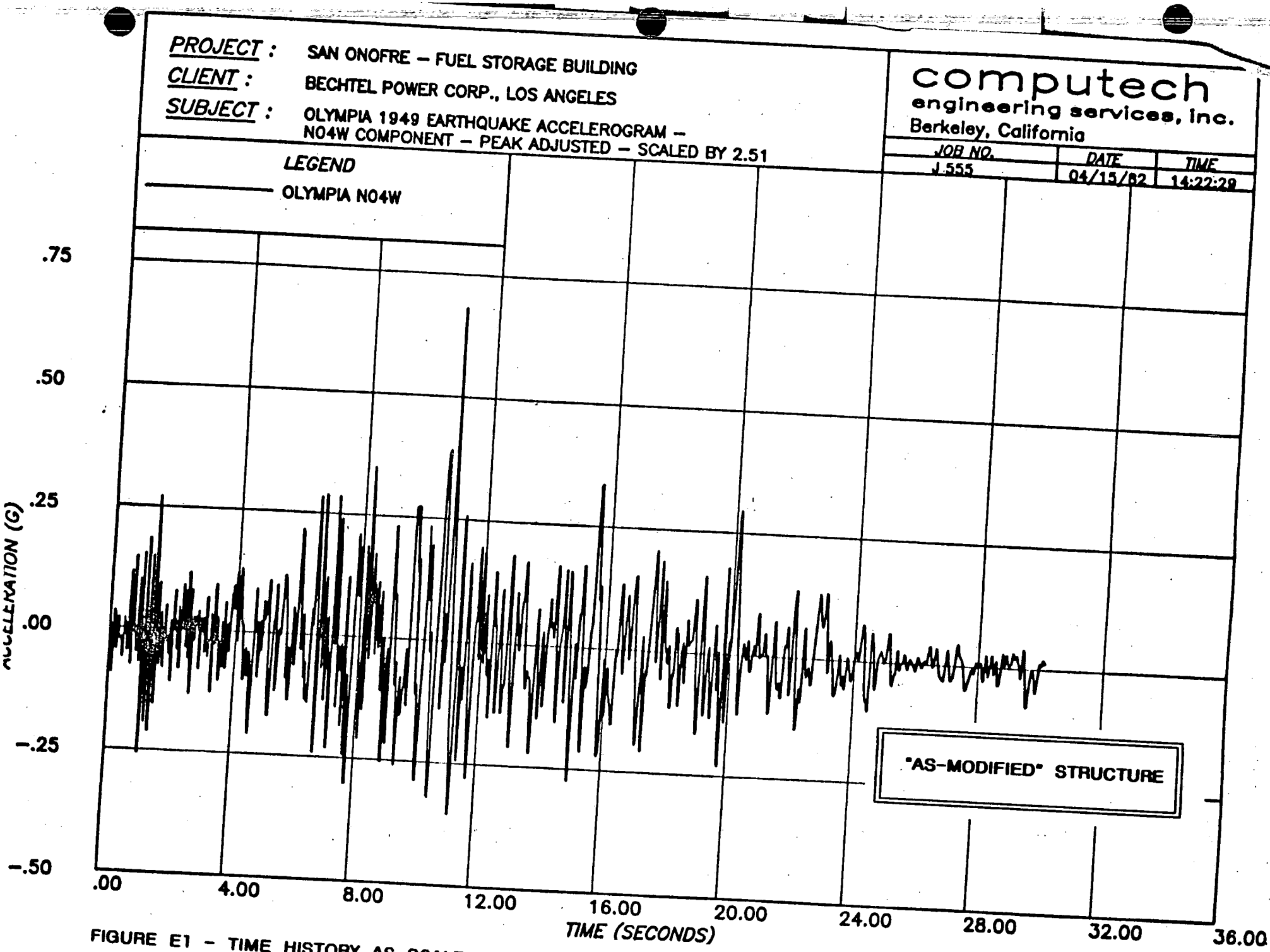

FIGURE E1 – TIME HISTORY AS SCALED [Y(N-S)]

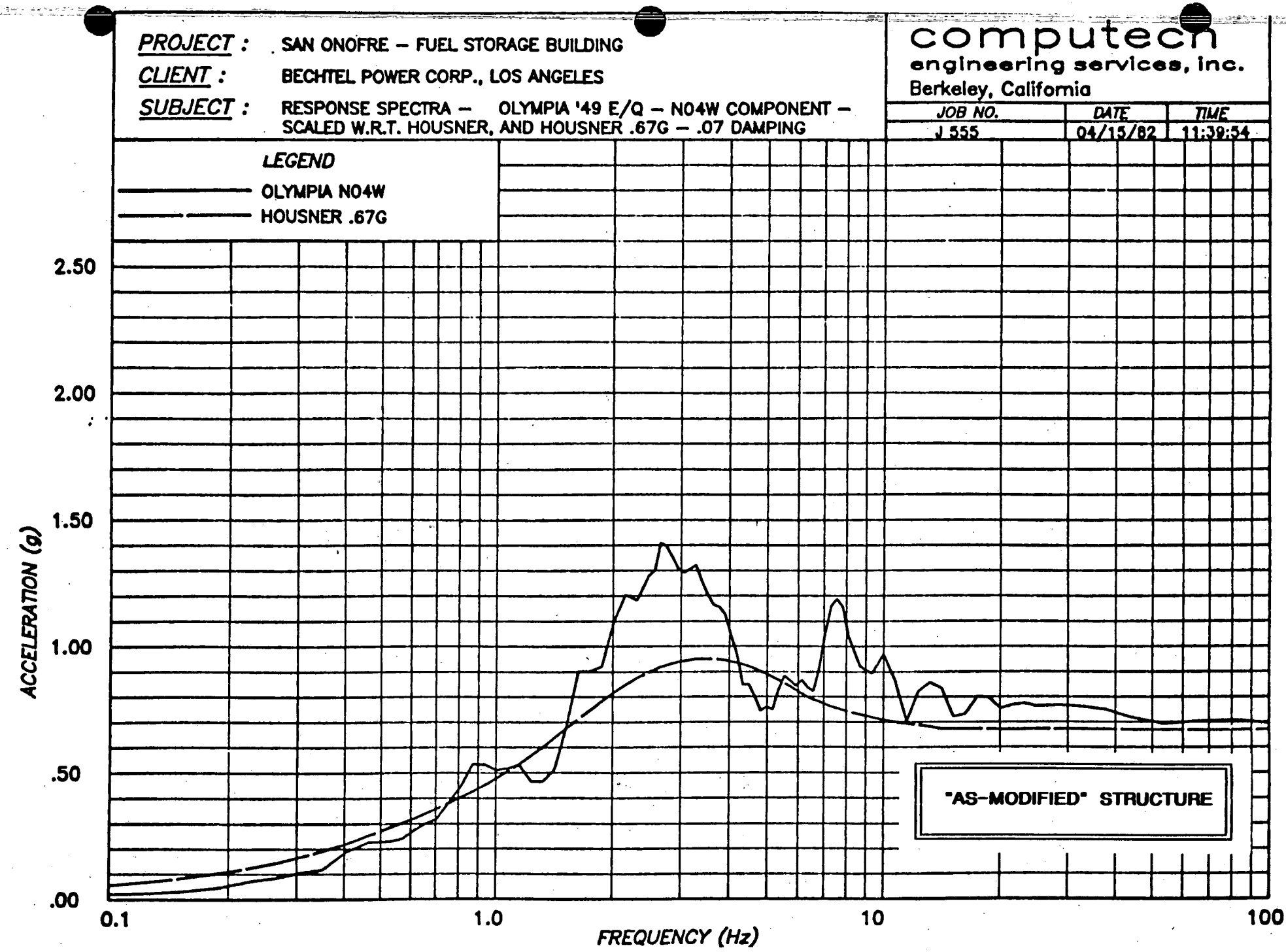

FIGURE E2 – RESPONSE SPECTRUM [Y(N-S)]

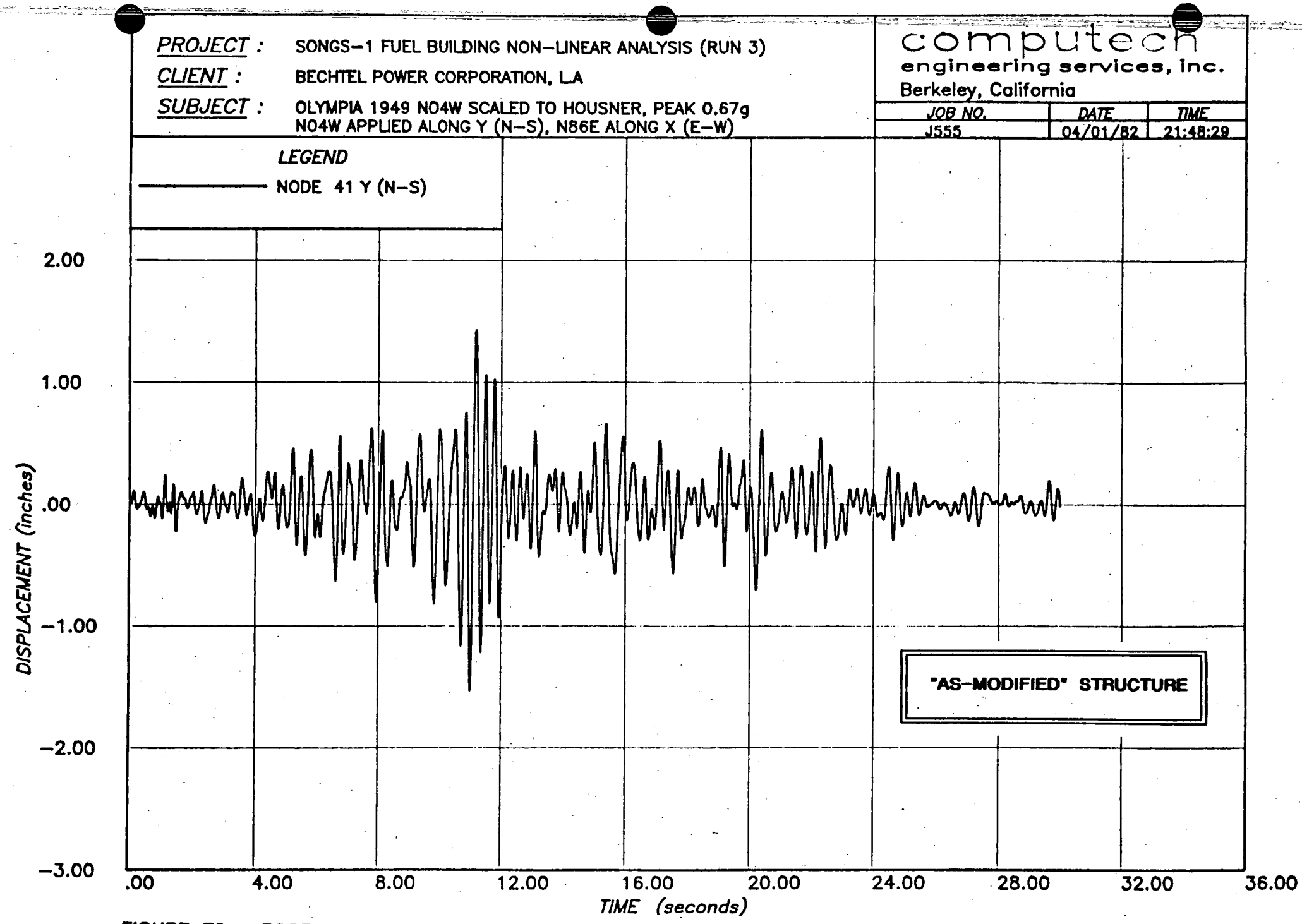

FIGURE E3 – ROOF DISPLACEMENT

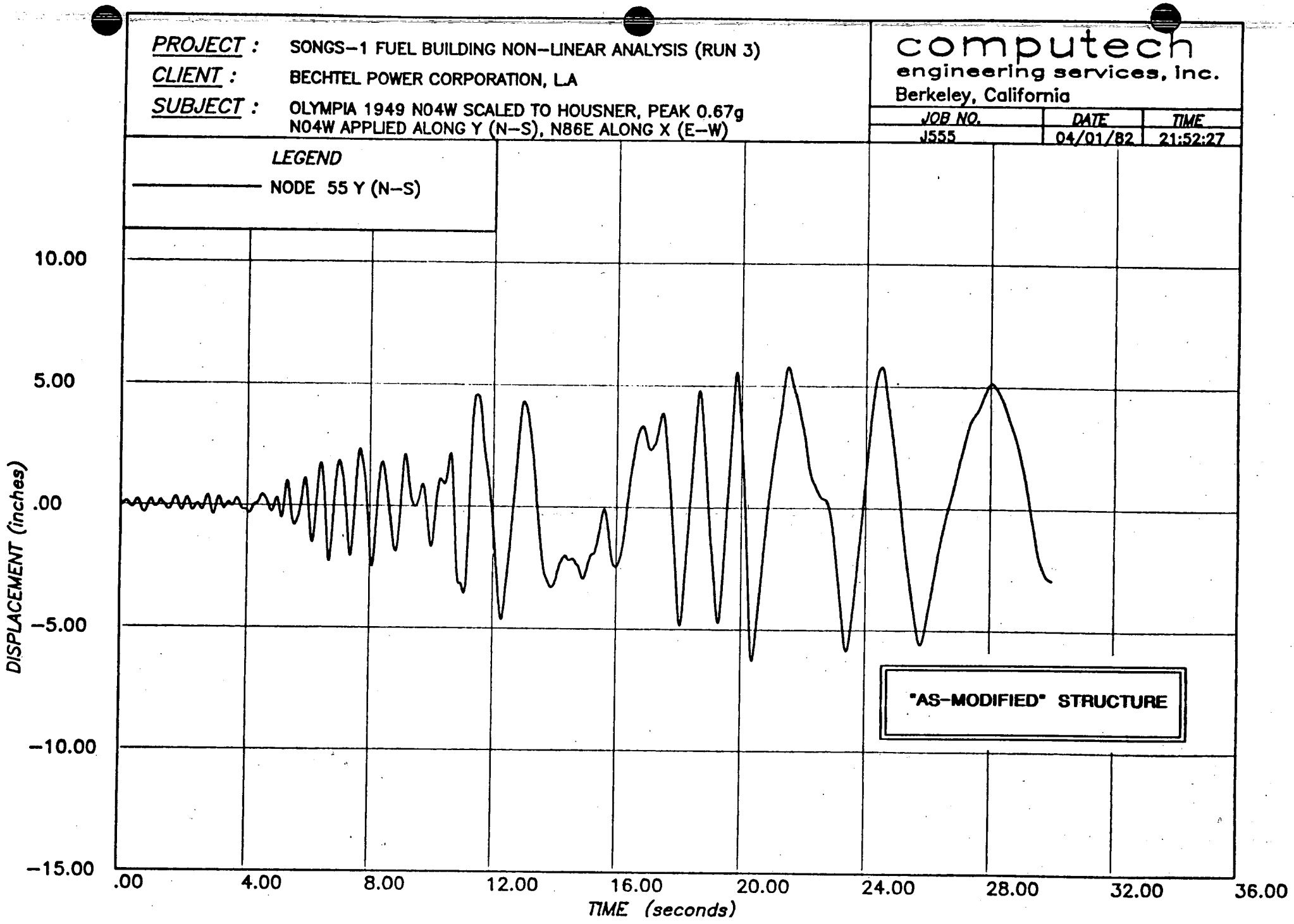

FIGURE E4 – OUT–OF–PLANE WALL DISPLACEMENTS – CENTER

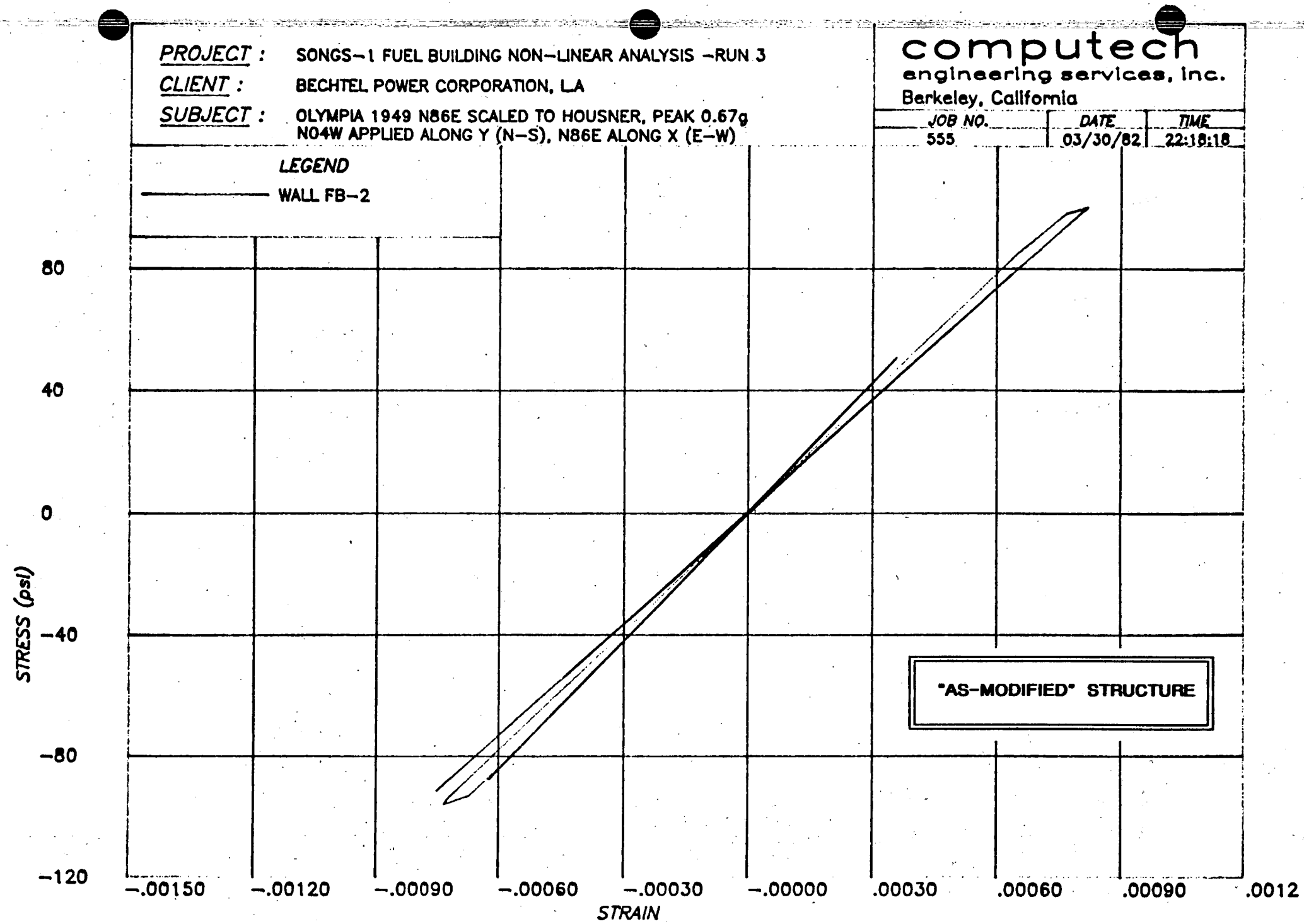

FIGURE E5 - IN-PLANE WALL STRESS-STRAIN - EL 42'

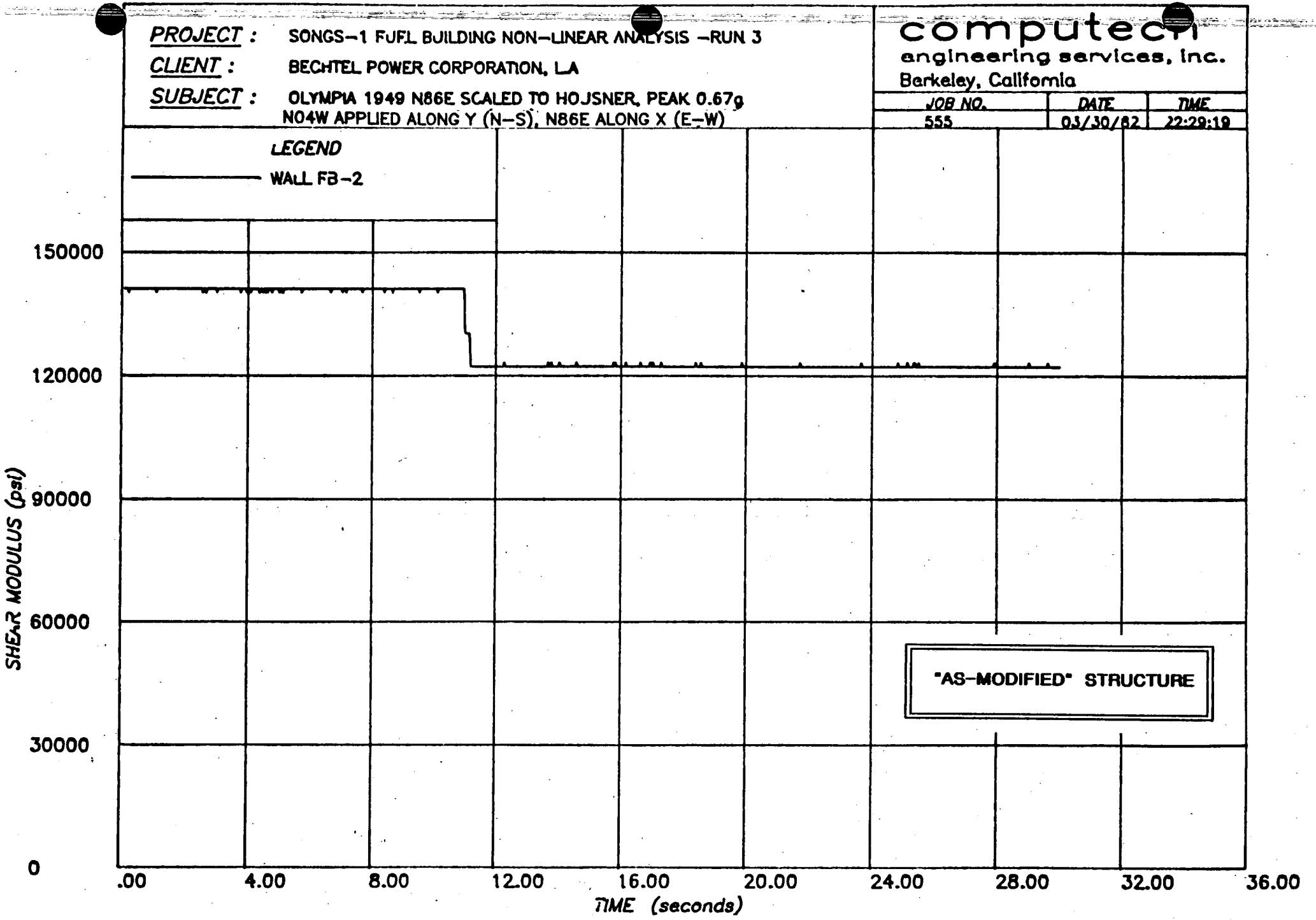

FIGURE E6 - IN-PLANE WALL STIFFNESS - EL 42'

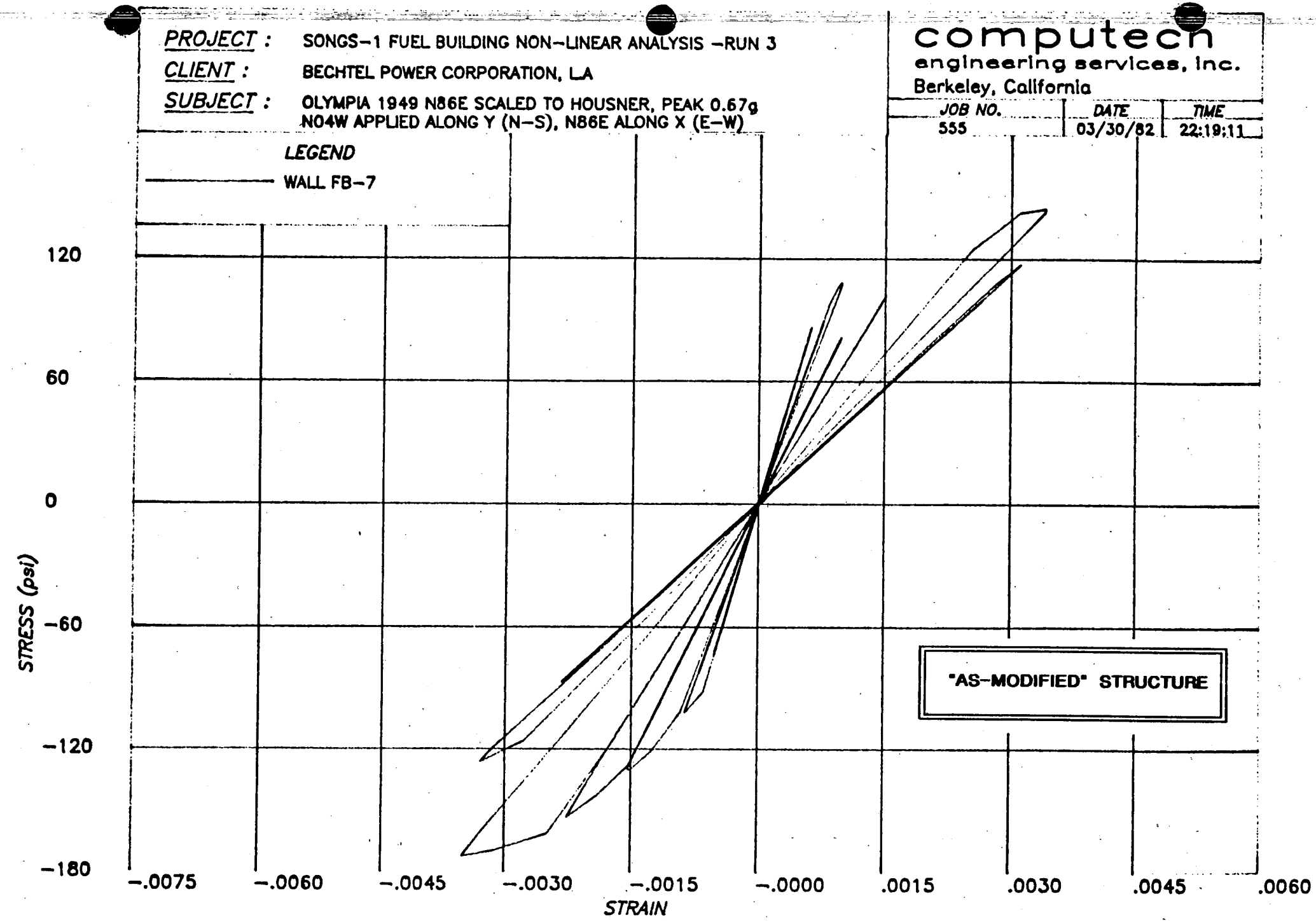

FIGURE E7 - IN-PLANE WALL STRESS-STRAIN - EL 42'

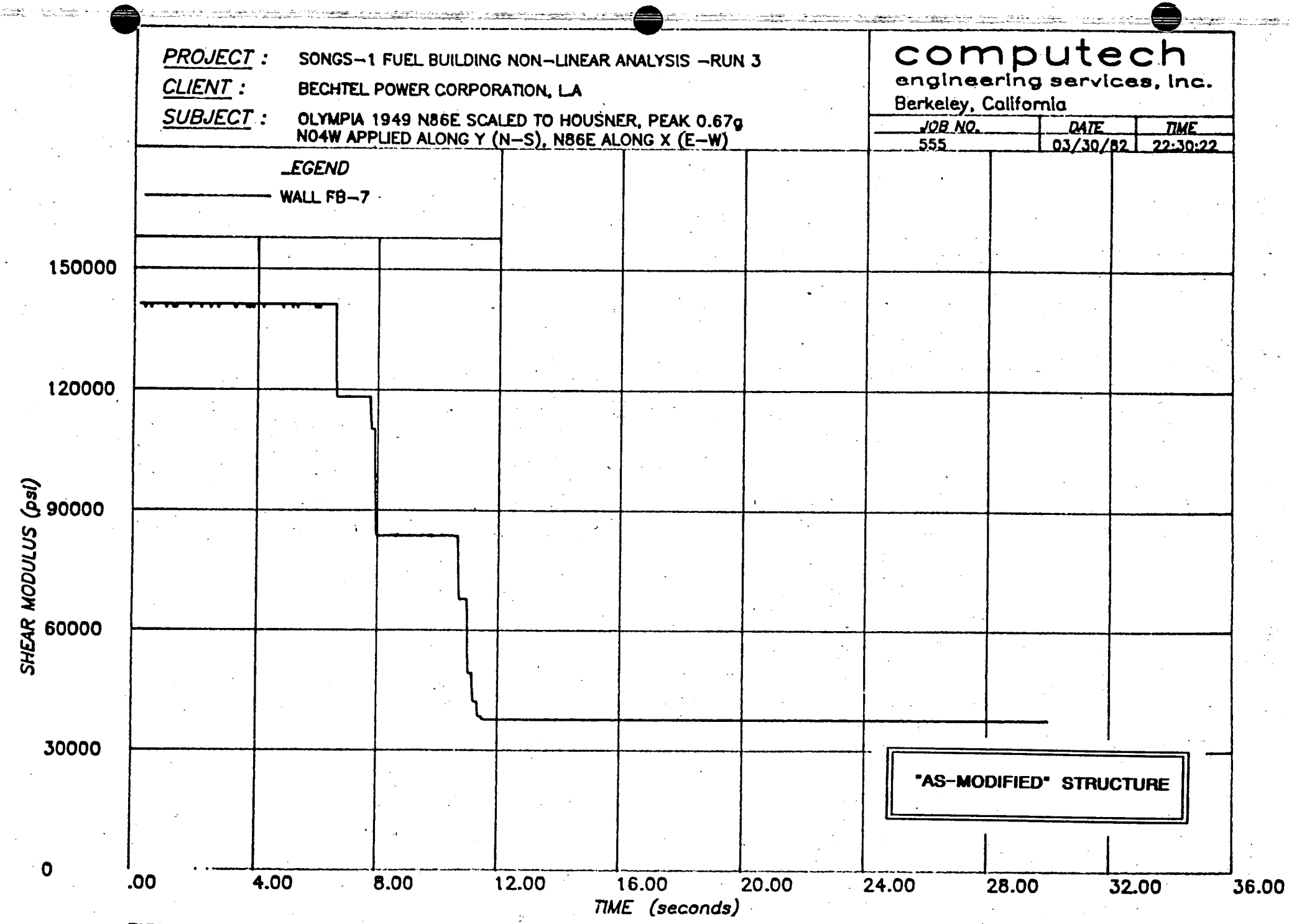

FIGURE E8 - IN-PLANE WALL STIFFNESS - EL 42'

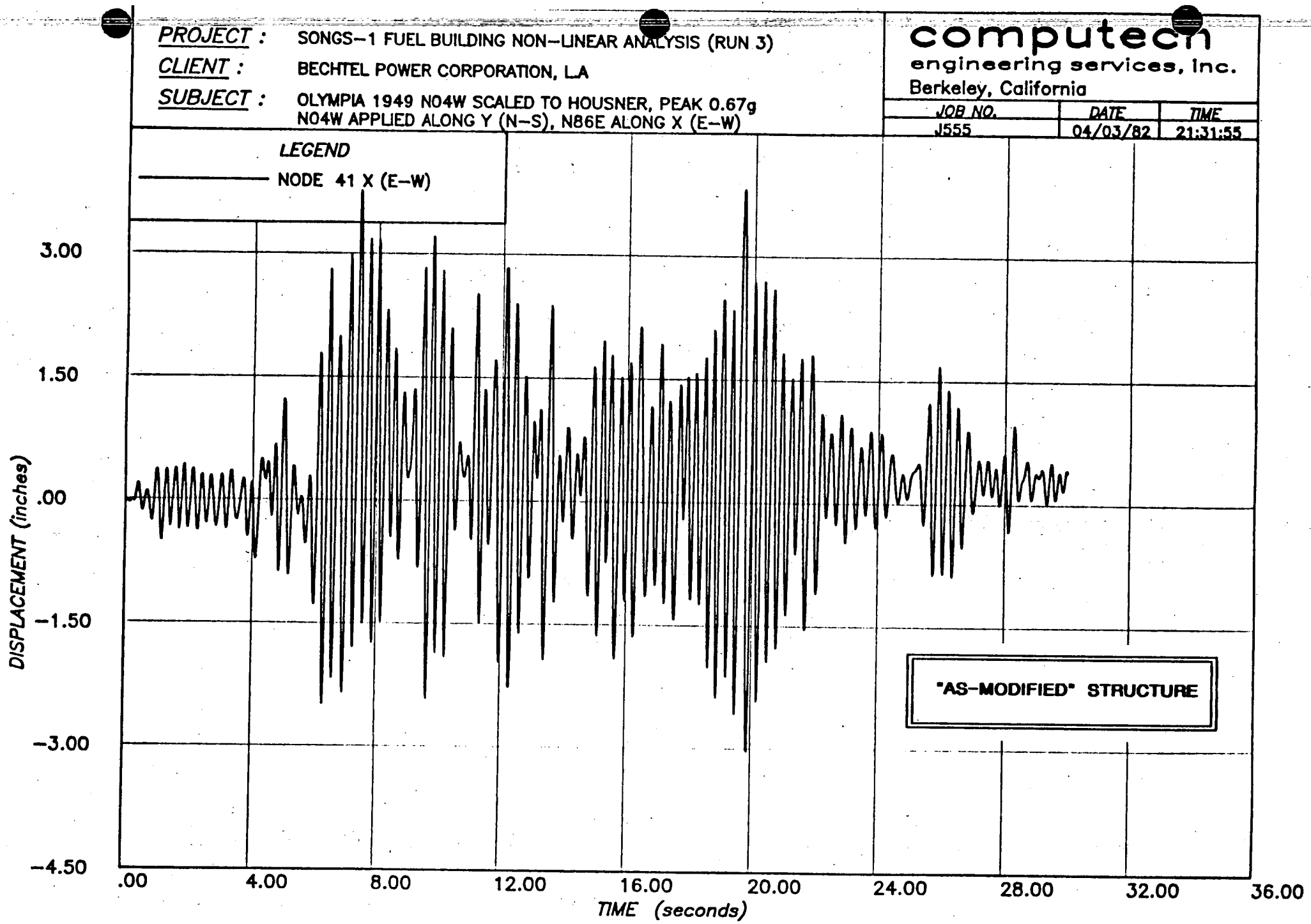

FIGURE E9 – DISPLACEMENT AT ROOF OPENING – EAST

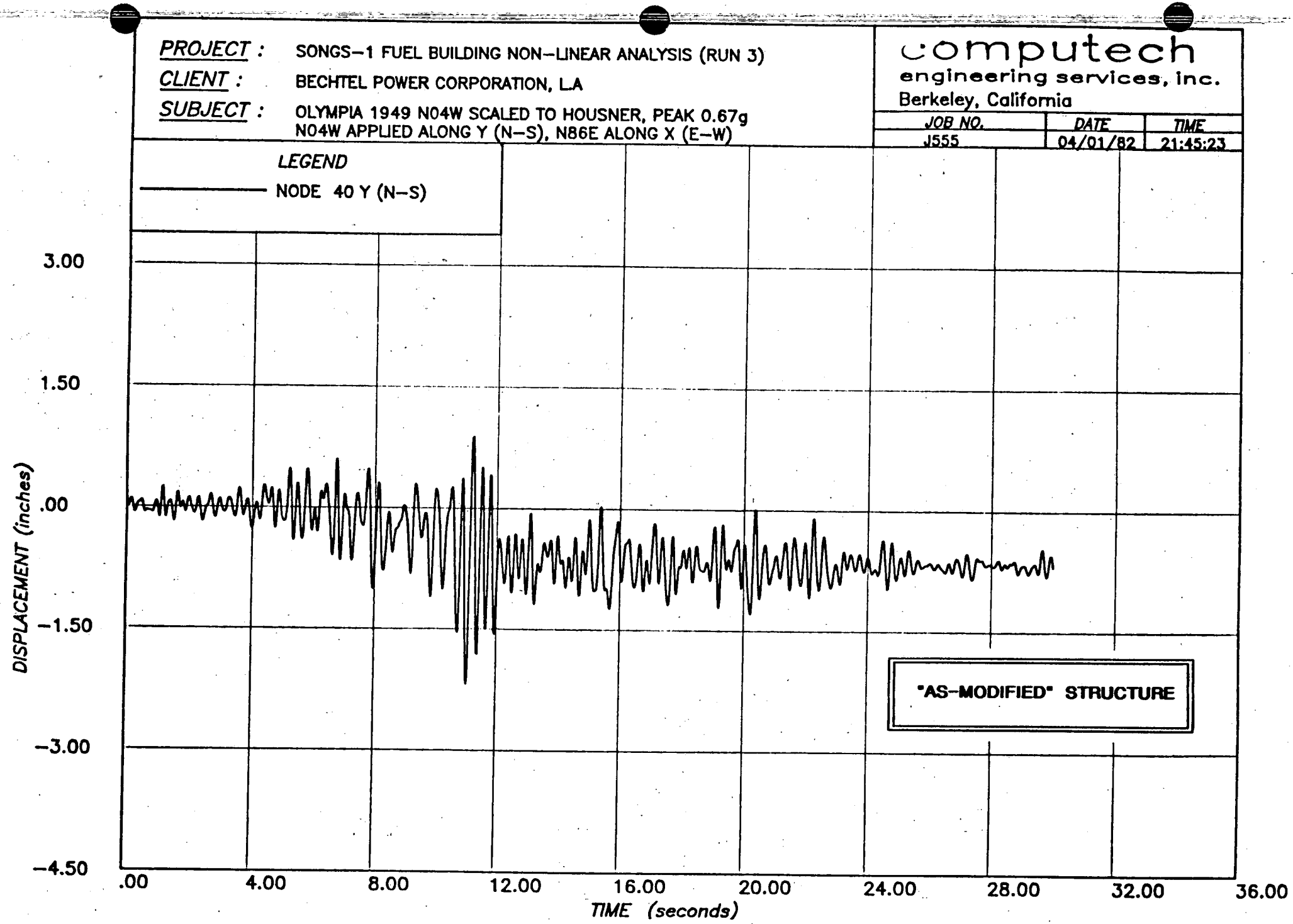

FIGURE E10 – DISPLACEMENT AT ROOF OPENING – SOUTH

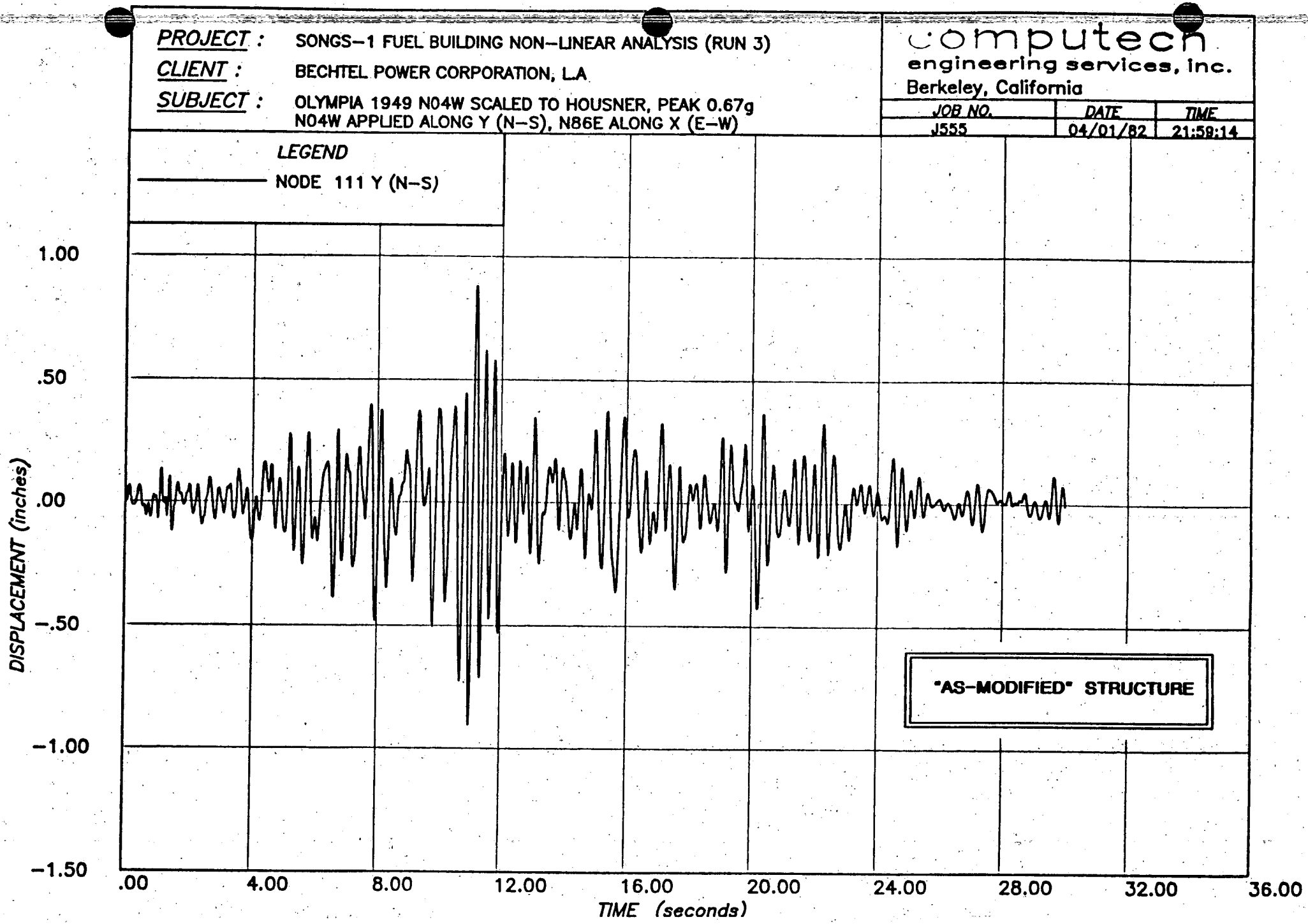

FIGURE E11 – TOP OF POOL: DISPLACEMENT

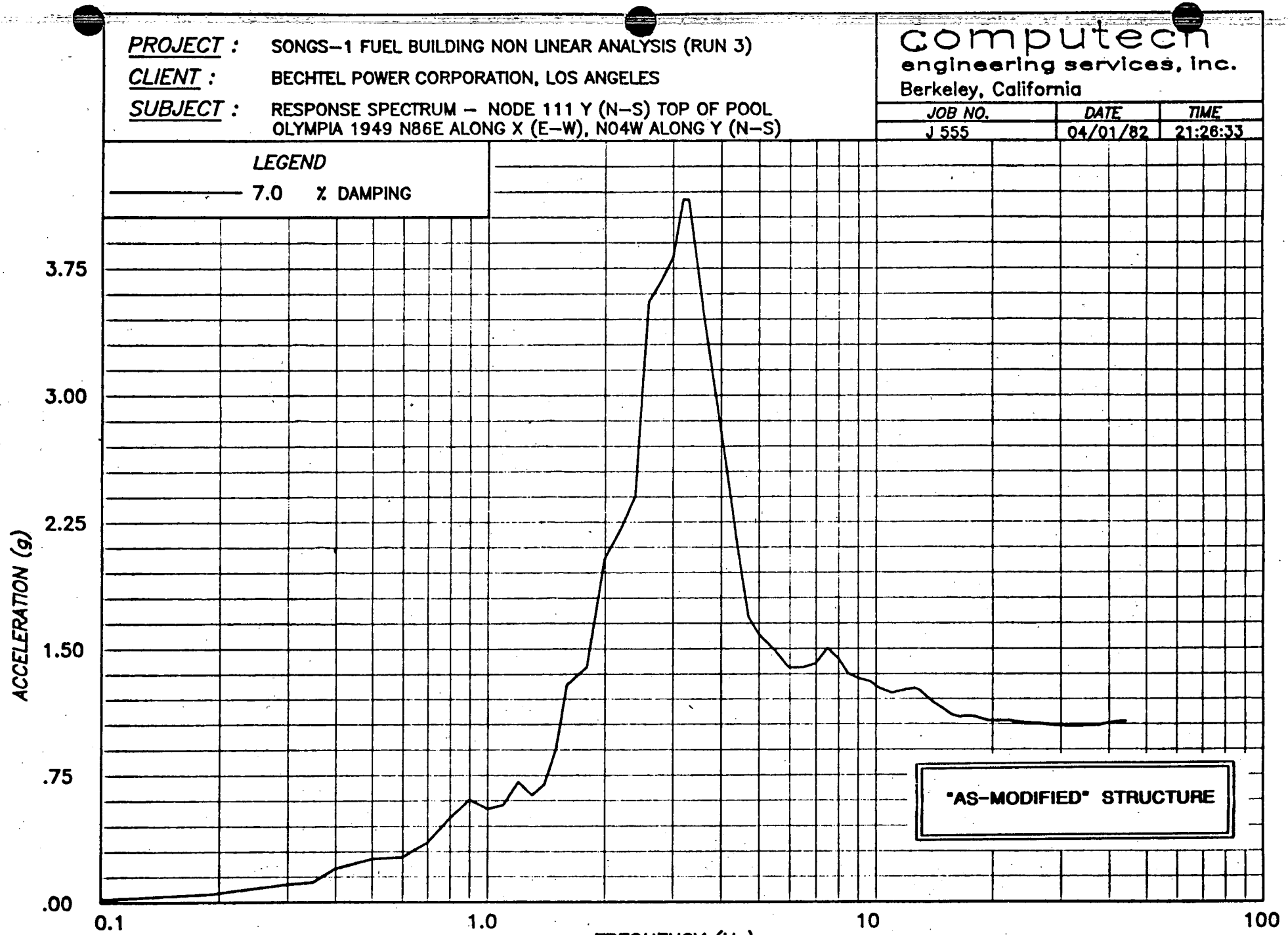

FIGURE E12 – TOP OF POOL: RESPONSE SPECTRUM – HORIZONTAL

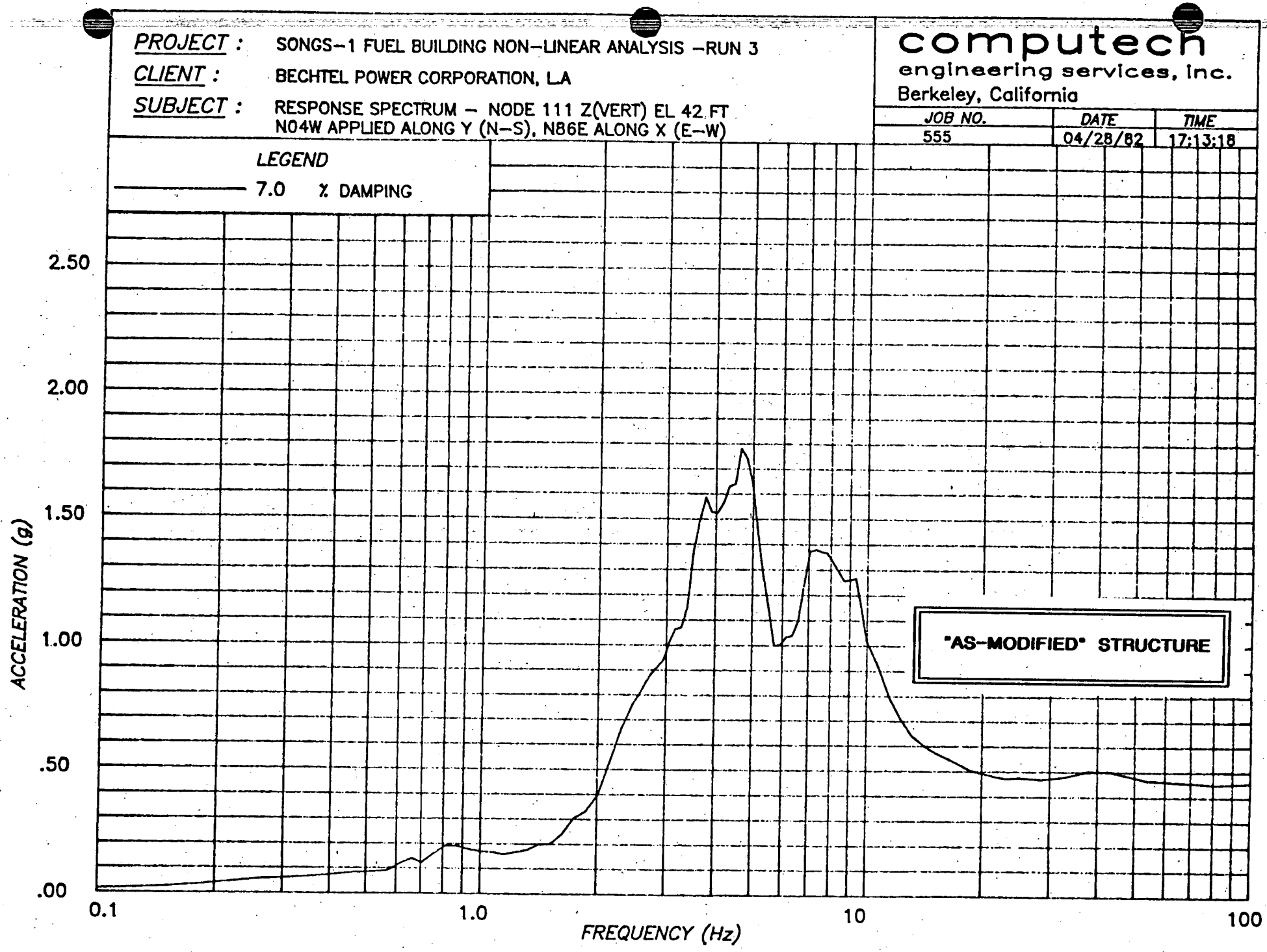

FIGURE E13 – TOP OF POOL: RESPONSE SPECTRUM – VERTICAL

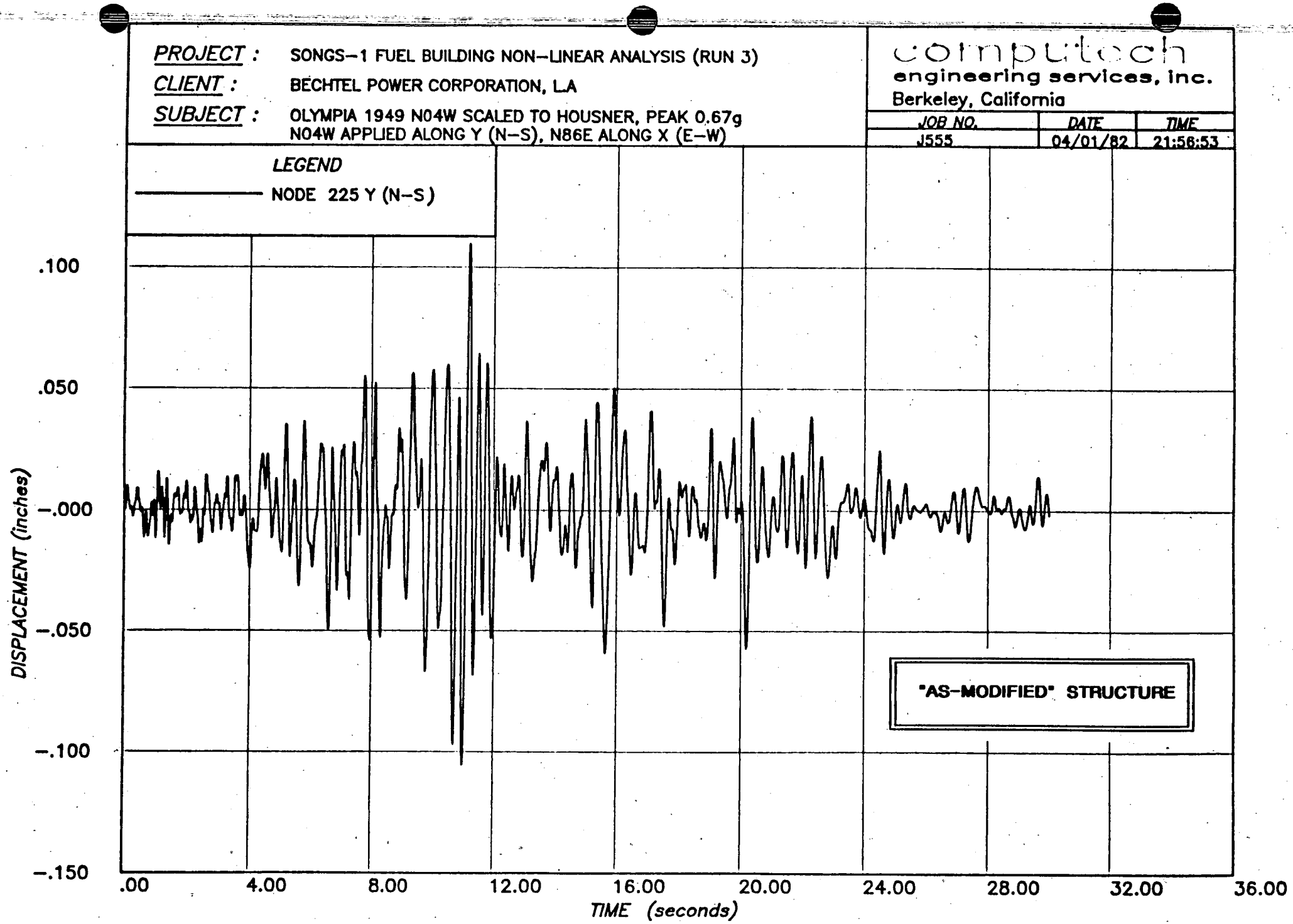

FIGURE E14 – BASE OF POOL: DISPLACEMENT

APPENDIX F: DETAILED RESULTS

Y(N-S) EARTHQUAKE: Olympia 1949 S86E. Scaled 2.51

X(E-W) EARTHQUAKE: Olympia 1949 N04W. Scaled 2.51. Peak 0.67g

LOCATION	DISPLACEMENT (inches)	
	MAXIMUM	MINIMUM
ROOF		
N-W Corner	0.319	-0.490
S-W Corner	0.465	-0.602
N-E Corner	0.355	-0.533
S-E Corner	0.389	-0.537
TOP OF FUEL POOL		
N-W Corner	0.204	-0.296
S-W Corner	0.232	-0.328
N-E Corner	0.204	-0.297
S-E Corner	0.231	-0.326
BASE OF FUEL POOL		
N-W Corner	0.057	-0.085
S-W Corner	0.065	-0.097
N-E Corner	0.057	-0.085
S-E Corner	0.065	-0.097

ANALYSIS NUMBER 4

EARTHQUAKE: Olympia

PRINCIPAL COMPONENT DIRECTION: X

TABLE F1: MAXIMUM DISPLACEMENTS

("AS-MODIFIED" STRUCTURE)

WALL NUMBER	SHEAR STRESS (p.s.D	SHEAR STRAIN	RATIO OF MAXIMUM STRAIN TO ALLOWABLE
FB-1	-442.35	-0.00030	0.1136
FB-2	-116.6	-0.00116	0.4394
FB-3	64.68	0.00046	0.1742
FB-4	-59.53	-0.00042	0.1591
FB-5	-50.88	-0.00036	0.1364
FB-6	-49.64	-0.00035	0.1326
FB-7	-178.4	-0.00478	0.9053
FB-8	-132.4	-0.00159	0.6023
FB-9	-157.1	-0.00237	0.8977
FB-10	-89.77	-0.00064	0.2424

ANALYSIS NUMBER: 4

EARTHQUAKE: Olympia

PRINCIPAL COMPONENT DIRECTION: X

TABLE F2 : MAXIMUM IN-PLANE WALL RESPONSE
("AS-MODIFIED" STRUCTURE)

WALL	STEEL STRAIN RATIO		MASONRY STRESS	CENTER DISPLACEMENT
	CENTER	END	fm (p.s.i.)	(inches)
FB-1	16.47	19.92	655.9	7.70
FB-2	9.13	12.33	656.0	5.14
FB-3	9.76	13.47	655.9	5.41
FB-4				
FB-5	16.77	16.80	655.9	7.46
FB-6	13.30	16.97	655.3	6.75
FB-7				
FB-8	.98	.61	643.2	.94
FB-9	.88	.49	577.6	.79
FB-10	.96	.74	632.2	1.22

ANALYSIS NUMBER: 4

EARTHQUAKE: Olympia

PRINCIPAL COMPONENT DIRECTION: X

TABLE F3: MAXIMUM OUT-OF-PLANE MASONRY WALL RESPONSE

("AS-MODIFIED" STRUCTURE)

WALL NUMBER	LOCATION	SHEAR STRESS (lb/ft)	TENSION (lb/ft)
FB-1	Roof	707.1	257.0
FB-2	Roof	1044.1	232.8
FB-3	Roof	316.5	113.6
FB-4	Roof	378.4	-
FB-5	Roof	714.2	226.3
FB-6	Roof	1332.8	214.0
FB-7	Roof	1831.0	-
FB-8	El 42'-0"	2829.3	591.5
FB-9	El 42'-0"	1046.1	106.4
FB-10	El 42'-0"	1953.1	629.3
FB-8	El 42'-0"	-	710.3
FB-9	El 42'-0"	-	566.7
FB-10	El 42'-0"	-	1025.0

ANALYSIS NUMBER: 4

EARTHQUAKE: Olympia

PRINCIPAL COMPONENT DIRECTION: X

TABLE F4: MAXIMUM CONNECTION FORCES

("AS-MODIFIED" STRUCTURE)

WALL NUMBER	LOCATION	SHEAR STRESS (lb/ft)	RATIO OF MAXIMUM STRESS TO ALLOWABLE
FB-1	Roof	1064.7	0.3594
FB-2	Roof	1454.6	0.4910
FB-3	Roof	756.1	0.2552
FB-4	Roof	955.8	0.3226
FB-5	Roof	947.4	0.3198
FB-6	Roof	2687.7	0.9072
FB-7	Roof	2687.7	0.9072
FB-8	El 42'-0"	3965.8	0.3869
FB-9	El 42'-0"	3881.5	0.3786
FB-10	El 42'-0"	2805.6	0.2737

ANALYSIS NUMBER: 4

EARTHQUAKE: Olympia

PRINCIPAL COMPONENT DIRECTION: X

TABLE F5 : MAXIMUM DIAPHRAGM FORCES
("AS-MODIFIED" STRUCTURE)

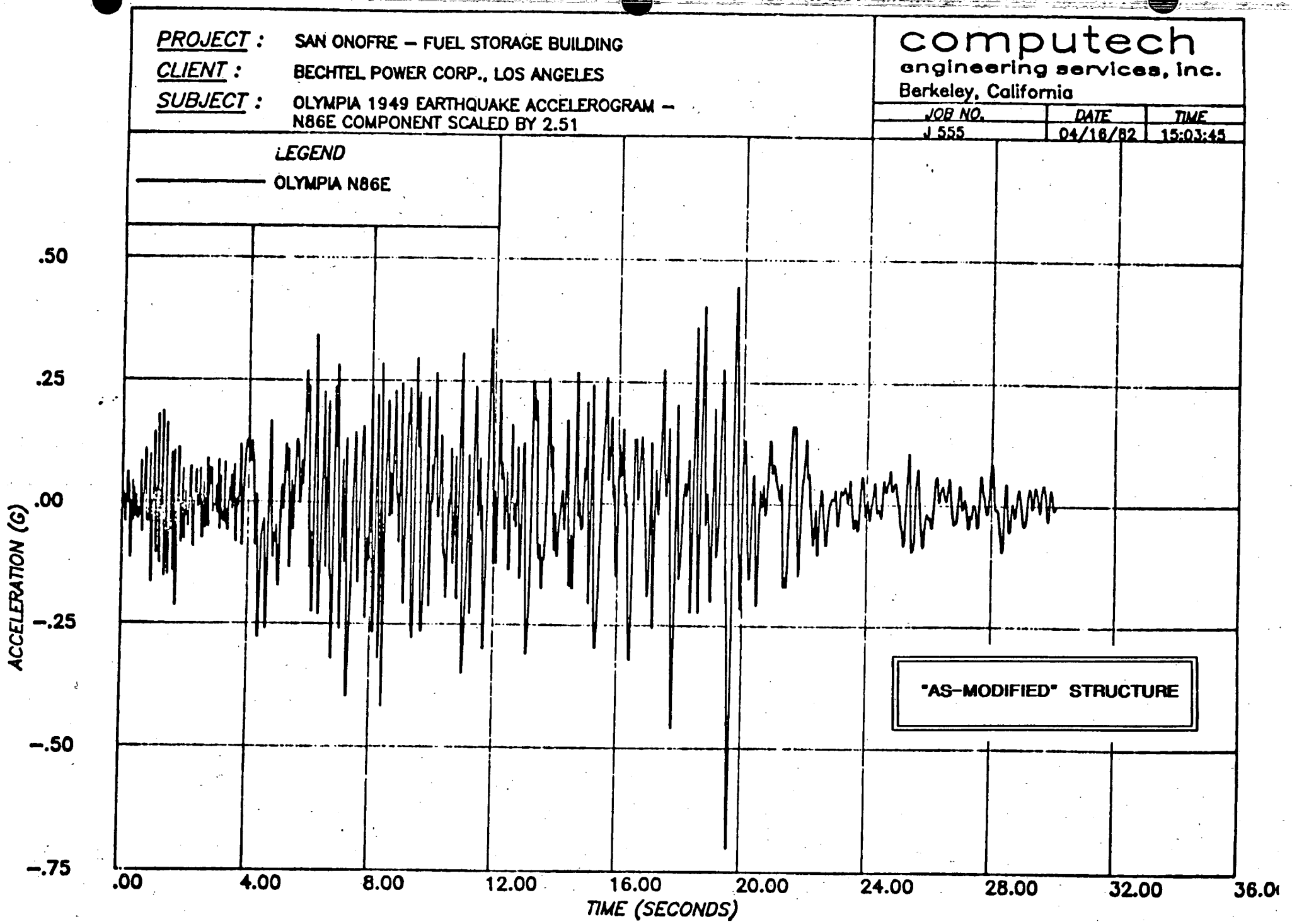

FIGURE F1 – TIME HISTORY AS SCALED [Y(N-S)]

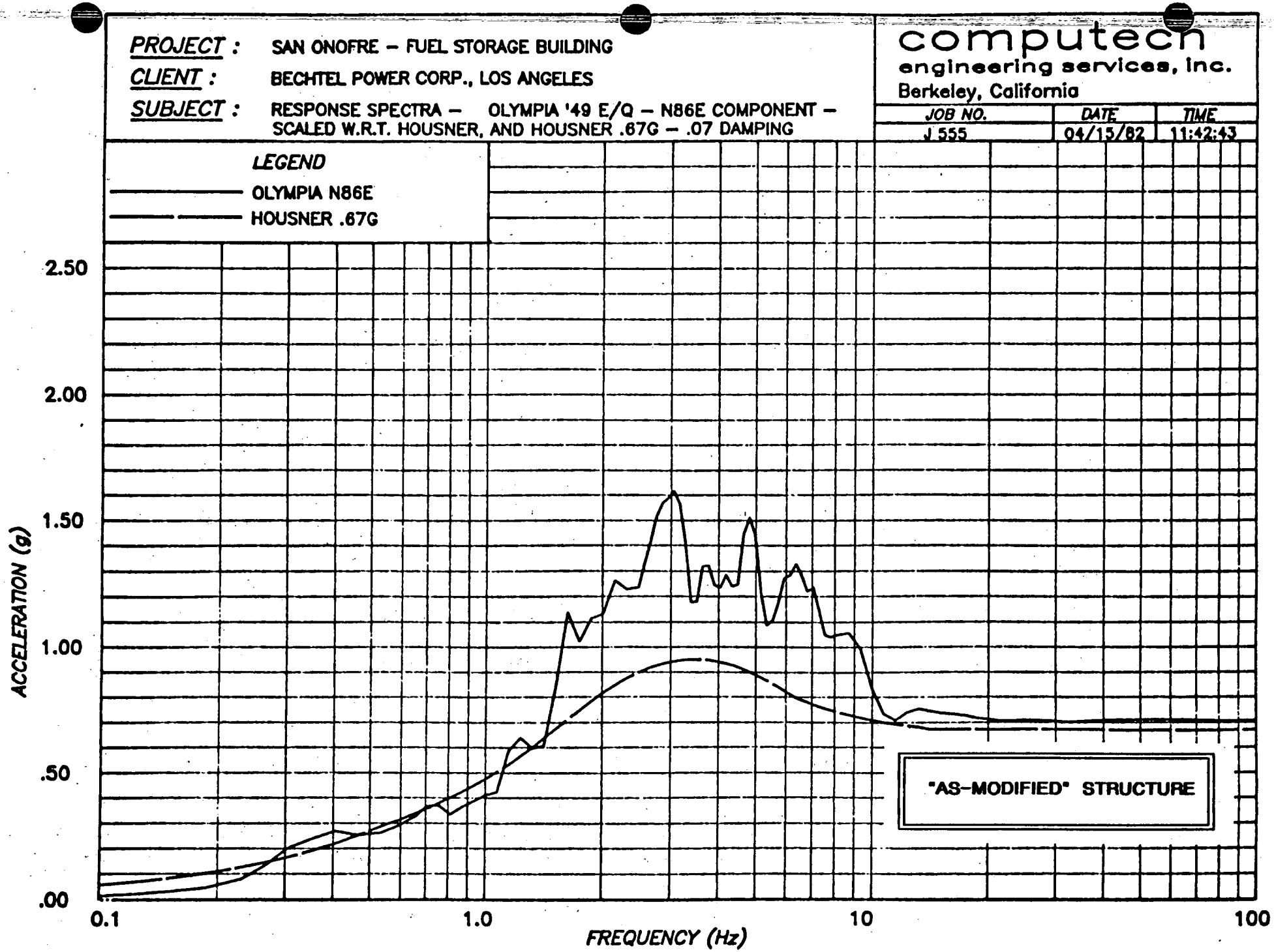

FIGURE F2 – RESPONSE SPECTRUM [Y(N-S)]

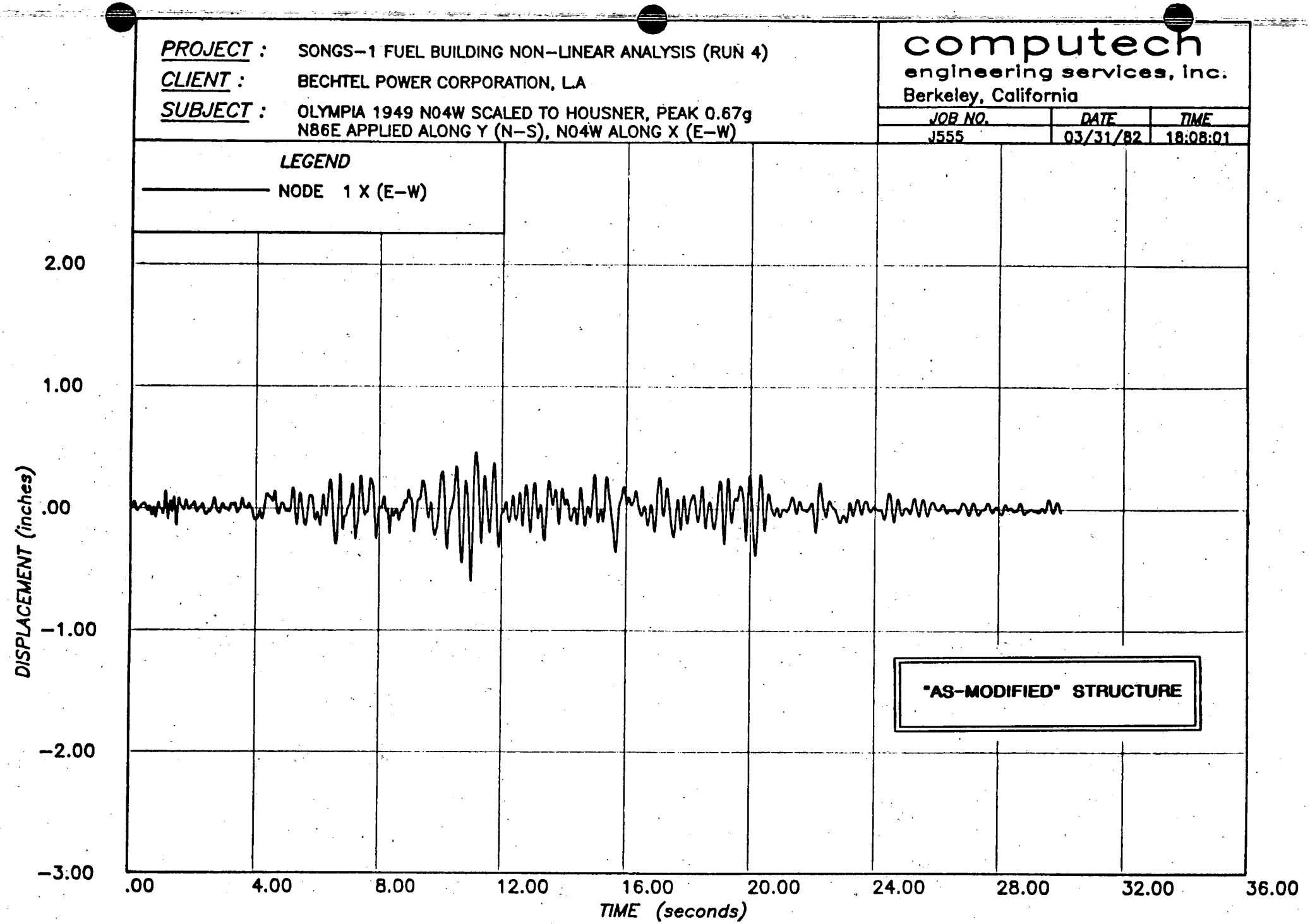

FIGURE F3 – ROOF DISPLACEMENT

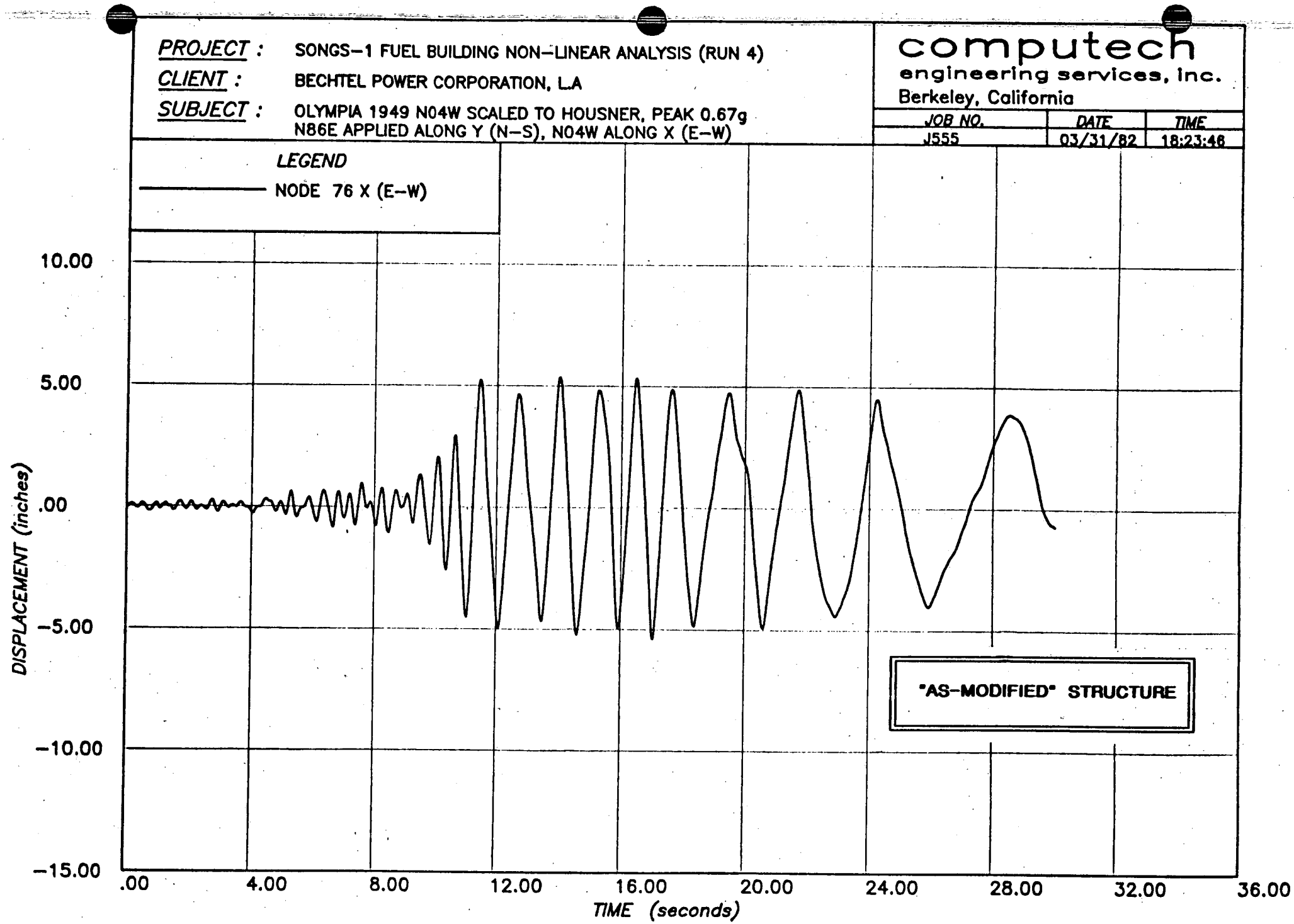

FIGURE F4 - OUT-OF-PLANE WALL DISPLACEMENTS - CENTER

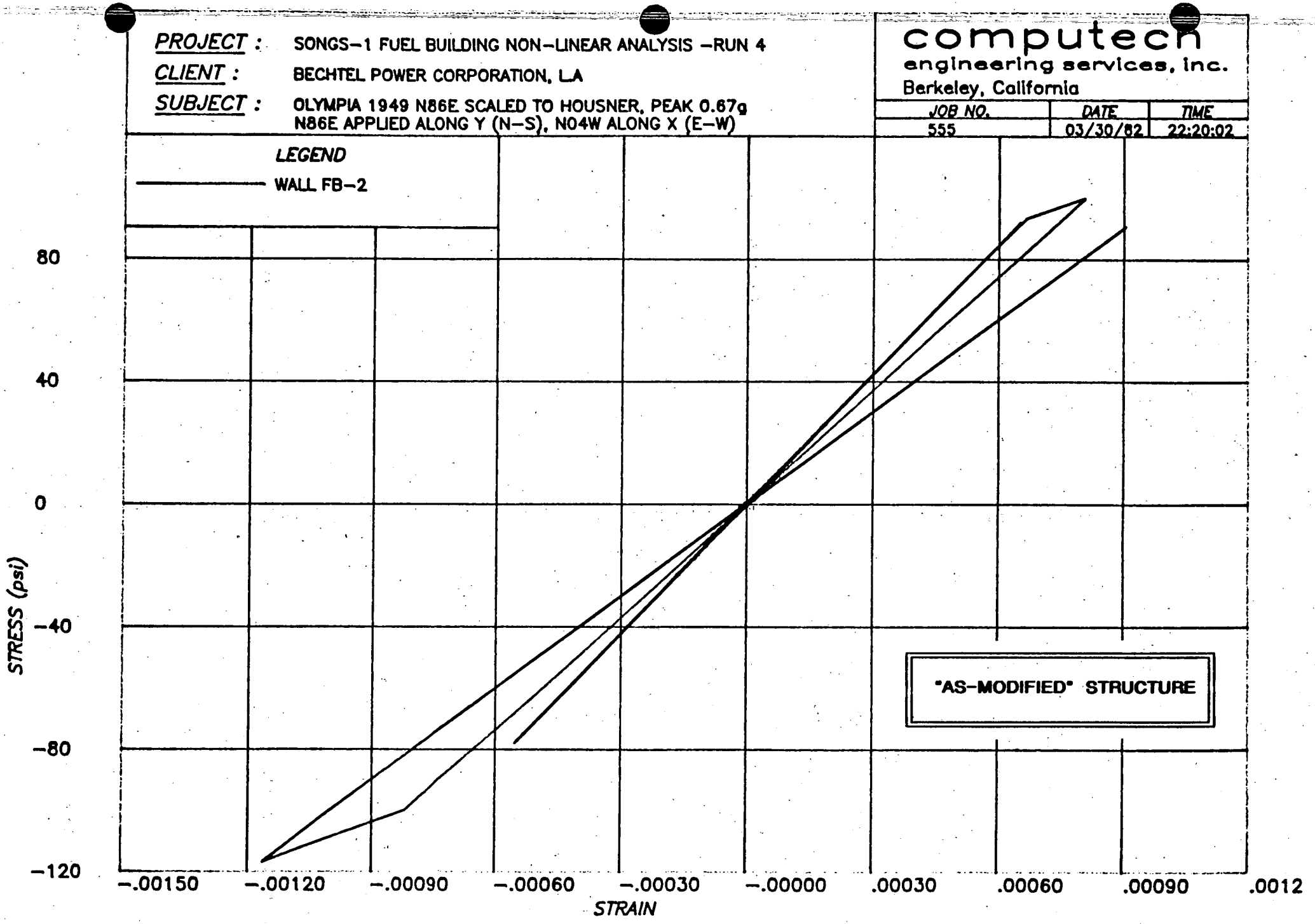

FIGURE F5 - IN-PLANE WALL STRESS-STRAIN - EL 42'

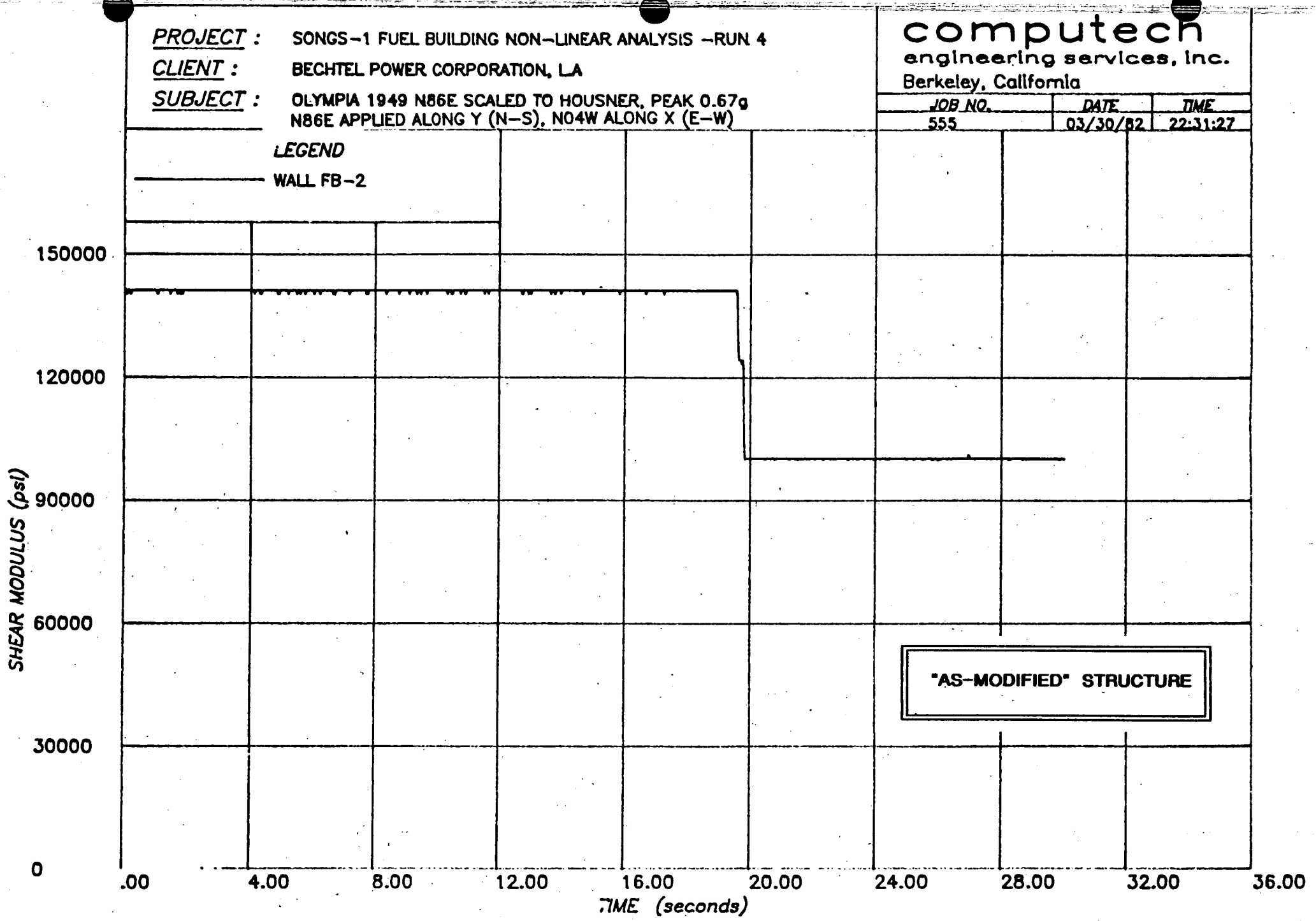

FIGURE F6 - IN-PLANE WALL STIFFNESS - EL 42'

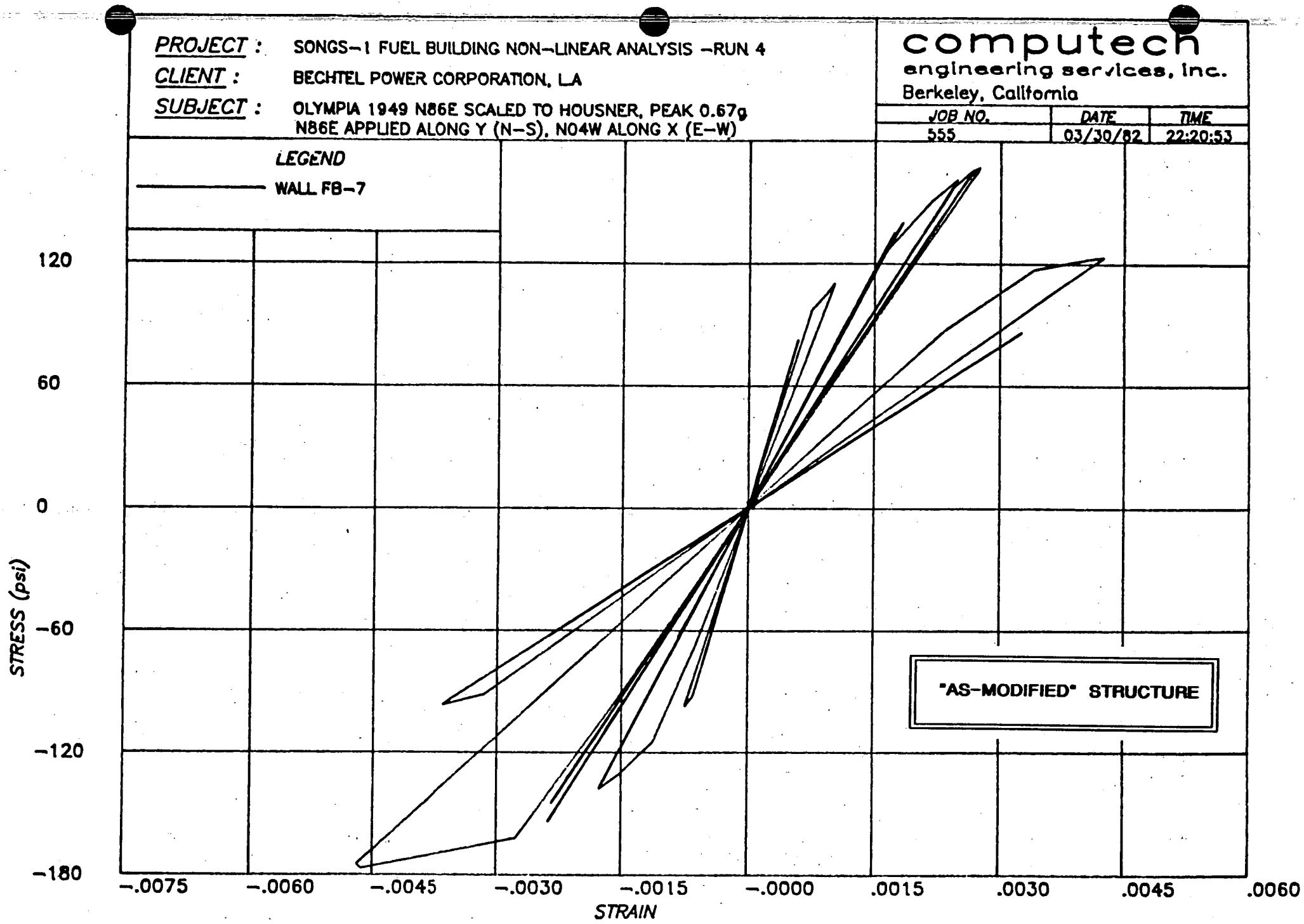

FIGURE F7 - IN-PLANE WALL STRESS-STRAIN - EL 42'

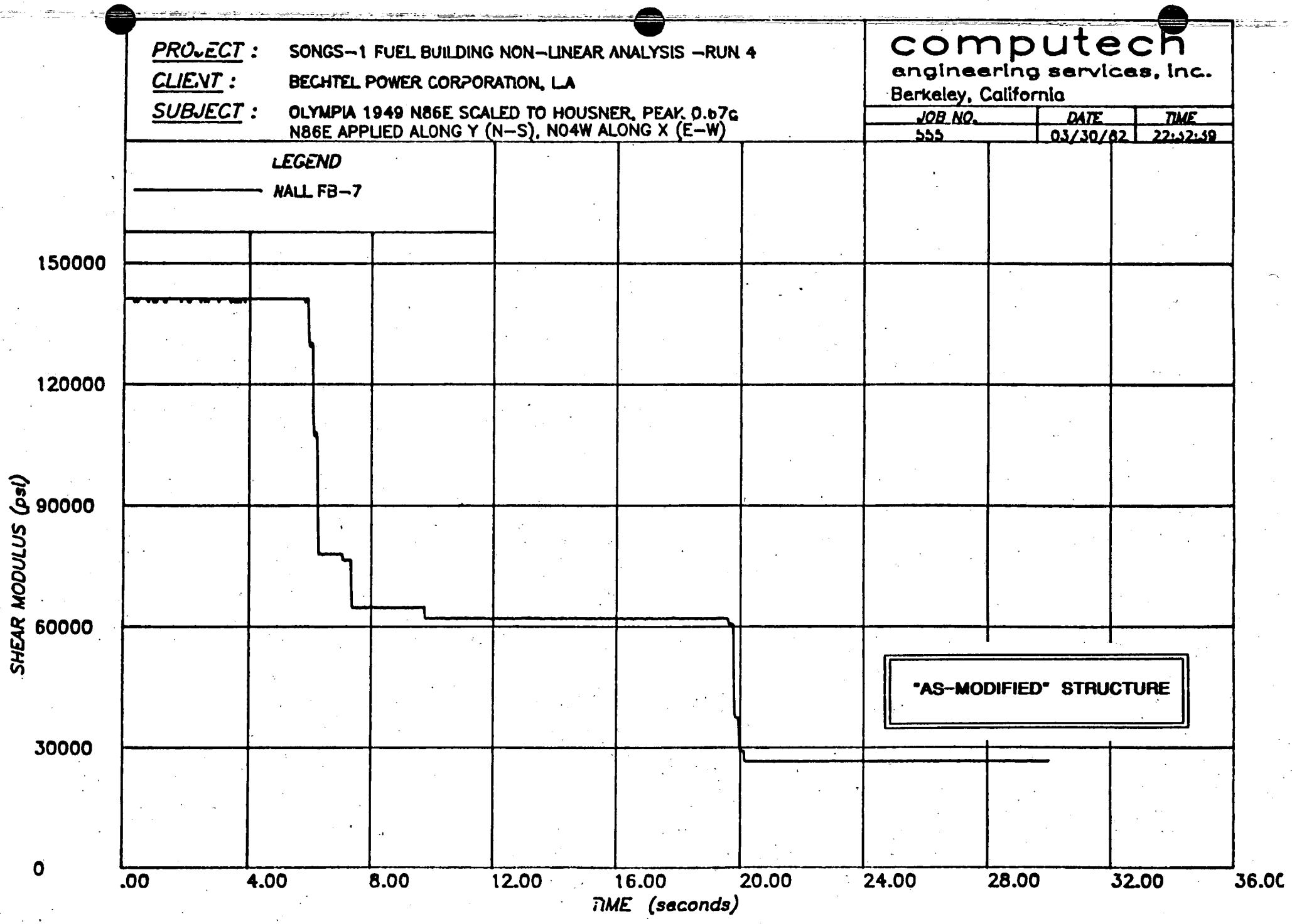

FIGURE F8 - IN-PLANE WALL STIFFNESS - EL 42'

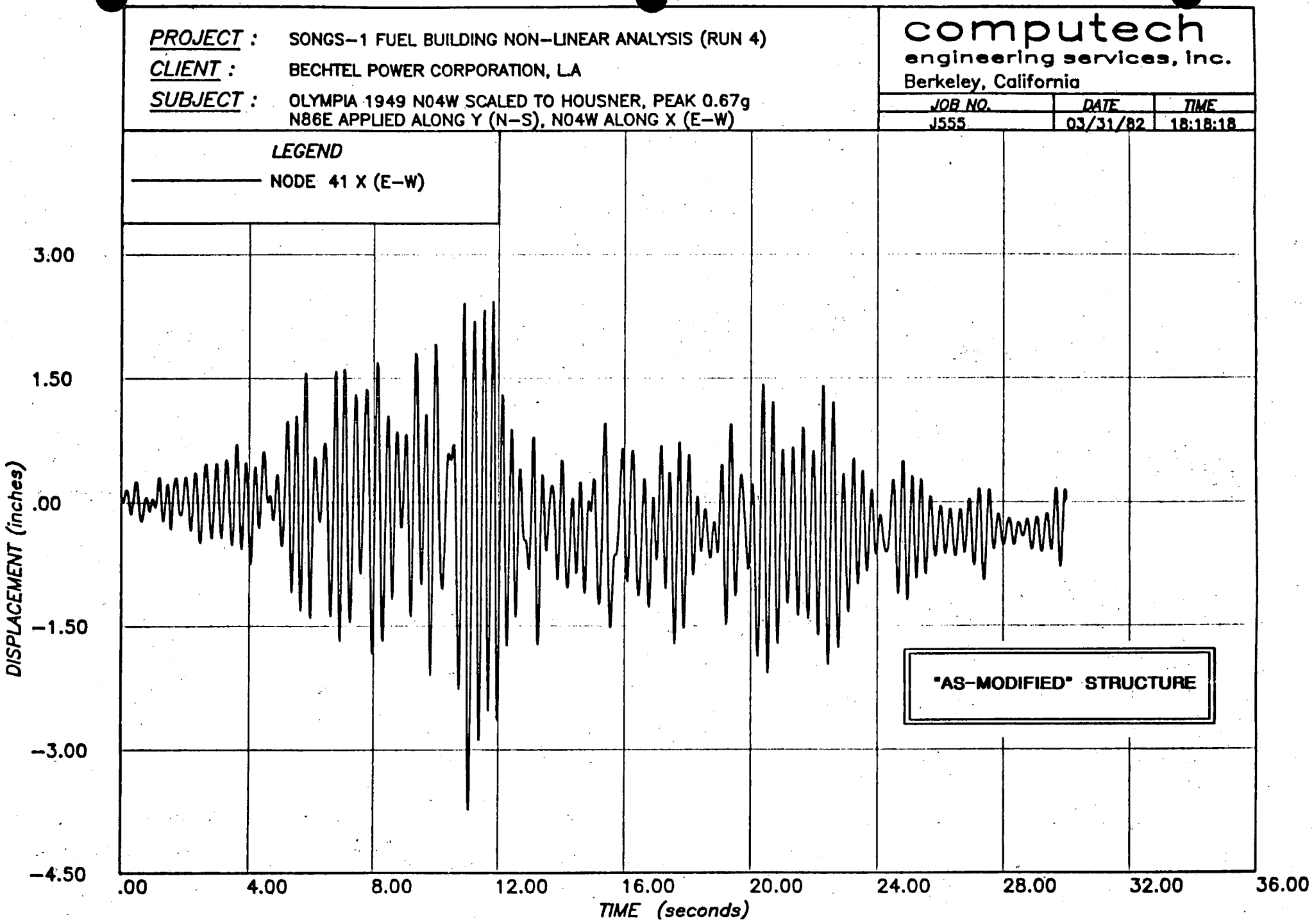

FIGURE F9 – DISPLACEMENT AT ROOF OPENING – EAST

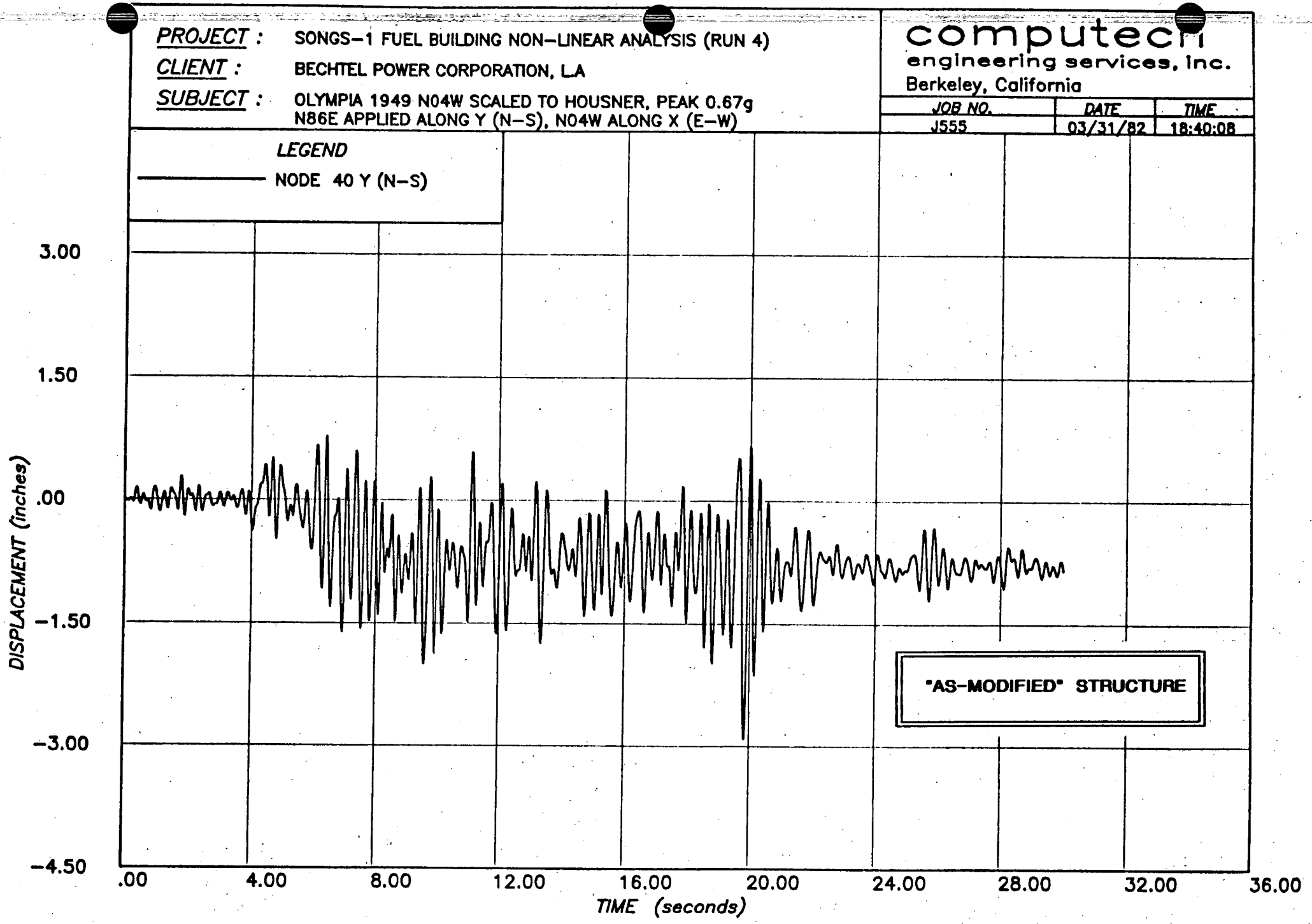

FIGURE F10 – DISPLACEMENT AT ROOF OPENING – SOUTH

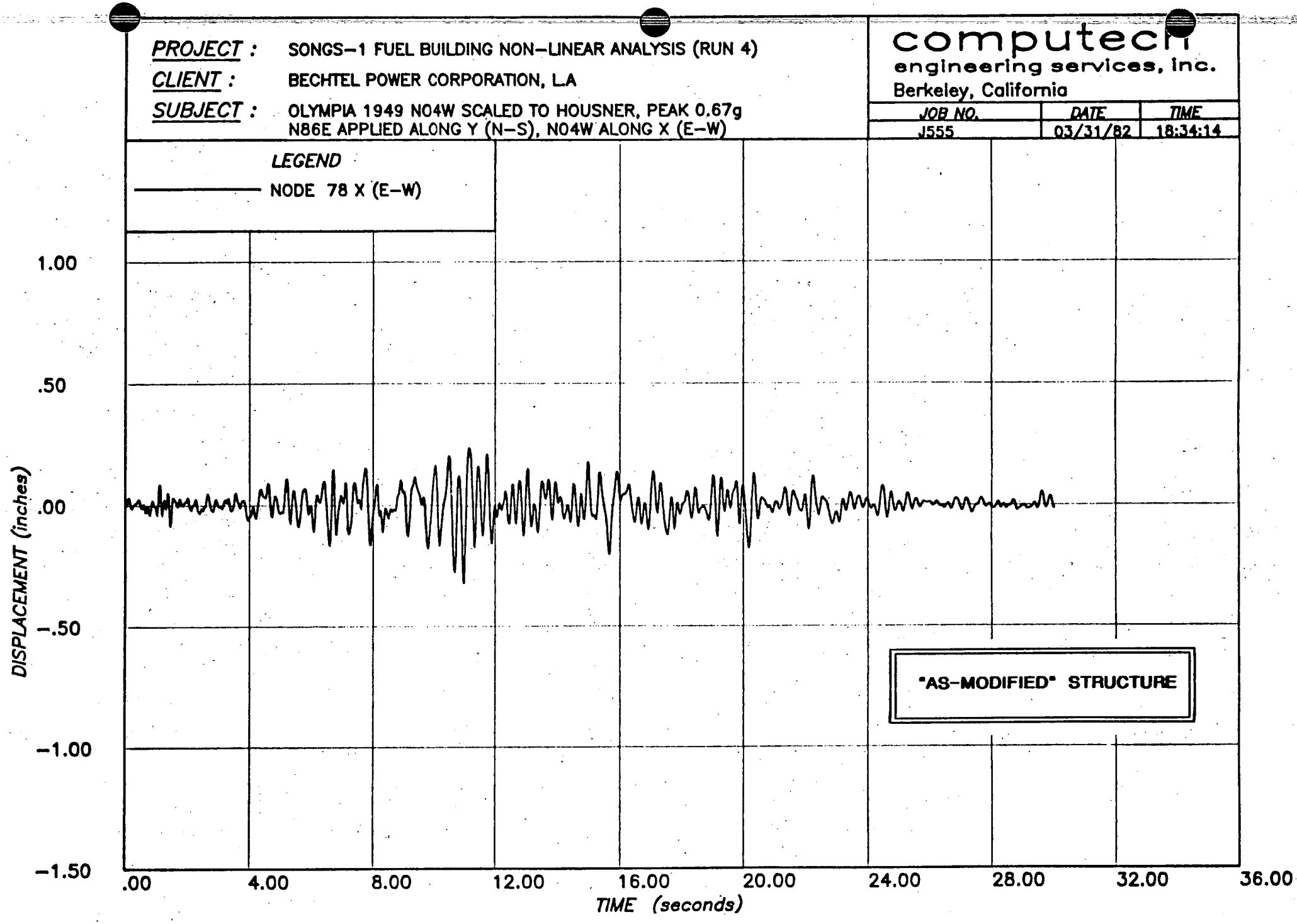

FIGURE F11 – TOP OF POOL: DISPLACEMENT

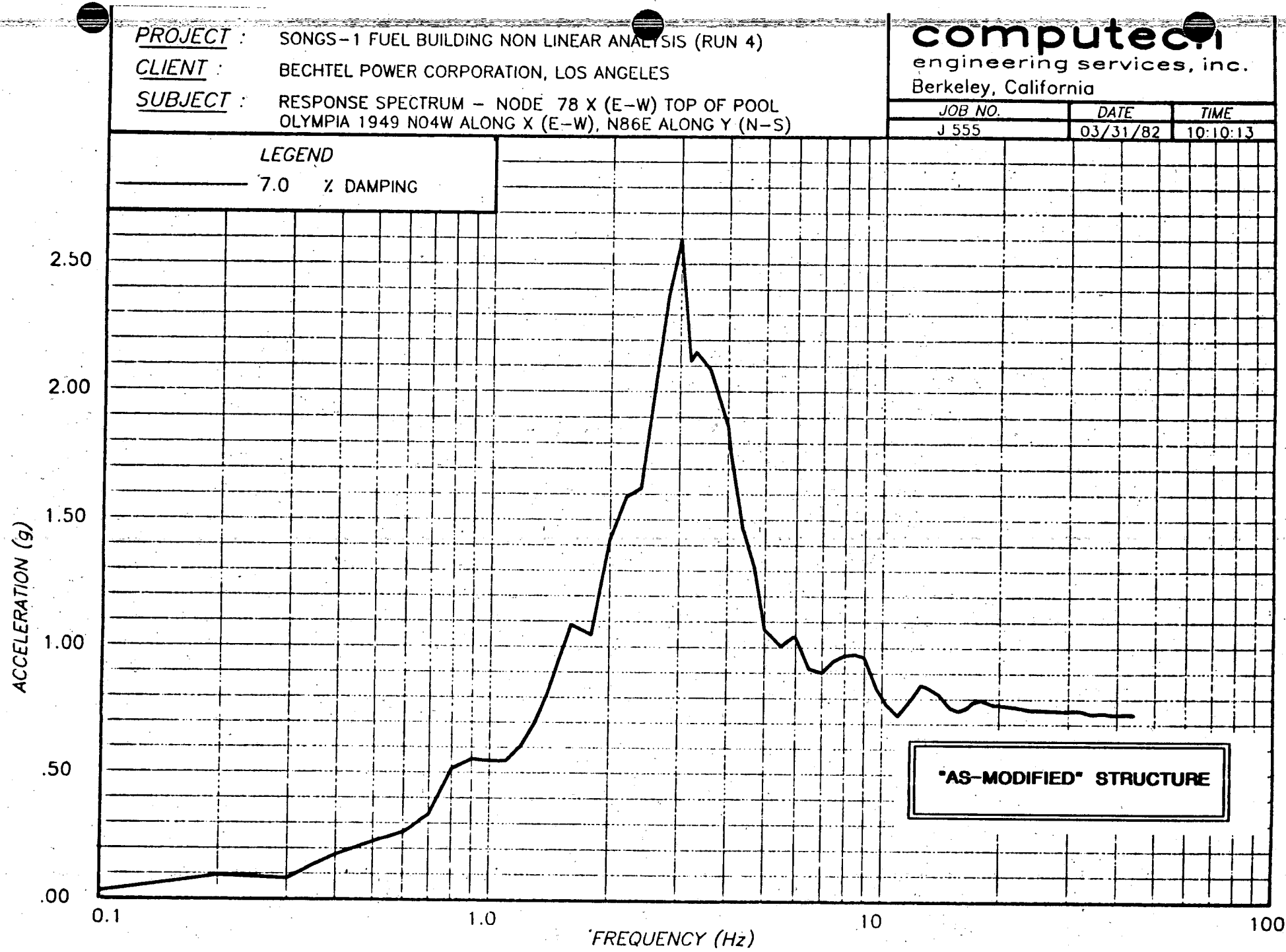

FIGURE F12 - TOP OF POOL: RESPONSE SPECTRUM - HORIZONTAL

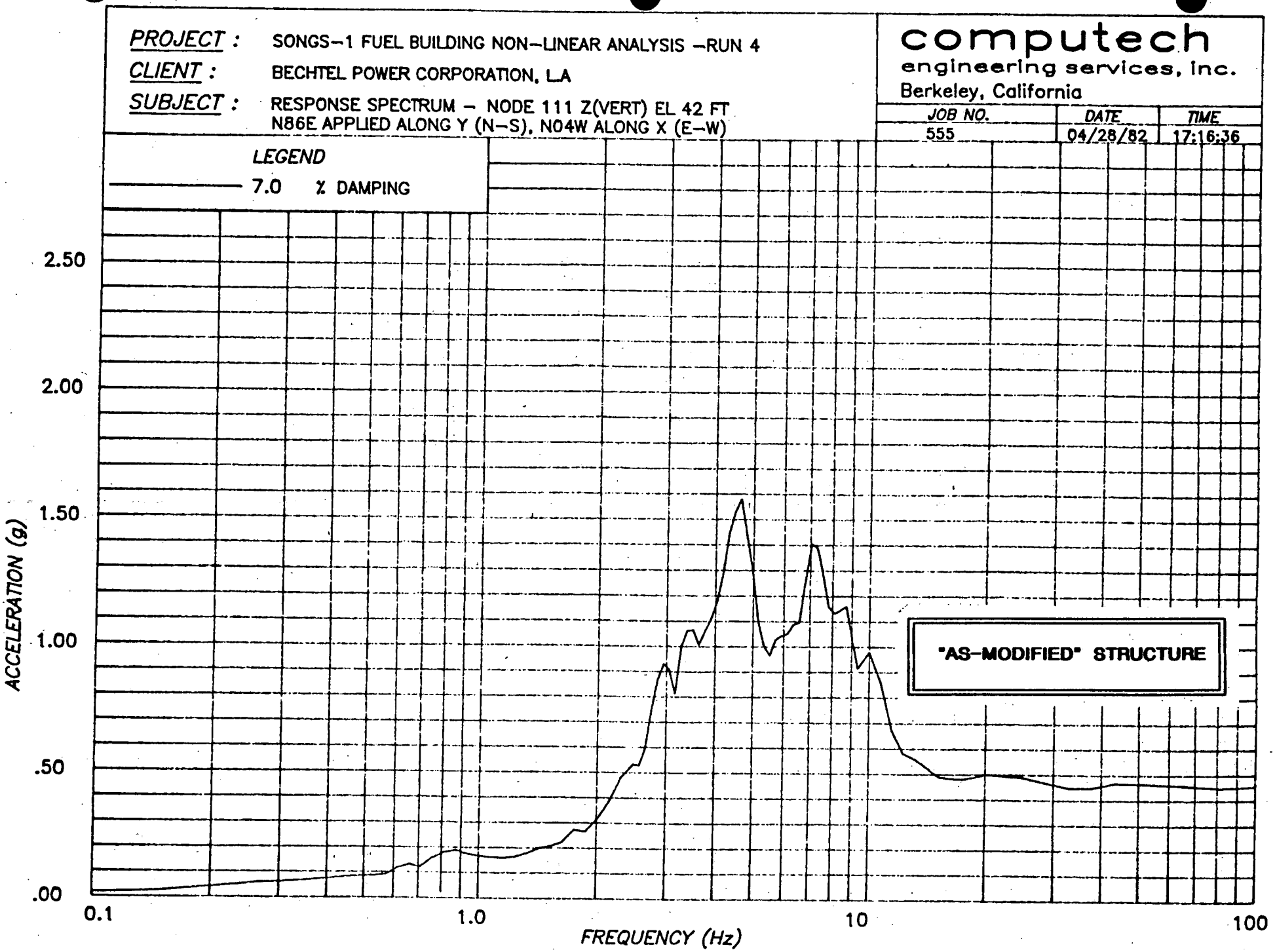

FIGURE F13 - TOP OF POOL: RESPONSE SPECTRUM - VERTICAL

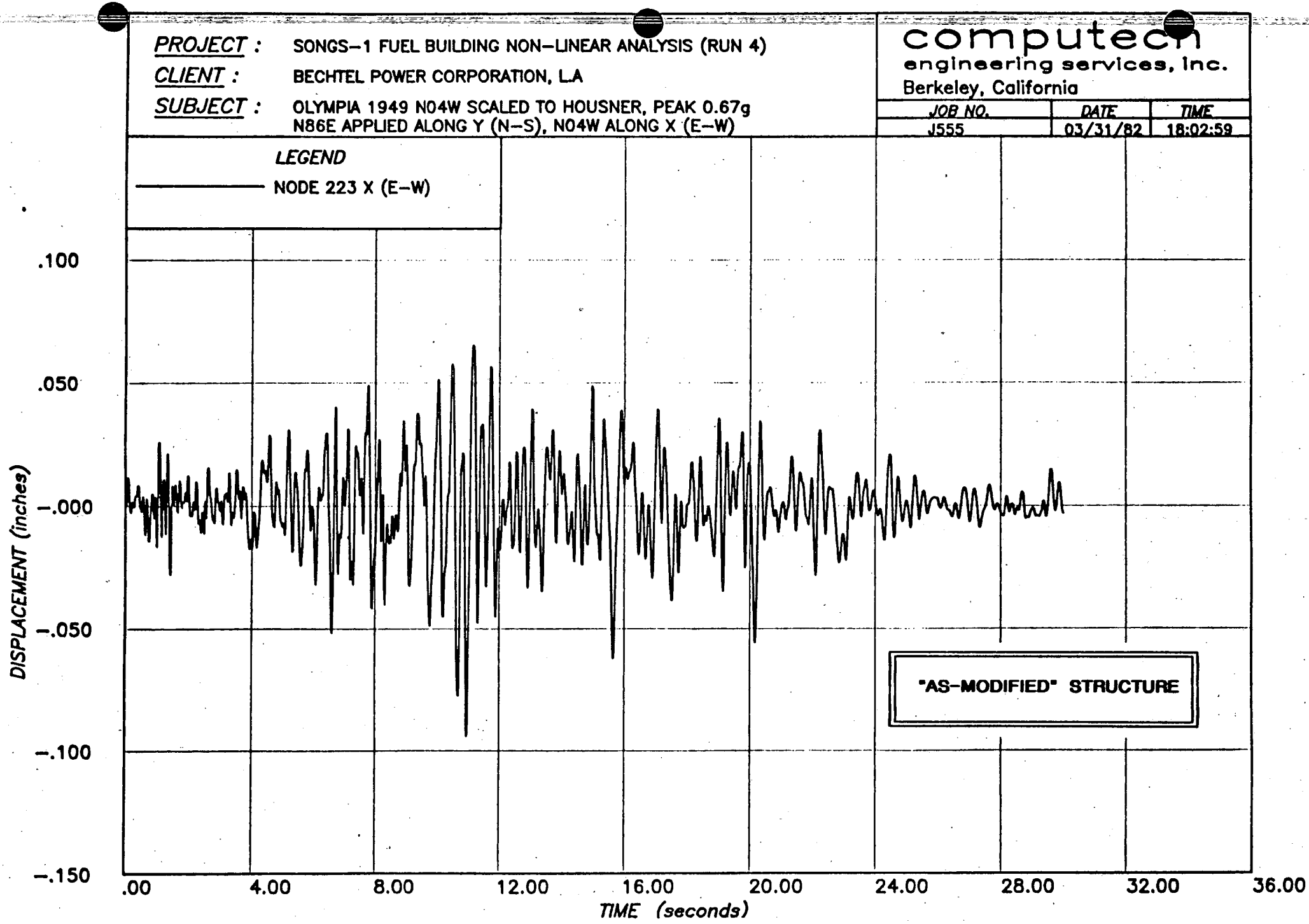

FIGURE F14 – BASE OF POOL: DISPLACEMENT

APPENDIX G: DETAILED RESULTS

Y(N-S) EARTHQUAKE: Taft 1952 S69E, Scaled 2.90, 0.67g Peak

X(E-W) EARTHQUAKE: Taft 1952 N21W, Scaled 2.90,

LOCATION	DISPLACEMENT (inches)	
	MAXIMUM	MINIMUM
ROOF		
N-W Corner	1.357	-1.126
S-W Corner	1.277	-1.102
N-E Corner	1.411	-1.216
S-E Corner	1.379	-1.193
TOP OF FUEL POOL		
N-W Corner	0.810	-0.694
S-W Corner	0.812	-0.696
N-E Corner	0.866	-0.747
S-E Corner	0.868	-0.749
BASE OF FUEL POOL		
N-W Corner	0.067	-0.066
S-W Corner	0.067	-0.066
N-E Corner	0.118	-0.109
S-E Corner	0.117	-0.109

ANALYSIS NUMBER 5

EARTHQUAKE: Taft

PRINCIPAL COMPONENT DIRECTION: Y

TABLE G1: MAXIMUM DISPLACEMENTS

("AS-MODIFIED" STRUCTURE)

WALL NUMBER	SHEAR STRESS (p.s.i)	SHEAR STRAIN	RATIO OF MAXIMUM STRAIN TO ALLOWABLE
FB-1	-36.32	-0.00026	0.0985
FB-2	97.00	0.00075	0.2841
FB-3	-56.07	-0.00040	0.1515
FB-4	-48.58	-0.00035	0.1326
FB-5	48.98	0.00035	0.1326
FB-6	48.22	0.00034	0.1288
FB-7	167.3	0.00284	0.5379
FB-8	123.7	0.00132	0.5000
FB-9	132.2	0.00158	0.5985
FB-10	-68.47	-0.00049	0.1856

ANALYSIS NUMBER: 5

EARTHQUAKE: Taft

PRINCIPAL COMPONENT DIRECTION: Y

TABLE G2 : MAXIMUM IN-PLANE WALL RESPONSE
("AS-MODIFIED" STRUCTURE)

WALL	STEEL STRAIN RATIO		MASONRY STRESS	CENTER DISPLACEMENT
	CENTER	END	fm (p.s.i.)	(inches)
FB-1	11.72	15.44	655.9	6.01
FB-2	7.18	1050	656.0	4.21
FB-3	5.81	9.65	655.9	3.70
FB-4				
FB-5	10.35	11.21	655.9	5.63
FB-6	7.34	11.51	655.3	5.18
FB-7				
FB-8	.81	.50	528.3	.79
FB-9	.68	.35	442.7	.60
FB-10	.84	.64	549.3	1.07

ANALYSIS NUMBER: 5

EARTHQUAKE: Taft

PRINCIPAL COMPONENT DIRECTION: Y

TABLE G3: MAXIMUM OUT-OF-PLANE MASONRY WALL RESPONSE

("AS-MODIFIED" STRUCTURE)

WALL NUMBER	LOCATION	SHEAR STRESS (lb/ft)	TENSION (lb/ft)
FB-1	Roof	620.3	257.5
FB-2	Roof	931.0	233.2
FB-3	Roof	311.7	113.6
FB-4	Roof	267.5	-
FB-5	Roof	620.9	225.9
FB-6	Roof	1252.3	214.3
FB-7	Roof	1600.5	-
FB-8	El 42'-0"	2558.1	576.6
FB-9	El 42'-0"	1037.5	137.1
FB-10	El 42'-0"	1823.5	589.6
FB-8	El 42'-0"	-	583.0
FB-9	El 42'-0"	-	418.3
FB-10	El 42'-0"	-	878.6

ANALYSIS NUMBER: 5

EARTHQUAKE: Taft

PRINCIPAL COMPONENT DIRECTION: Y

TABLE G4: MAXIMUM CONNECTION FORCES

("AS-MODIFIED" STRUCTURE)

WALL NUMBER	LOCATION	SHEAR STRESS (lb/ft)	RATIO OF MAXIMUM STRESS TO ALLOWABLE
FB-1	Roof	929.9	0.3139
FB-2	Roof	1406.7	0.4748
FB-3	Roof	744.7	0.2514
FB-4	Roof	675.9	0.2282
FB-5	Roof	894.7	0.3020
FB-6	Roof	2153.6	0.7270
FB-7	Roof	2153.6	0.7270
FB-8	El 42'-0"	3445.2	0.3361
FB-9	El 42'-0"	3535.1	0.3449
FB-10	El 42'-0"	2954.7	0.2882

ANALYSIS NUMBER: 5

EARTHQUAKE: Taft

PRINCIPAL COMPONENT DIRECTION: Y

TABLE G5 : MAXIMUM DIAPHRAGM FORCES

("AS-MODIFIED" STRUCTURE)

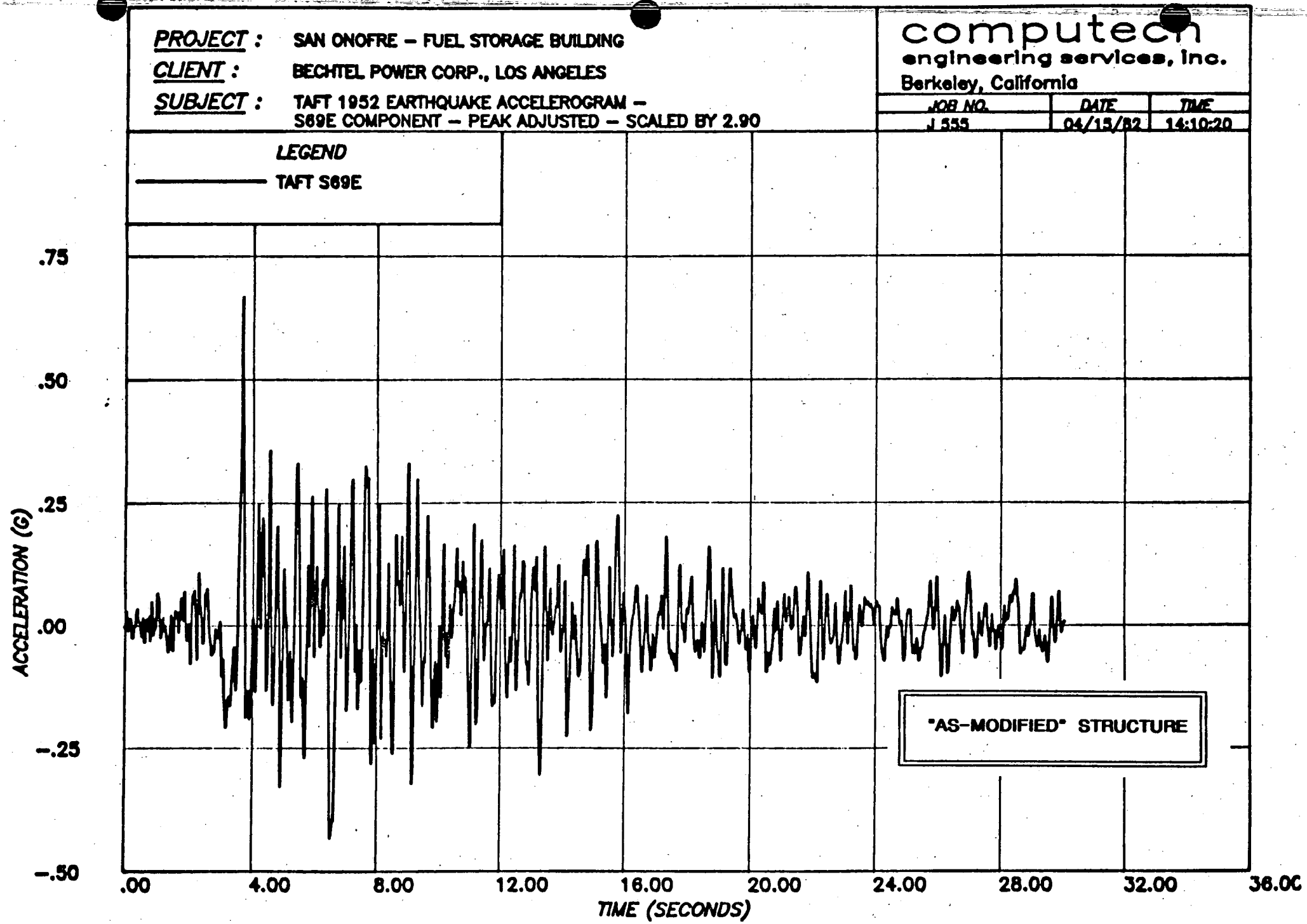

FIGURE G1 – TIME HISTORY AS SCALED [Y(N-S)]

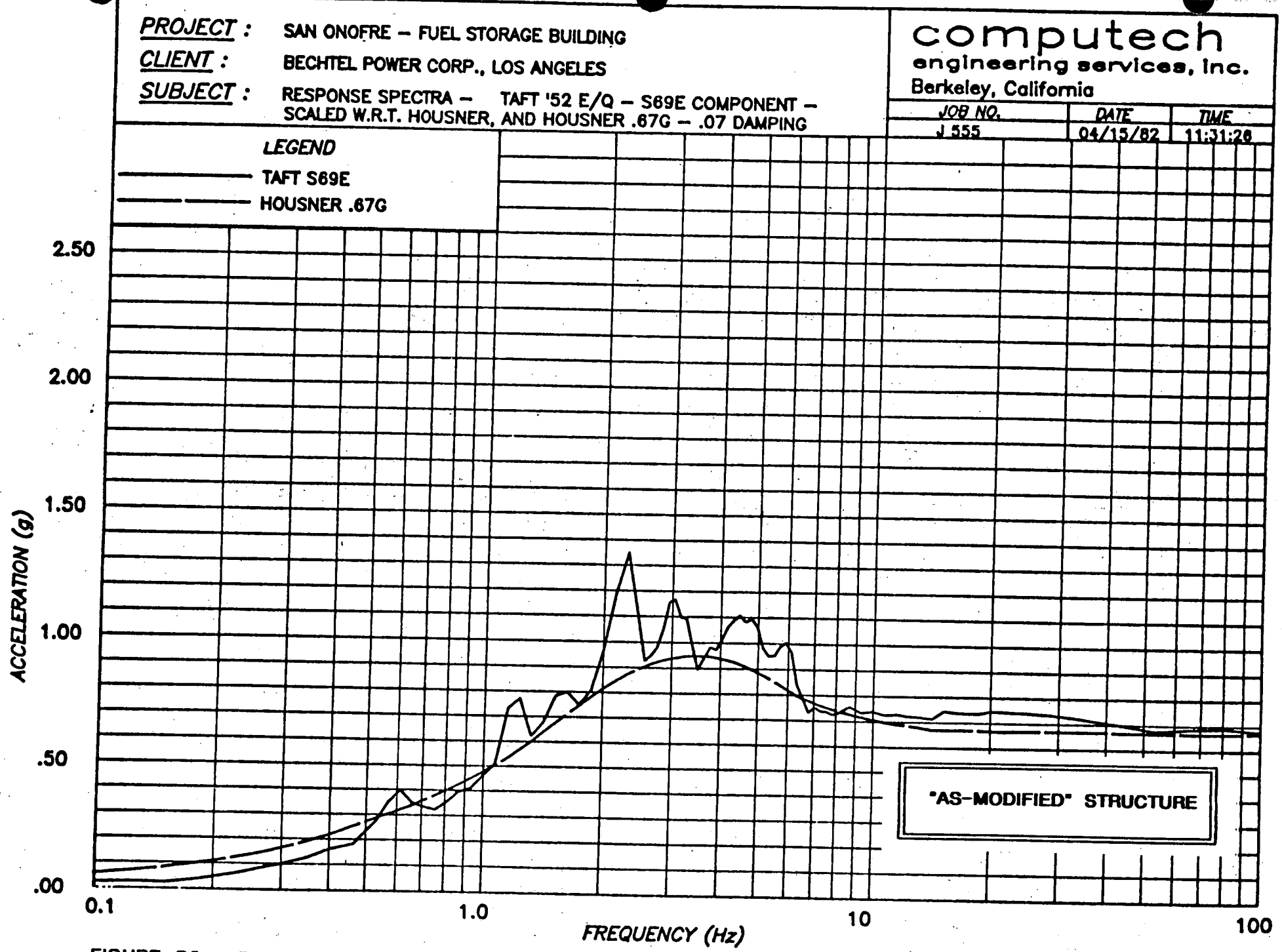

FIGURE G2 – RESPONSE SPECTRUM [Y(N-S)]

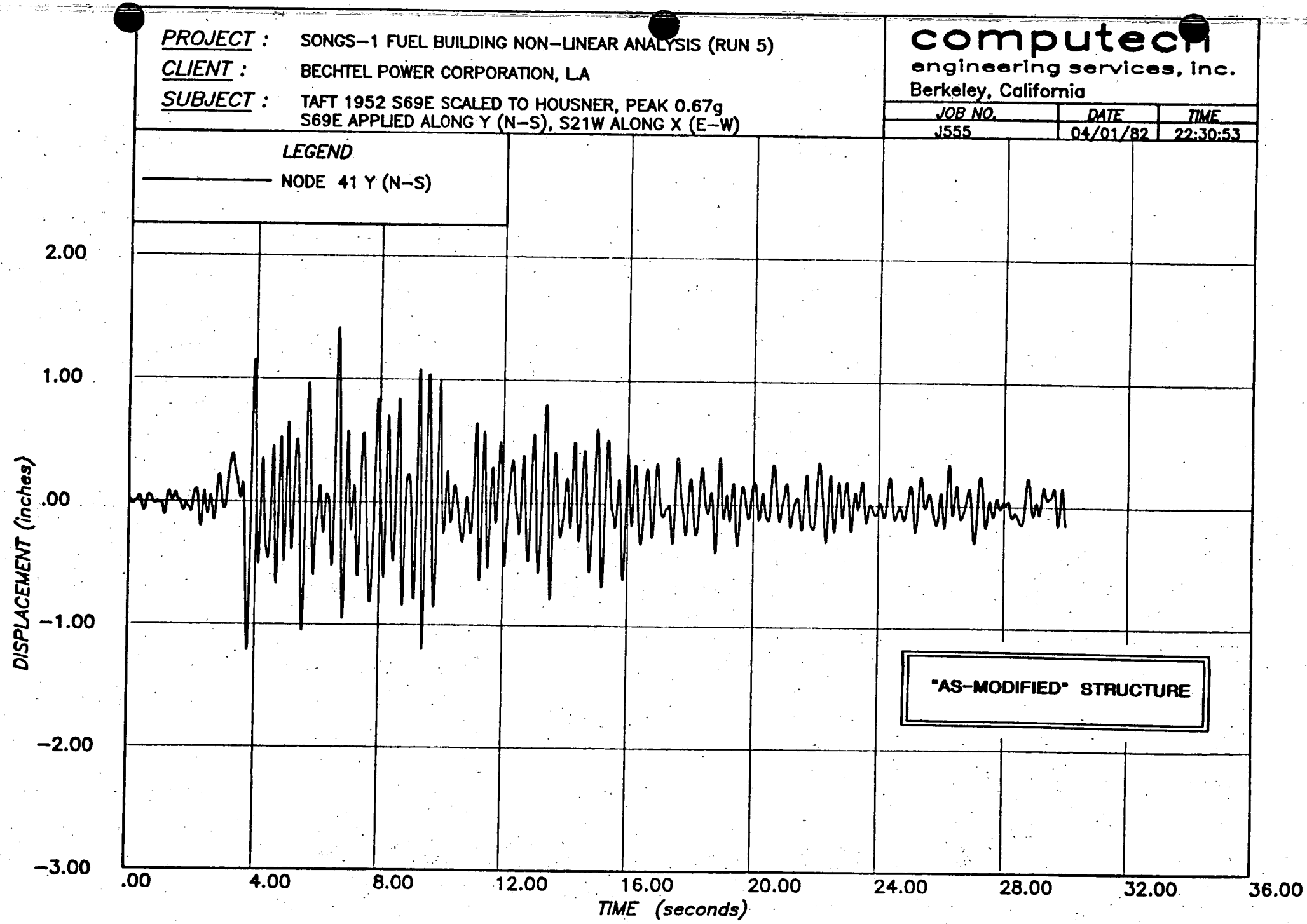

FIGURE G3 – ROOF DISPLACEMENT

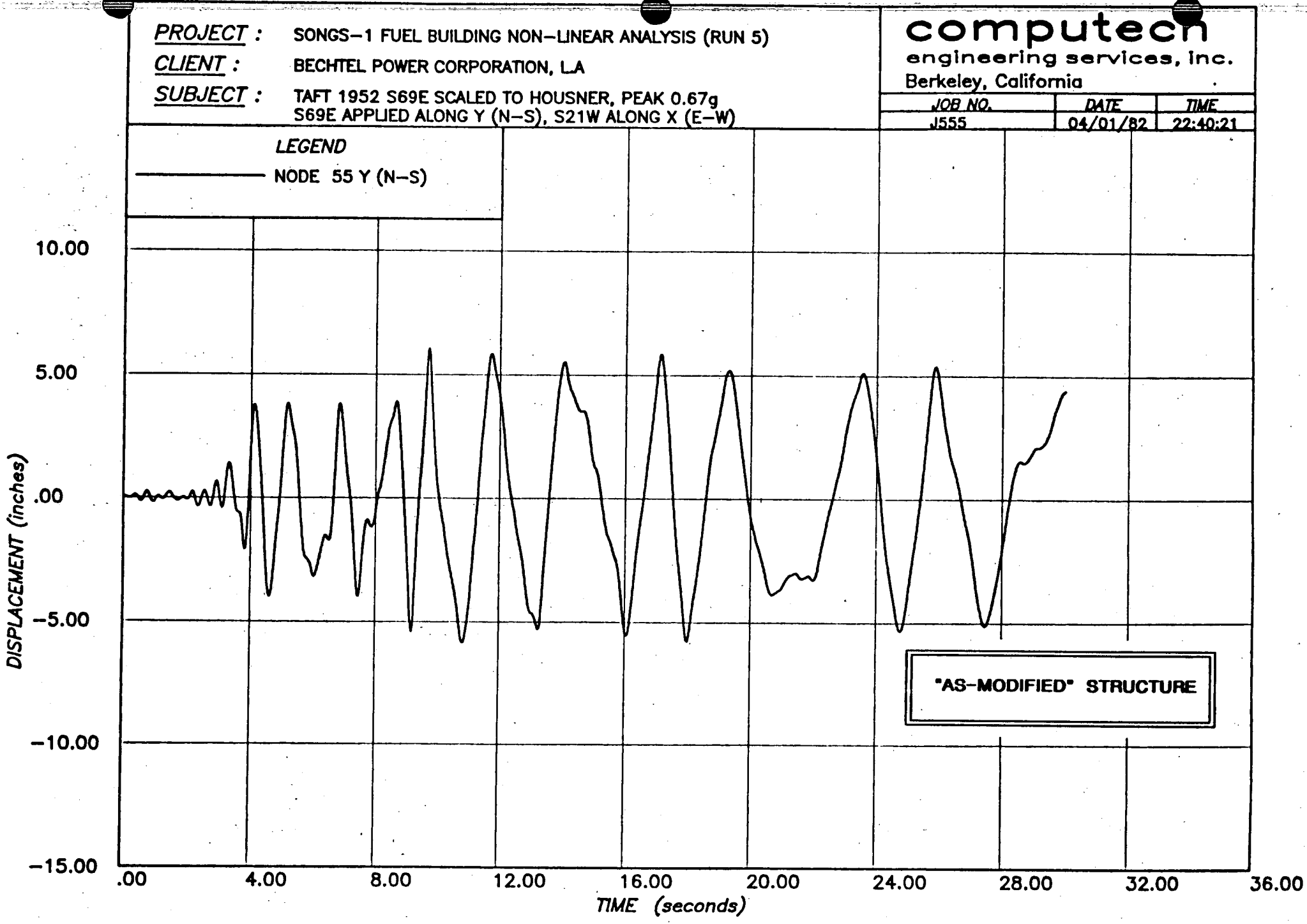

FIGURE G4 – OUT–OF–PLANE WALL DISPLACEMENTS – CENTER

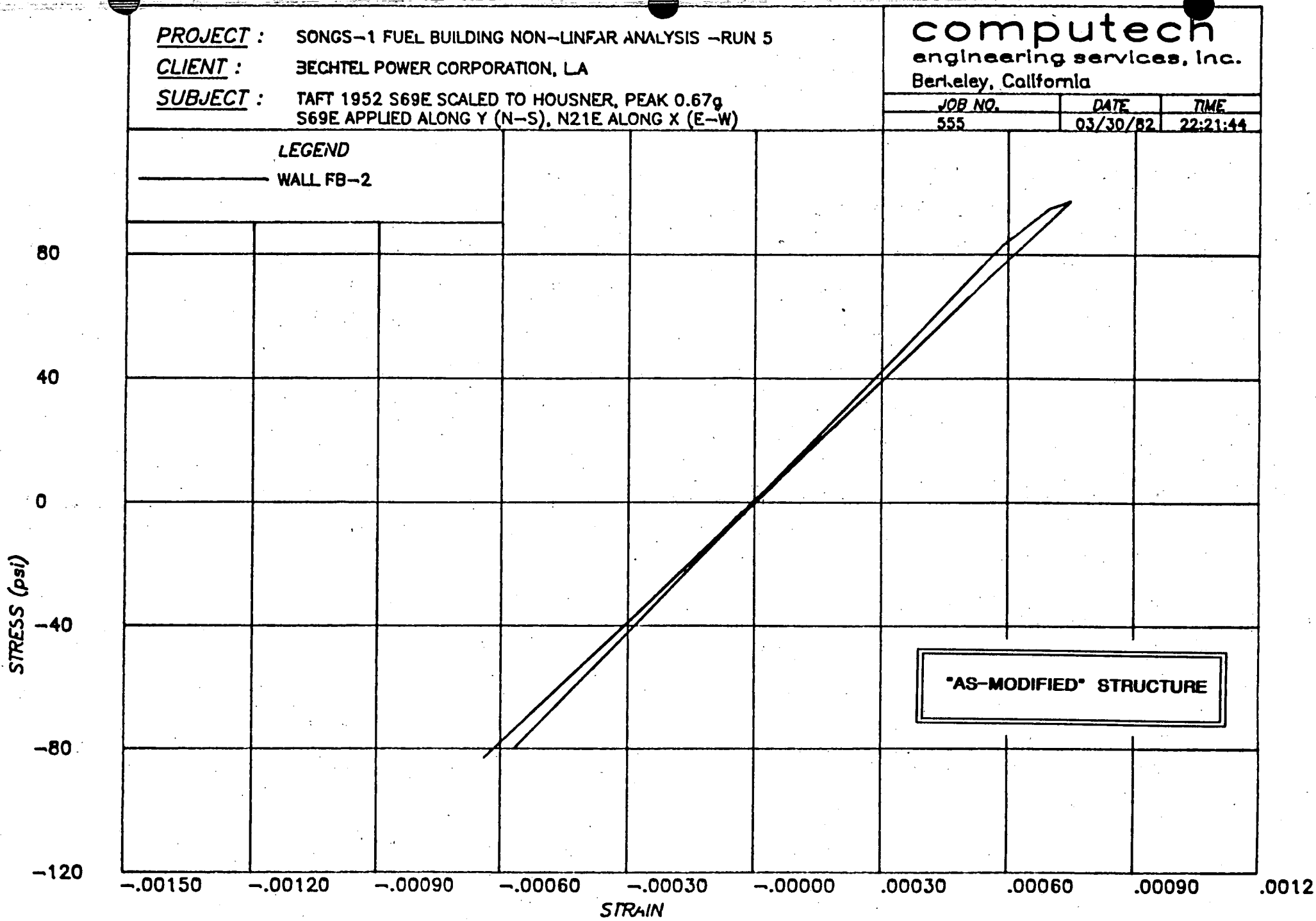

FIGURE G5 - IN-PLANE WALL STRESS-STRAIN - EL 42'

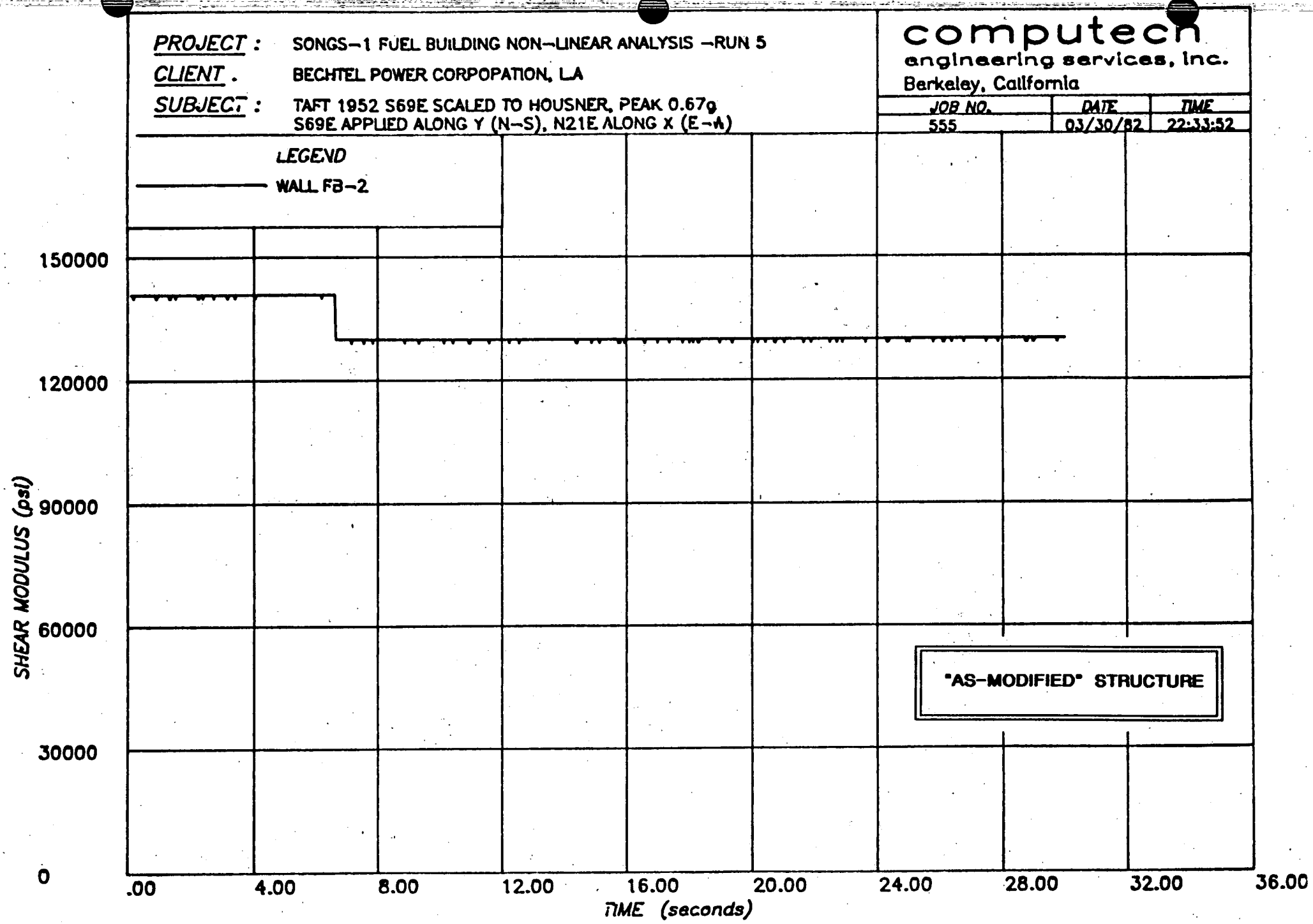

FIGURE G6 - IN-PLANE WALL STIFFNESS - EL 42'

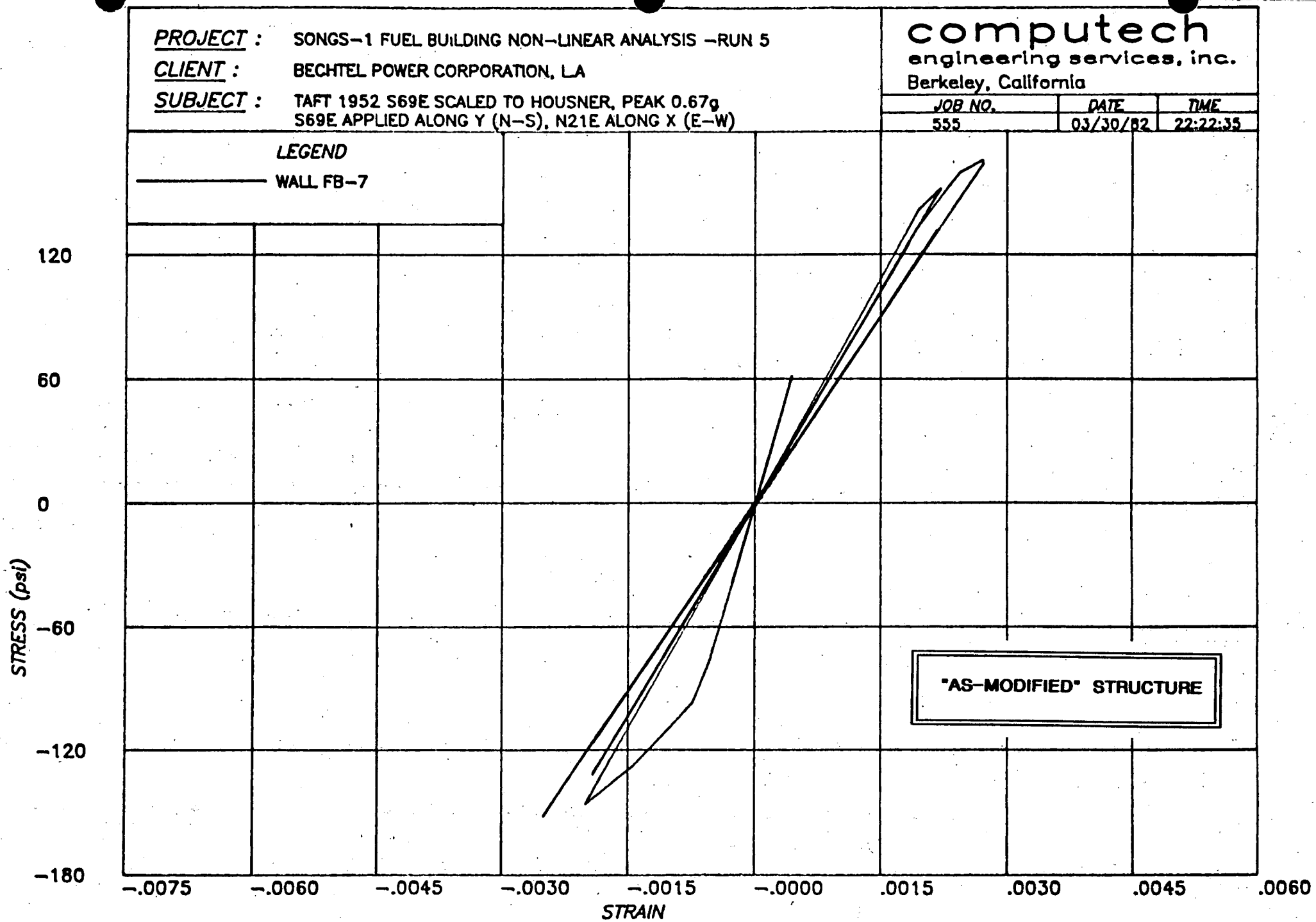

FIGURE G7 - IN-PLANE WALL STRESS-STRAIN - EL 42'

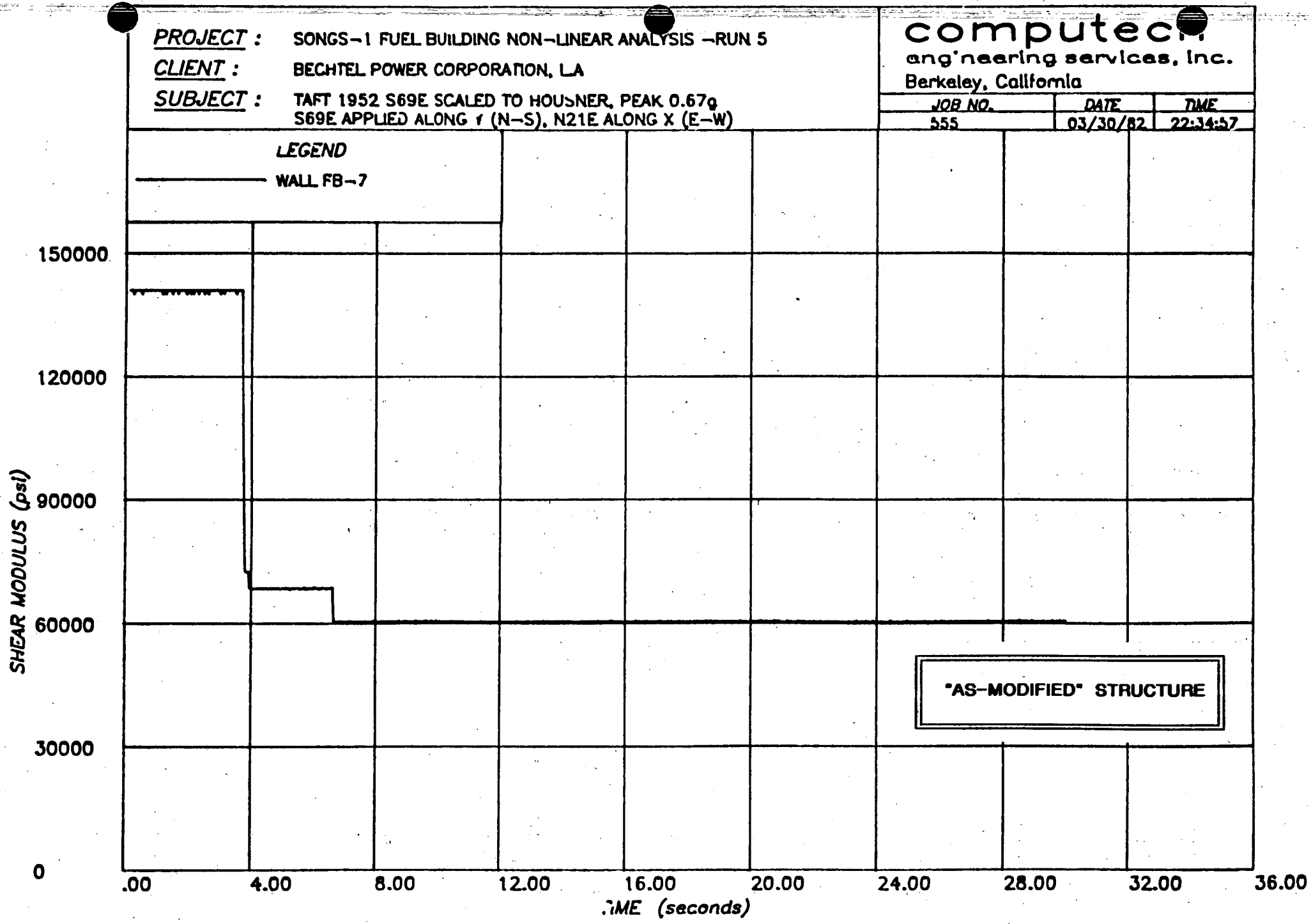

FIGURE G8 - IN-PLANE WALL STIFFNESS - EL 42'

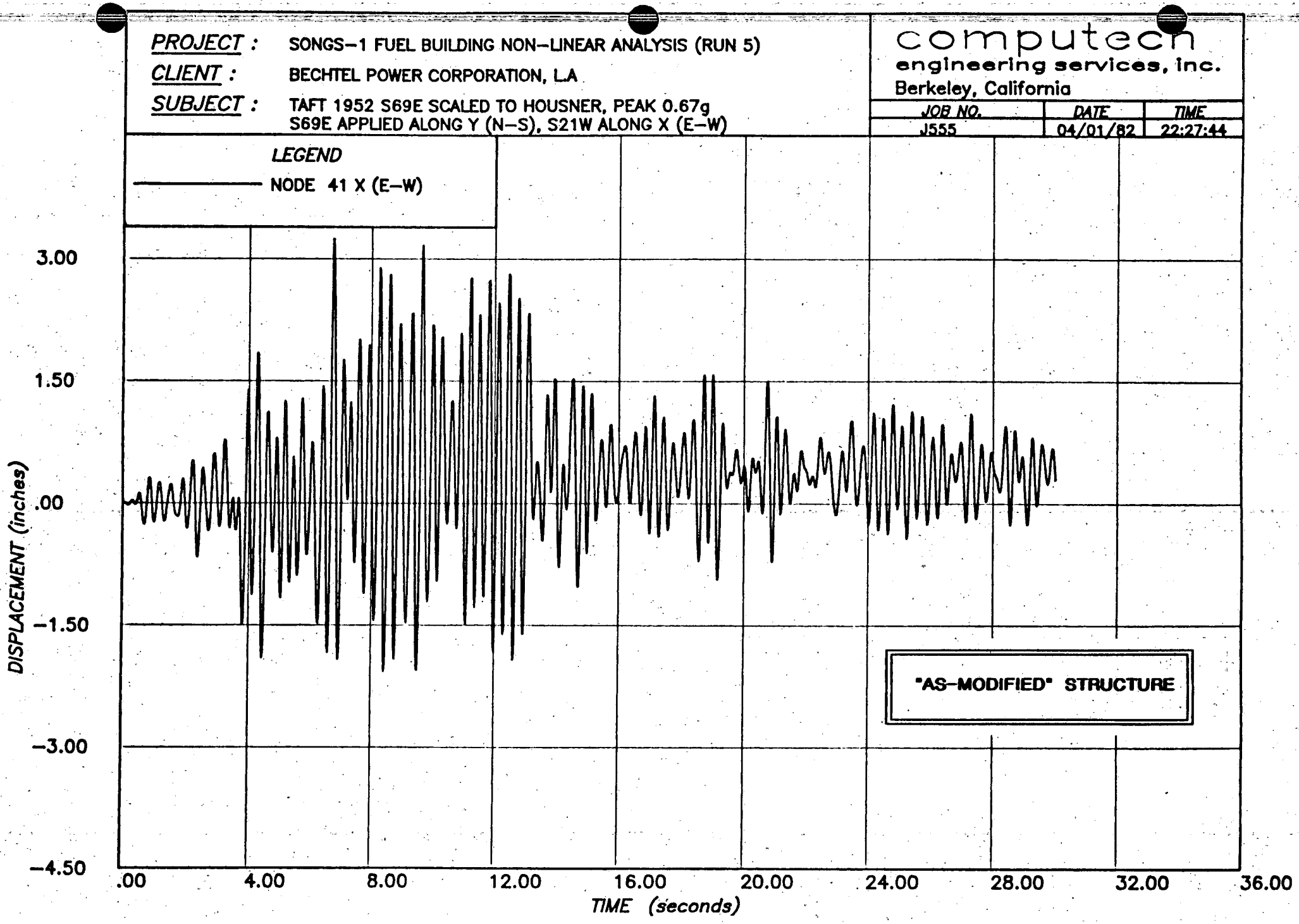

FIGURE G9 – DISPLACEMENT AT ROOF OPENING – EAST

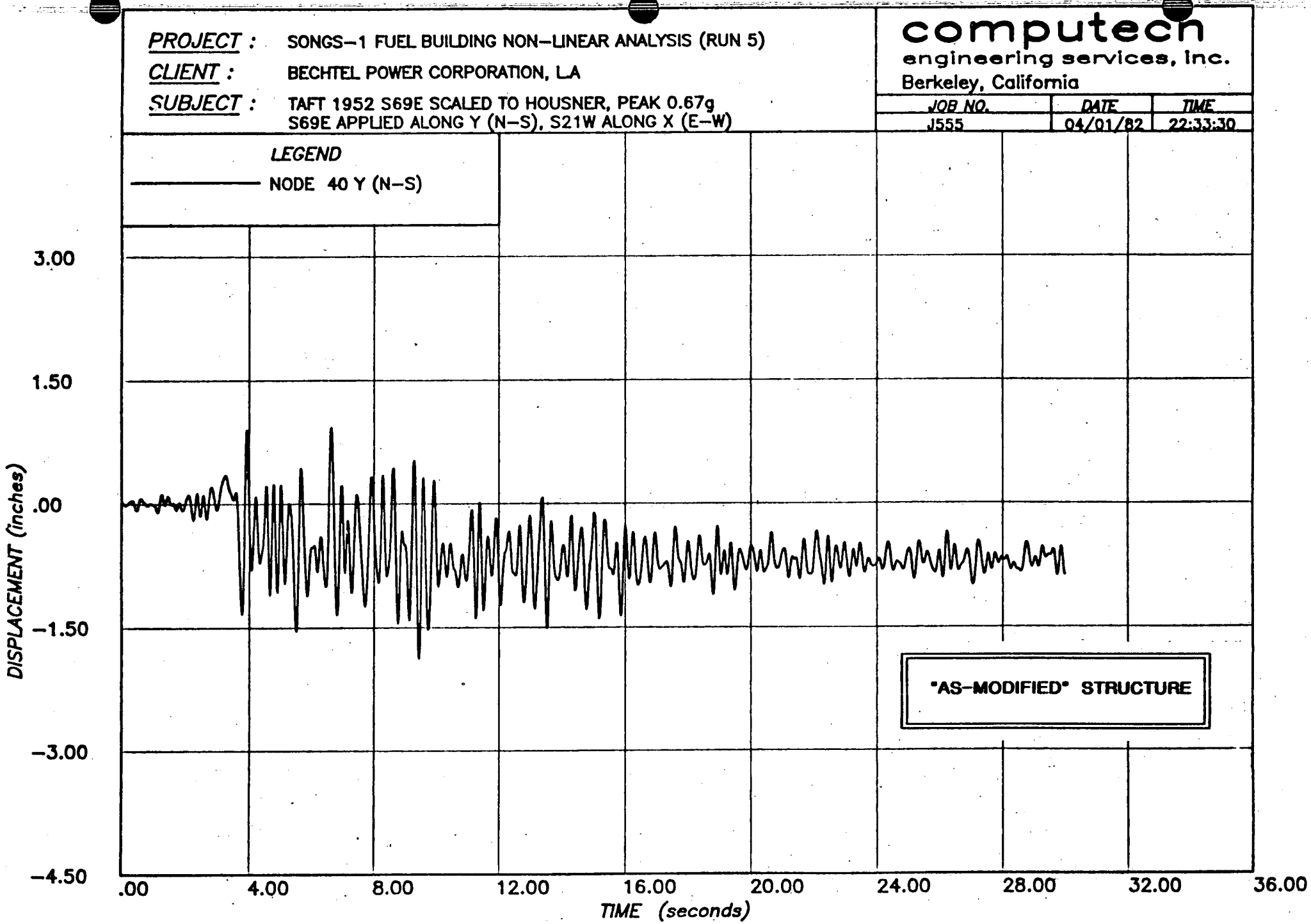

FIGURE G10 – DISPLACEMENT AT ROOF OPENING – SOUTH

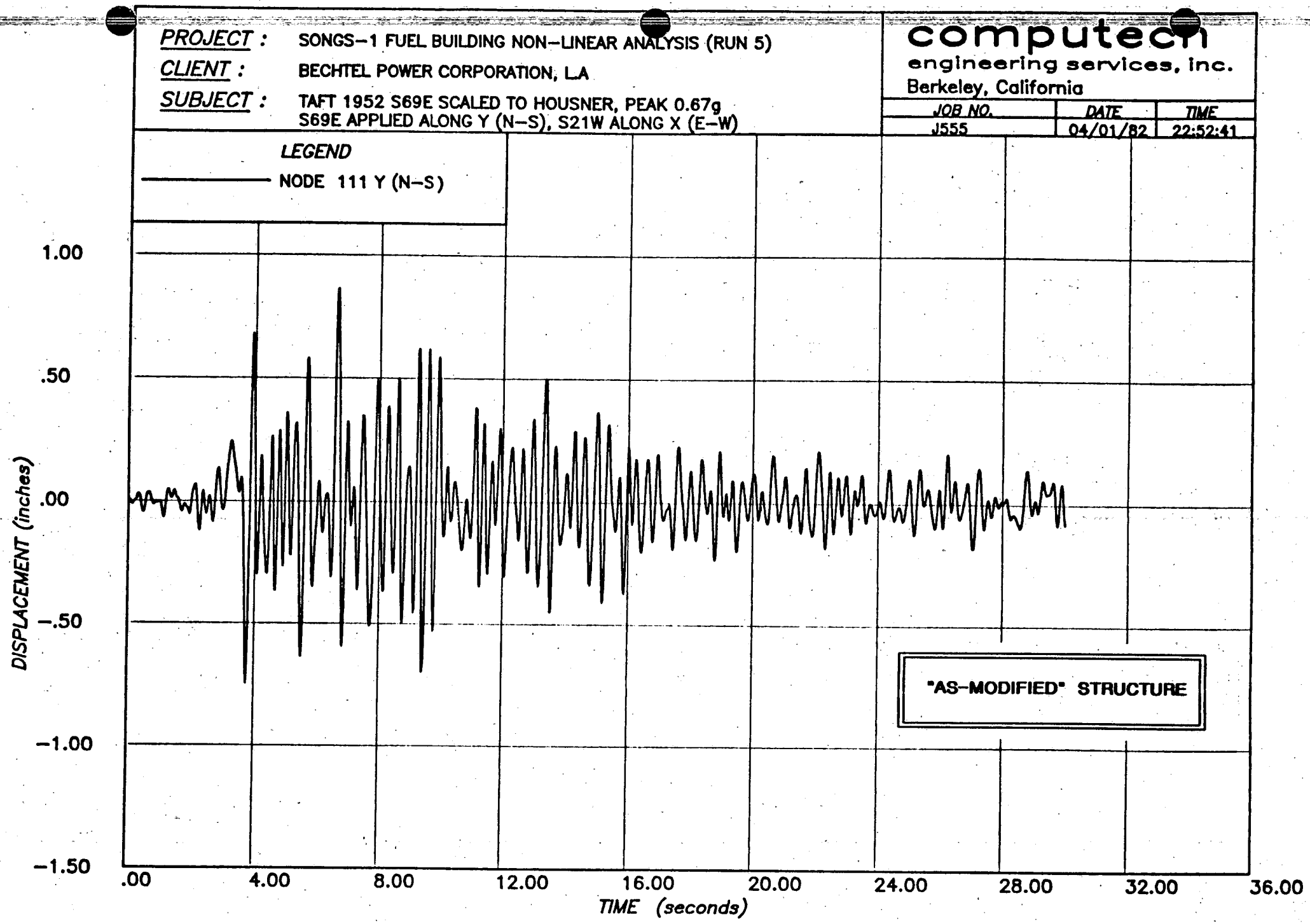

FIGURE G11 – TOP OF POOL: DISPLACEMENT

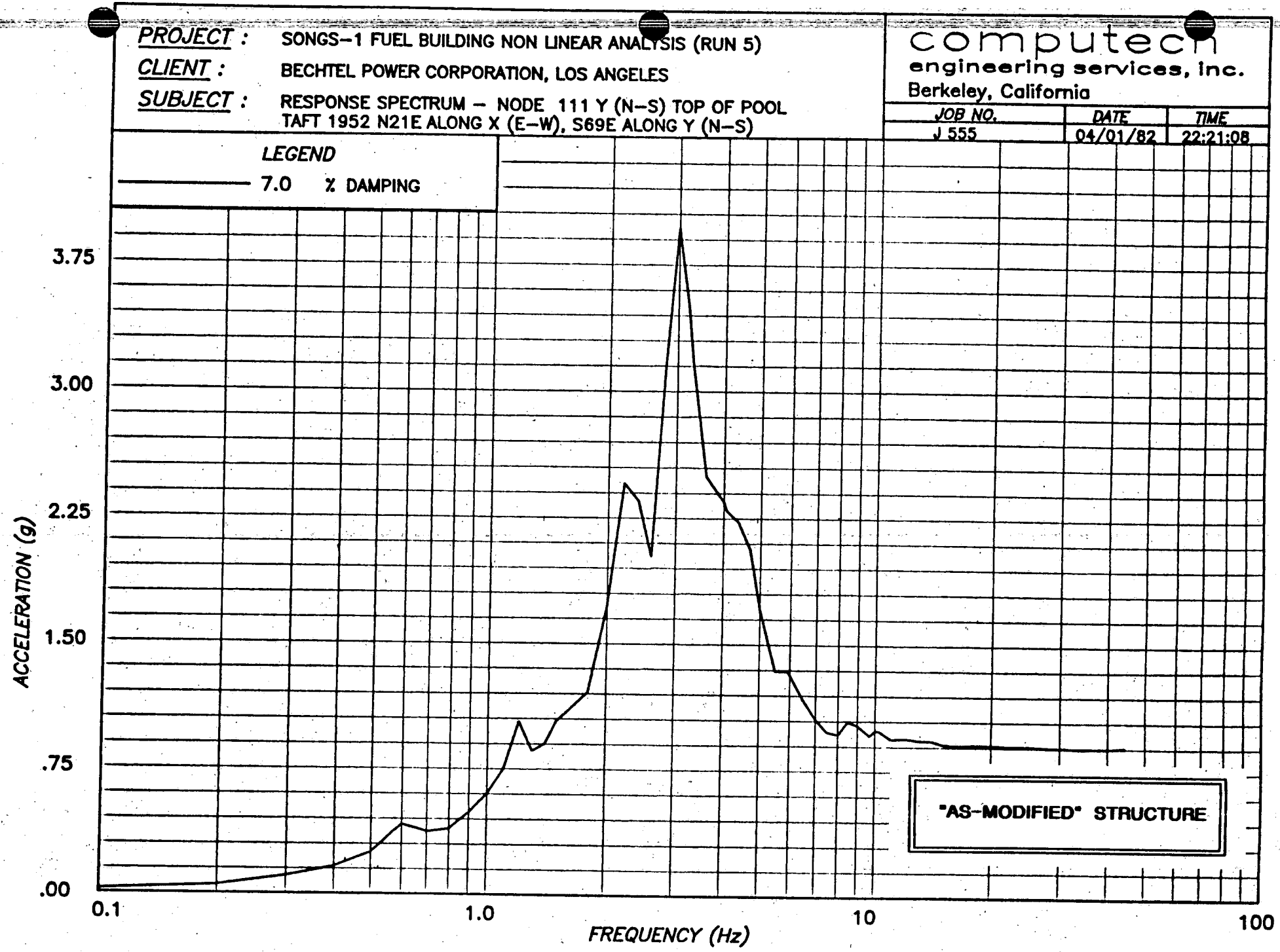

FIGURE G12 - TOP OF POOL: RESPONSE SPECTRUM - HORIZONTAL

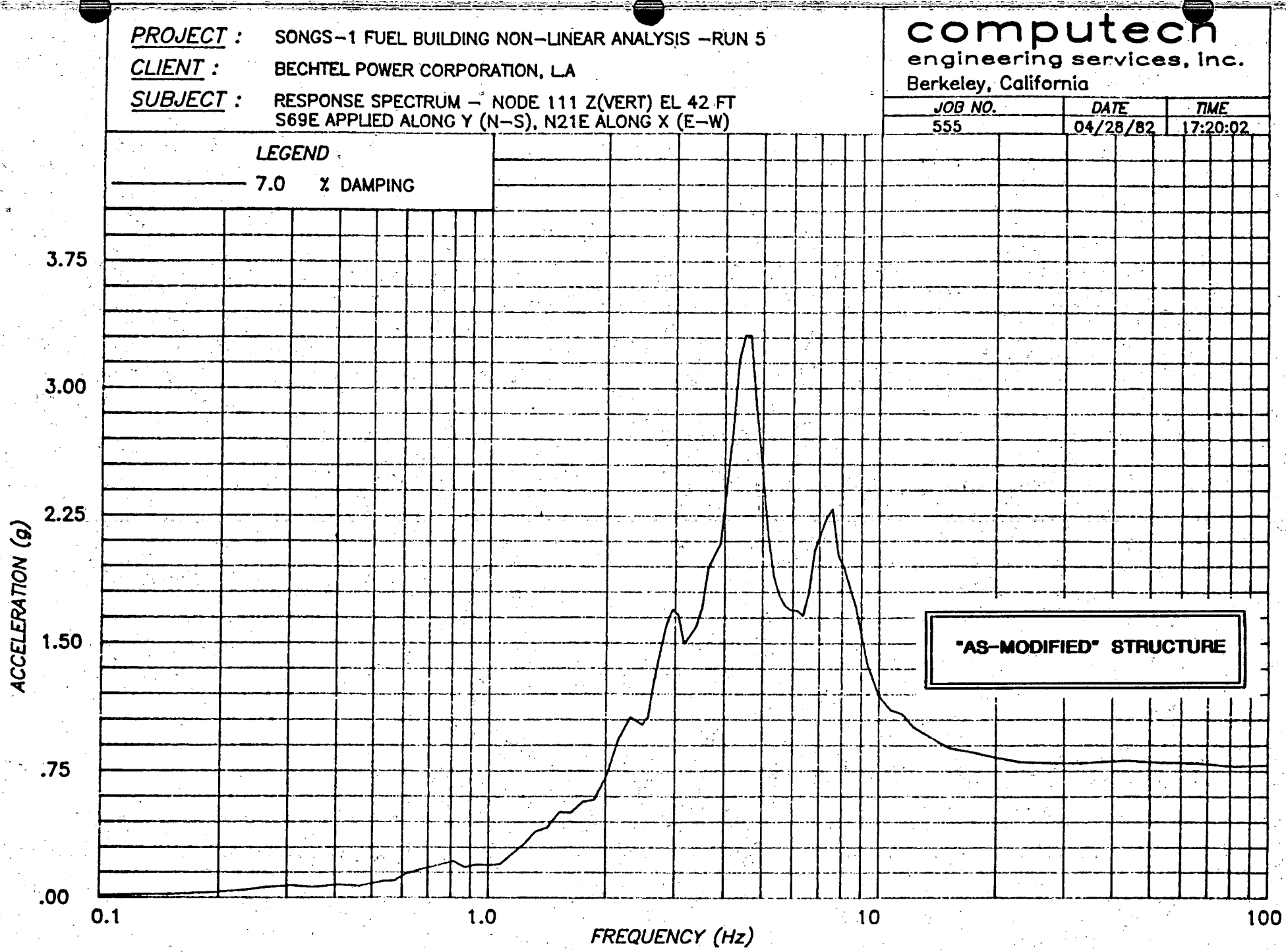

FIGURE G13 - TOP OF POOL: RESPONSE SPECTRUM - VERTICAL

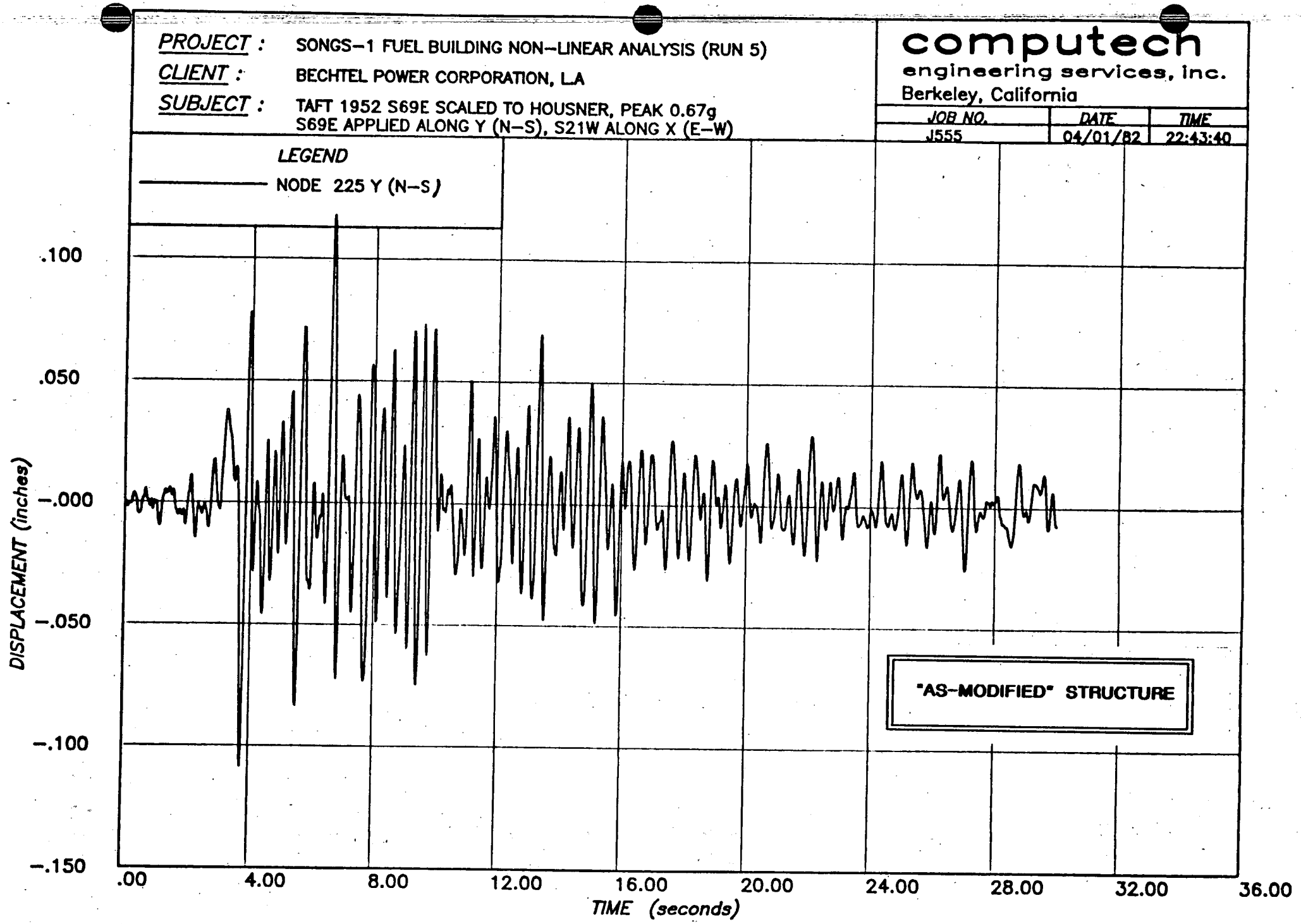

FIGURE G14 – BASE OF POOL: DISPLACEMENT

APPENDIX H: DETAILED RESULTS

Y(N-S) EARTHQUAKE: Taft 1952 N21W. Scaled 2.90

X(E-W) EARTHQUAKE: Taft 1952 S69E. Scaled 2.90. 0.67g Peak

LOCATION	DISPLACEMENT (Inches)	
	MAXIMUM	MINIMUM
ROOF		
N-W Corner	0.499	-0.480
S-W Corner	0.457	-0.558
N-E Corner	0.494	-0.497
S-E Corner	0.466	-0.501
TOP OF FUEL POOL		
N-W Corner	0.301	-0.295
S-W Corner	0.305	-0.324
N-E Corner	0.301	-0.295
S-E Corner	0.304	-0.323
BASE OF FUEL POOL		
N-W Corner	0.015	-0.091
S-W Corner	0.083	-0.101
N-E Corner	0.085	-0.091
S-E Corner	0.083	-0.101

ANALYSIS NUMBER **6**

EARTHQUAKE: **Taft**

PRINCIPAL COMPONENT DIRECTION: **X**

TABLE H1: MAXIMUM DISPLACEMENTS

("AS-MODIFIED" STRUCTURE)

WALL NUMBER	SHEAR STRESS (p.s.i)	SHEAR STRAIN	RATIO OF MAXIMUM STRAIN TO ALLOWABLE
FB-1	35.16	0.00025	0.0947
FB-2	90.62	0.00064	0.2424
FB-3	55.99	0.00040	0.1515
FB-4	64.50	0.00046	0.1742
FB-5	-45.92	-0.00033	0.1250
FB-6	-43.53	-0.00031	0.1174
FB-7	165.8	0.00266	0.5038
FB-8	114.1	0.00111	0.4205
FB-9	137.5	0.00175	0.6629
FB-10	97.29	0.00075	0.2841

ANALYSIS NUMBER: 6

EARTHQUAKE: Taft

PRINCIPAL COMPONENT DIRECTION: X

TABLE H2 : MAXIMUM IN-PLANE WALL RESPONSE

("AS-MODIFIED" STRUCTURE)

WALL	STEEL STRAIN RATIO		MASONRY STRESS	CENTER DISPLACEMENT
	CENTER	END	fm (p.s.i.)	(inches)
FB-1	14.02	17.60	655.9	7.17
FB-2	6.01	9.40	656.0	3.62
FB-3	5.95	9.83	655.9	3.88
FB-4				
FB-5	13.88	14.58	655.9	7.00
FB-6	14.05	17.78	655.3	7.46
FB-7				
FB-8	.81	.49	533.0	.78
FB-9	.85	.45	554.1	.73
FB-10	.85	.65	559.2	1.05

ANALYSIS NUMBER: 6

EARTHQUAKE: Taft

PRINCIPAL COMPONENT DIRECTION: X

TABLE H3: MAXIMUM OUT-OF-PLANE MASONRY WALL RESPONSE

("AS-MODIFIED" STRUCTURE)

WALL NUMBER	LOCATION	SHEAR STRESS (lb/ft)	TENSION (lb/ft)
FB-1	Roof	642.6	257.8
FB-2	Roof	982.1	233.2
FB-3	Roof	270.6	113.2
FB-4	Roof	250.4	-
FB-5	Roof	639.9	226.6
FB-6	Roof	1153.0	214.6
FB-7	Roof	1546.6	-
FB-8	El 42'-0"	2521.5	605.8
FB-9	El 42'-0"	978.6	118.9
FB-10	El 42'-0"	1664.9	572.1
FB-8	El 42'-0"	-	574.9
FB-9	El 42'-0"	-	486.3
FB-10	El 42'-0"	-	863.5

ANALYSIS NUMBER: 6

EARTHQUAKE: Taft

PRINCIPAL COMPONENT DIRECTION: X

TABLE H4: MAXIMUM CONNECTION FORCES

("AS-MODIFIED" STRUCTURE)

WALL NUMBER	LOCATION	SHEAR STRESS (lb/ft)	RATIO OF MAXIMUM STRESS TO ALLOWABLE
FB-1	Roof	1111.3	0.3751
FB-2	Roof	1581.1	0.5337
FB-3	Roof	646.3	0.2182
FB-4	Roof	632.7	0.2136
FB-5	Roof	901.9	0.3044
FB-6	Roof	2269.9	0.7662
FB-7	Roof	2269.9	0.7662
FB-8	El 42'-0"	3571.6	0.3484
FB-9	El 42'-0"	3571.6	0.3484
FB-10	El 42'-0"	2040.1	0.1990

ANALYSIS NUMBER: 6

EARTHQUAKE: Taft

PRINCIPAL COMPONENT DIRECTION: X

TABLE H5 : MAXIMUM DIAPHRAGM FORCES

("AS-MODIFIED" STRUCTURE)

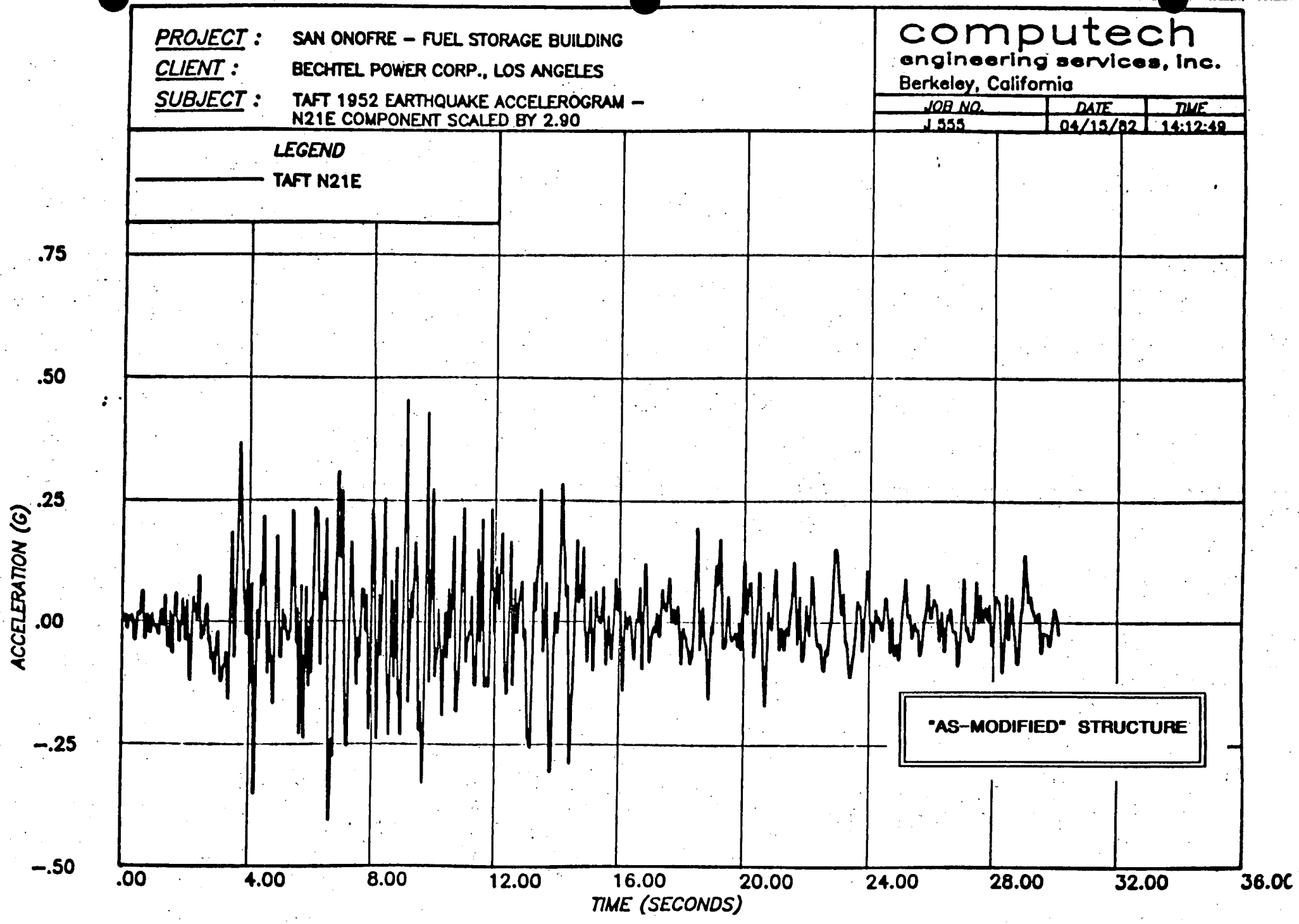

FIGURE H1 – TIME HISTORY AS SCALED [Y(N–S)]

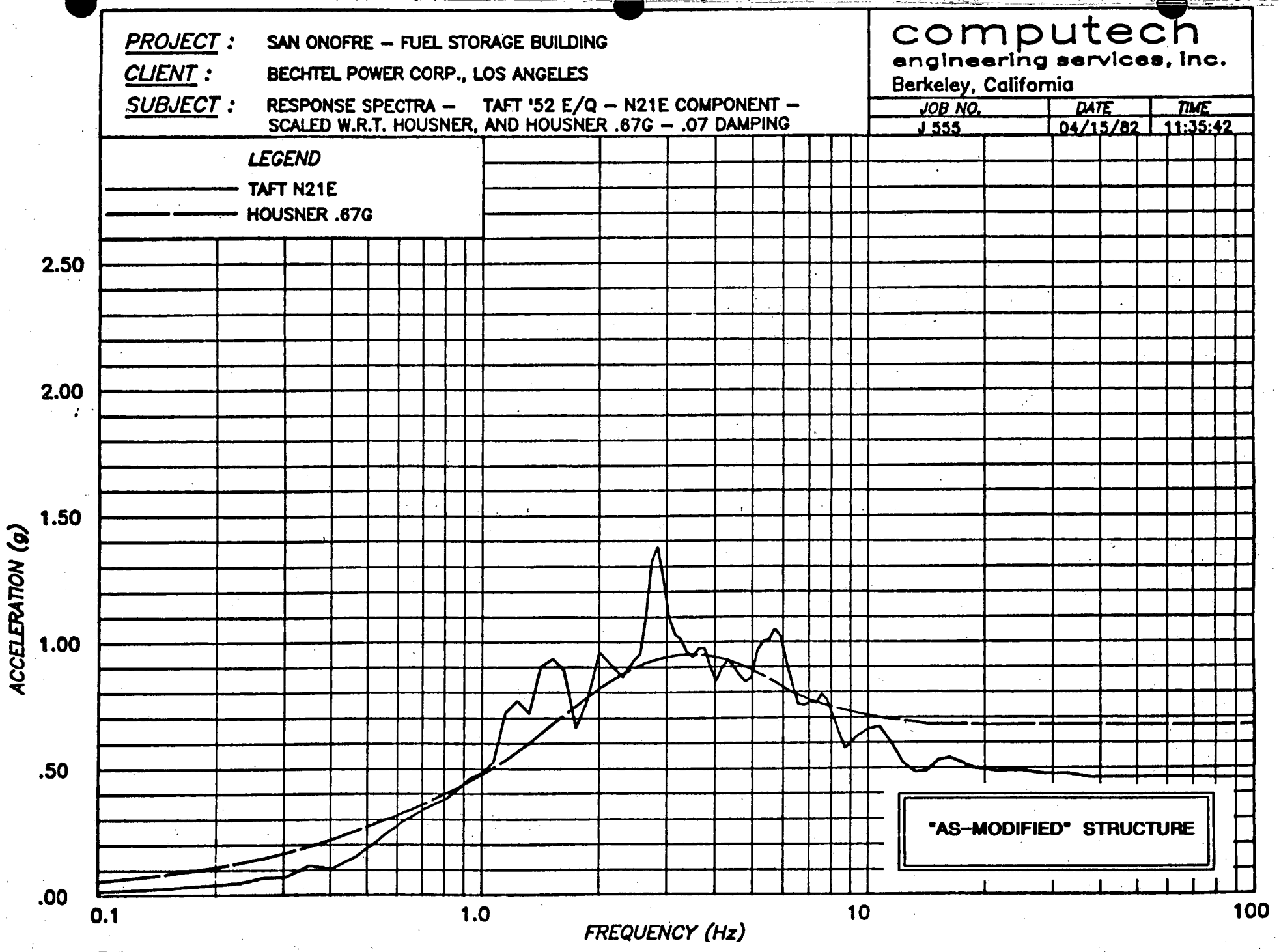

FIGURE H2 – RESPONSE SPECTRUM [Y(N-S)]

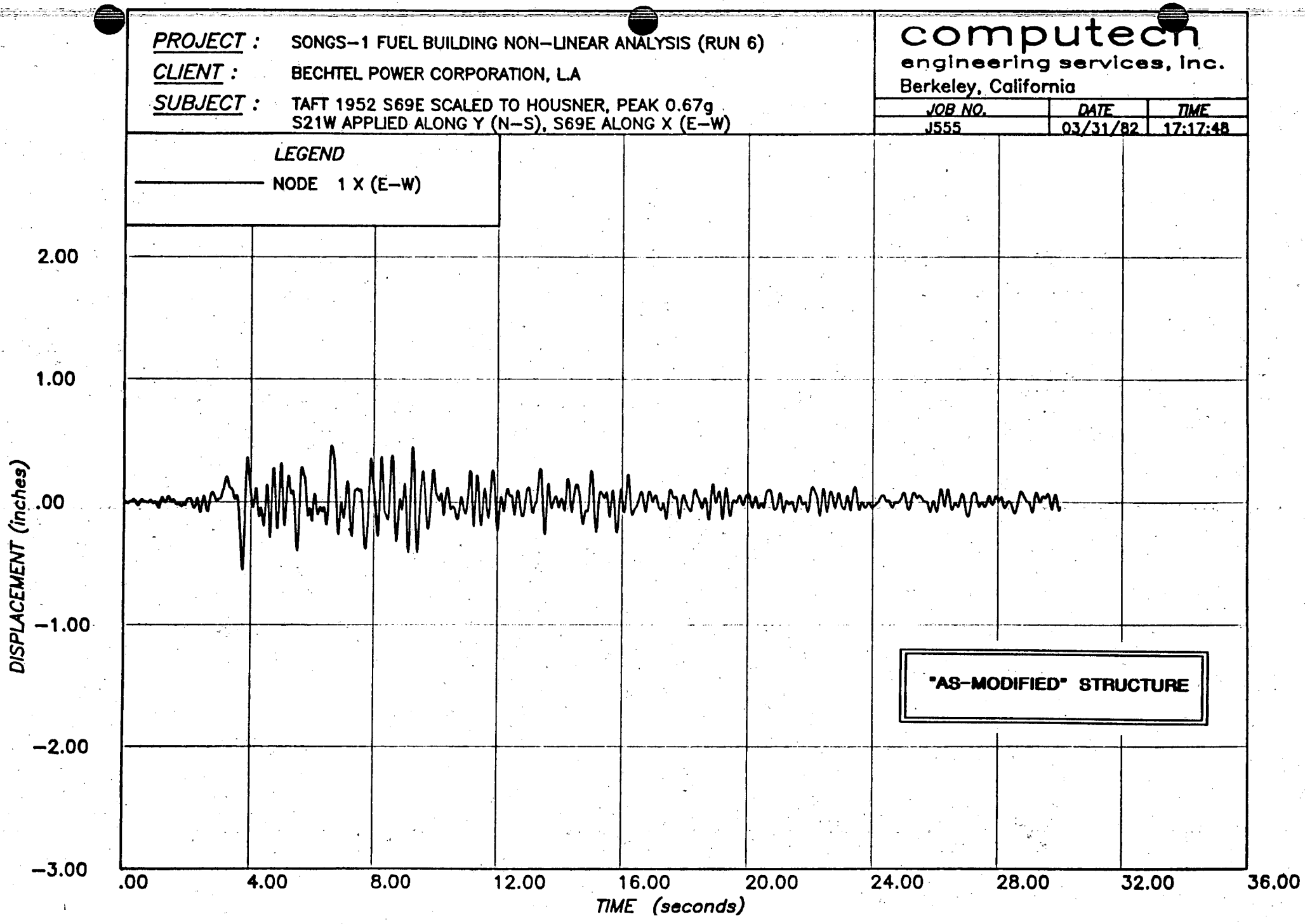

FIGURE H3 – ROOF DISPLACEMENT

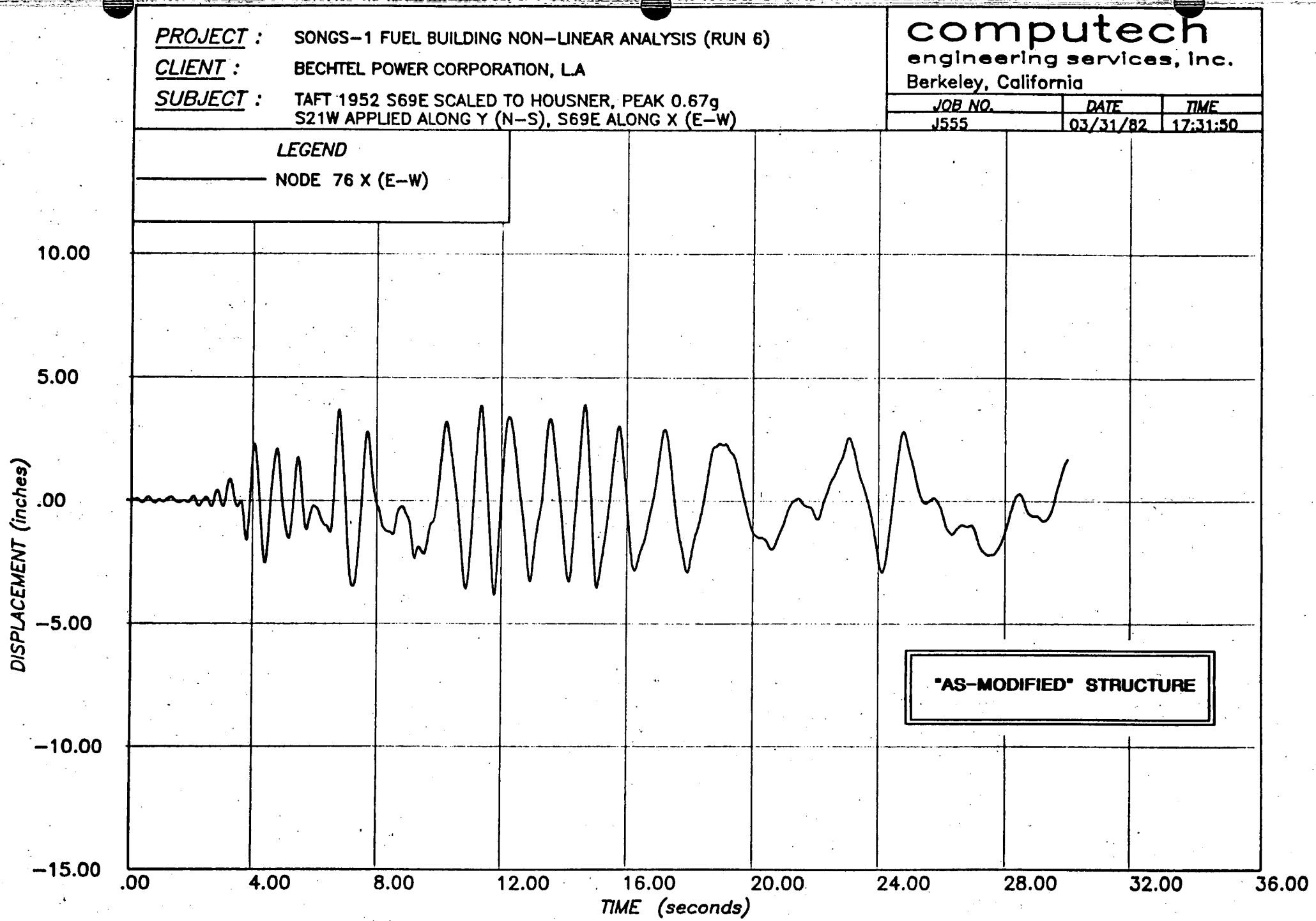

FIGURE H4 - OUT-OF-PLANE WALL DISPLACEMENTS - CENTER

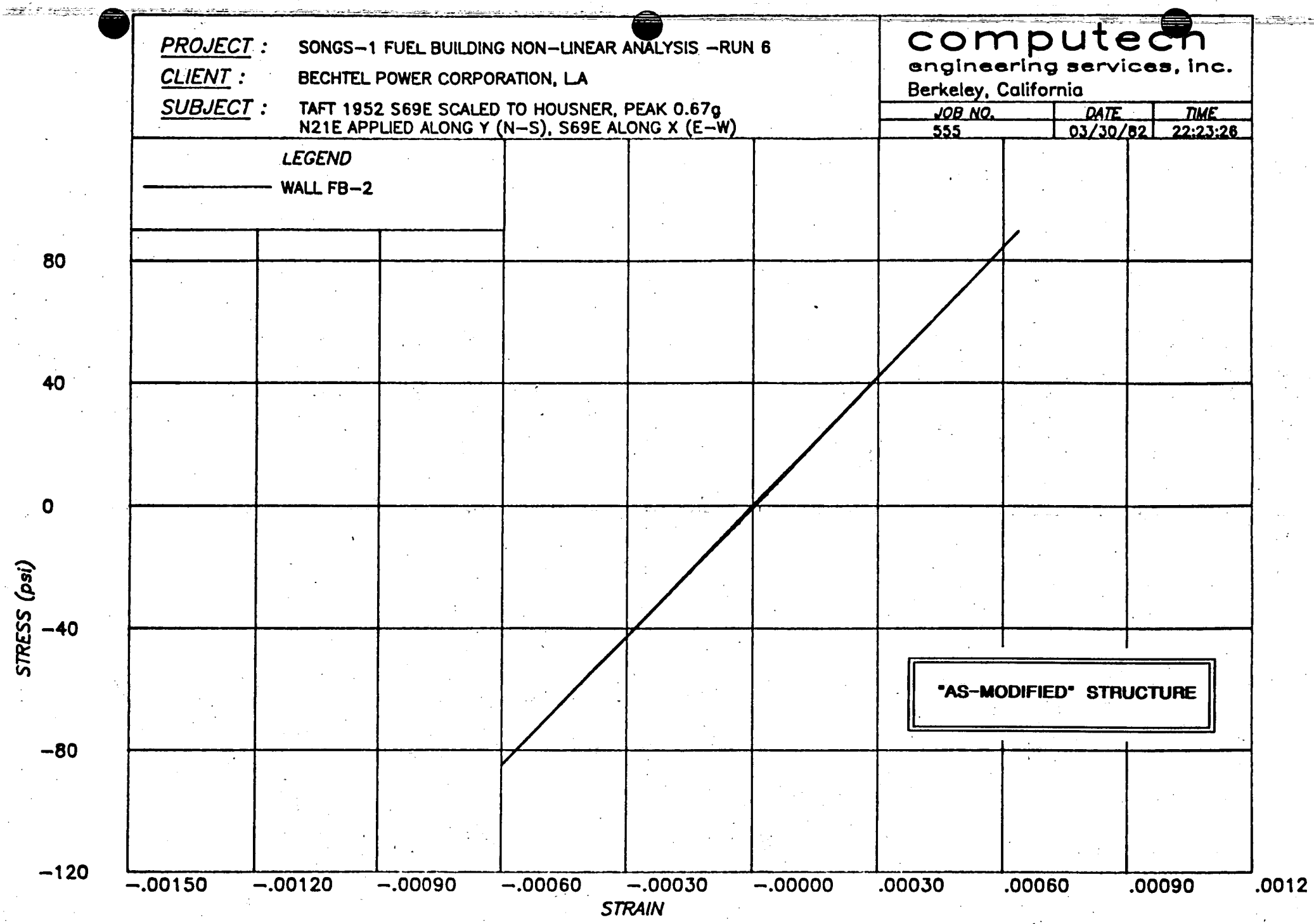

FIGURE H5 – IN-PLANE WALL STRESS-STRAIN – EL 42'

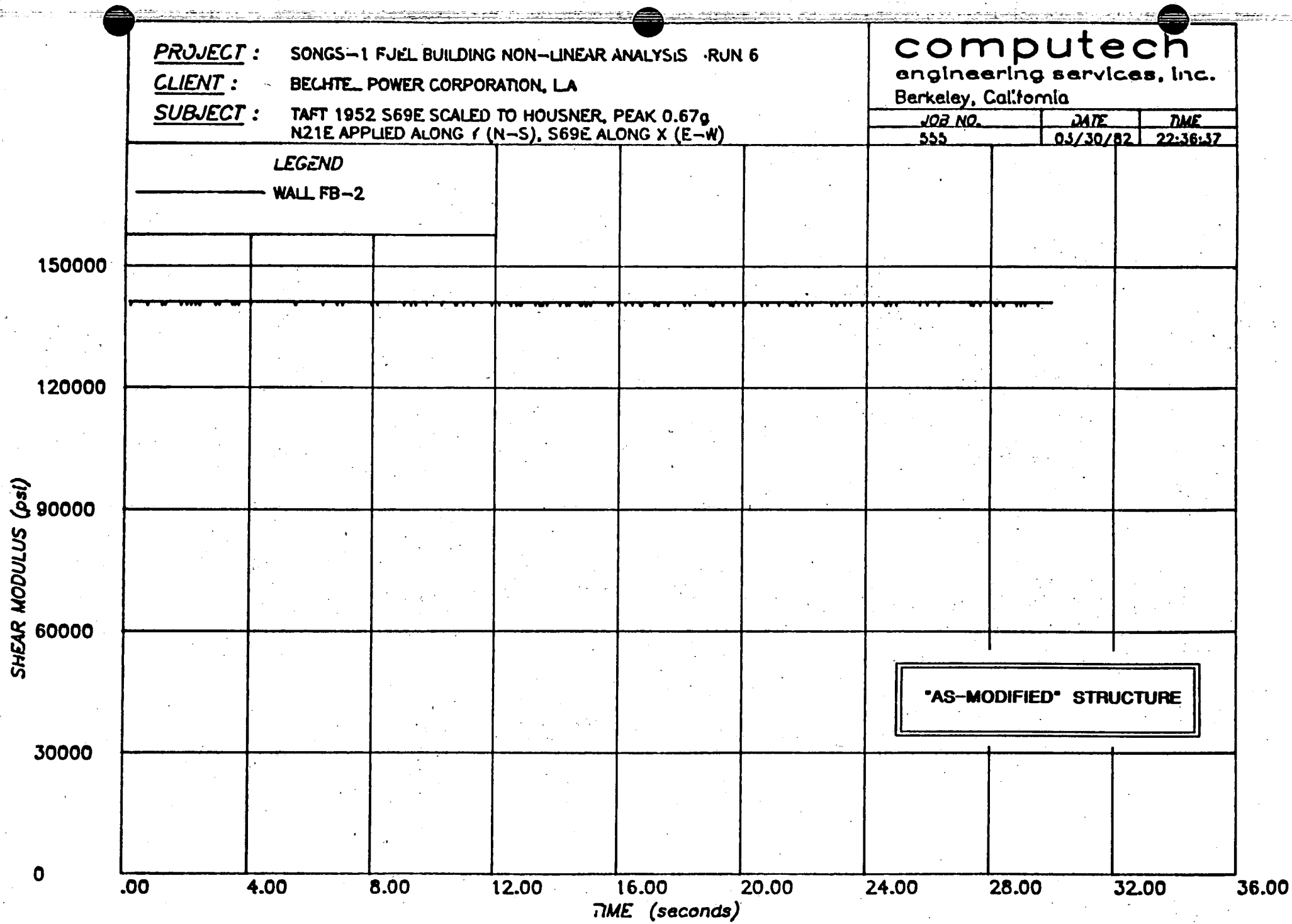

FIGURE H6 - IN-PLANE WALL STIFFNESS - EL 42'

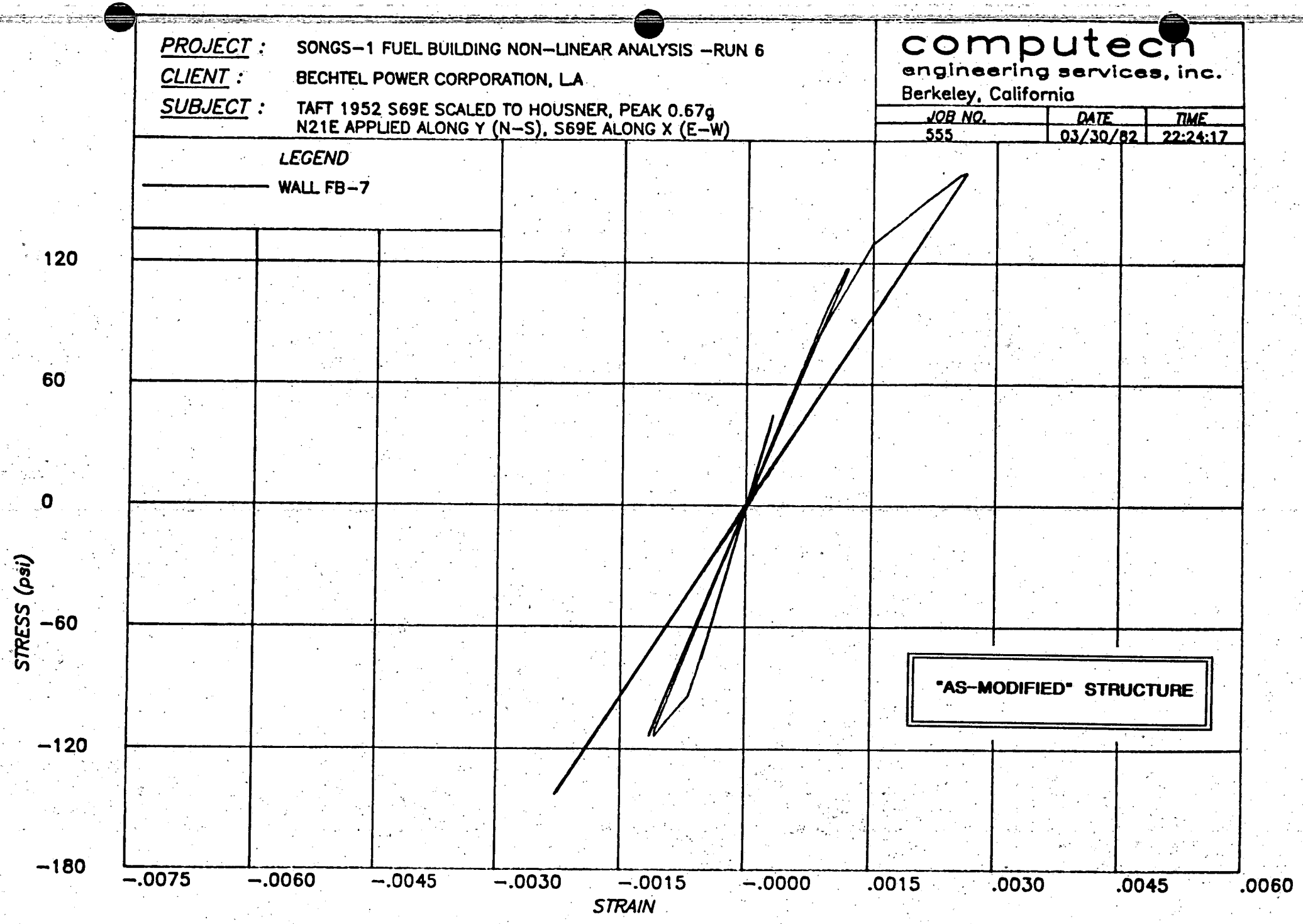

FIGURE H7 - IN-PLANE WALL STRESS-STRAIN - EL 42'

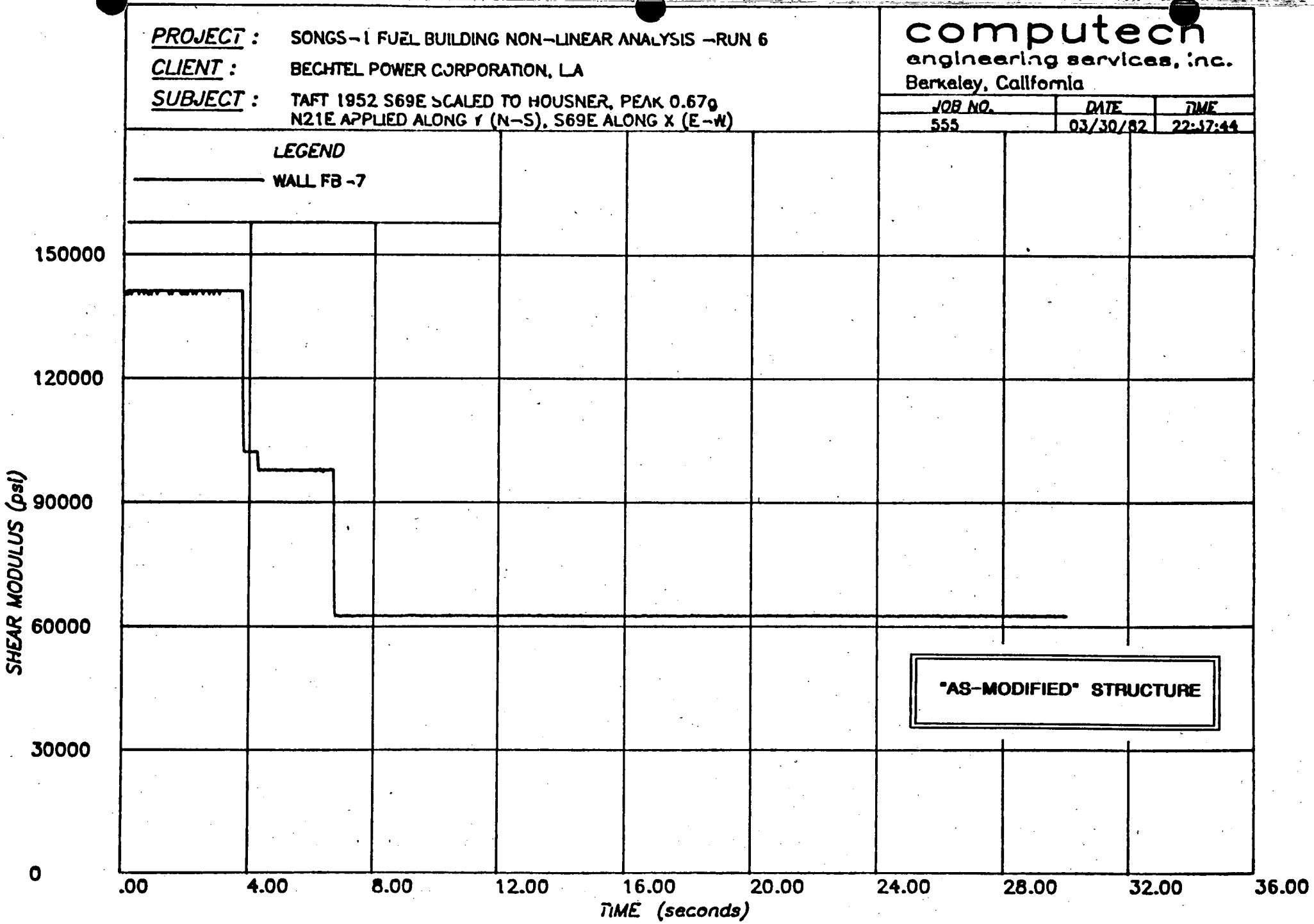

FIGURE H8 - IN-PLANE WALL STIFFNESS - EL 42'

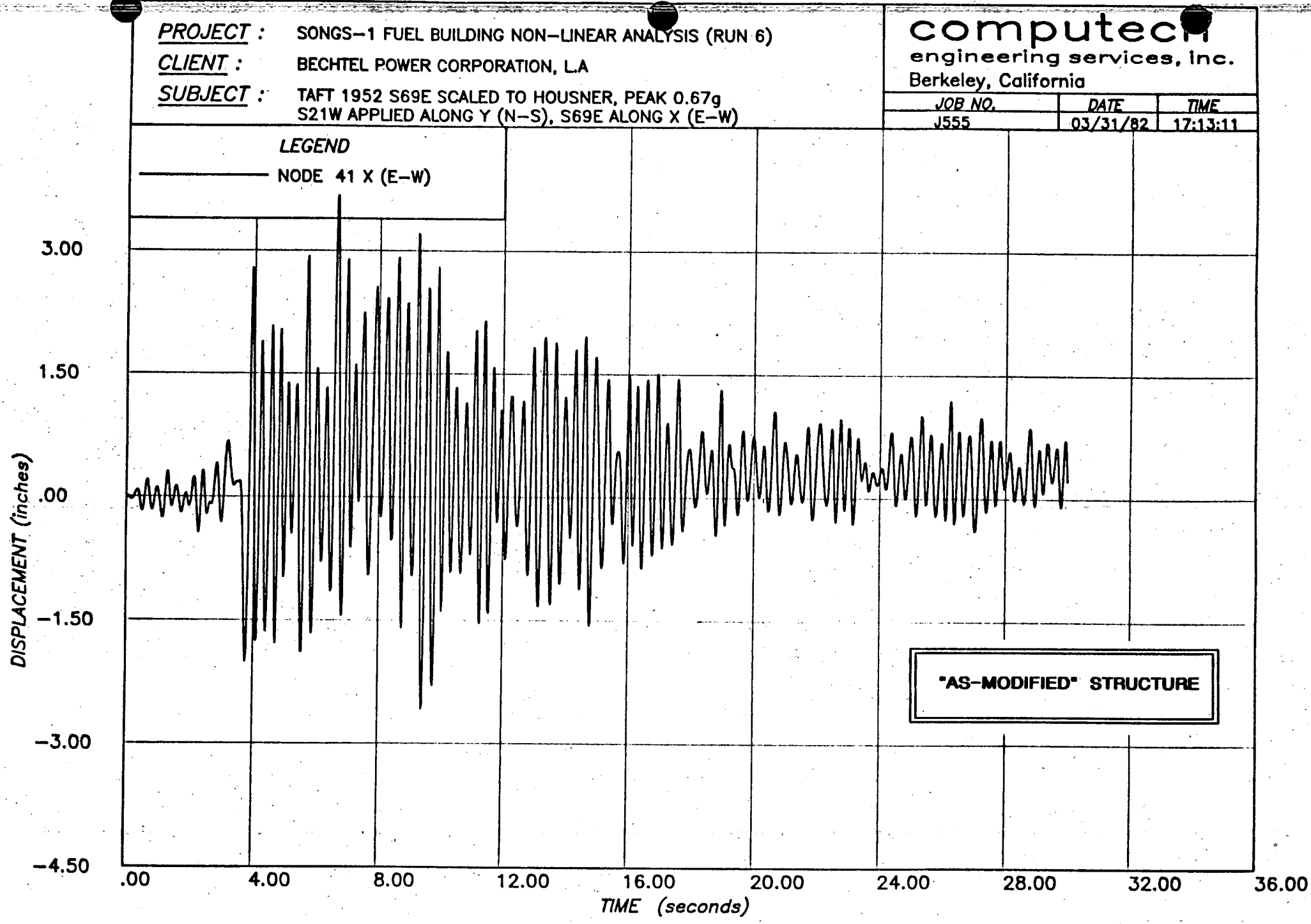

FIGURE H9 – DISPLACEMENT AT ROOF OPENING – EAST

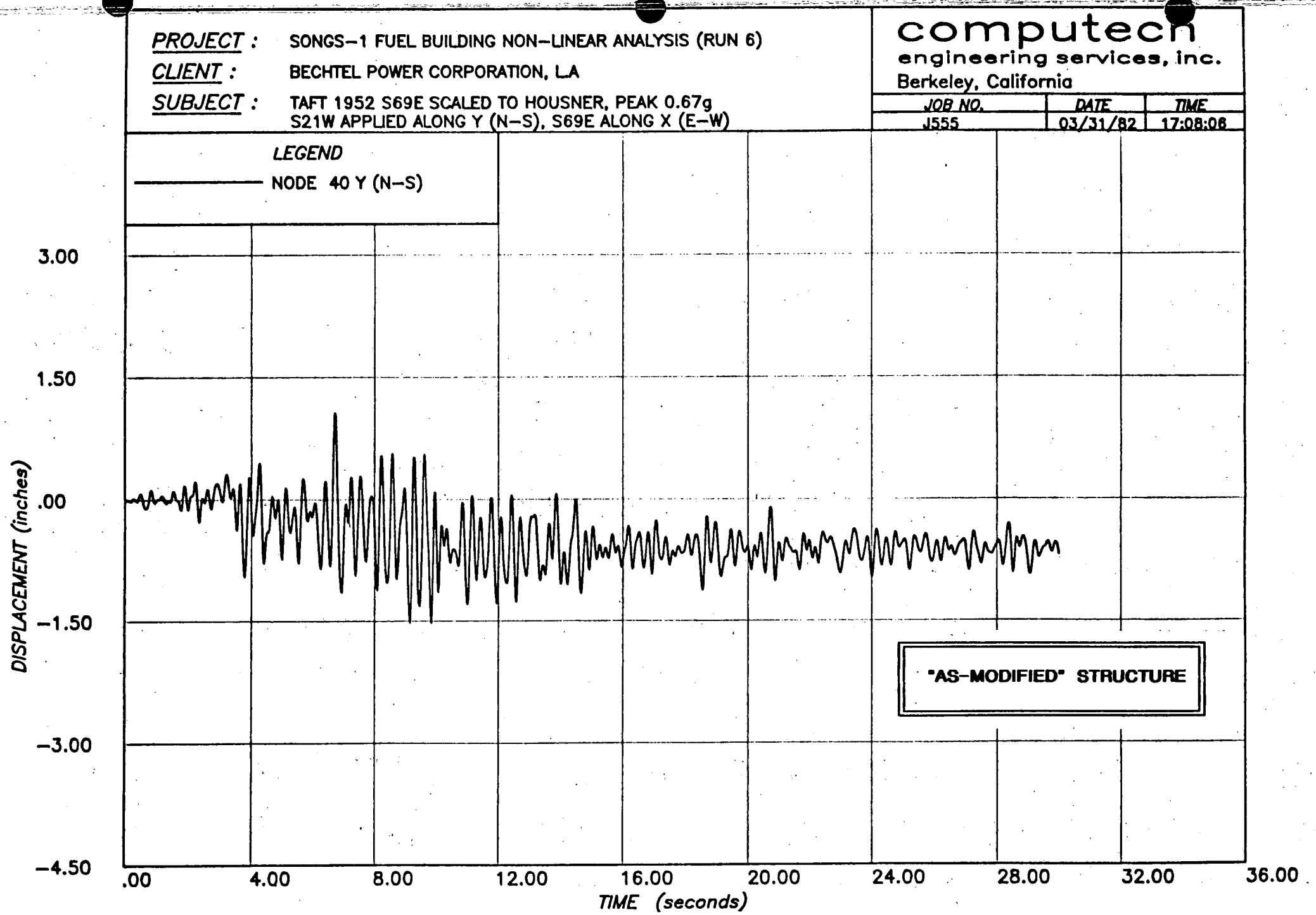

FIGURE H10 - DISPLACEMENT AT ROOF OPENING - SOUTH

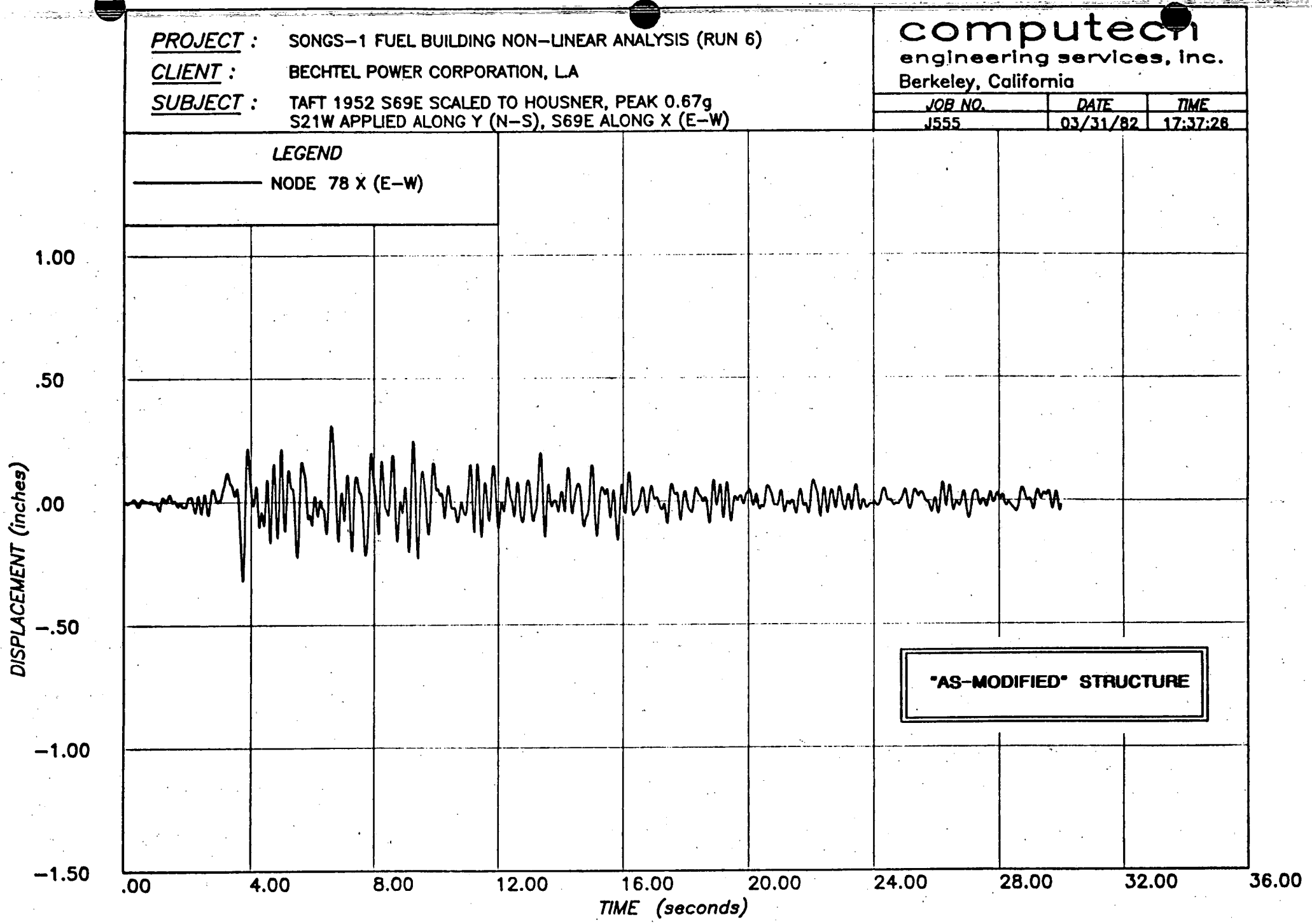

FIGURE H11 - TOP OF POOL: DISPLACEMENT

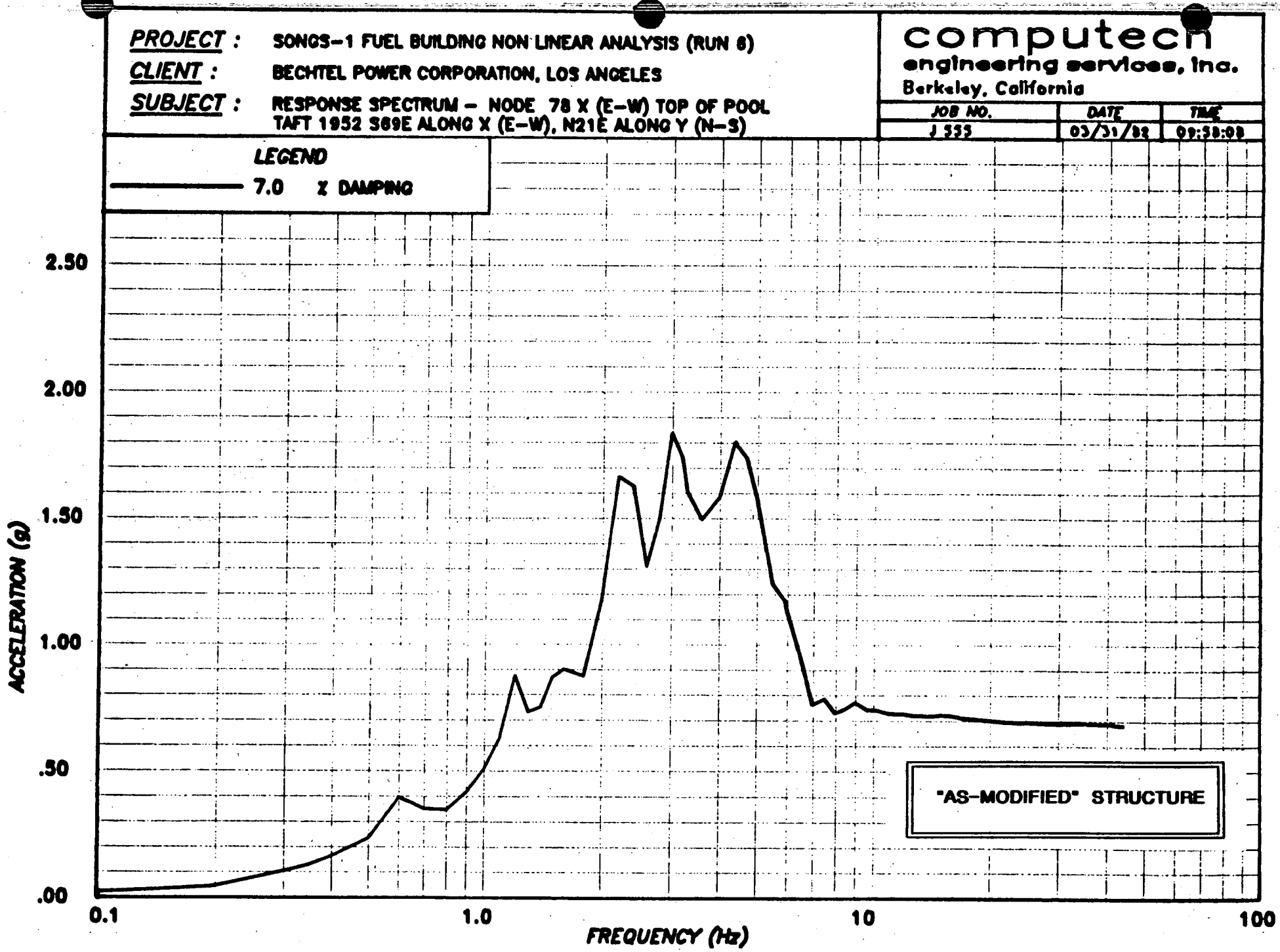

FIGURE H12 - TOP OF POOL: RESPONSE SPECTRUM - HORIZONTAL

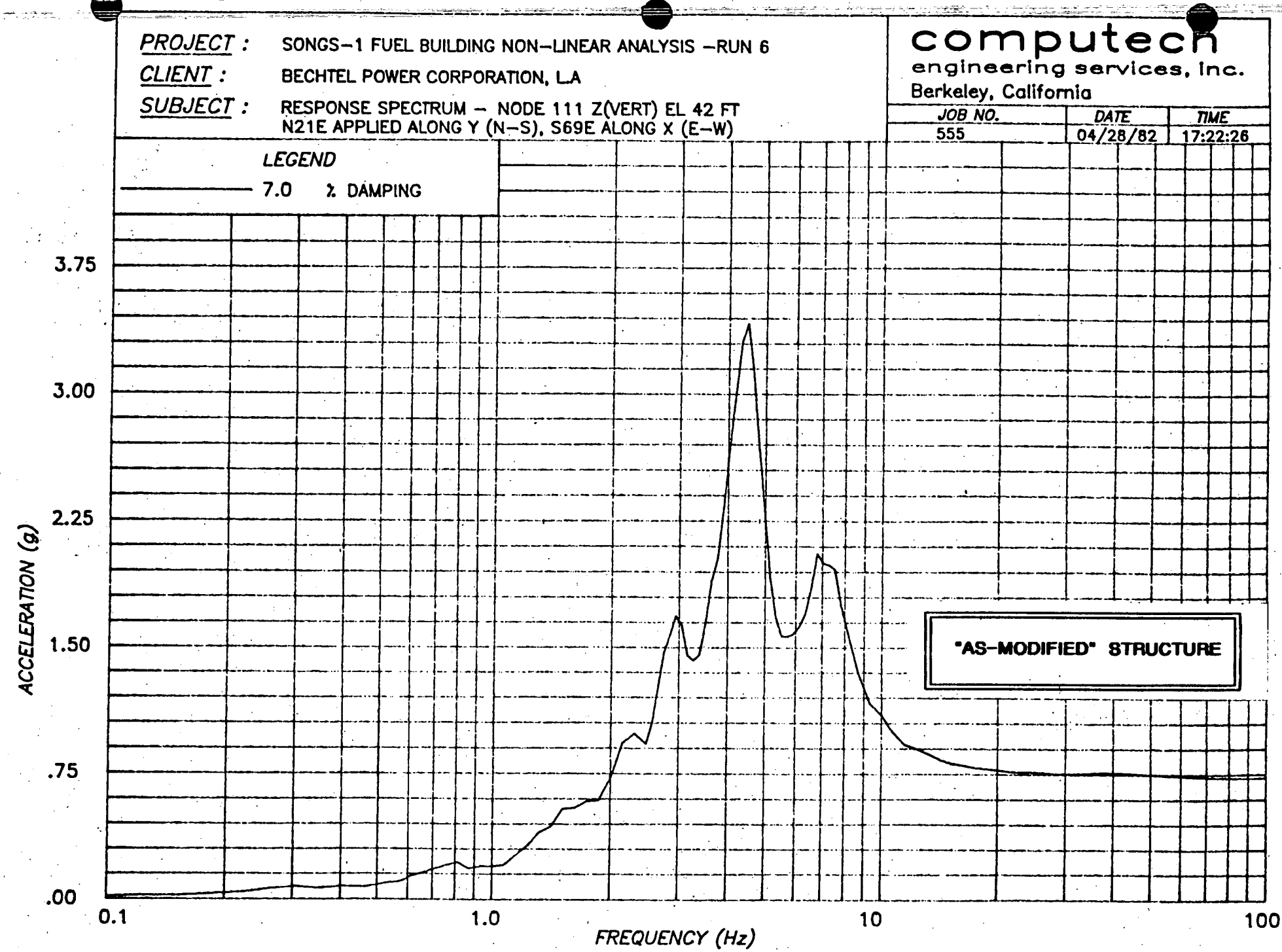

FIGURE H13 - TOP OF POOL: RESPONSE SPECTRUM - VERTICAL

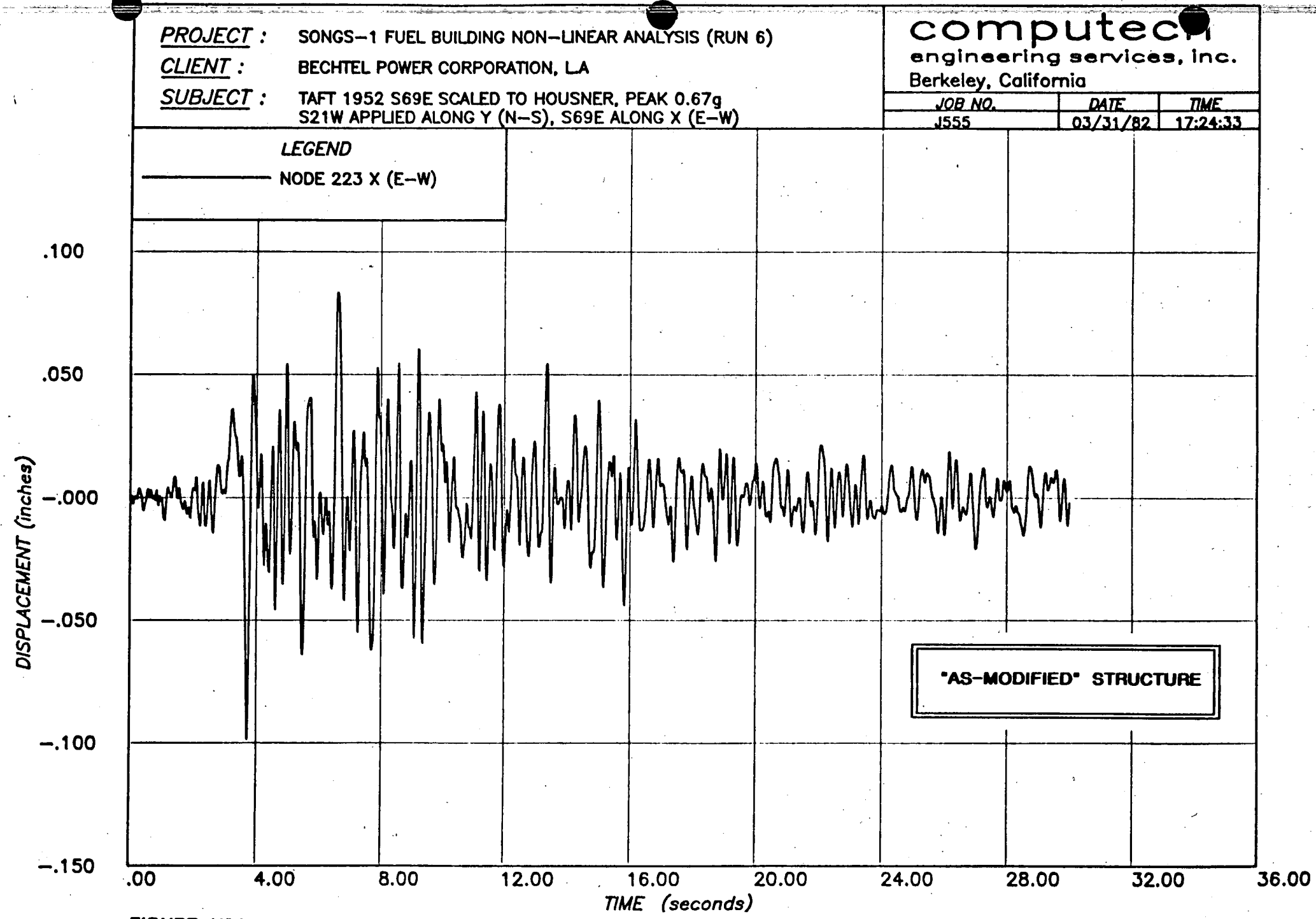

FIGURE H14 – BASE OF POOL: DISPLACEMENT